Complexity

Hyperchaotic Fractional-Order Systems and Their Applications

Lead Guest Editor: Ahmed Elsaid
Guest Editors: Delfim F. M. Torres, Sachin Bhalekar, Abdelalim Elsadany, and Amr Elsonbaty

Hyperchaotic Fractional-Order Systems and Their Applications

Complexity

Hyperchaotic Fractional-Order Systems and Their Applications

Lead Guest Editor: Ahmed Elsaid
Guest Editors: Delfim F. M. Torres, Sachin Bhalekar, Abdelalim Elsadany, and Amr Elsonbaty

Editorial Board

Contents

Hindawi
Complexity
Volume 2017, Article ID 7476090, 1 page
https://doi.org/10.1155/2017/7476090

Editorial

Hyperchaotic Fractional-Order Systems and Their Applications

Ahmed Elsaid,[1] Delfim F. M. Torres,[2] Sachin Bhalekar,[3] Abdelalim Elsadany,[4] and Amr Elsonbaty[1]

[1] *Mathematics & Engineering Physics Department, Faculty of Engineering, Mansoura University, P.O. 35516, Mansoura, Egypt*
[2] *Department of Mathematics and CIDMA, University of Aveiro, 3810-193 Aveiro, Portugal*
[3] *Department of Mathematics, Shivaji University, Kolhapur 416004, India*
[4] *Department of Basic Science, Faculty of Computers and Informatics, Suez Canal University, Ismailia 41522, Egypt*

Correspondence should be addressed to Ahmed Elsaid; a_elsaid@mans.edu.eg

Received 12 November 2017; Accepted 12 November 2017; Published 7 December 2017

Research about fractional-order hyperchaotic systems gains a lot of interest from both theoretical and applied point of view. Some fractional-order hyperchaotic systems have been investigated, such as the fractional-order hyperchaotic Rossler system and the fractional-order hyperchaotic Chen system. Recent publications in this area include nonlinear circuits, secure communication, laser applications, spread spectrum communication, communication in star coupled network, video encryption communication, color image encryption algorithm, and applications of different types of synchronization.

We are pleased to announce the publication of this special issue focusing on novel topics in hyperchaotic fractional-order systems and their applications. The main objective of this special issue is to provide an opportunity to study the new developments related to novel chaotic systems, synchronization schemes, bifurcations, and control in hyperchaotic fractional-order systems along with their applications. Among the articles that were submitted for review, our editorial team has selected seven articles for publication. These articles cover the topics of adaptive fuzzy synchronization, image encryption algorithm, dynamical analysis of a novel hyperchaotic system, eigenvalue problems, BAM neural networks with distributed delays and impulses, complex synchronization scheme between integer-order and fractional-order chaotic systems with different dimensions, and fractional-order FPGA implementation. We are confident that this special issue advances the understanding and research of hyperchaotic fractional-order systems and their applications.

Acknowledgments

We would also like to thank all the reviewers who have participated in the review process of the articles submitted to this special issue.

Ahmed Elsaid
Delfim F. M. Torres
Sachin Bhalekar
Abdelalim Elsadany
Amr Elsonbaty

Hindawi
Complexity
Volume 2017, Article ID 9010251, 13 pages
https://doi.org/10.1155/2017/9010251

Research Article

A Novel Image Encryption Algorithm Based on a Fractional-Order Hyperchaotic System and DNA Computing

Taiyong Li,[1,2,3,4] Minggao Yang,[1] Jiang Wu,[1] and Xin Jing[1]

[1] *School of Economic Information Engineering, Southwestern University of Finance and Economics, 55 Guanghuacun Street, Chengdu 610074, China*
[2] *Collaborative Innovation Center for the Innovation and Regulation of Internet-Based Finance, Southwestern University of Finance and Economics, 55 Guanghuacun Street, Chengdu 610074, China*
[3] *Laboratory for Financial Intelligence and Financial Engineering, Southwestern University of Finance and Economics, 55 Guanghuacun Street, Chengdu 610074, China*
[4] *Institute of Chinese Payment System, Southwestern University of Finance and Economics, 55 Guanghuacun Street, Chengdu 610074, China*

Correspondence should be addressed to Taiyong Li; litaiyong@gmail.com

Received 20 July 2017; Accepted 12 October 2017; Published 23 November 2017

Academic Editor: Ahmed Elsaid

In the era of the Internet, image encryption plays an important role in information security. Chaotic systems and DNA operations have been proven to be powerful for image encryption. To further enhance the security of image, in this paper, we propose a novel algorithm that combines the fractional-order hyperchaotic Lorenz system and DNA computing (FOHCLDNA) for image encryption. Specifically, the algorithm consists of four parts: firstly, we use a fractional-order hyperchaotic Lorenz system to generate a pseudorandom sequence that will be utilized during the whole encryption process; secondly, a simple but effective diffusion scheme is performed to spread the little change in one pixel to all the other pixels; thirdly, the plain image is encoded by DNA rules and corresponding DNA operations are performed; finally, global permutation and 2D and 3D permutation are performed on pixels, bits, and acid bases. The extensive experimental results on eight publicly available testing images demonstrate that the encryption algorithm can achieve state-of-the-art performance in terms of security and robustness when compared with some existing methods, showing that the FOHCLDNA is promising for image encryption.

1. Introduction

Images, as one of the most popular media types, are widespread over various networks. How to prevent images from illegal copying and distribution in the era of the Internet is a critical issue. Therefore, image encryption has become one of the hottest research topics of information security in recent years. Although there exist some classical schemes such as Data Encryption Standard (DES), Advanced Encryption Standard (AES), and International Data Encryption Algorithm (IDEA) for information security [1], they usually cannot be directly applied to image encryption to yield satisfactory results due to some intrinsic properties of images such as bulky data capacity, strong correlation, and high redundancy [2–4]. In contrast, the chaos-based image encryption has attracted much attention for research purposes and has been demonstrated to be effective and secure in recent years [5–9].

Chaotic systems have the following properties: pseudorandomness, extreme sensitivity to the initial values and system parameters, ergodicity, and unpredictability, which make it very suitable for image encryption [10]. Typically, chaos-based image encryption framework includes chaotic sequence generation, pixel position permutation, and pixel value diffusion. One-dimensional (1D) chaotic systems have simple forms and are easy to implement, and thus some researchers used them to encrypt images. For example, the authors used two 1D chaotic Logistic maps to generate the pseudorandom sequence for image encryption in [11]. Boriga et al. presented a new 1D chaotic map for real-time

image encryption [12]. However, since the 1D chaotic systems usually have only one variable and a few parameters, along with relatively simple structures and chaotic orbits, it is easy to estimate the orbits and to predict the initial values and/or parameters by little information extracted from them [13]. Therefore, in order to improve the security of image encryption, chaotic systems with two or more dimensions have been applied to image encryption. Fridrich put forward symmetric ciphers with two-dimensional (2D) chaotic maps and the experimental results demonstrated good diffusion properties with respect to the key and the plain image [14]. Hua et al. proposed an image encryption algorithm using 2D Sine Logistic modulation map that has better properties of chaos when compared with some existing chaotic systems [15]. Using the chaotic three-dimensional (3D) cat map extended from 2D Arnold's cat map [16] and 3D Chen's chaotic system [17], Chen et al. proposed a symmetric image encryption scheme for alternative permutation and diffusion [5]. The Lyapunov exponent (LE) is a type of measurement methodology for chaotic level, and a chaotic system is said to be hyperchaotic if it has two or more positive LEs [18]. Since hyperchaotic systems have more advantages such as richer dynamic phenomena and higher randomness than common chaotic systems, lots of hyperchaotic systems have been employed to encrypt images [19–23]. For example, Norouzi et al. used the key stream generated by a hyperchaotic system to perform one round diffusion on the image to attain good results [20]. A novel image encryption algorithm based on genetic recombination and hyperchaotic Lorenz system was put forward by Wang and Zhang [21]. Yuan et al. proposed a parallel image cryptosystem by combining the Logistic map and a five-dimensional (5D) hyperchaotic system [23].

Most of the above-mentioned literature uses integral-order chaotic systems for image encryption. It has been reported that fractional-order hyperchaotic systems, as a counterpart of integral-order chaos, show higher nonlinearity and degrees owing to the complex geometrical interpretation of fractional derivatives for the nonlocal effects either in time or in space [24, 25]. Therefore, the fractional-order hyperchaotic systems have great potential in information security. Wang et al. applied the fractional-order hyperchaotic Lorenz system to color image encryption. To enhance the security of images, both system parameters and derivative order were embedded in the scheme [25]. The 3D fractional-order Lorenz system and Chen chaotic systems were employed to encrypt images by Wu et al. and Zhao et al., respectively [3, 26]. Huang et al. used a four-dimensional (4D) fractional-order hyperchaotic neural network system to cipher color images, and the experiments demonstrated the effectiveness of the system [27].

Most image encryption algorithms are performed on pixel-level or bit-level data. With the development of bioinformatics, some image encryption algorithms based on deoxyribonucleic acid (DNA) have emerged since Adleman completed the first experiment on DNA computing [28], due to the properties of DNA: massive parallelism, huge storage, and ultralow power consumption [29–34]. Typically, DNA-based image encryption consists of three steps: DNA encoding, DNA operations, and DNA decoding. The bit stream of images is encoded as DNA sequences with some encoding rules in the step of DNA encoding. Then, different DNA operations such as addition, subtraction, and exclusive OR (XOR) are performed on DNA. The types of both encoding and operations are usually determined by chaotic sequences. Finally, the results of DNA operations are decoded to bits with the counterpart of corresponding encoding rules. Zhang et al. used Logistic maps and two DNA operations (addition and complement) to encrypt image blocks, but the blocks led to low robustness against noise [33]. In the RGB image encryption scheme by Liu et al., DNA addition and complement operations were carried out on each channel of RGB image with the DNA sequence matrix generated from Logistic map [34]. Zhan et al. jointly used a hyperchaotic system and DNA computing to encrypt images, where the hyperchaotic sequence was applied to all steps. However, two important evaluation standards, that is, the number of pixels change rate (NPCR) and the unified average changing intensity (UACI), still need to be improved [29].

Motivated by the above analysis, this paper aims at proposing a novel image encryption algorithm that incorporates the fractional-order hyperchaotic Lorenz (FOHCL) system and fractional-order hyperchaotic Lorenz DNA (FOHCLDNA) computing in order to improve the security of image encryption. Specifically, the proposed FOHCLDNA is mainly composed of six stages: (1) the FOHCL is firstly applied to generating the pseudorandom sequence for encryption; (2) global pixel diffusion, global pixel permutation, and 2D permutation are carried out on pixels; (3) global bit permutation and 3D permutation are conducted on bits; (4) the bit stream of image is encoded as DNA sequence according to the encoding rules decided by the hyperchaotic sequence; (5) one of the DNA operations (addition, subtraction, or XOR) is carried out on each acid base, and, at the same time, global DNA permutation and 3D permutation further improve the security. Both the types of DNA operations and the orders of DNA permutation are determined by the hyperchaotic sequence; (6) the encrypted DNA sequence is decoded to bit stream, followed by bit-to-pixel decoding. Finally, the encrypted image is obtained. The main contributions of this paper are four aspects: (1) different from most existing literature that uses integral-order chaotic or hyperchaotic systems, the proposed FOHCLDNA uses a fractional-order hyperchaotic system for image encryption; (2) a simple but effective pixel diffusion is proposed; (3) permutation is carried out at different levels, that is, pixels, bits, and acid bases, while both the DNA encoding rule and DNA operation for each acid base are determined by corresponding hyperchaotic sequence; (4) extensive experiments demonstrate that the FOHCLDNA is promising for image encryption. The novelty of this paper is threefold: (1) it is a good attempt to integrate fractional-order hyperchaotic system and DNA computing to enhance the security of image encryption; (2) the simple pixel diffusion can spread the little change in one pixel to all other pixels; (3) several permutation operations performed at different levels can further improve the security.

The remainder of this paper is organized as follows. A brief description of the fractional-order hyperchaotic

Table 1: Encoding and decoding rules of DNA.

Rule	Rule 1	Rule 2	Rule 3	Rule 4	Rule 5	Rule 6	Rule 7	Rule 8
00	A	A	T	T	C	C	G	G
01	C	G	C	G	A	T	A	T
10	G	C	G	C	T	A	T	A
11	T	T	A	A	G	G	C	C

system and DNA computing is given in Section 2. In Section 3, we propose the novel image encryption algorithm (FOHCLDNA) in detail. Experimental results, analysis, and comparison are presented in Section 4. Concluding remarks of the FOHCLDNA are summarized in Section 5.

2. Related Work

2.1. Fractional-Order Hyperchaotic Lorenz System. The Lorenz systems and their variants are among the most popular chaotic/hyperchaotic systems in image encryption. The fractional-order hyperchaotic Lorenz (FOHCL) system shows good complex dynamics [35, 36], and some previous research has demonstrated its power in image encryption [25, 37, 38]. Therefore, in this paper, we use a four-dimensional FOHCL system to generate the chaotic sequence that the algorithm needs [25, 35]. The FOHCL can be described as follows:

$$\begin{aligned}
\frac{d^{q1}x_1}{dt^{q1}} &= \alpha\left(x_2 - x_1\right) + x_4,\\
\frac{d^{q2}x_2}{dt^{q2}} &= \gamma x_1 - x_2 - x_1 x_3,\\
\frac{d^{q3}x_3}{dt^{q3}} &= x_1 x_2 - \beta x_3,\\
\frac{d^{q4}x_4}{dt^{q4}} &= -x_2 x_3 + \phi x_4,
\end{aligned} \tag{1}$$

where α, β, γ, ϕ, and q_i $(i = 1, 2, 3, 4)$ are the system parameters. When $\alpha = 10$, $\beta = 8/3$, $\gamma = 28$, $\phi = -1$, $q_i = 0.98$ $(i = 1, 2, 3, 4)$, and the initial values $x_1^0 = 12$, $x_2^0 = 22$, $x_3^0 = 31$, and $x_4^0 = 4$, the system exhibits a hyperchaotic behavior with 2 positive values among all the 4 Lyapunov exponents ($\lambda_1 = 0.3362$, $\lambda_2 = 0.1568$, $\lambda_3 = 0$, and $\lambda_4 = -15.1724$) [35]. Figure 1 shows the attractor of the FOHCL system.

2.2. Deoxyribonucleic Acid (DNA) Computing. Deoxyribonucleic acid (DNA) is a kind of biological macromolecule, and the knowledge of DNA sequence is widely used in genetic engineering, biotechnology, and identification. An individual DNA sequence is mainly composed of carbohydrate and four different nucleic acid bases: A (Adenine), G (Guanine), C (Cytosine), and T (Thymine), where T and A; C and G are complementary pairs. The number of DNA coding combinations is 4! = 24 in total, which only have eight kinds of DNA bases legally to meet the DNA complementary rules, as shown in Table 1 [29, 39]. In the theory of binary system, 0 and 1 are complementary pairs such as 00 (0) and 11 (3), 01 (1) and 10 (2). Each pixel value of grayscale image in binary sequence is 8 bits, and if every 2 bits is represented by a letter, the representation of a pixel would be a 4-length nucleotide string. For example, for a pixel value 161 in decimal, its binary combination is "10010011," and the corresponding DNA sequence is "GCAT" by adopting the first encoding rule. If any other DNA coding rules are used to code the same binary sequence, the result will definitely be different.

Table 2: Addition (++) operation.

++	A	G	C	T
A	C	T	A	G
G	T	C	G	A
C	A	G	C	T
T	G	A	T	C

Table 3: Subtraction (−−) operation.

--	A	G	C	T
A	C	T	G	A
G	T	C	A	G
C	A	G	C	T
T	G	A	T	C

Table 4: XOR (⊗⊗) operation.

⊗⊗	A	G	C	T
A	A	G	C	T
G	G	A	T	C
C	C	T	A	G
T	T	C	G	A

With the encoding rules, the operations of addition (++), subtraction (−−), and XOR (⊗⊗) are listed in Tables 2–4.

3. Image Encryption Scheme

3.1. Hyperchaotic Sequence Generation. Since fractional-order hyperchaotic systems have good properties for image encryption, we use the FOHCL system described in Section 2.1 for generating the hyperchaotic sequence. The generating process is comprised of three steps.

Step 1. To eliminate the adverse effects, the FOHCL system is firstly iterated N_0 times and then the generated sequence is removed.

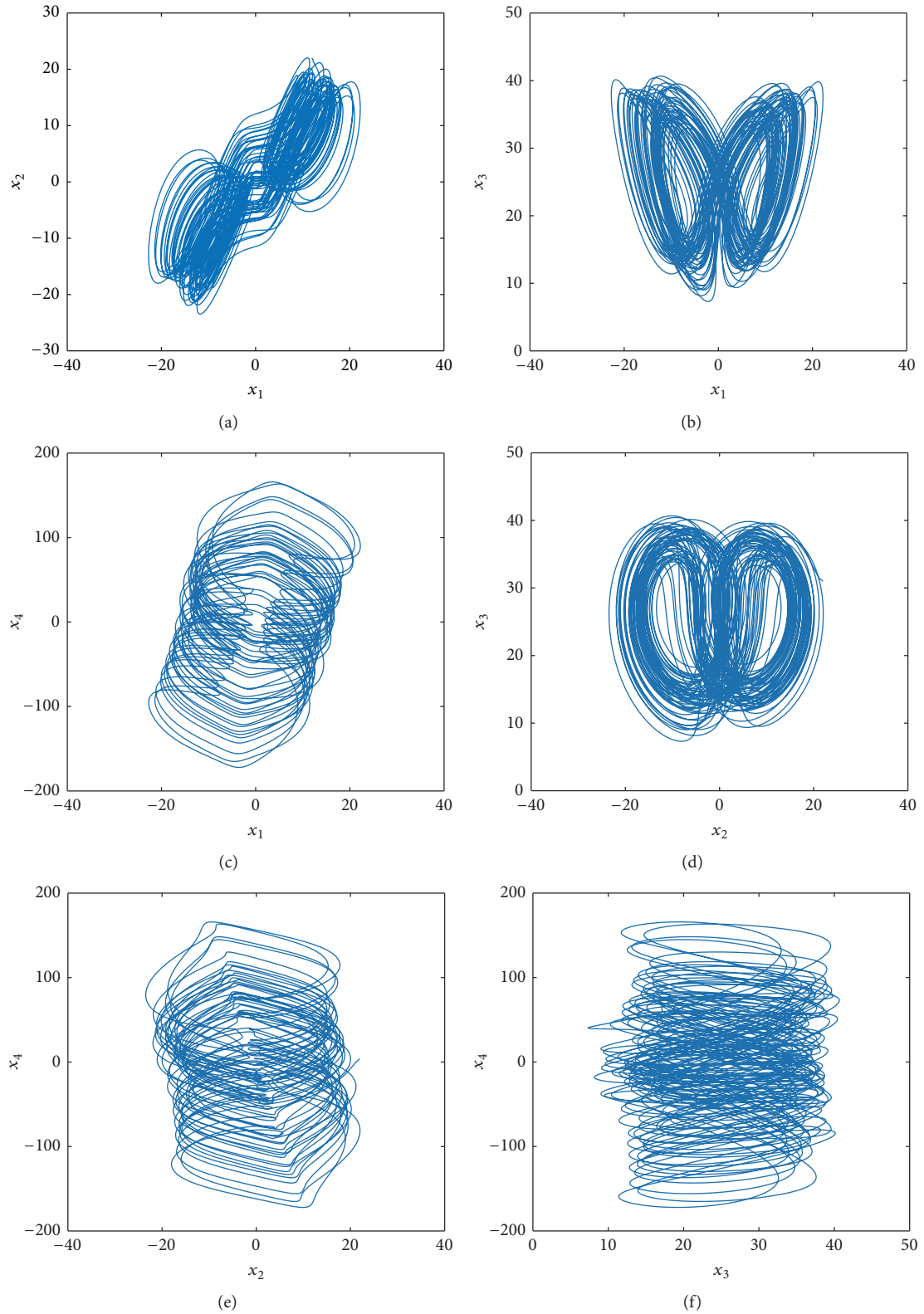

Figure 1: Phase diagrams of the fractional-order Lorenz hyperchaotic attractor. (a) x_1-x_2 plane, (b) x_1-x_3 plane, (c) x_1-x_4 plane, (d) x_2-x_3 plane, (e) x_2-x_4 plane, and (f) x_3-x_4 plane.

Step 2. The FOHCL system continues to iterate $N = \lceil (30hw + 3(h+w)+13)/4 \rceil$ times, where $\lceil \cdot \rceil$ denotes the ceiling operation and h and w denote the width (column) and the height (row) of the image to encrypt, respectively. For the jth iteration, four state values denoted by $s^j = \{x_1^j, x_2^j, x_3^j, x_4^j\}$ are obtained by (1).

Step 3. After the whole iteration, the fractional-order hyperchaotic sequences K can be obtained by concatenating all the s^j $(j = 1, 2, \ldots, N)$ as

$$\begin{aligned} K &= \left\{s^1, s^2, \ldots, s^N\right\} \\ &= \left\{x_1^1, x_2^1, x_3^1, x_4^1, \ldots, x_1^N, x_2^N, x_3^N, x_4^N\right\} \\ &= \left\{k^1, k^2, k^3, \ldots, k^{4N-2}, k^{4N-1}, k^{4N}\right\}. \end{aligned} \tag{2}$$

The purposes of the generated sequence K for encryption are two aspects: (1) sorting subsequence of K to get the index of original data for permutation; (2) using subsequence of K to change the values of images for diffusion. In our scheme, for the first purpose, we directly use the original values of K for sorting while, for the second purpose, we map the hyperchaotic subsequence of K with n values to the integer range of $[0, 255]$ by

$$S^i = \mathrm{mod}\left(\left\lfloor \mathrm{mod}\left(\left(\left|k^i\right| - \left\lfloor \left|k^i\right| \right\rfloor\right) \times 10^{15}, 10^8\right)\right\rfloor, 256\right), \quad i = 1, 2, 3, \ldots, n, \tag{3}$$

where S^i is the ith integer in the generated integer sequence, mod is the modulo operation, $|\cdot|$ is the absolute value operation, and $\lfloor \cdot \rfloor$ denotes flooring operation [29].

3.2. Global Pixel Diffusion. In our scheme, we carry out a simple two-step diffusion for image on pixels. Specifically, for a given image I of size $h \times w$, we can transform the image into a 1D pixel sequence $S = \{s^i\}$, $i = 1, 2, \ldots, L$, where $L = h \times w$. Suppose we have an initial key C^0 and a key sequence $K = \{k^i \in [0, 255]\}$, $i = 1, 2, \ldots, L$; the first-step diffusion can be described as follows:

$$\begin{aligned} D^1 &= s^1 \otimes \mathrm{mod}\left(C^0 + k^1, 256\right), \\ D^i &= s^i \otimes \mathrm{mod}\left(D^{i-1} + k^i, 256\right), \end{aligned} \tag{4}$$

and the second-step diffusion can be formulated as follows:

$$\begin{aligned} D^1 &= D^1 \otimes \mathrm{mod}\left(\left|D^L - k^1\right|, 256\right), \\ D^i &= D^i \otimes \mathrm{mod}\left(\left|D^{i-1} - k^i\right|, 256\right), \end{aligned} \tag{5}$$

and in both (4) and (5), $\otimes$ is XOR operation and D is the result of pixel diffusion.

3.3. Global Permutation and 2D and 3D Permutation. In this approach, several permutations are carried out at different levels, that is, pixel level, bit level, and DNA level. For an image of size $h \times w$, global pixel/bit/DNA permutation means permuting all pixels/bits/DNA with corresponding hyperchaotic subsequences. Since pixel-level data is a 2D plane of size $h \times w$, we can permute the image firstly by row and then by column, which is called 2D permutation. Bit-level and DNA-level data are a 3D cube of size $h \times w \times 8$ and $h \times w \times 4$, respectively, and we can permute the image by row, column, and depth, respectively, which is called 3D permutation in this paper. Specifically, the global permutation can be summarized as follows.

Step 1. Arrange the pixels/bits/acid bases into a 1D vector v with the length of $L = h \times w / h \times w \times 8 / h \times w \times 4$.

Step 2. Extract a subsequence with the length of L from the hyperchaotic sequence K. Sort the subsequence in ascending order to get the index sequence i^x, $x = 1, 2, \ldots, L$.

Step 3. According to i^x, rearrange the vector v to get the new vector v' by

$$v'_x = v_{i^x}, \quad x = 1, 2, \ldots, L. \tag{6}$$

The 3D permutation is to permute planes at different directions in 3D spaces. The operations in each direction are very similar. For simplicity, here we only give the operation in the direction of width as follows.

Step 1. Extract a subsequence of length $L = h$ from the hyperchaotic sequence K. Sort the subsequence in ascending order to get the index sequence i^x, $x = 1, 2, \ldots, L$.

Step 2. According to i^x, rearrange the plane p to get the new vector p' by

$$p'_x = p_{i^x}, \quad x = 1, 2, \ldots, L. \tag{7}$$

It is clear that the 2D permutation is a special case of the 3D permutation. The proposed scheme extracts subsequence with $L = h + w$, $h + w + 8$, and $h + w + 4$ from K for 2D pixel permutation, 3D bit permutation, and 3D DNA permutation, respectively. Note that the proposed global permutation and 3D permutation at bit-level data or DNA-level data can change the positions of bits or DNAs to lead the values of pixels changed, and thus they can simultaneously permute and diffuse the images at bit-level or DNA-level data.

3.4. FOHCLDNA: The Proposed Image Encryption Scheme. With the above-mentioned description, the flowchart of the proposed FOHCLDNA is shown in Figure 2, and the details are as follows.

Step 1. Let $h \times w$ denote the size of the input image P. Concatenate the four sequences generated by (1) to compose one hyperchaotic sequence K using (2).

Step 2 (conduct pixel-level encryption). Extract the first $h+w$ items from K to carry out row and column permutation (2D permutation) on P to obtain P^0. Extract the next $h \times w$ items from K to carry out global pixel permutation on P^0 to obtain P^1. Extract the next $h \times w + 1$ items from K to compose a new

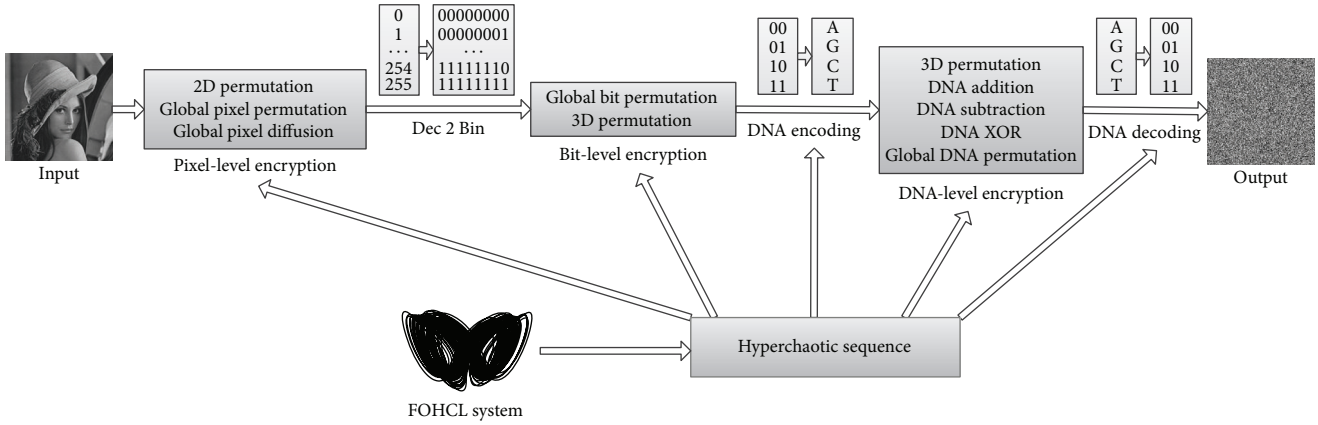

Figure 2: The flowchart of the proposed FOHCLDNA algorithm.

sequence S^0 and then map S^0 to the integer range of $[0, 255]$ by (3) to obtain sequence S^1. Use the first item in S^1 as the initial value and the rest as the key to carry out global pixel diffusion on P^1 to obtain P^2.

Step 3. P^2 is encoded to a bit sequence B^0.

Step 4 (conduct bit-level encryption). Use the next $h \times w \times 8$ items from K to perform global bit permutation on B^0 to obtain B^1. Use the next $h + w + 8$ items from K to perform 3D permutation on B^1 to obtain B^2.

Step 5 (DNA encoding). Map the next $h \times w \times 4$ items in K to the integer range of $[0, 255]$ by (3) to obtain sequence S^2. Encode the ith pair bits in B^2 with the DNA rule decided by (8) to obtain D^0:

$$\text{Rule} = \text{mod}\left(S_i^2, 8\right) + 1, \tag{8}$$

where S_i^2 denotes the ith item in the sequence S^2.

Step 6 (conduct DNA-level encryption). Use the next $h+w+4$ items from K to perform 3D permutation on D^0 to obtain D^1. Map the next $h \times w \times 4$ items in K to the integer range of $[0, 255]$ by (3) to obtain sequence S^3. Create a mask DNA matrix M of size $h \times w \times 4$ using the next $h \times w \times 4$ items in K. For the ith DNA in D^1, conduct DNA operation with ith DNA in M to obtain D^2. The operation type is decided by

$$\text{op} = \text{mod}\left(S_i^3, 3\right) + 1, \tag{9}$$

where op denotes the type of DNA operation. When op equals 1, 2, and 3, the corresponding DNA operation is $+$, $-$, and $\otimes$, respectively. Extract the next $h \times w \times 4$ items from K to carry out global DNA permutation on D^2 to obtain D^3.

Step 7 (DNA decoding). Map the next $h \times w \times 4$ items in K to the integer range of $[0, 255]$ by (3) to obtain sequence S^4. Decode the ith DNA in D^2 with the DNA rule decided by (10) to obtain a binary sequence B^3:

$$\text{Rule} = \text{mod}\left(S_i^4, 8\right) + 1. \tag{10}$$

Note that for a specified acid base, the encoding rule to generate it and the decoding rule to decode it may be different because of the difference between S^2 and S^4.

Step 8. The binary sequence B^3 is converted to the cipher image Q.

The decryption process is the reverse version of the encryption process.

The proposed FOHCLDNA enhances the security of images in several aspects. Firstly, the hyperchaotic sequence with high nonlinearity and complex dynamics generated by the FOHCL is used throughout the process of image encryption. Secondly, the global pixel diffusion can spread little change in one pixel to all the other pixels, leading to a good result of diffusion. Thirdly, permutations are performed on different levels, that is, pixels, bits, and acid bases. Specially, for each two adjacent bits in a pixel and each acid base, a unique DNA rule determined by the hyperchaotic sequence is used to perform DNA encoding and DNA decoding, respectively. The operation type of each acid base is also decided by the sequence when the image is operated with the DNA mask image. All these properties enhance the security of images.

4. Experimental Results

4.1. Experimental Settings. In order to evaluate the performance of the proposed FOHCLDNA, we compare it with some state-of-the-art schemes, such as the hyperchaotic and DNA sequence-based method (HC-DNA) [29], the image encryption using cipher diffusion in crisscross pattern (CDCP) [40], and a class hyperchaos-based scheme (CHC) [41]. The parameters for the compared schemes are set as given by the authors. We set the parameters of the FOHCLDNA as follows. The initial values for the FOHCL system are $x_1^0 = 12$, $x_2^0 = 22$, $x_3^0 = 31$, and $x_4^0 = 4$. And

Table 5: Testing images.

Image	Size ($h \times w$)
Lena	256×256
Cameraman	256×256
Circuit	280×272
Peppers	512×512
Barbara	566×402
Bridge	512×512
Plane	512×512
Aerial	366×364

the preiterating times N_0 are set to 10000. All the fractional orders q_i, $i = (1, 2, 3, 4)$ are set to a fixed value 0.98.

Eight publicly accessed images with different sizes are used to test the proposed FOHCLDNA, as listed in Table 5.

All the experiments were conducted by Matlab 8.6 (Mathworks, Natick, MA, USA) on a 64-bit Windows 7 (Microsoft, Redmond, WA, USA) with 32 GB memory and 3.4 GHz I7 CPU.

4.2. Security Key Analysis. Key space and sensitivity to secret key are two essential points in encryption. A good encryption scheme should have an enough large key space and be extremely sensitive to any small changes in its security key. Both a large key space and extreme sensitivity can resist brute-force attacks.

4.2.1. Key Space. Basically, the security keys of the proposed FOHCLDNA are composed of 4 initial values, that is, $(x_1^0, x_2^0, x_3^0, x_4^0)$. If the precision of each initial value is 10^{-16}, the key space size is $10^{16\times4} = 10^{64} \approx 2^{212}$. From the view of cryptology, the size of the key space larger than 2^{100} is capable of providing a high-level security [1, 42]. Therefore, the key space of the FOHCLDNA is large enough to resist brute-force attacks from current computers. In addition, the fractional orders of the FOHCL can also be used as keys to further enhance the key space.

4.2.2. Sensitivity to Secret Key. The extreme sensitivity of an image encryption algorithm implies that even one bit changed in the keys will lead to a completely different encrypted image. In other words, if the security key changes a little, the decrypted image will be completely different from the input image.

To demonstrate the sensitivity to secret key of the FOHCLDNA, we decrypt the cipher images twice. In the first run, we use the exact encryption keys ($x_1^0 = 12$, $x_2^0 = 22$, $x_3^0 = 31$, $x_4^0 = 4$) to decrypt the cipher images, while, in the second run, we attempt to decrypt the cipher images with slightly different keys ($x_1^0 = 12 + 10^{-15}$, $x_2^0 = 22$, $x_3^0 = 31$, and $x_4^0 = 4$). We conduct the experiments on the images of Lena, Circuit, Peppers, and Plane, and the results are shown in Figure 3. As we can see, the decrypted images with the slightly different keys are completely different from those decrypted with the correct keys, showing that the proposed FOHCLDNA has high sensitivity to secret key.

4.3. Statistical Analysis. A good cryptosystem should have the ability to resist all kinds of statistical attacks. Hence statistical analysis is another widely used and effective way to analyze a cryptosystem. Typical statistical analysis includes histogram analysis, information entropy, and correlation analysis.

4.3.1. Histogram Analysis. For image encryption, histogram is a popular tool to measure the distribution of pixel values in the plain image and the cipher image. The histogram of a plain image is usually unevenly distributed while that of cipher image by a good encryption scheme should be close to a uniform distribution. To put it another way, as far as the effectiveness of encryption schemes, the flatter the histogram of the cipher image is, the better the encryption scheme is.

The histograms of the plain images and their corresponding cipher images are shown in Figure 4. It can be seen from Figure 4 that the histograms of the plain images are irregularly distributed while all those of cipher images are very close to a uniform distribution. The results demonstrate that the proposed FOHCLDNA can resist histogram attacks.

4.3.2. Information Entropy. Information entropy (IE) is used to reflect the complexity of a system. For the 8-bit grayscale images used in the experiments, their intensity has 2^8 kinds of possible values ($[0, 255]$). The IE can be defined as

$$\mathrm{IE} = -\sum_{i=0}^{255} p(i) \log_2 p(i), \tag{11}$$

where $p(i)$ is the probability that the pixel value i appears [29]. When each pixel of cipher image has the same probability, that is, 1/256, IE reaches the ideal value 8.

The IEs of input images and cipher images are shown in Table 6. It can be seen that the IEs of input images are far below 8, while those of cipher images are very close to the ideal value. Among the encryption schemes, the FOHCLDNA achieves 4 out of 8 optimal values while all the IEs by HC-DNA are less than those by any other schemes. It is demonstrated that the FOHCLDNA is secure enough to resist entropy attacks.

4.3.3. Correlation Analysis. Two adjacent pixels in a natural image usually have high correlation. A good image encryption algorithm should be capable of reducing such correlation dramatically. Correlation coefficient γ is a popular metric to measure the correlation that can be formulated as follows [25]:

$$\begin{aligned} E(x) &= \frac{1}{N}\sum_{i=1}^{N} x_i, \\ D(x) &= \frac{1}{N}\sum_{i=1}^{N} \left(x_i - E(x)\right)^2, \\ \mathrm{cov}(x, y) &= \frac{1}{N}\sum_{i=1}^{N} \left(x_i - E(x)\right)\left(y_i - E(y)\right), \\ \gamma &= \frac{\mathrm{cov}(x, y)}{\sqrt{D(x)\, D(y)}}, \end{aligned} \tag{12}$$

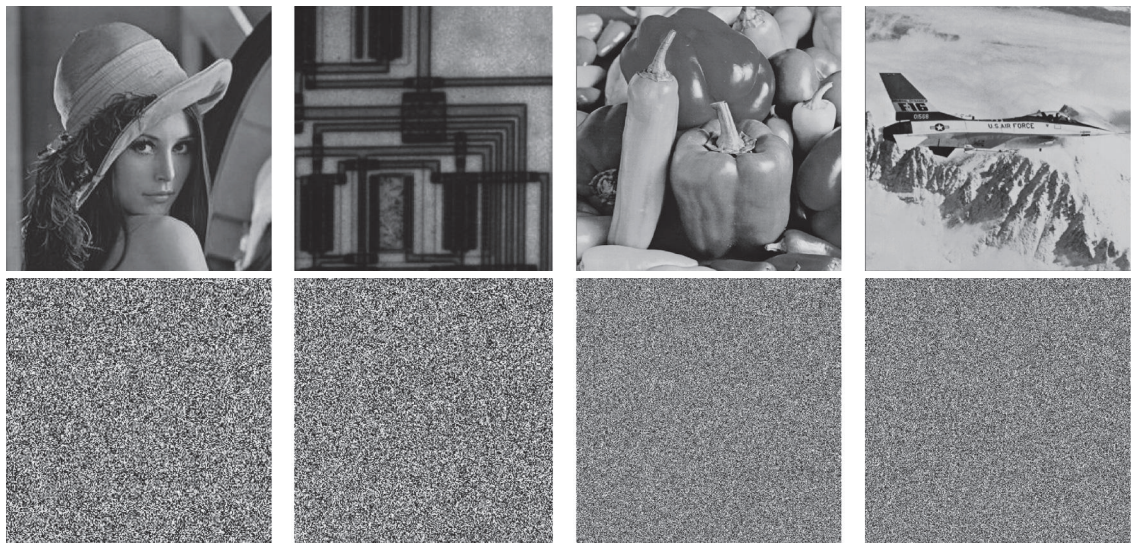

Figure 3: Decrypted images of Lena, Circuit, Peppers, and Plane. The first row is with correct keys: $x_1^0 = 12$, $x_2^0 = 22$, $x_3^0 = 31$, and $x_4^0 = 4$. The second row is with slightly different keys: $x_1^0 = 12 + 10^{-15}$, $x_2^0 = 22$, $x_3^0 = 31$, and $x_4^0 = 4$.

Table 6: The IE of the testing images.

Image	Input images	Cipher images			
		FOHCLDNA	HC-DNA [29]	CDCP [40]	CHC [41]
Lena	7.2283	7.9971	7.9964	7.9968	**7.9974**
Cameraman	7.1048	7.9973	7.9964	**7.9976**	7.9972
Circuit	7.2069	7.9975	7.9946	**7.9976**	7.9974
Peppers	7.5925	**7.9994**	7.9992	7.9993	**7.9994**
Barbara	7.1674	**7.9993**	7.9991	**7.9993**	7.9992
Bridge	5.7056	**7.9993**	7.9990	**7.9993**	**7.9993**
Plane	6.7059	**7.9993**	7.9990	7.9992	7.9992
Aerial	7.7357	7.9986	7.9985	**7.9987**	**7.9987**

where x and y are the gray levels of two neighbouring pixels in an image and N denotes the total number of pixels involved in the image.

To analyze the correlation of the image encryption schemes, we firstly calculate the correlation coefficients for all input images and cipher images in different directions, that is, horizontal γ_h, vertical γ_v, and diagonal γ_d, respectively [29], as listed in Table 7. From this table, it can be found that the correlation coefficients of all the input images are close to 1 in all directions, while those of the cipher images are round 0, showing that the encryption schemes can dramatically reduce the correlation of the adjacent pixels of the images. Specifically, the FOHCLDNA outperforms the rest schemes on 7 out of 24 correlation coefficients, whereas the HC-DNA achieves the optimal value only three times.

To have a further correlation analysis, we randomly select 4000 pairs of adjacent pixels in horizontal direction from each input image and corresponding cipher image by the FOHCLDNA, respectively, to show their adjacent-pixel distribution maps in Figure 5. It can be seen that the values of input images are distributed near the diagonal of coordinate plane, indicating strong correlation of input images. However, the correlation is completely destroyed by the FOHCLDNA so that the values of cipher images are distributed over almost the whole plane, showing very weak correlation in cipher images.

4.4. Analysis of Resisting Differential Attacks. According to the theory of cryptography, a good image encryption algorithm should also be very sensitive to the plain images; that is, a little change (e.g., a bit change) in a plain image can lead to a completely different cipher image. An image encryption scheme that has such a property can effectively resist differential attacks.

The number of pixels change rate (NPCR) and the unified average changing intensity (UACI) are two important metrics for differential attack analysis. NPCR is defined as the variation ratio of two cipher images when the value of a pixel in the input image is slightly changed. UACI indicates the average intensity of the differences between the same cipher images. Mathematically, NPCR and UACI between

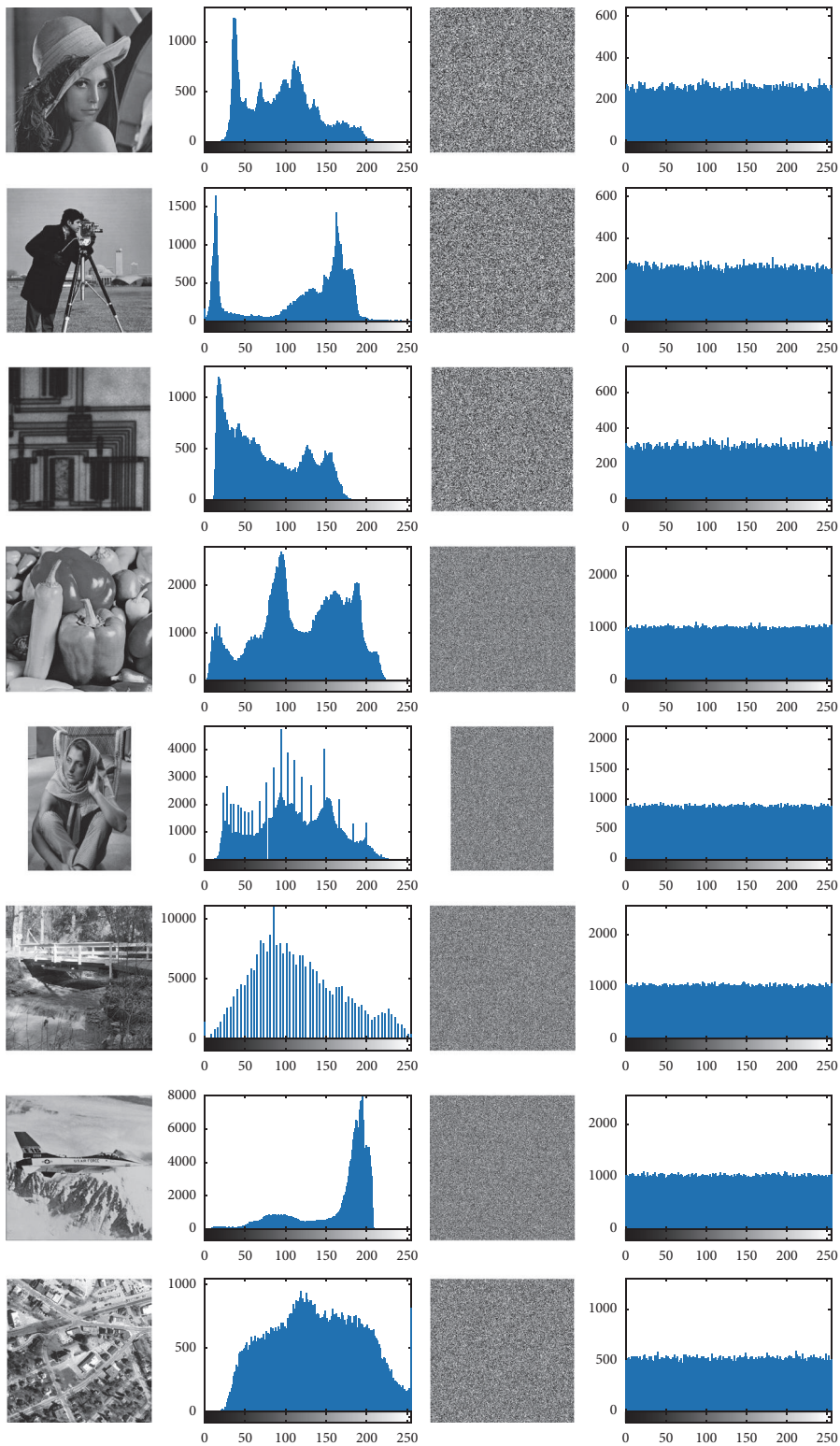

Figure 4: Histograms of the plain images and their corresponding cipher images. The first column is plain images. The second column is the histograms of the plain images. The third column is cipher images. And the fourth column is the histograms of the cipher images.

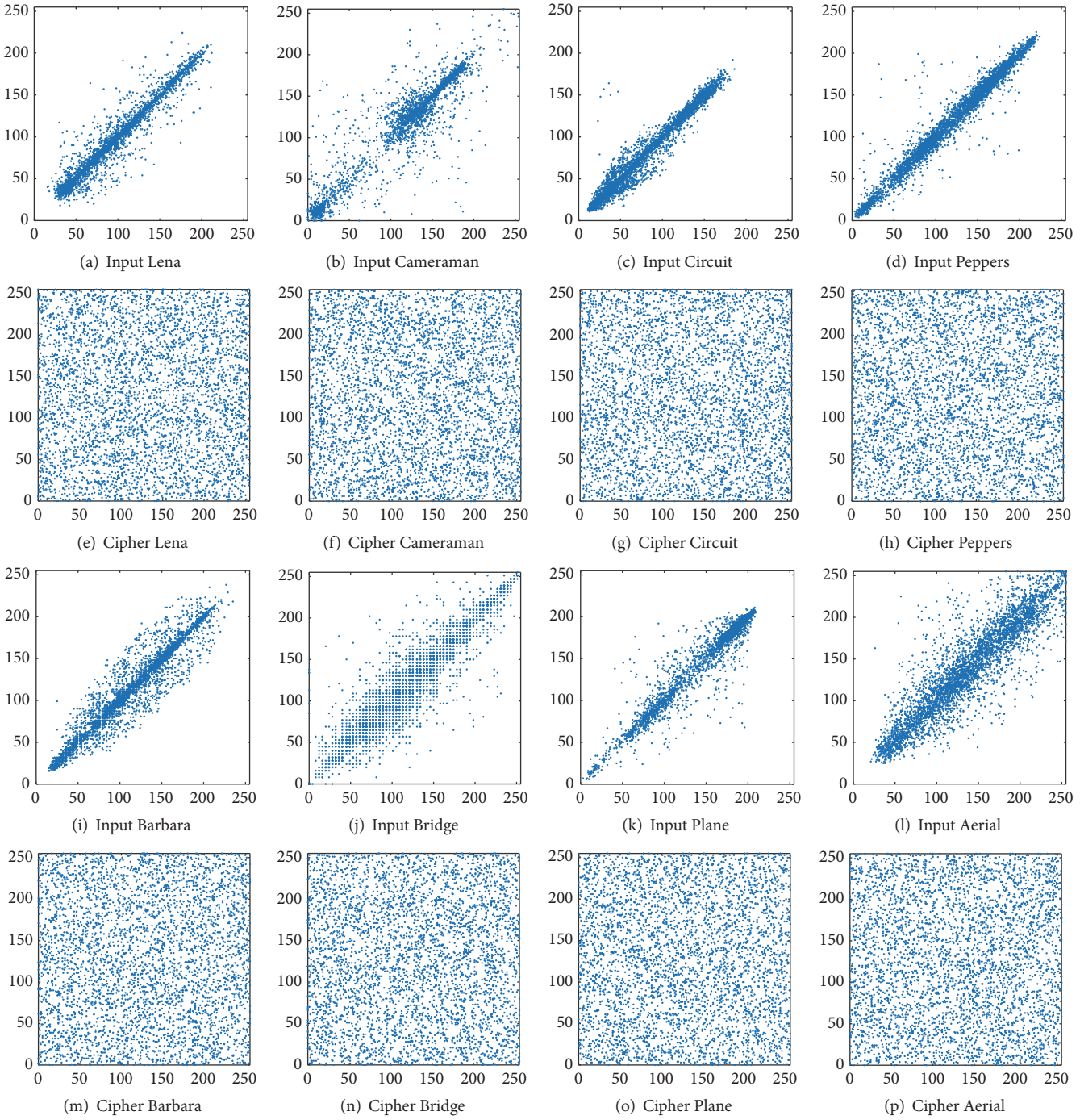

Figure 5: The adjacent-pixel distribution maps of the input images and the corresponding cipher images in horizontal direction.

two cipher images Q^1 and Q^2 can be formulated as (13) and (14), respectively:

$$\text{NPCR} = \frac{1}{hw}\sum_{i=1}^{h}\sum_{j=1}^{w} d_{ij} \times 100\%, \tag{13}$$

$$\text{UACI} = \frac{1}{hw}\sum_{i=1}^{h}\sum_{j=1}^{w} \frac{\left|Q_{ij}^1 - Q_{ij}^2\right|}{255} \times 100\%, \tag{14}$$

where h and w are the height and the width of the image, respectively, and d_{ij} is defined as follows:

$$d_{ij} = \begin{cases} 0, & Q_{ij}^1 = Q_{ij}^2, \\ 1, & Q_{ij}^1 \neq Q_{ij}^2. \end{cases} \tag{15}$$

Generally speaking, the more NPCR gets close to 100% and the bigger UACI is, the more encryption scheme becomes

Table 7: The correlation coefficients γ of the testing images.

Image	γ	Input images	Cipher images			
			FOHCLDNA	HC-DNA [29]	CDCP [40]	CHC [41]
Lena	γ_h	0.9494	0.0054	0.0019	−0.0021	**0.0006**
	γ_v	0.9667	0.0035	−0.0030	−0.0042	**−0.0003**
	γ_d	0.9366	**0.0016**	0.0018	−0.0022	0.0048
Cameraman	γ_h	0.9329	**−0.0010**	0.0076	−0.0022	−0.0069
	γ_v	0.9566	−0.0088	−0.0091	−0.0054	**−0.0044**
	γ_d	0.9117	0.0027	−0.0012	0.0048	**0.0010**
Circuit	γ_h	0.9766	**0.0012**	0.0019	0.0026	−0.0036
	γ_v	0.9775	−0.0071	0.0041	0.0030	**0.0022**
	γ_d	0.9678	**−0.0001**	−0.0012	0.0021	0.0018
Peppers	γ_h	0.9733	**−0.0009**	**0.0009**	−0.0015	−0.0017
	γ_v	0.9763	−0.0021	0.0041	−0.0012	**−0.0003**
	γ_d	0.9650	−0.0013	0.0008	0.0017	**−0.0006**
Barbara	γ_h	0.8271	**0.0010**	0.0011	−0.0038	0.0034
	γ_v	0.9501	−0.0030	0.0006	−0.0028	**0.0003**
	γ_d	0.8310	0.0007	−0.0038	**−0.0004**	0.0009
Bridge	γ_h	0.9388	−0.0029	**0.0007**	0.0036	0.0008
	γ_v	0.9217	−0.0033	0.0036	**0.0014**	0.0035
	γ_d	0.8988	**−0.0002**	0.0023	0.0018	0.0027
Plane	γ_h	0.9599	0.0017	−0.0017	**0.0004**	0.0005
	γ_v	0.9613	0.0021	0.0020	0.0018	**−0.0003**
	γ_d	0.9359	0.0015	**−0.0007**	0.0013	0.0010
Aerial	γ_h	0.9083	0.0015	−0.0010	**−0.0006**	−0.0025
	γ_v	0.8891	−0.0022	0.0034	**0.0010**	−0.0045
	γ_d	0.8502	−0.0015	0.0022	0.0026	**−0.0014**

Table 8: The average NPCR (%) of running the schemes 10 times.

Image	FOHCLDNA	HC-DNA [29]	CDCP [40]	CHC [41]
Lena	99.5723	68.1731	**100.0000**	99.6103
Cameraman	99.5853	44.7412	**100.0000**	99.6089
Circuit	99.5962	44.1423	**99.6663**	99.6026
Peppers	99.5845	58.9414	**99.7145**	99.6061
Barbara	99.5857	58.6456	**100.0000**	99.6035
Bridge	99.5798	49.3543	**99.7100**	99.6089
Plane	99.5846	65.2526	99.5881	**99.6067**
Aerial	99.5802	53.0030	**100.0000**	99.6093

effective in resisting differential attacks. For a 256-level gray image, the maximum theoretical values for NPCR and UACI are 99.6094% and 33.4635%, respectively [29].

We randomly change one bit in the plain images to compute one value of NPCR and UACI. We repeat the process 10 times and report the average values of NPCR and UACI in Tables 8 and 9, respectively.

It can be shown that although the values by the FOHCLDNA are not as good as those by CDCP and CHC, they are very close to the maximum theoretical values. The FOHCLDNA apparently outperforms HC-DNA in terms of NPCR and UACI. The results show that the global pixel diffusion is effective and the FOHCLDNA has the capability of resisting differential attacks.

5. Conclusions

In this paper, we propose a novel image encryption algorithm based on a fractional-order hyperchaotic Lorenz system and DNA computing (FOHCLDNA). The fractional-order hyperchaotic Lorenz system is adopted to generate the pseudorandom sequence that is utilized throughout the process of encryption. Besides pixel-level and bit-level operations, DNA operations such as DNA addition, DNA subtraction, and DNA XOR are also introduced to the algorithm. A simple pixel diffusion is used to spread the slight change in one pixel to all other pixels. Several types of permutation are carried out on different level data. Through the results of extensive experiments and corresponding security analysis,

Table 9: The average UACI (%) of running the schemes 10 times.

Image	FOHCLDNA	HC-DNA [29]	CDCP [40]	CHC [41]
Lena	33.3159	31.7168	**33.5530**	33.4333
Cameraman	33.3727	17.3423	33.4064	**33.4724**
Circuit	33.1996	15.2453	33.4253	**33.5338**
Peppers	33.2703	23.4302	33.4135	**33.4672**
Barbara	33.3261	24.0960	**33.4946**	33.4446
Bridge	33.3062	18.0547	**33.4779**	33.4620
Plane	33.3532	24.9252	**33.4753**	33.4446
Aerial	33.3311	20.3190	**33.4911**	33.4392

it can be found that the FOHCLDNA is highly sensitive to the secret key, has a larger secret key space, and can resist some known attacks, such as brute-force attacks, statistical attacks, and differential attacks. All these properties indicate that the FOHCLDNA is promising for image encryption. In the future, the FOHCLDNA could be extended to color image encryption.

Conflicts of Interest

The authors declare that there are no conflicts of interest regarding the publication of this paper.

Acknowledgments

This work was supported in part by the Major Research Plan of the National Natural Science Foundation of China (Grant no. 91218301), the Fundamental Research Funds for the Central Universities (Grants no. JBK170944, no. JBK170505, and no. JBK130503), the Natural Science Foundation of China (Grant no. 71473201), and the Scientific Research Fund of Sichuan Provincial Education Department (Grant no. 17ZB0433).

References

[1] B. Schneier, *Applied Cryptography: Protocols, Algorithms, and Source Code in C*, John Wiley and Sons, Indianapolis, IN, USA, 2015.

[2] A. A. A. El-Latif, L. Li, and X. Niu, "A new image encryption scheme based on cyclic elliptic curve and chaotic system," *Multimedia Tools and Applications*, vol. 70, no. 3, pp. 1559–1584, 2014.

[3] X. Wu, H. Kan, and J. Kurths, "A new color image encryption scheme based on DNA sequences and multiple improved 1D chaotic maps," *Applied Soft Computing*, vol. 37, pp. 24–39, 2015.

[4] X. Zhang, X. Fan, J. Wang, and Z. Zhao, "A chaos-based image encryption scheme using 2D rectangular transform and dependent substitution," *Multimedia Tools and Applications*, vol. 75, no. 4, pp. 1745–1763, 2016.

[5] G. Chen, Y. Mao, and C. K. Chui, "A symmetric image encryption scheme based on 3D chaotic cat maps," *Chaos, Solitons & Fractals*, vol. 21, no. 3, pp. 749–761, 2004.

[6] Z. Zhu, W. Zhang, K. Wong, and H. Yu, "A chaos-based symmetric image encryption scheme using a bit-level permutation," *Information Sciences*, vol. 181, no. 6, pp. 1171–1186, 2011.

[7] N. Zhou, S. Pan, S. Cheng, and Z. Zhou, "Image compression-encryption scheme based on hyper-chaotic system and 2D compressive sensing," *Optics & Laser Technology*, vol. 82, pp. 121–133, 2016.

[8] L. Xu, Z. Li, J. Li, and W. Hua, "A novel bit-level image encryption algorithm based on chaotic maps," *Optics and Lasers in Engineering*, vol. 78, pp. 17–25, 2016.

[9] L. Xu, X. Gou, Z. Li, and J. Li, "A novel chaotic image encryption algorithm using block scrambling and dynamic index based diffusion," *Optics and Lasers in Engineering*, vol. 91, pp. 41–52, 2017.

[10] Y. Wu, G. Yang, H. Jin, and J. P. Noonan, "Image encryption using the two-dimensional logistic chaotic map," *Journal of Electronic Imaging*, vol. 21, no. 1, Article ID 013014, 2012.

[11] N. K. Pareek, V. Patidar, and K. K. Sud, "Image encryption using chaotic logistic map," *Image and Vision Computing*, vol. 24, no. 9, pp. 926–934, 2006.

[12] R. Boriga, A. C. Dascalescu, and A.-V. Diaconu, "A new one-dimensional chaotic map and its use in a novel real-time image encryption scheme," *Advances in Multimedia*, vol. 2014, Article ID 409586, 15 pages, 2014.

[13] D. Arroyo, R. Rhouma, G. Alvarez, S. Li, and V. Fernandez, "On the security of a new image encryption scheme based on chaotic map lattices," *Chaos: An Interdisciplinary Journal of Nonlinear Science*, vol. 18, no. 3, Article ID 033112, 2008.

[14] J. Fridrich, "Symmetric ciphers based on two-dimensional chaotic maps," *International Journal of Bifurcation and Chaos*, vol. 8, no. 6, pp. 1259–1284, 1998.

[15] Z. Hua, Y. Zhou, C.-M. Pun, and C. L. P. Chen, "2D Sine Logistic modulation map for image encryption," *Information Sciences*, vol. 297, pp. 80–94, 2015.

[16] G. Chen and X. Dong, *From Chaos to Order: Methodologies, Perspectives, and Applications*, Series on Nonlinear Science, World Scientific, 1998.

[17] T. Ueta and G. Chen, "Bifurcation analysis of Chen's equation," *International Journal of Bifurcation and Chaos*, vol. 10, no. 8, pp. 1917–1931, 2000.

[18] A. Wolf, J. B. Swift, and H. L. A. Swinney, "Determining Lyapunov exponents from a time series," *Physica D: Nonlinear Phenomena*, vol. 16, no. 3, pp. 285–317, 1985.

[19] C. Zhu, "A novel image encryption scheme based on improved hyperchaotic sequences," *Optics Communications*, vol. 285, no. 1, pp. 29–37, 2012.

[20] B. Norouzi, S. Mirzakuchaki, S. M. Seyedzadeh, and M. R. Mosavi, "A simple, sensitive and secure image encryption algorithm based on hyper-chaotic system with only one round diffusion process," *Multimedia Tools and Applications*, vol. 71, no. 3, pp. 1469–1497, 2014.

[21] X. Wang and H. Zhang, "A novel image encryption algorithm based on genetic recombination and hyper-chaotic systems," *Nonlinear Dynamics*, vol. 1, pp. 333–346, 2016.

[22] N. Zhou, Y. Hu, L. Gong, and G. Li, "Quantum image encryption scheme with iterative generalized Arnold transforms and quantum image cycle shift operations," *Quantum Information Processing*, vol. 16, no. 6, 2017.

[23] H.-M. Yuan, Y. Liu, T. Lin, T. Hu, and L.-H. Gong, "A new parallel image cryptosystem based on 5D hyper-chaotic system," *Signal Processing: Image Communication*, vol. 52, pp. 87–96, 2017.

[24] I. Podlubny, I. Petráš, B. M. Vinagre, and L. Dorcák, "Analogue realizations of fractional-order controllers," *Nonlinear Dynamics*, vol. 29, no. 1–4, pp. 281–296, 2002.

[25] Z. Wang, X. Huang, Y.-X. Li, and X.-N. Song, "A new image encryption algorithm based on the fractional-order hyperchaotic Lorenz system," *Chinese Physics B*, vol. 22, no. 1, Article ID 010504, 2013.

[26] J. Zhao, S. Wang, Y. Chang, and X. Li, "A novel image encryption scheme based on an improper fractional-order chaotic system," *Nonlinear Dynamics*, vol. 80, no. 4, pp. 1721–1729, 2015.

[27] X. Huang, T. Sun, Y. Li, and J. Liang, "A color image encryption algorithm based on a fractional-order hyperchaotic system," *Entropy*, vol. 17, no. 1, pp. 28–38, 2014.

[28] L. M. Adleman, "Molecular computation of solutions to combinatorial problems," *Science*, vol. 266, no. 5187, pp. 1021–1024, 1994.

[29] K. Zhan, D. Wei, J. Shi, and J. Yu, "Cross-utilizing hyperchaotic and DNA sequences for image encryption," *Journal of Electronic Imaging*, vol. 26, no. 1, Article ID 013021, 2017.

[30] Q. Zhang, L. Liu, and X. Wei, "Improved algorithm for image encryption based on DNA encoding and multi-chaotic maps," *AEU-International Journal of Electronics and Communications*, vol. 68, no. 3, pp. 186–192, 2014.

[31] P. Zhen, G. Zhao, L. Min, and X. Jin, "Chaos-based image encryption scheme combining DNA coding and entropy," *Multimedia Tools and Applications*, vol. 75, no. 11, pp. 6303–6319, 2016.

[32] R. Guesmi, M. A. B. Farah, A. Kachouri, and M. Samet, "A novel chaos-based image encryption using DNA sequence operation and Secure hash algorithm SHA-2," *Nonlinear Dynamics*, vol. 83, no. 3, pp. 1123–1136, 2016.

[33] Q. Zhang, L. Guo, and X. Wei, "Image encryption using DNA addition combining with chaotic maps," *Mathematical and Computer Modelling*, vol. 52, no. 11-12, pp. 2028–2035, 2010.

[34] L. Liu, Q. Zhang, and X. Wei, "A RGB image encryption algorithm based on DNA encoding and chaos map," *Computers & Electrical Engineering*, vol. 38, no. 5, pp. 1240–1248, 2012.

[35] X. Wang and J. Song, "Synchronization of the fractional order hyperchaos lorenz systems with activation feedback control," *Communications in Nonlinear Science and Numerical Simulation*, vol. 14, no. 8, pp. 3351–3357, 2009.

[36] S. Wang and R. Wu, "Dynamic analysis of a 5D fractional-order hyperchaotic system," *International Journal of Control, Automation, and Systems*, vol. 15, no. 3, pp. 1–8, 2017.

[37] J. He, S. Yu, and J. Cai, "A method for image encryption based on fractional-order hyperchaotic systems," *Journal of Applied Analysis and Computation*, vol. 5, no. 2, pp. 197–209, 2015.

[38] X. Wu, "A color image encryption algorithm using the fractional-order hyperchaotic systems," in *Proceedings of the 5th International Workshop on Chaos-Fractals Theories and Applications, IWCFTA ('12)*, pp. 196–201, China, October 2012.

[39] X. Wang and C. Liu, "A novel and effective image encryption algorithm based on chaos and DNA encoding," *Multimedia Tools and Applications*, vol. 76, no. 5, pp. 6229–6245, 2017.

[40] C. Zhu, Y. Hu, and K. Sun, "New image encryption algorithm based on hyperchaotic system and ciphertext diffusion in criss-cross pattern," *Journal of Electronics & Information Technology*, vol. 34, no. 7, pp. 1735–1743, 2012.

[41] C.-X. Zhu and K.-H. Sun, "Cryptanalysis and improvement of a class of hyperchaos based image encryption algorithms," *Acta Physica Sinica*, vol. 61, no. 12, p. 120503, 2012.

[42] D. R. Stinson, *Cryptography: Theory and Practice*, CRC Press, 2005.

Hindawi
Complexity
Volume 2017, Article ID 4962739, 23 pages
https://doi.org/10.1155/2017/4962739

Research Article

Dynamical Analysis, Synchronization, Circuit Design, and Secure Communication of a Novel Hyperchaotic System

Li Xiong,[1,2] Zhenlai Liu,[1] and Xinguo Zhang[3]

[1]*School of Physics and Electromechanical Engineering, Hexi University, Zhangye 734000, China*
[2]*State Key Laboratory of ASIC & System, Fudan University, Shanghai 200433, China*
[3]*School of Information Science and Engineering, Lanzhou University, Lanzhou 730000, China*

Correspondence should be addressed to Li Xiong; xl-427814@163.com

Received 19 May 2017; Revised 22 August 2017; Accepted 26 September 2017; Published 15 November 2017

Academic Editor: Amr Elsonbaty

This paper is devoted to introduce a novel fourth-order hyperchaotic system. The hyperchaotic system is constructed by adding a linear feedback control level based on a modified Lorenz-like chaotic circuit with reduced number of amplifiers. The local dynamical entities, such as the basic dynamical behavior, the divergence, the eigenvalue, and the Lyapunov exponents of the new hyperchaotic system, are all investigated analytically and numerically. Then, an active control method is derived to achieve global chaotic synchronization of the novel hyperchaotic system through making the synchronization error system asymptotically stable at the origin based on Lyapunov stability theory. Next, the proposed novel hyperchaotic system is applied to construct another new hyperchaotic system with circuit deformation and design a new hyperchaotic secure communication circuit. Furthermore, the implementation of two novel electronic circuits of the proposed hyperchaotic systems is presented, examined, and realized using physical components. A good qualitative agreement is shown between the simulations and the experimental results around 500 kHz and below 1 MHz.

1. Introduction

The Lorenz chaotic system was proposed [1] and later the chaotic synchronization was implemented in the electronic circuit [2], which greatly inspired many scientists and accelerated the pace of chaos research [3–7]. A hyperchaotic system is defined as an attractor with at least two positive Lyapunov exponents and an autonomous system with phase space of dimension at least four [8]. The sum of Lyapunov exponents must be negative to ensure that the system is dissipative [9]. The hyperchaotic systems have more complex structure, higher unpredictability, and more randomness than ordinary chaotic systems. Thus, the hyperchaotic attractors are more suitable for many important fields in applied nonlinear sciences such as secure communications, neural network, image encryption, laser physics, and nonlinear circuits [10–19].

With the deep development of chaotic systems, synchronization of hyperchaotic systems is an important nonlinear phenomenon. In recent years, Mahmoud et al. introduced some chaotic and hyperchaotic systems with complex variables, analyzed their chaotic behavior, and proposed several types of synchronization methods [20–25]. Usually, increasingly novel chaotic systems are generated from low-order chaotic systems to hyperchaotic systems [26–28] and from two-wing systems to four-wing or multiloop systems [29–32]. A significant application of chaotic systems is to form chaotic secure communication circuit [33]. From the perspective of improving the security of secure communication system, the novel hyperchaotic system should be selected. Accordingly, most hyperchaotic systems are generated and verified by numerical simulations; there is a certain degree of deviation from the physical circuit system [34]. Therefore, hardware circuit simulation and physical verification are also important for hyperchaotic system generation.

The contribution of this paper is that we introduce a novel fourth-order hyperchaotic system on the basis of a modified Lorenz-like chaotic circuit with reduced number of

amplifiers. Then we perform a detailed qualitative analysis, active control, synchronous stability analysis, and applications of the novel hyperchaotic system. The active control and synchronization results derived in this paper are established by using Lyapunov stability theory. The corresponding physical circuit design for the novel hyperchaotic system is also proposed to show the accuracy and efficiency of circuit realization. The analog circuit implementation results match the Multisim and Matlab simulation results. These proposed circuit design methods can also be applied in other complex hyperchaotic systems.

This paper is organized as follows. In Section 2, a modified Lorenz-like chaotic circuit is constructed with reduced number of amplifiers. Based on the modified Lorenz-like chaotic circuit, several qualitative issues about a novel hyperchaotic system, such as the basic dynamical behavior, divergence, equilibria, Lyapunov exponents, and synchronous stability, are investigated analytically and numerically in Section 3. In Section 4, another z-u-y hyperchaotic system and a new hyperchaotic secure communication circuit are proposed based on the novel $(y + z)$-u-x hyperchaotic circuit. In Section 5, the proposed hyperchaotic circuits are, respectively, implemented in analog electronic circuits. Finally, some conclusions and discussions are drawn in Section 6.

2. Circuit Design of a Modified Lorenz-Like Chaotic System

A modified Lorenz-like chaotic system is proposed by the following autonomous nonlinear system of differential equations:

$$\begin{aligned} \dot{x} &= a(y - x) \\ \dot{y} &= bx - y + cxz \\ \dot{z} &= -dxy - ez, \end{aligned} \tag{1}$$

where x, y, and z are the state variables and a, b, c, d, and e are constant, positive parameters of the system. When choosing $a = 10$, $b = 45$, $c = 20$, $d = 5$, and $e = 3.7$, there exists a typical chaotic attractor in system (1).

$$\begin{aligned} \dot{x} &= -10x + 10y \\ \dot{y} &= 45x - y + 20xz \\ \dot{z} &= -5xy - 3.7z. \end{aligned} \tag{2}$$

The two- and three-dimensional chaotic attractors with Matlab simulation of the modified Lorenz-like chaotic system (2) are shown in Figure 1. It can be seen from the numerical simulation results that the numerical range of each variable parameter is within −10 V to +10 V, and it fully meets the requirements of circuit design in practical applications. That is because the working voltage range of electronic components is generally from −15 V to +15 V in practical electronic circuits. Therefore, it must be the equation of scaling if the circuit is to be implemented.

Based on the modified Lorenz-like chaotic system (2), the normalized resistor is set as $R = 100\text{k}\,\Omega$ in order to design the Lorenz-like chaotic circuit. Thus, the state equation of the Lorenz-like chaotic circuit is obtained as follows:

$$\begin{aligned} \dot{x} &= -\frac{100\text{k}}{10\text{k}}x + \frac{100\text{k}}{10\text{k}}y \\ \dot{y} &= \frac{100\text{k}}{2.2\text{k}}x - \frac{100\text{k}}{100\text{k}}y + \frac{100\text{k}}{0.51\text{k}} \times 0.1xz \\ \dot{z} &= -\frac{100\text{k}}{2\text{k}} \times 0.1xy - \frac{100\text{k}}{27\text{k}}z. \end{aligned} \tag{3}$$

Therefore, the Lorenz-like chaotic circuit schematic is designed as shown in Figure 2. It can be seen from Figure 2 that the circuit is composed of five operational amplifiers and two analog multipliers. It can output three waveforms and three phase portraits, and it can output stable third-order double vortex chaotic signal. Being different from the general Lorenz-like circuit, it can output inverted phase portrait shape like butterfly wings. However, lacking of improvement on the Lorenz-like chaotic circuit precluded comprehensive statements. Although it can implement the function of (2), it is not the most optimal circuit. In order to obtain the most optimal circuit, the Lorenz-like chaotic circuit shown in Figure 2 needs to be improved. The basic idea of improved design is to simplify, minimize, and merge the circuit by using the main knowledge of circuit theory under the condition of not changing the circuit function. Thus, an improved Lorenz-like chaotic circuit consisting of four operational amplifiers and two analog multipliers is designed based on Figure 2.

The final improved design result of the Lorenz-like circuit is shown in Figure 3. It consists of 4 operational amplifiers, 2 analog multipliers, 9 resistors, and 3 capacitors. As can be seen from Figure 3, the number of operational amplifiers is reduced from 5 to 4, and other passive components are correspondingly reduced. Through improvement, the complexity of the circuit, the thermal noise of the total resistance, and the total error of the circuit can also be reduced. Meanwhile, the cost can be reduced. Thus, the improved Lorenz-like chaotic circuit is simple, easy to debug, and suitable for mass production. From this, the various curves of chaos evolution of the improved Lorenz-like chaotic circuit can be observed.

The beneficial effects of the improved Lorenz-like circuit are as follows: (i) It can output three chaotic waveform signals of x, y, and z and three chaotic phase portraits of xy, xz, and zy. (ii) A variety of chaotic signals can be displayed on the oscilloscope. (iii) It can output inverted phase portrait shape like butterfly wings and other kinds of experiments can also be carried out by the improved circuit. Using these values, some simulations are implemented. All of the electronic components are easily available. The chaotic phase portraits of the improved Lorenz-like chaotic circuit by Multisim are shown in Figure 4. It can be seen from the Multisim simulation results that it is consistent with the Matlab simulation results shown in Figure 1. That is, it fully conforms to the requirements of the circuit design in practical applications.

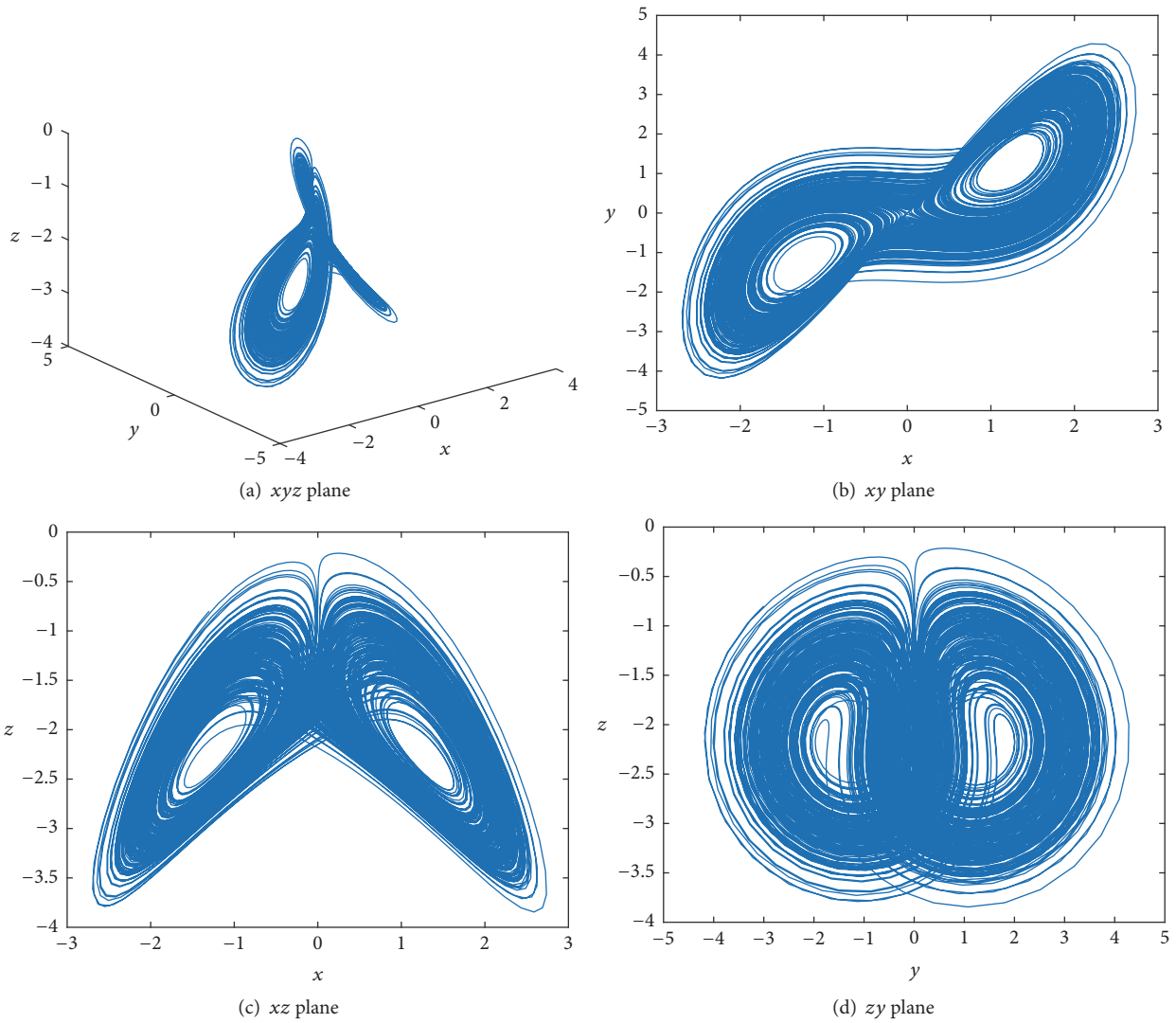

(a) xyz plane (b) xy plane

(c) xz plane (d) zy plane

Figure 1: The chaotic attractors of the modified Lorenz-like chaotic system.

3. Dynamical Analysis of the Novel Hyperchaotic System Based on the Improved Lorenz-Like Chaotic Circuit

It can be seen from the analysis and simulations above that the improved Lorenz-like chaotic circuit can only output three chaotic waveforms and three chaotic phase portraits. What is more, it can only output inverted phase portrait shape like butterfly wings. However, in order to meet certain conditions of displaying four chaotic waveforms, six chaotic phase portraits, and upright phase portrait shape like butterfly wings, the improved Lorenz-like chaotic circuit as shown in Figure 3 needs to be deformed from low-order chaotic system to hyperchaotic system.

3.1. Divergence and Equilibria of the Novel Hyperchaotic System. On the basis of the improved Lorenz-like chaotic circuit shown in Figure 3, the input is introduced by $(y + z)$ end, and feedback is given to the x input stage after the u stage. Thus, a novel fourth-order hyperchaotic circuit is constructed and the proposed hyperchaotic circuit schematic is shown in Figure 5. It is composed of 5 operational amplifiers, 2 analog multipliers, 12 resistors, and 4 capacitors. In order to facilitate the narrative, we call this novel circuit $(y + z)$-u-x hyperchaotic circuit.

The beneficial effects of the novel $(y + z)$-u-x fourth-order hyperchaotic circuit are as follows: it not only can output four chaotic waveforms and six phase portraits, but also can output stable fourth-order double vortex chaotic signals. Also, operational amplifier TL082 or TL084 and analog multiplier AD633 are used. According to the new $(y+z)$-u-x hyperchaotic circuit, the normalized resistor is set as $R = 100\text{k}\,\Omega$. Thus, the state equation of the corresponding hyperchaotic circuit is obtained as follows:

$$\dot{x} = -\frac{100\text{k}}{100\text{k}}x - \frac{100\text{k}}{100\text{k}}y - \frac{100\text{k}}{100\text{k}} \times 0.1u$$

$$\dot{y} = -\frac{100\text{k}}{22\text{k}}x + \frac{100\text{k}}{510\,\Omega} \times 0.01xz$$

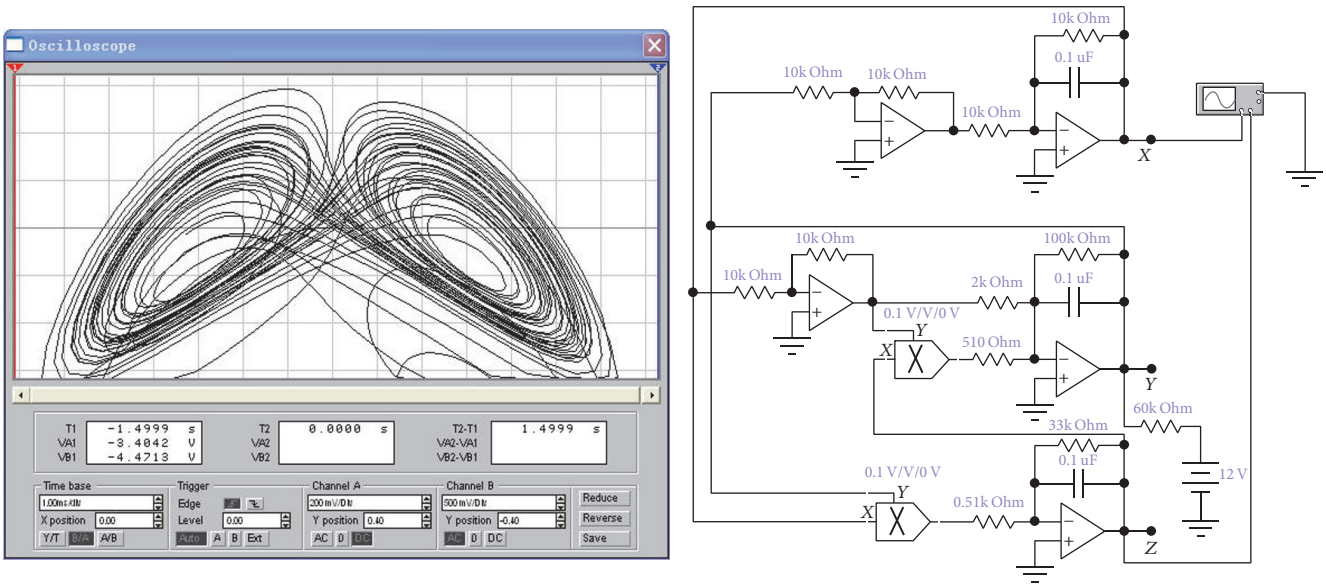

Figure 2: Lorenz-like chaotic circuit of system (2) using 5 amplifiers.

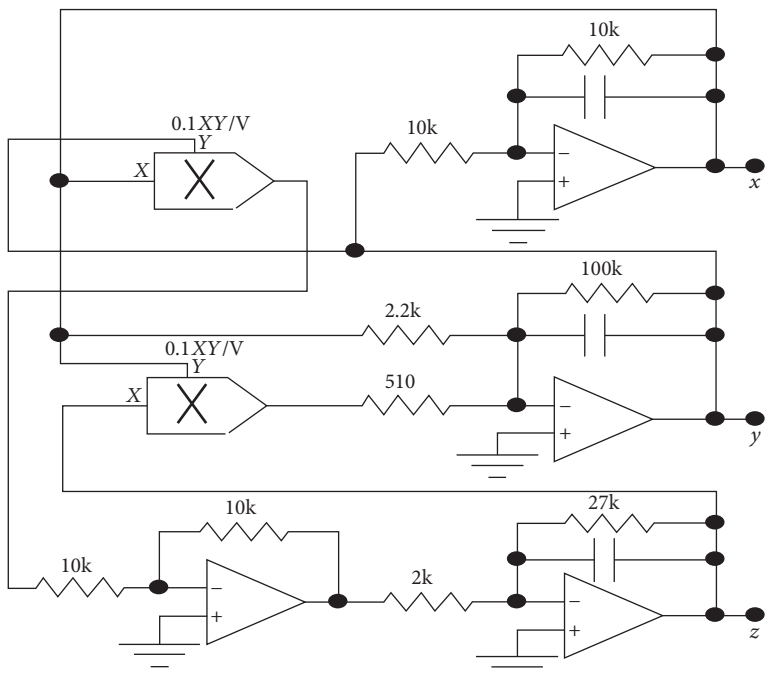

Figure 3: Lorenz-like chaotic circuit of system (2) with reduced number of amplifiers.

$$\dot{z} = -\frac{100\text{k}}{270\text{k}}z - \frac{100\text{k}}{2\text{k}} \times 0.01xy$$

$$\dot{u} = -\frac{100\text{k}}{100\text{k}}y - \frac{100\text{k}}{100\text{k}}z - \frac{100\text{k}}{20\text{k}} \times 0.1u. \quad (4)$$

Then, a novel fourth-order hyperchaotic system is obtained by (4):

$$\dot{x} = -x - y - au$$

$$\dot{y} = -bx + cxz$$

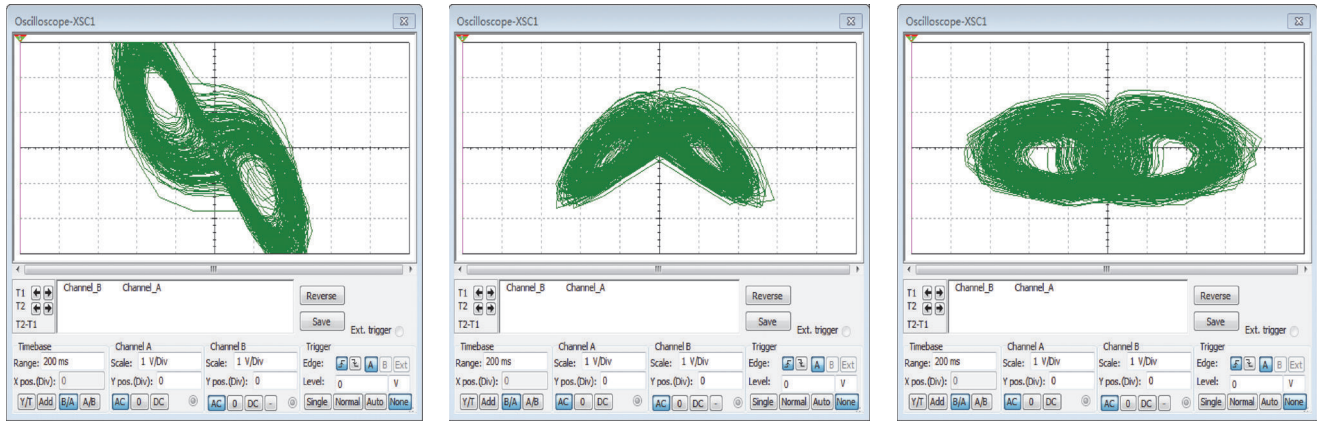

(a) xy phase portrait (b) xz phase portrait (c) zy phase portrait

Figure 4: Chaotic phase portraits of the Lorenz-like chaotic circuit with reduced number of amplifiers.

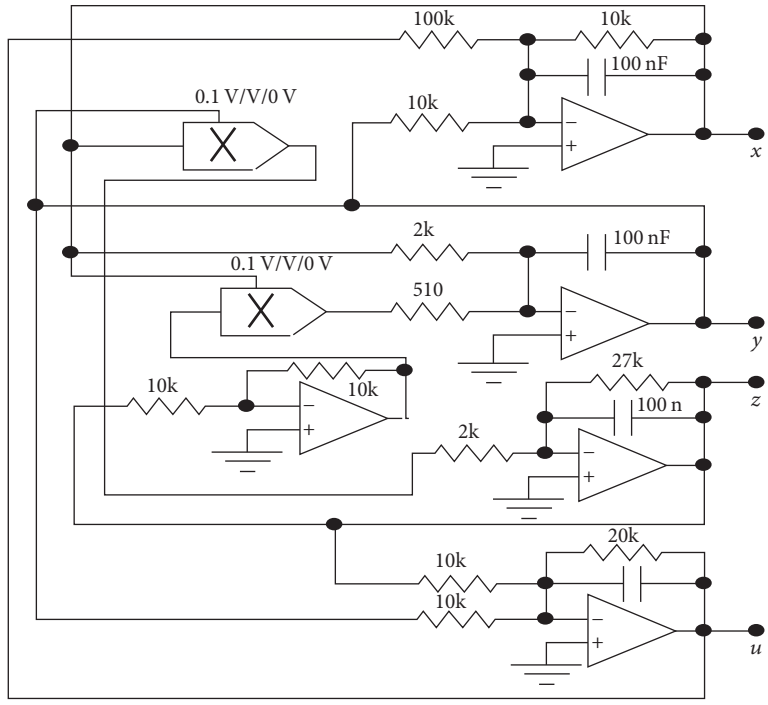

Figure 5: $(y + z)$-u-x hyperchaotic circuit schematic.

$$pt]\dot{z} = -dz - exy$$

$$\dot{u} = -y - z - eu, \tag{5}$$

where x, y, z, and u are the state variables and a, b, c, d, and e are constant, positive parameters of the system. When choosing $a = 0.1$, $b = 4.55$, $c = 1.96$, $d = 0.37$, and $e = 0.5$, the novel system (5) is chaotic. Substituting the specific parameter values, (5) becomes

$$\dot{x} = -x - y - 0.1u$$

$$\dot{y} = -4.55x + 1.96xz$$

$$\dot{z} = -0.37z - 0.5xy$$

$$\dot{u} = -y - z - 0.5u. \tag{6}$$

This is the novel fourth-order hyperchaotic system. The divergence of the hyperchaotic system (5) is easily calculated as

$$\nabla = \frac{\partial \dot{x}}{\partial x} + \frac{\partial \dot{y}}{\partial y} + \frac{\partial \dot{z}}{\partial z} + \frac{\partial \dot{u}}{\partial u} = -1 - d - e = -1.87 < 0. \tag{7}$$

The divergence is less than 0. A necessary and sufficient condition for system (5) to be dissipative is that the divergence of the vector field is negative when the time tends to be

infinite, and the corresponding dynamic characteristics will be presented.

Consider $\dot{x} = \dot{y} = \dot{z} = \dot{u} = 0$; then the equilibrium equation of system (5) is easily obtained as follows:

$$\begin{aligned} \dot{x} &= -x - y - au = 0 \\ \dot{y} &= -bx + cxz = 0 \\ \dot{z} &= -dz - exy = 0 \\ \dot{u} &= -y - z - eu = 0. \end{aligned} \tag{8}$$

Clearly, the solution of (8) is the origin; that is, the equilibrium point of system (5) is obtained as

$$\begin{aligned} x &= 0, \\ y &= 0, \\ z &= 0, \\ u &= 0. \end{aligned} \tag{9}$$

The Jacobian matrix for system (5) at equilibrium point (9) is obtained as

$$J = \begin{bmatrix} -1 & -1 & 0 & -a \\ -b + cz & 0 & cx & 0 \\ -ey & -ex & -d & 0 \\ 0 & -1 & -1 & -e \end{bmatrix}, \tag{10}$$

where $a = 0.1$, $b = 4.55$, $c = 1.96$, $d = 0.37$, and $e = 0.5$. Then, the Jacobian matrix for system (5) at equilibrium point is easily obtained as

$$J = \begin{bmatrix} -1 & -1 & 0 & -0.1 \\ -4.55 + 1.96z & 0 & 1.96x & 0 \\ -0.5y & -0.5x & -0.37 & 0 \\ 0 & -1 & -1 & -0.5 \end{bmatrix}. \tag{11}$$

The characteristic polynomial of the Jacobian matrix (11) is described as follows:

$$\det(\lambda I - J) = 0. \tag{12}$$

Therefore, the solutions of (12) are obtained as $\lambda_1 = -2.7368$, $\lambda_2 = 1.6419$, $\lambda_3 = -0.4050$, and $\lambda_4 = 0.3700$. Because there are two positive values in the four eigenvalues above, the equilibrium point $\{x = y = z = u = 0\}$ is an unstable equilibrium point. It shows that the novel fourth-order hyperchaotic system is unstable in two directions and stable in the other two directions.

3.2. Chaotic Attractors and Lyapunov Exponents. All of the electronic components are easily available. The hyperchaotic phase portraits of the new hyperchaotic circuit by Multisim are shown in Figure 6. And the hyperchaotic phase portraits by Matlab are shown in Figure 7. It can be seen from the simulation results that it can output six chaotic phase portraits of xy, xz, zy, xu, yu, and zu. More importantly, being different from the modified Lorenz-like circuit, it can output upright phase portrait shape like butterfly wings. Moreover, it can be seen from the numerical simulation results that the numerical range of each variable parameter is within −10 V to +10 V, and it is consistent with the Multisim and Matlab simulation results shown in Figures 6 and 7. That is, it fully conforms to the requirements of circuit design in practical applications. A variety of hyperchaotic signals can be displayed on the oscilloscope.

In order to further verify the chaotic dynamical behavior of the novel hyperchaotic system (5), the Lyapunov exponents of the novel hyperchaotic system are determined numerically. With the parameters chosen as $a = 0.1, b = 4.55, c = 1.96, d = 0.37$, and $e = 0.5$, the corresponding Lyapunov exponents are obtained as follows: $L_1 = 0.0717$, $L_2 = 0.0209$, $L_3 = -0.4187$, and $L_4 = -1.5439$. Thus, the Lyapunov dimension [8, 21] of the new hyperchaotic system (5) is also calculated as

$$D_L = M + \frac{1}{|L_{M+1}|} \sum_{i=1}^{M} L_i. \tag{13}$$

such that M is the largest integer, for which

$$\begin{aligned} \sum_{i=1}^{M} L_i &> 0, \\ \sum_{i=1}^{M+1} L_i &< 0. \end{aligned} \tag{14}$$

This means that system (5) is a hyperchaotic system since L_1 and L_2 are positive values and a dissipative system since the sum of the Lyapunov exponents is negative. It meets the condition of at least two positive Lyapunov exponents for the hyperchaotic systems. The Lyapunov dimension of this hyperchaotic attractor using (13) and (14) is $D_L = 2.2211$. Therefore, we conclude that the Lyapunov dimension of the new hyperchaotic system (5) is fractional. And the corresponding Lyapunov exponents diagram of the novel hyperchaotic system (6) is shown in Figure 8.

3.3. Synchronous Stability Analysis. From a physical point of view, synchronization means that the trajectory of a system converges to another system and maintains a consistent dynamic phenomenon. Consider two chaotic systems, and one of the chaotic systems is described as

$$\dot{X} = F(X, t). \tag{15}$$

This system can be referred to as the drive system or, as being called in the communication system, the transmitter.

Another chaotic system is described as

$$\dot{Y} = F'(Y, t) + G, \tag{16}$$

where G is the controller. Usually, this system is called the response system or, as being referred to in the communication system, the receiving system. Here t is the time, and

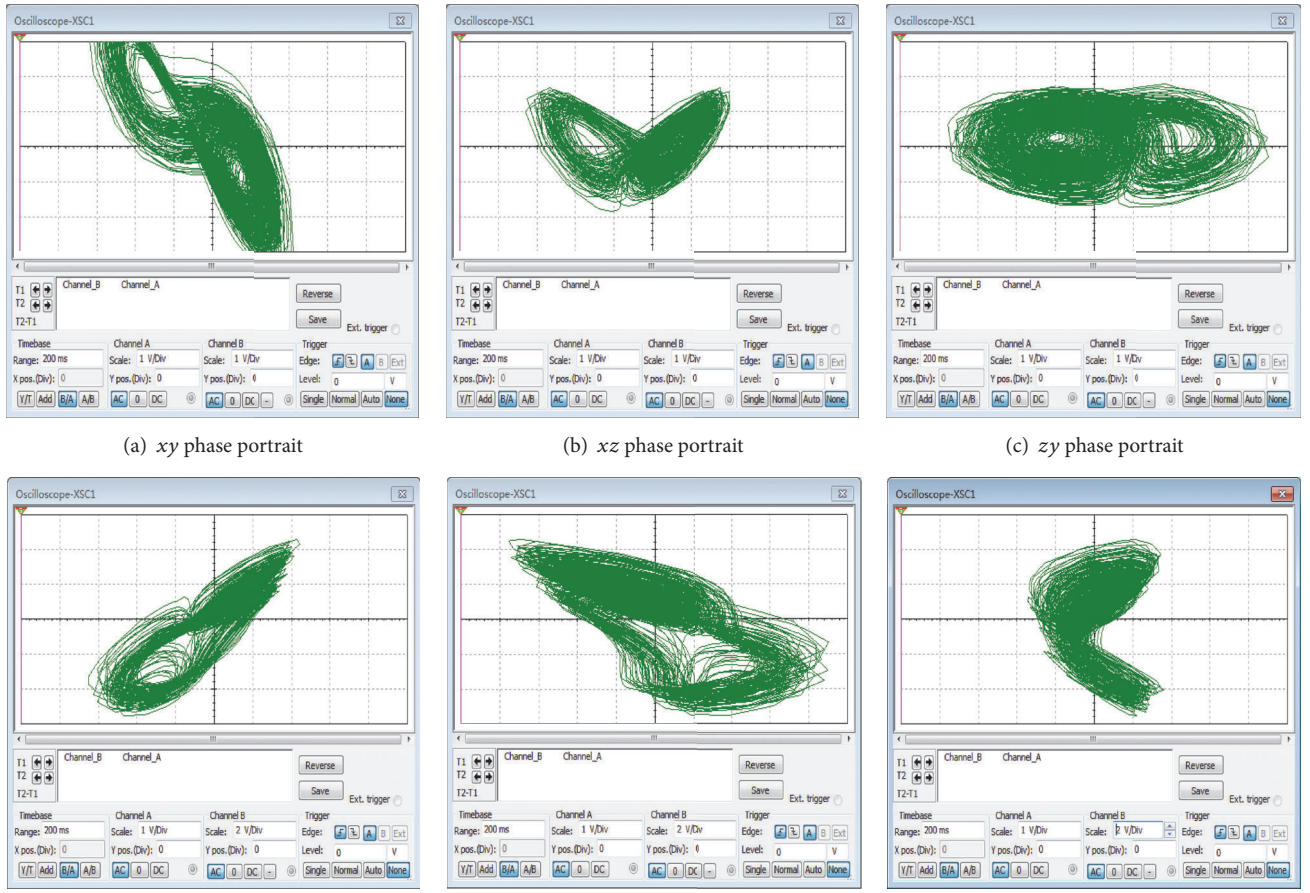

(a) xy phase portrait (b) xz phase portrait (c) zy phase portrait

(d) xu phase portrait (e) yu phase portrait (f) zu phase portrait

FIGURE 6: $(y + z)$-u-x hyperchaotic phase portraits with Multisim.

vectors $X, Y \in R^n$. They have dimensional components $(x_1, x_2, \ldots, x_n)$ and $(y_1, y_2, \ldots, y_n)$, respectively. The two chaotic systems can be the same or different, but their initial conditions are different. If the two chaotic systems are connected in some way by the controller, we consider $X(t; t_0, X_0)$ and $Y(t; t_0, Y_0)$ are the solutions of system (15) and system (16), respectively, and satisfy the smooth condition of the function. If R^n has a subset of $D(t_0)$ and the initial value $X_0, Y_0 \in D(t_0)$, then, when $t \to \infty$, the following exists:

$$\zeta \equiv \lim_{t\to\infty} \left\| X(t; t_0, X_0) - Y(t; t_0, Y_0) \right\| \longrightarrow 0. \tag{17}$$

Then, the response system (15) is synchronized with the drive system (16). In short, the synchronization error system of the chaotic systems is defined as $\dot{e} = \dot{y} - \dot{x}$. Chaotic synchronization means the asymptotic stability of the error system for the drive system and the response system at the origin; that is, $\lim_{t\to\infty} \|e(t)\| \to 0$. Obviously, the controller plays a key role, and the goal of the controller is to stabilize the synchronization error system at the origin. Therefore, through the design of a variety of different controllers, there will be a variety of synchronization methods.

Thus, we consider the novel drive system described by

$$\begin{aligned} \dot{x}_1 &= -x_1 - x_2 - ax_4 \\ \dot{x}_2 &= -bx_1 + cx_1x_3 \\ \dot{x}_3 &= -dx_3 - ex_1x_2 \\ \dot{x}_4 &= -x_2 - x_3 - ex_4, \end{aligned} \tag{18}$$

where x_1, x_2, x_3, and x_4 are the states and a, b, c, d, and e are system parameters. When choosing $a = 0.1$, $b = 4.55$, $c = 1.96$, $d = 0.37$, and $e = 0.5$, the novel system (18) is chaotic. Next, we consider the novel response system described by

$$\begin{aligned} \dot{y}_1 &= -y_1 - y_2 - ay_4 + u_1 \\ \dot{y}_2 &= -by_1 + cy_1y_3 + u_2 \\ \dot{y}_3 &= -dy_3 - ey_1y_2 + u_3 \\ \dot{y}_4 &= -y_2 - y_3 - ey_4 + u_4, \end{aligned} \tag{19}$$

where y_1, y_2, y_3, y_4 are the states and u_1, u_2, u_3, u_4 are the controllers to be designed so as to achieve global chaos synchronization between systems (18) and (19).

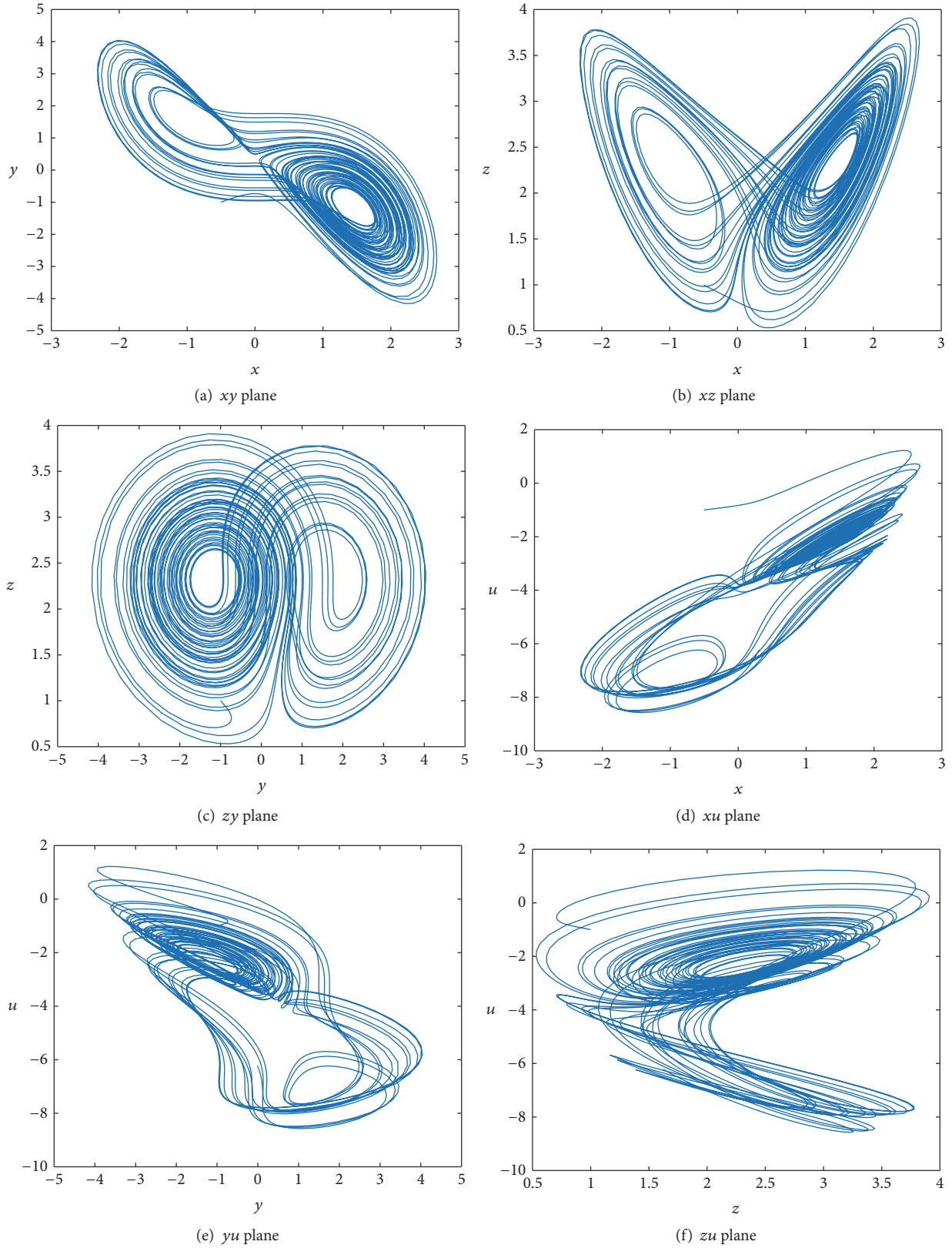

FIGURE 7: $(y + z)$-u-x hyperchaotic phase portraits with Matlab.

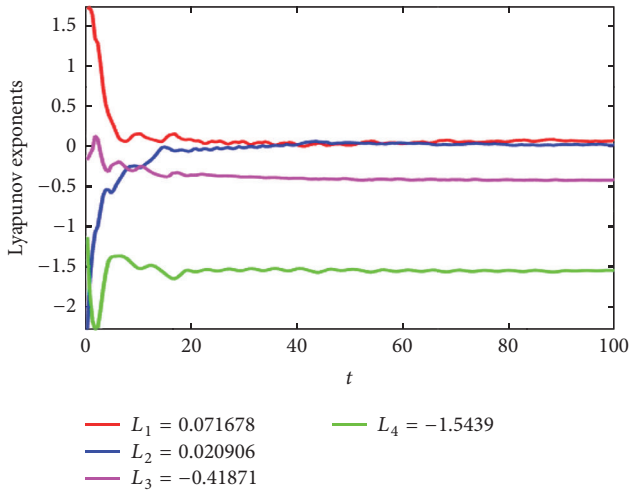

FIGURE 8: Lyapunov exponents of the new system (6).

The synchronization error is defined as

$$\dot{\xi}_i = \dot{y}_i - \dot{x}_i, \quad (i = 1, 2, 3, 4). \tag{20}$$

Then, the synchronization error system between the drive system (18) and the response system (19) is easily obtained as

$$\begin{aligned} \dot{\xi}_1 &= -\xi_1 - \xi_2 - a\xi_4 + u_1 \\ \dot{\xi}_2 &= -b\xi_1 + c\left(y_1 y_3 - x_1 x_3\right) + u_2 \\ \dot{\xi}_3 &= -d\xi_3 - e\left(y_1 y_2 - x_1 x_2\right) + u_3 \\ \dot{\xi}_4 &= -\xi_2 - \xi_3 - e\xi_4 + u_4. \end{aligned} \tag{21}$$

Construct the following controller system:

$$\begin{aligned} u_1 &= \xi_1 + \xi_2 + a\xi_4 - k_1\xi_1 \\ u_2 &= b\xi_1 - c\left(y_1 y_3 - x_1 x_3\right) - k_2\xi_2 \\ u_3 &= d\xi_3 + e\left(y_1 y_2 - x_1 x_2\right) - k_3\xi_3 \\ u_4 &= \xi_2 + \xi_3 + e\xi_4 - k_4\xi_4, \end{aligned} \tag{22}$$

where $k_i > 0$ $(i = 1, 2, 3, 4)$, for the use of controlling the synchronization speed. Substituting (22) into (21), we can obtain the error dynamics:

$$\begin{aligned} \dot{\xi}_1 &= -k_1\xi_1 \\ \dot{\xi}_2 &= -k_2\xi_2 \\ \dot{\xi}_3 &= -k_3\xi_3 \\ \dot{\xi}_4 &= -k_4\xi_4. \end{aligned} \tag{23}$$

Then, the Lyapunov function V is considered as

$$V = \frac{\left(\xi_1^2 + \xi_2^2 + \xi_3^2 + \xi_4^2\right)}{2}. \tag{24}$$

Clearly, V is a positive definite function. Differentiating V from (24), we can obtain

$$\begin{aligned} \dot{V} &= \xi_1\dot{\xi}_1 + \xi_2\dot{\xi}_2 + \xi_3\dot{\xi}_3 + \xi_4\dot{\xi}_4 \\ &= \xi_1\left(-k_1\xi_1\right) + \xi_2\left(-k_2\xi_2\right) + \xi_3\left(-k_3\xi_3\right) \\ &\quad + \xi_4\left(-k_4\xi_4\right) = -k_1\xi_1^2 - k_2\xi_2^2 - k_3\xi_3^2 - k_4\xi_4^2. \end{aligned} \tag{25}$$

Thus, we can easily obtain $\dot{V} = -k_1\xi_1^2 - k_2\xi_2^2 - k_3\xi_3^2 - k_4\xi_4^2 \leq 0$, which shows that $\dot{V}$ is a negative semidefinite function. According to the Lyapunov stability theory, it follows that if V is a positive definite function and $\dot{V}$ is a negative semidefinite function, then the system is consistent and stable at the origin of the equilibrium state. Hence, it follows that $\xi_1(t) \to 0$, $\xi_2(t) \to 0$, $\xi_3(t) \to 0$, and $\xi_4(t) \to 0$ exponentially as $t \to \infty$. That is, the active synchronization error system (21) is asymptotically stable at the origin and the synchronization is effectively realized. This completes the proof.

For the numerical simulations, the fourth-order Runge-Kutta method is used to solve the novel drive system (18) and the novel response system (19) with active control method. In the following simulations, suppose that the initial values of the novel drive system are chosen as $x_1(0) = -14$, $x_2(0) = -5$, $x_3(0) = 43$, and $x_4(0) = 0.3$. The initial values of the novel response system are chosen as $y_1(0) = -12$, $y_2(0) = -3$, $y_3(0) = 35$, and $y_4(0) = 0.2$. The control gains are chosen as $k_1 = 1$, $k_2 = 0.5$, $k_3 = 0.8$, and $k_4 = 0.5$. The history of the synchronization errors is shown in Figure 9. It can be seen from Figure 9 that the synchronization errors ξ_1, ξ_2, ξ_3, ξ_4 are asymptotically stabilized at the origin. The timing diagrams of x_1-y_1, x_2-y_2, x_3-y_3, x_4-y_4 are shown in Figure 10. The synchronous waveforms of the two chaotic systems are shown to be the same in a very short period of time; thus the active control synchronization is implemented.

The advantages of active control method are presented as follows: this method is a simple but applicable tool for analyzing synchronization stability, and the synchronization speed is very fast. In practical applications, it has always been known that the less the control signal is, the more easily the hardware circuit of the control process is realized. Therefore, the active control synchronization method is easier to be realized in the hardware circuits because of its less control signal and lower cost compared with other control methods [20–22]. By the use of this control method in chaotic secure communication, the number of signals transmitted through the public channel can be greatly decreased to further guarantee the security and good robustness. Thus, it is easy to be implemented in engineering. But the disadvantage of this control method is that the anti-interference ability is weaker.

4. Applications of the Novel Hyperchaotic System

4.1. Circuit Deformation. In the following, another new fourth-order hyperchaotic circuit is constructed successfully through circuit deformation based on the novel $(y + z)$-u-x

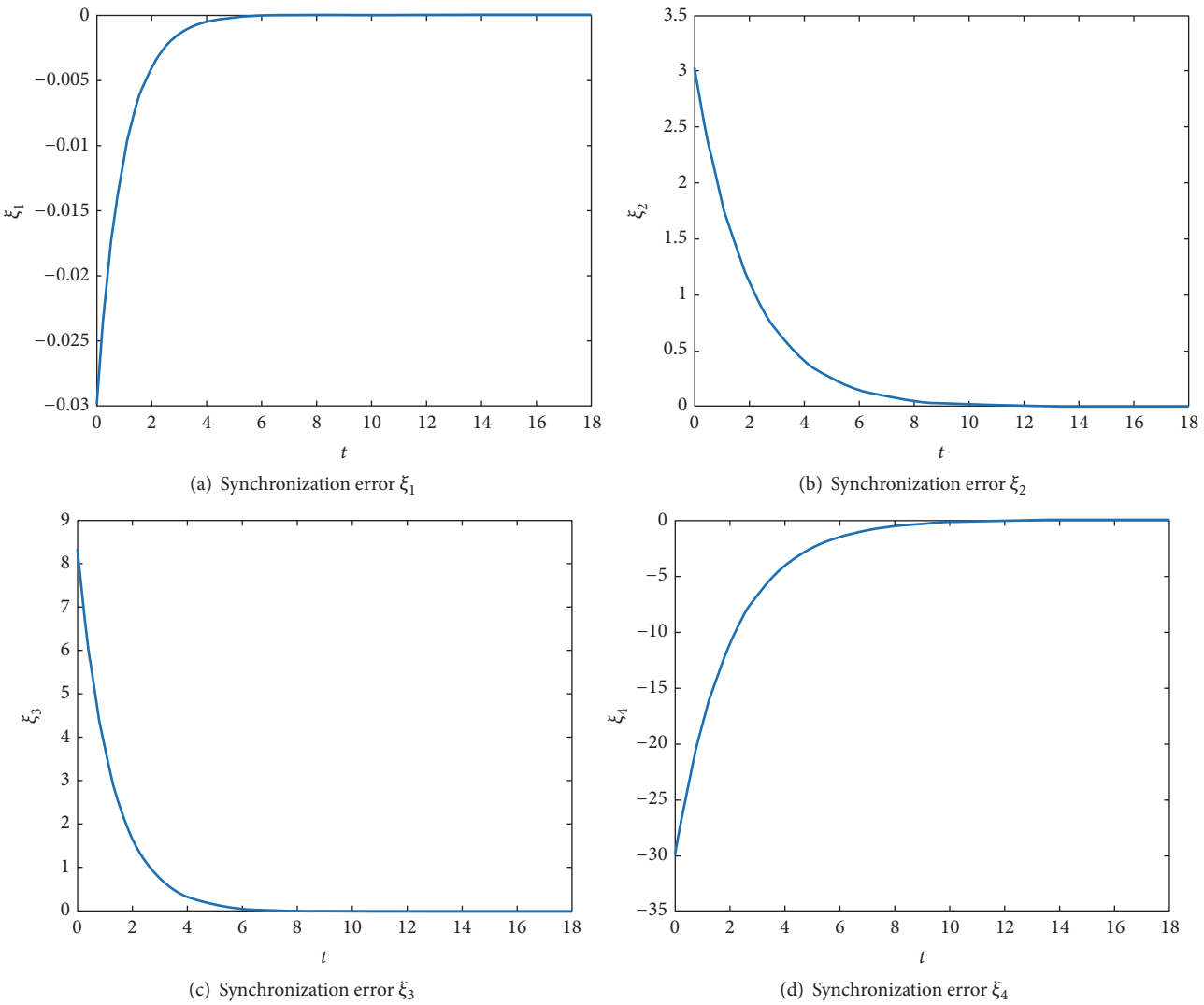

(a) Synchronization error ξ_1

(b) Synchronization error ξ_2

(c) Synchronization error ξ_3

(d) Synchronization error ξ_4

FIGURE 9: The history of synchronization errors.

hyperchaotic circuit. The circuit deformation principle is given as follows: according to the fourth-order $(y + z)$-u-x hyperchaotic circuit, the input is introduced from the z end, and feedback is given to the y input stage after the u stage. Thus, another novel fourth-order hyperchaotic circuit is proposed, and the novel hyperchaotic circuit schematic is shown in Figure 11. It is composed of 5 operational amplifiers, 2 analog multipliers, 11 resistors, and 4 capacitors. In order to facilitate the narrative, we call this novel fourth-order circuit z-u-y hyperchaotic circuit.

The beneficial effects of the novel fourth-order z-u-y hyperchaotic circuit are as follows: it not only can output four chaotic waveforms and six phase portraits, but also can output upright phase portrait shape like butterfly wings and stable fourth-order double vortex chaotic signals. Also, operational amplifier TL082 or TL084 and analog multiplier AD633 are used. According to the novel z-u-y hyperchaotic circuit shown in Figure 11, the normalized resistor is set as $R = 100\text{k}\,\Omega$. Thus, the state equation of the corresponding z-u-y hyperchaotic circuit is obtained as follows:

$$\begin{aligned}
\dot{x} &= -\frac{100\text{k}}{100\text{k}}x - \frac{100\text{k}}{100\text{k}}y \\
\dot{y} &= -\frac{100\text{k}}{22\text{k}}x + \frac{100\text{k}}{510\,\Omega} \times 0.01xz - \frac{100\text{k}}{100\text{k}} \times 0.1u \\
\dot{z} &= -\frac{100\text{k}}{270\text{k}}z - \frac{100\text{k}}{2\text{k}} \times 0.01xy \\
\dot{u} &= -\frac{100\text{k}}{100\text{k}}y - \frac{100\text{k}}{20\text{k}} \times 0.1u.
\end{aligned} \tag{26}$$

Then, another novel fourth-order hyperchaotic system is obtained by (26):

$$\begin{aligned}
\dot{x} &= -x - y \\
\dot{y} &= -ax + bxz - cu
\end{aligned}$$

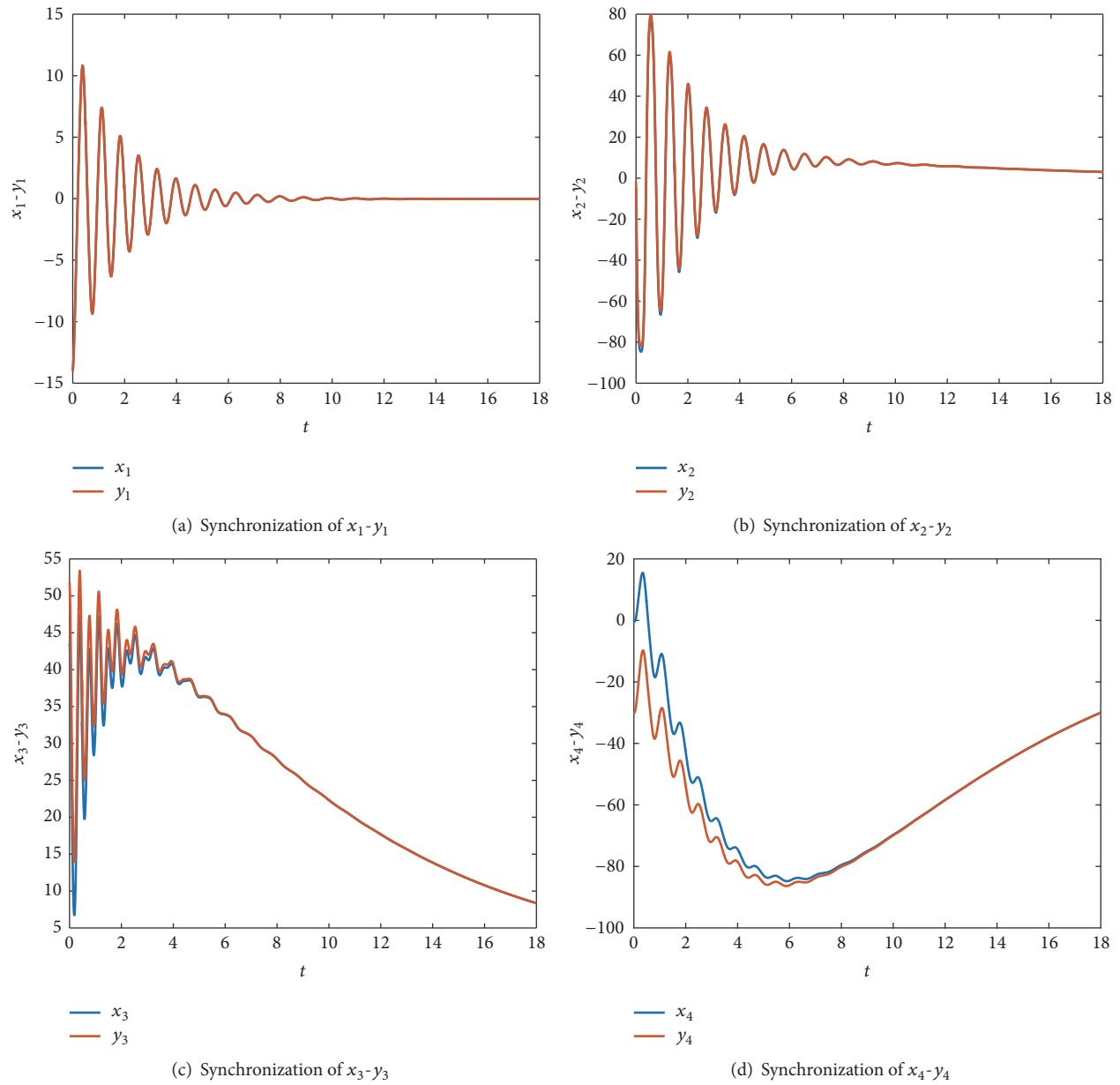

(a) Synchronization of x_1-y_1

(b) Synchronization of x_2-y_2

(c) Synchronization of x_3-y_3

(d) Synchronization of x_4-y_4

Figure 10: Synchronization of the two chaotic systems.

$$\begin{aligned}\dot{z} &= -dz - exy\\ \dot{u} &= -y - eu.\end{aligned} \tag{27}$$

When choosing $a = 4.55$, $b = 1.96$, $c = 0.1$, $d = 0.37$, and $e = 0.5$, the novel system (27) is chaotic. Substituting the specific parameter values, (27) becomes

$$\begin{aligned}\dot{x} &= -x - y\\ \dot{y} &= -4.55x + 1.96xz - 0.1u\\ \dot{z} &= -0.37z - 0.5xy\\ \dot{u} &= -y - 0.5u.\end{aligned} \tag{28}$$

This is another novel hyperchaotic system through circuit deformation based on the $(y + z)$-u-x hyperchaotic circuit. Similarly, the divergence of the novel chaotic system (27) is easily calculated as

$$\nabla = \frac{\partial \dot{x}}{\partial x} + \frac{\partial \dot{y}}{\partial y} + \frac{\partial \dot{z}}{\partial z} + \frac{\partial \dot{u}}{\partial u} = -1 - d - e < 0. \tag{29}$$

The divergence is less than 0. A necessary and sufficient condition for system (27) to be dissipative is that the divergence of the vector field is negative when the time tends to be infinite, and the corresponding dynamic characteristics will be presented.

All of the electronic components are easily available. In order to illustrate the effectiveness of the proposed z-u-y

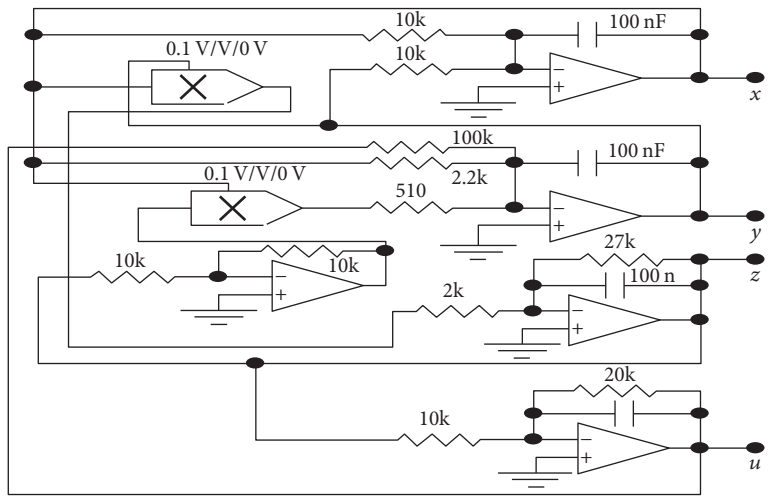

FIGURE 11: z-u-y hyperchaotic circuit schematic.

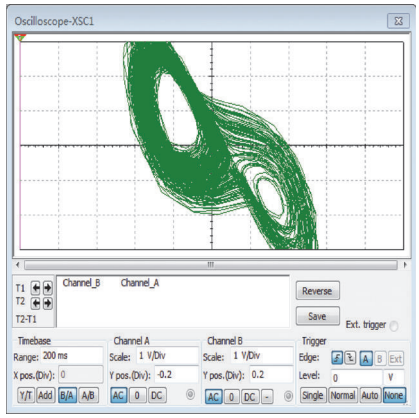

(a) xy phase portrait

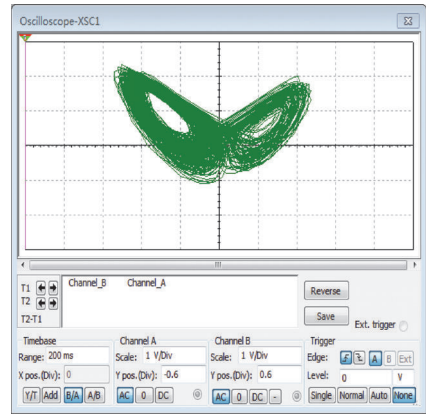

(b) xz phase portrait

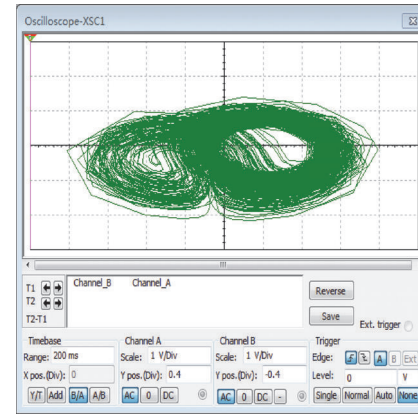

(c) zy phase portrait

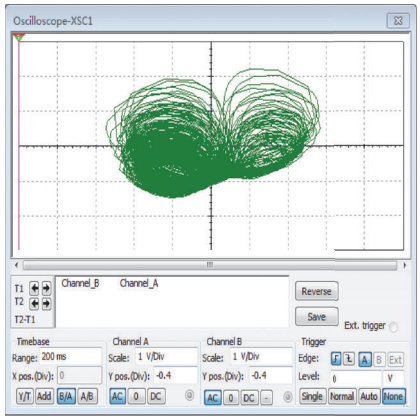

(d) xu phase portrait

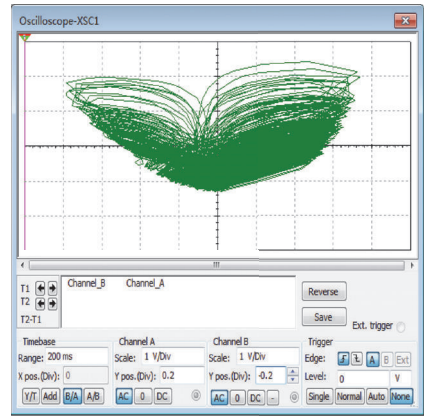

(e) yu phase portrait

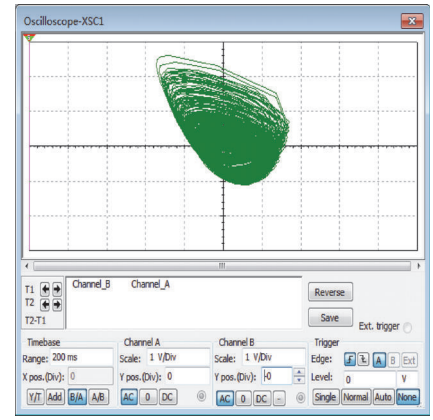

(f) zu phase portrait

FIGURE 12: z-u-y hyperchaotic phase portraits with Multisim.

hyperchaotic circuit, some simulations are presented by Multisim. The z-u-y hyperchaotic phase portraits are shown in Figure 12 with Multisim. It can be seen from the simulation results that it can output six chaotic phase portraits of xy, xz, zy, xu, yu, and zu. A variety of chaotic signals can be displayed on the oscilloscope. Similarly, other kinds of experiments can also be implemented through the novel z-u-y hyperchaotic circuit.

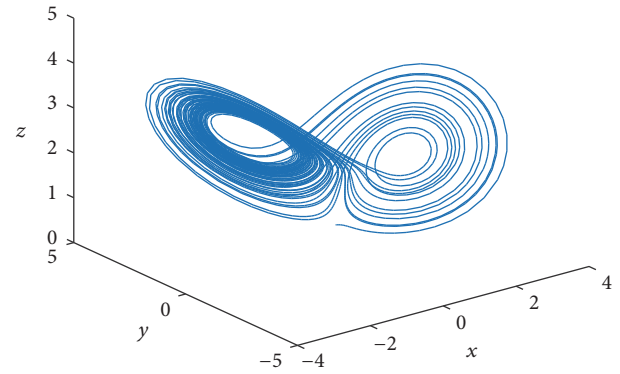

Figure 13: Three-dimensional chaotic attractor.

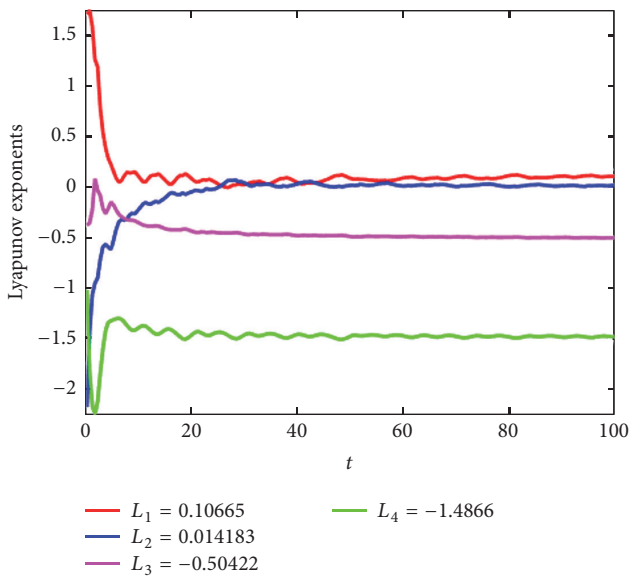

Figure 14: Lyapunov exponents of system (28).

In order to further study the chaotic dynamical behavior of the novel z-u-y hyperchaotic system (27), some numerical analysis and simulations are implemented. The three-dimensional chaotic attractor of the z-u-y hyperchaotic system is shown in Figure 13. And the Lyapunov exponents of the novel z-u-y hyperchaotic system are also strictly calculated. With the parameters chosen as $a = 4.55$, $b = 1.96$, $c = 0.1$, $d = 0.37$, and $e = 0.5$, the corresponding Lyapunov exponents are obtained as $L_1 = 0.1067$, $L_2 = 0.0142$, $L_3 = -0.5042$, and $L_4 = -1.4866$.

This means that system (28) is a hyperchaotic system since L_1 and L_2 are positive values and a dissipative system since the sum of the Lyapunov exponents is negative. It meets the condition of at least two positive Lyapunov exponents for the hyperchaotic systems. And the corresponding Lyapunov exponents diagram of the novel hyperchaotic system (28) is shown in Figure 14. It is further verified that the novel system (28) is a hyperchaotic system.

4.2. Hyperchaotic Secure Communication. It is well known that the hyperchaotic signals are especially suitable for the secure communication field. In order to improve the security of secure communication system, it is considered that the novel hyperchaotic system should be selected as the chaotic system. In the proposed hyperchaotic secure communication scheme, the hyperchaotic secure communication circuit is implemented by using some electronic components containing analog multipliers, operational amplifiers, resistors, and capacitors with a novel hyperchaotic system as chaos generator. On the basis of the proposed fourth-order $(y + z)$-u-x hyperchaotic circuit, the hyperchaotic secure communication circuit schematic by Multisim is shown in Figure 15. Its circuit principle is carefully presented as follows.

It consists of 12 operational amplifiers together with 4 analog multipliers. Its basic circuit is composed of two identical $(y + z)$-u-x hyperchaotic circuit units with a little change. The left side of the circuit is the transmitting system and the right side is the receiving system. The inverting input end of transmitter-modulator is connected with the transmitted signal to be transmitted. The same-phase input end is connected with the x output terminal of the novel $(y + z)$-u-x hyperchaotic circuit. The inverting input end of receiver-demodulator is connected with the communication channel signal, and the same-phase input end is connected with x output end of the novel $(y + z)$-u-x hyperchaotic circuit. The signal at the output is the output of the receiver. In this way the receiving system is more easily synchronized with the transmitting system and the robustness of the $(y + z)$-u-x hyperchaotic circuit is maintained. This method can effectively prevent the useful information from being intercepted in the communication process [34].

The advantages of the novel hyperchaotic secure communication circuit are described as follows: the implementation cost of the novel hyperchaotic system is reduced to improve the practicability of the secure communication system, the number of the state variables and transmission channels needed to access the drive system is also reduced, and the circuit structure of the designed control system is greatly simplified. In the following, some simulation experiments are presented to verify whether two identical parameters of the $(y + z)$-u-x hyperchaotic circuits can effectively achieve the signal transmission and reception without distortion. For example, an input sine wave with amplitude of 1 V and frequency of 1 kHz is given; the transmitting and receiving signal waveforms by Multisim are shown in Figure 16. It can be seen from the simulation results that, no matter what kinds of signals are input, the full synchronization can be realized in two identical $(y + z)$-u-x chaotic circuits if the component parameters of the transmitting circuit are completely consistent with the receiving circuit. Negligible distortion can be observed.

To illustrate the effectiveness of the proposed scheme, the intensity limit and stability of the transmitted signal, the broadband characteristics, and the accuracy requirements of electronic components are simulated by Multisim [34].

First of all, in order to verify whether the proposed hyperchaotic secure communication circuit has a choice for various input signals intensity, sine waves with frequency of 1 kHz and amplitude of 100 mV, 5 V, 15 V, 16 V, and 25 V are input. It can be concluded from these waveforms that

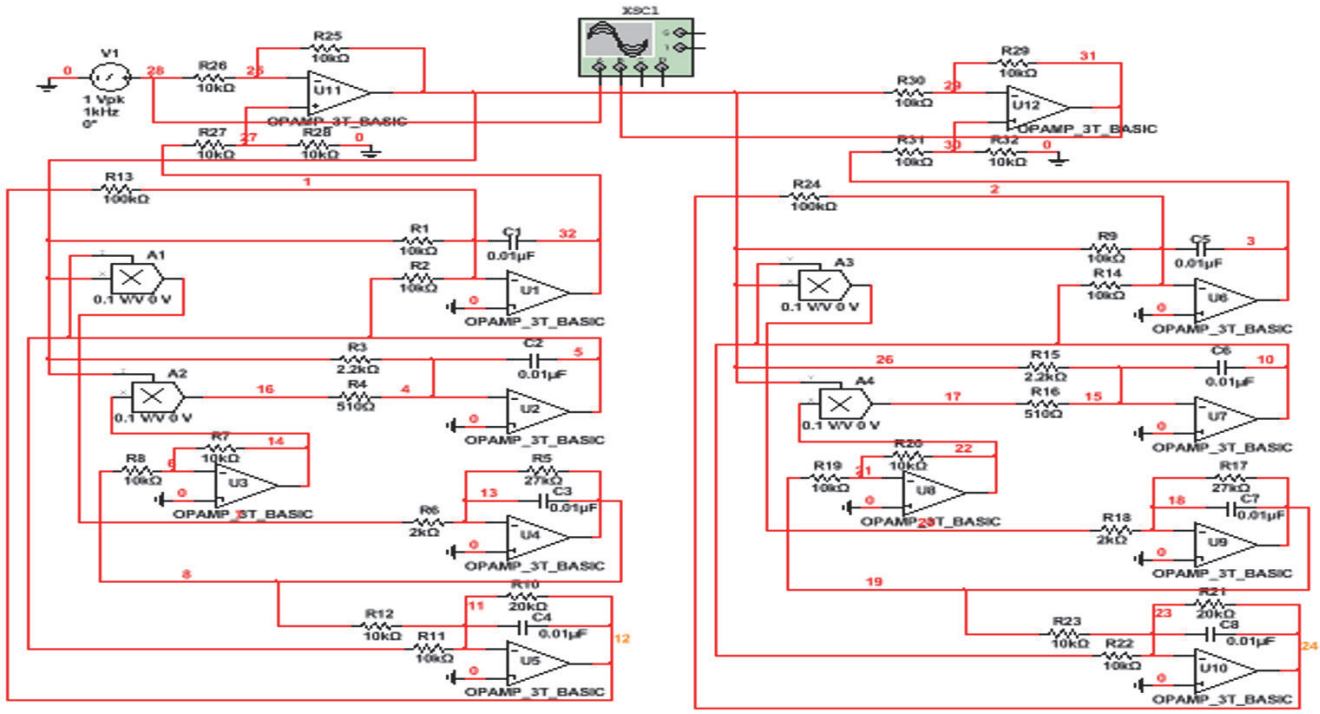

Figure 15: A novel hyperchaotic secure communication circuit by Multisim.

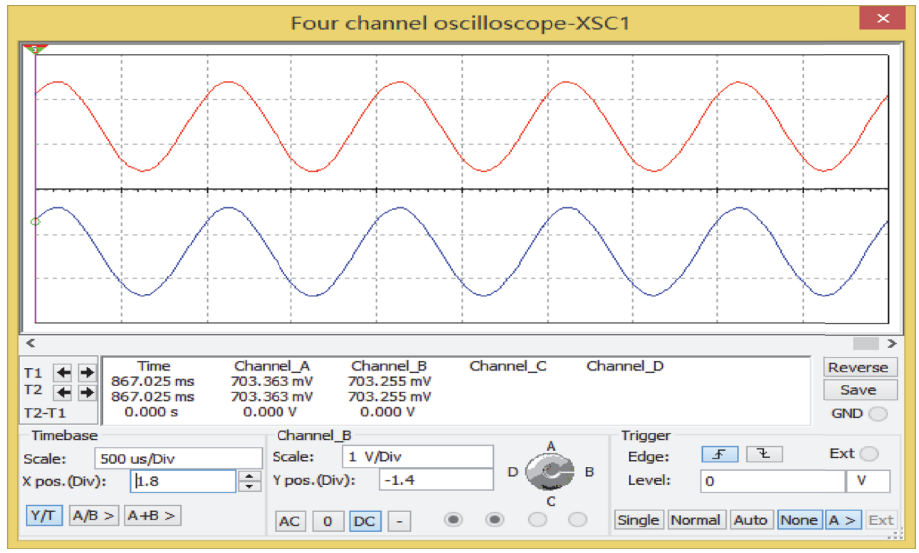

Figure 16: Transmitting and receiving waveforms with amplitude of 1 V and frequency of 1 kHz.

the signal transmission distortion will occur when the signal amplitude reaches 16 V, as shown in Figures 17, 18, 19, and 20. When the signal amplitude exceeds 16 V, the signal distortion is quite evident, as shown in Figures 21 and 22.

Secondly, in order to verify whether the proposed hyperchaotic secure communication circuit has a choice for the input signal frequency, sine waves with amplitude of 1 V and frequency of 100 Hz, 10 kHz, 100 kHz, 500 kHz, and 1 MHz are given. It can be seen from these waveforms that it can transmit the signal from 1 Hz to 500 kHz without distortion. This is due to the frequency limitations of the amplifiers, as already shown in [32]. When the signal frequency reaches 500 kHz to 1 MHz, the signal distortion is quite evident, as shown in Figures 23, 24, 25, and 26. Thus, it can be concluded that the circuit has the characteristic of broadband.

From the simulation results above, we can draw the conclusion that the proposed hyperchaotic secure communication circuit based on the $(y + z)$-u-x hyperchaotic

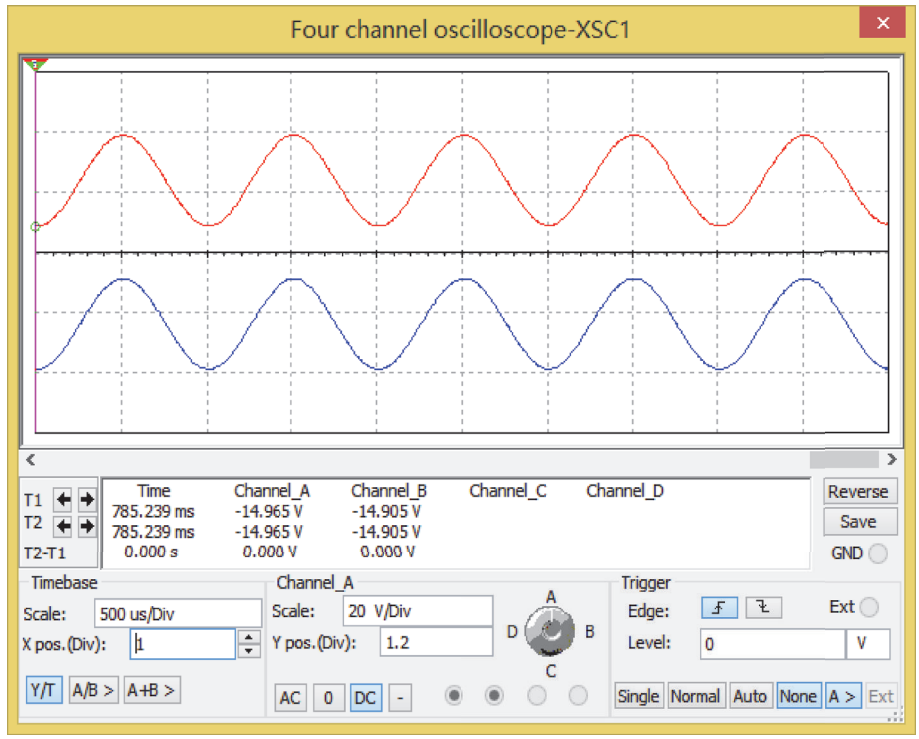

Figure 17: 15 V.

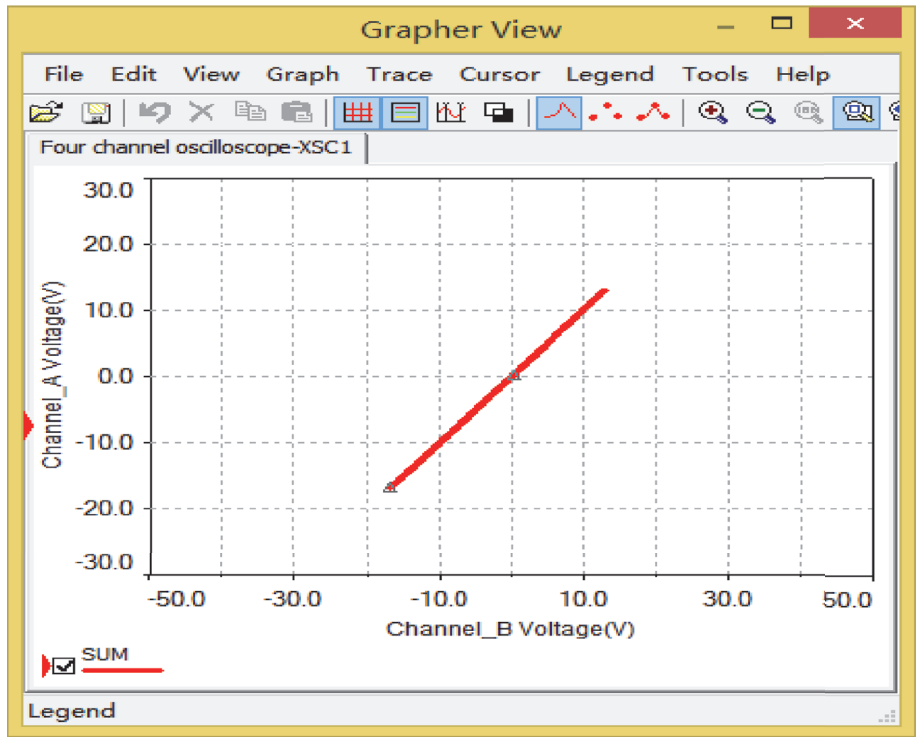

Figure 18: Synchronous phase portrait of 15 V.

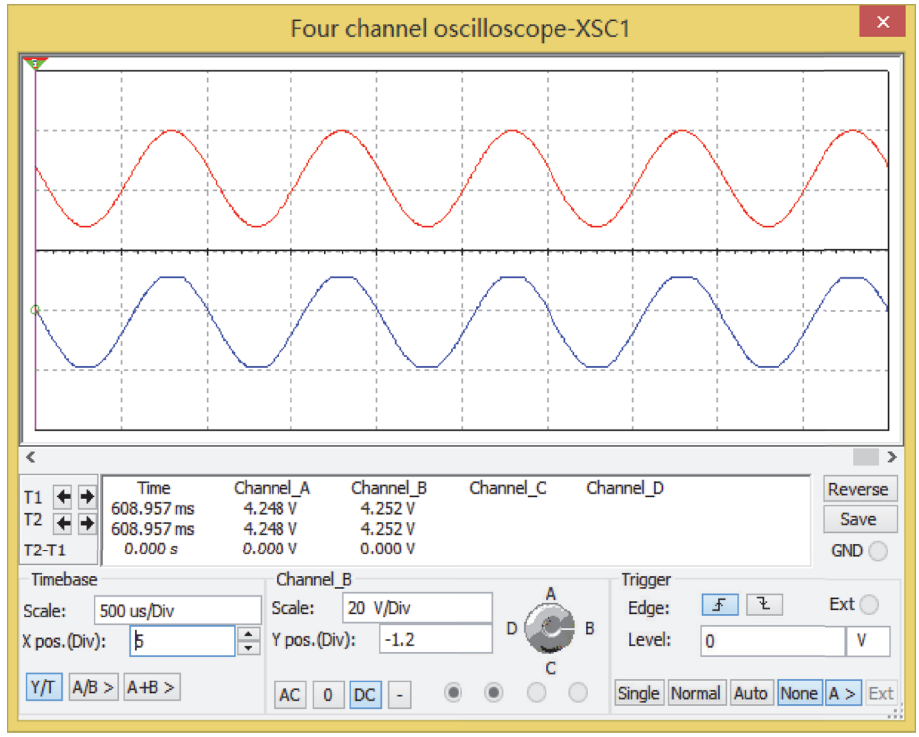

Figure 19: 16 V.

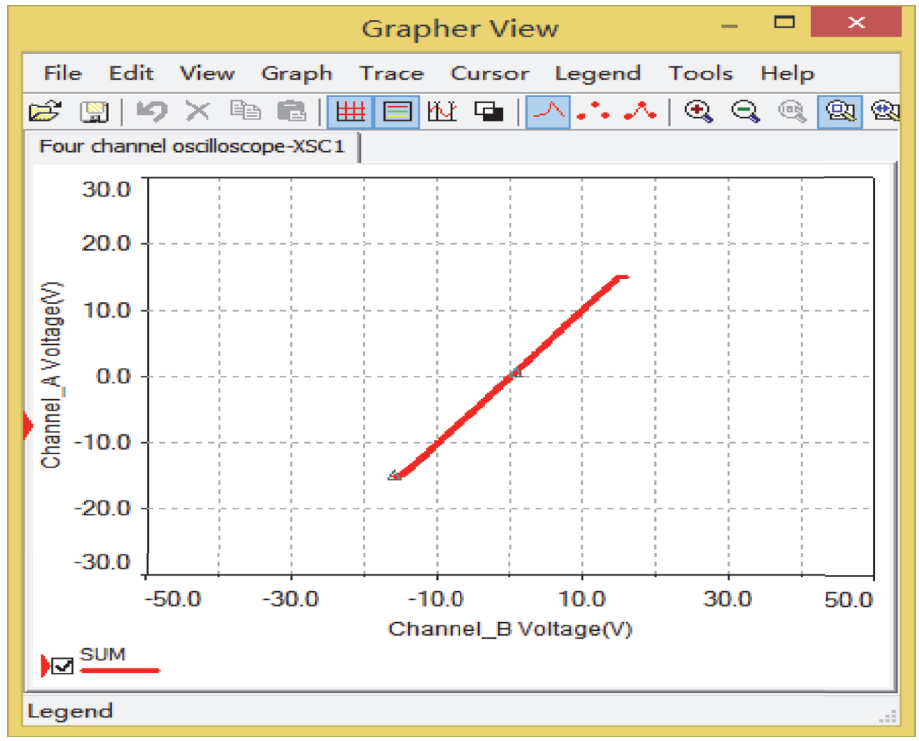

Figure 20: Synchronous phase portrait of 16 V.

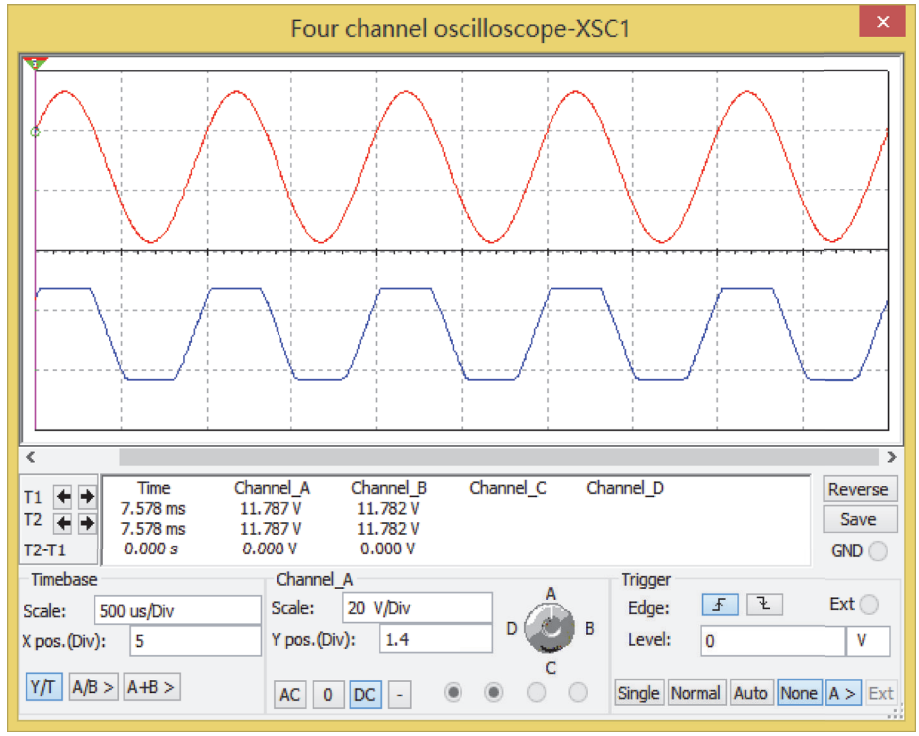

Figure 21: 25 V.

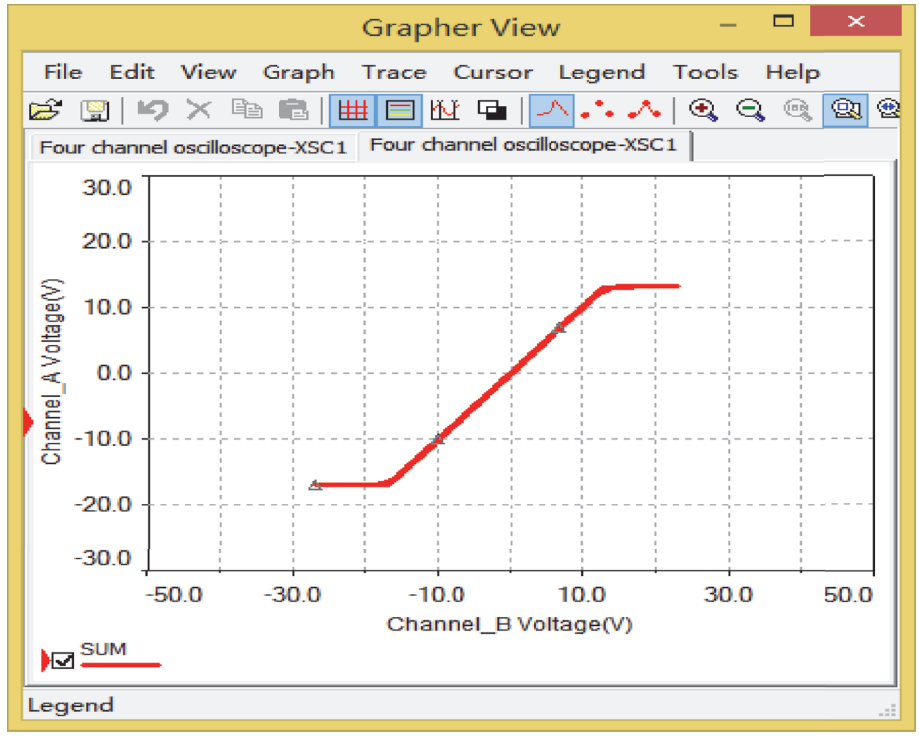

Figure 22: Synchronous phase portrait of 25 V.

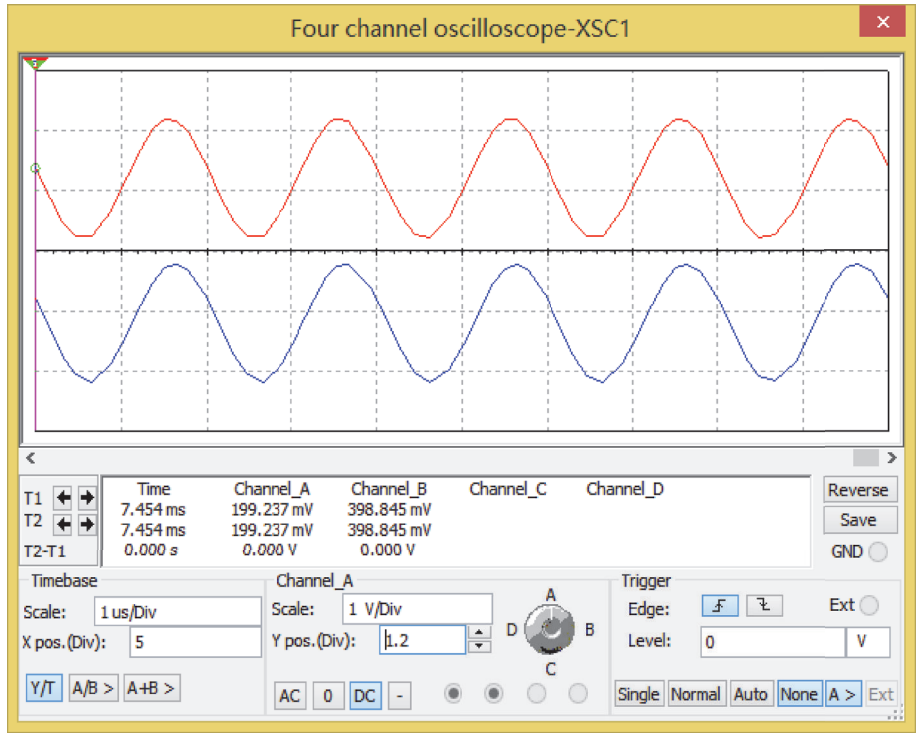

Figure 23: 500 KHZ.

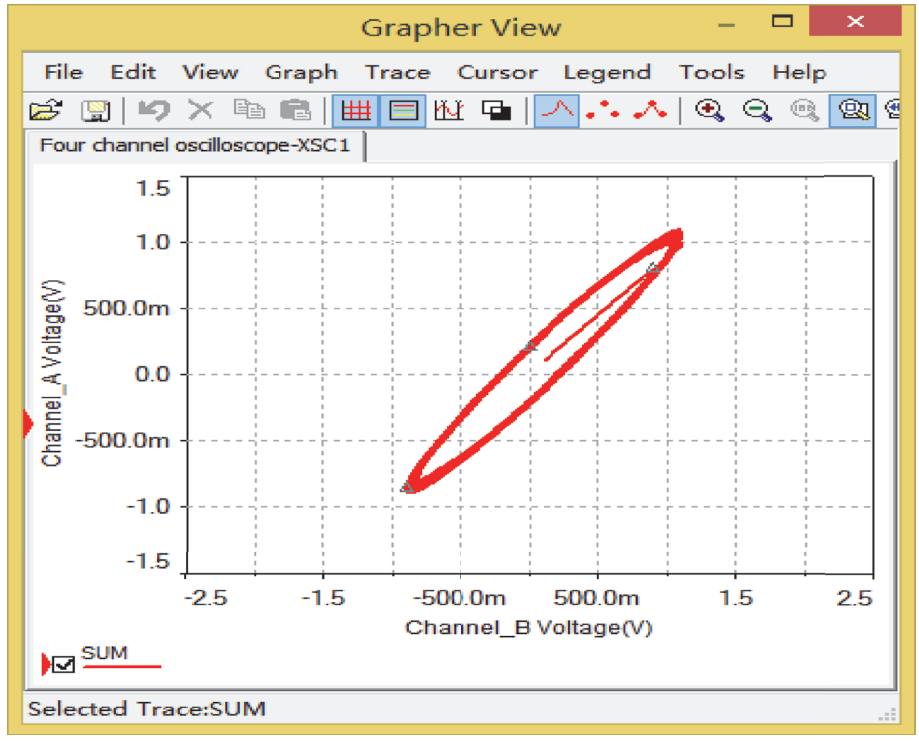

Figure 24: Phase portrait of 500 KHZ.

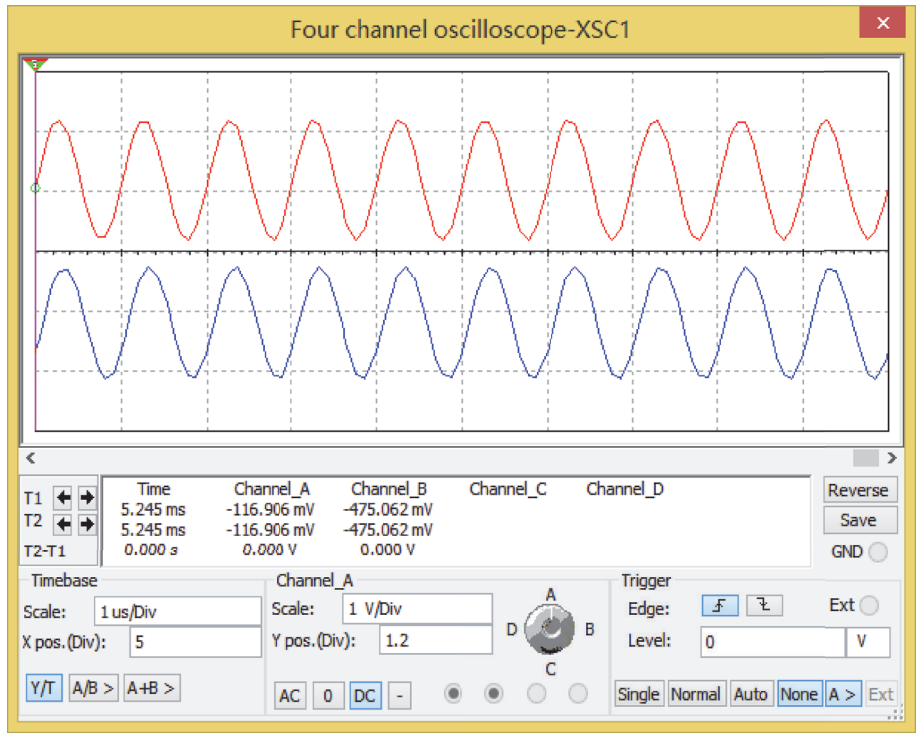

Figure 25: 1 MHZ.

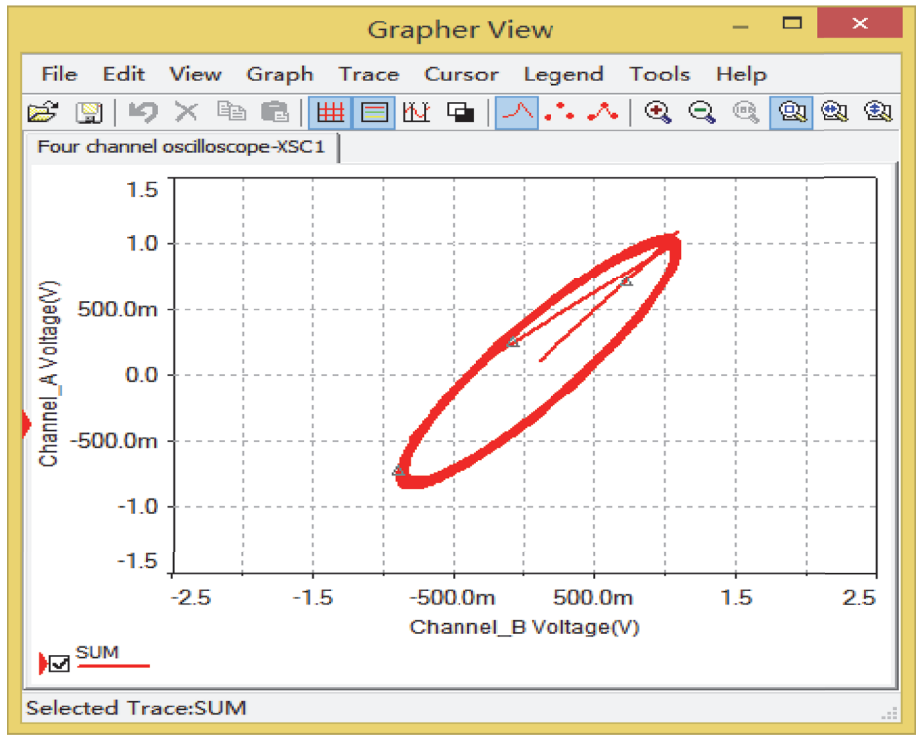

Figure 26: Phase portrait of 1 MHZ.

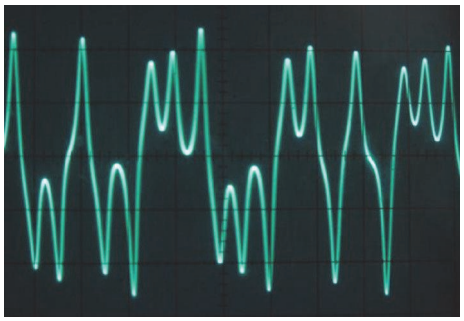

(a) x waveform

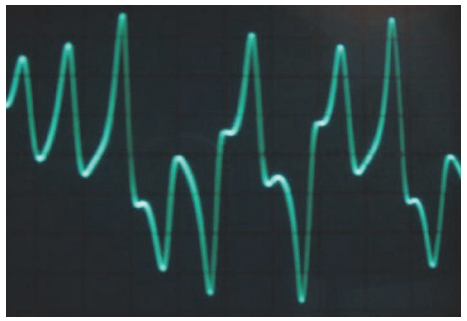

(b) y waveform

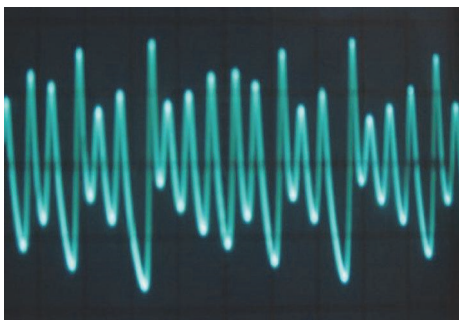

(c) z waveform

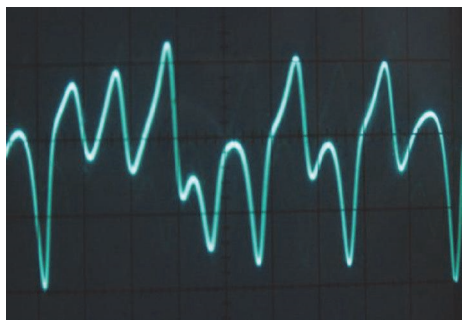

(d) u waveform

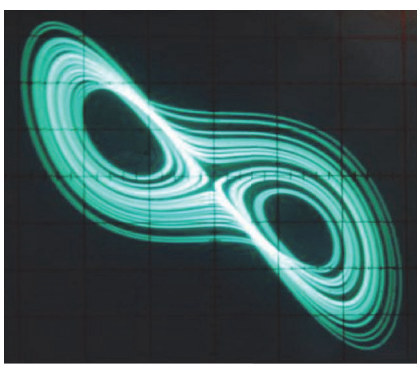

(e) xy phase portrait

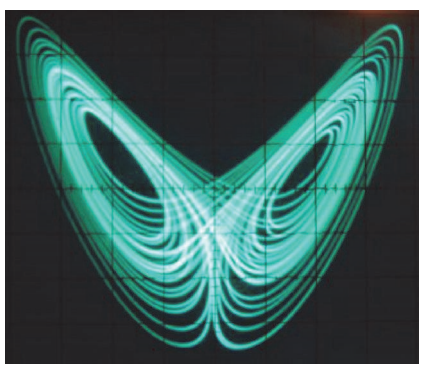

(f) xz phase portrait

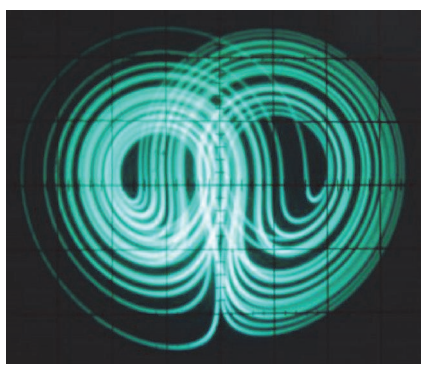

(g) zy phase portrait

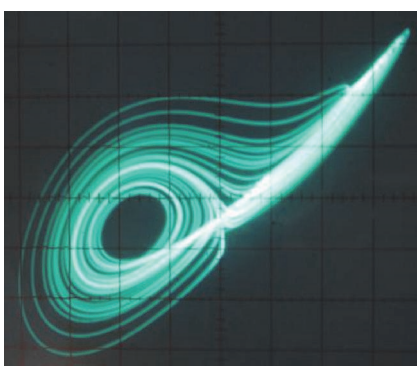

(h) xu phase portrait

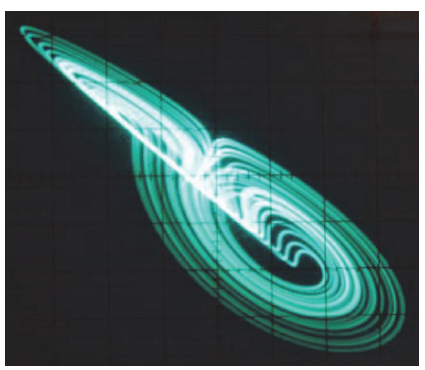

(i) yu phase portrait

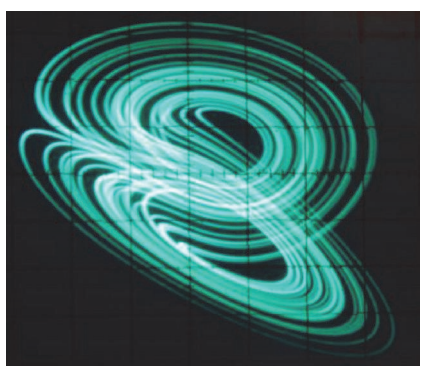

(j) zu phase portrait

Figure 27: The output waveforms and phase portraits signal photos of the novel $(y + z)$-u-x hyperchaotic system.

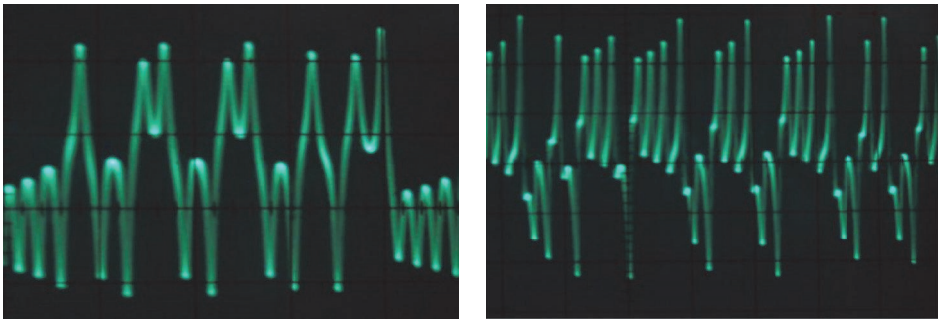

(a) x waveform (b) y waveform

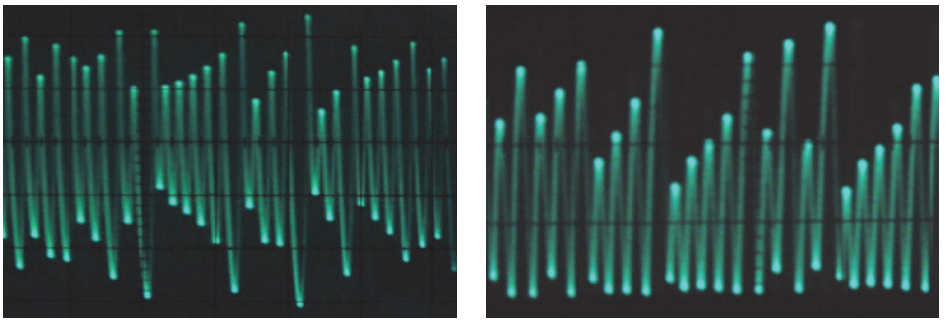

(c) z waveform (d) u waveform

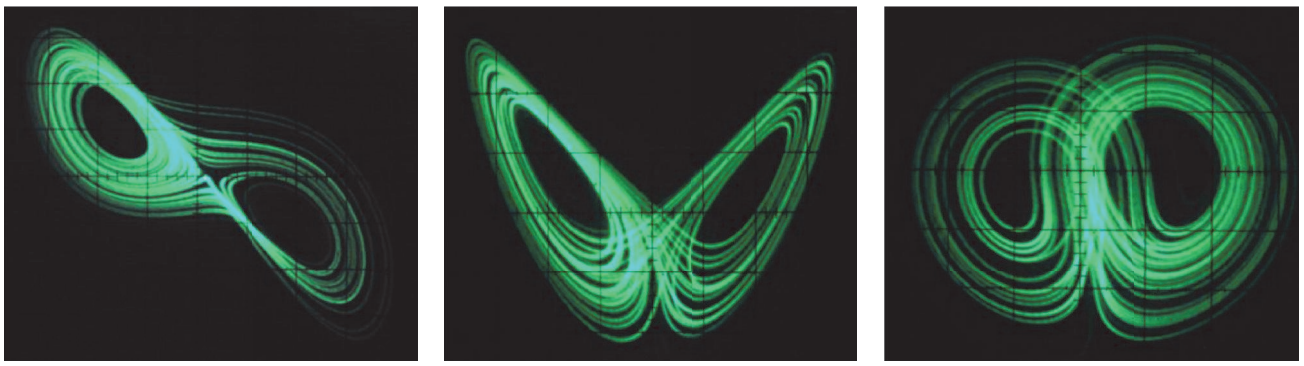

(e) xy phase portrait (f) xz phase portrait (g) zy phase portrait

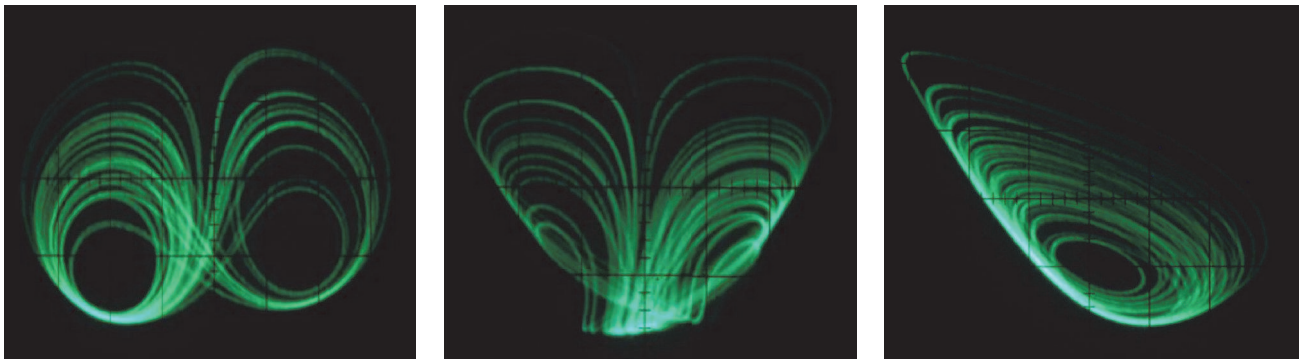

(h) xu phase portrait (i) yu phase portrait (j) zu phase portrait

Figure 28: The output waveforms and phase portraits signal photos of the novel z-u-y hyperchaotic system.

circuit has the following advantages: (i) higher intensity limit and stability of the transmitted signal, (ii) wider broadband characteristic than ordinary chaotic secure communication circuits, (iii) more stable working performance and smaller distortion, (iv) easier debugging and more convenience for mass production. Moreover, if three jumper pins are added, it can be used to control the new hyperchaotic secure communication circuit to realize the experiments of chaotic synchronization and chaotic nonsynchronization as well as experiments without signal and with signal. Similarly, the proposed chaotic secure communication method can also be applied to the z-u-y hyperchaotic circuit and other complex hyperchaotic systems.

5. Hardware Implementation of the Novel (y+z)-u-x and z-u-y Hyperchaotic Circuits

Despite the fact that chaotic circuits have many advantages, the study of chaotic circuit is still in the phase of laboratory research. Because most researchers still concentrate on the study of chaos theory in numerical simulations, there is a certain deviation from the physical circuit system. In order to verify that the novel ($y + z$)-u-x and z-u-y hyperchaotic circuits have high accuracy and good robustness and further study the chaotic dynamical characteristics of the novel hyperchaotic systems (5) and (27), two practical electronic circuits are constructed using some general electronic components such as operational amplifiers, analog multipliers, resistors, and capacitors. Figures 27(a), 27(b), 27(c), and 27(d) show the output waveform photos of the novel ($y + z$)-u-x hyperchaotic circuit. Figures 27(e), 27(f), 27(g), 27(h), 27(i), and 27(j) show the output phase portraits photos of the novel ($y + z$)-u-x hyperchaotic circuit. Figures 28(a), 28(b), 28(c), and 28(d) show the output waveform photos of the novel z-u-y hyperchaotic circuit. Figures 28(e), 28(f), 28(g), 28(h), 28(i), and 28(j) show the output phase portraits photos of the novel z-u-y hyperchaotic circuit.

It can be seen from the experimental results that the existence of the hyperchaotic attractors is proved, and it is also proved by the Multisim and Matlab simulation results. The proposed circuit design and circuit deformation methods of the novel fourth-order hyperchaotic system provide a reliable straightforward way of realizing chaotic circuits. The methods are easy to handle and prevent the output voltage from exceeding the limitation of the amplifier linear region efficiency.

6. Conclusion

In this paper, a novel hyperchaotic system is proposed based on a modified Lorenz-like chaotic circuit with reduced number of amplifiers. This paper is an attempt to investigate the dynamical behavior, synchronous stability, and applications in circuit deformation and secure communication field of the new hyperchaotic system. In order to enhance the confidentiality and security of the transmitted signals, the active control method is applied to achieve chaotic synchronization of the novel ($y + z$)-u-x hyperchaotic system based on the Lyapunov stability theory. Comparisons between Multisim as well as Matlab simulation results and physical experimental results show that they are consistent with each other and demonstrate that an attractor of the hyperchaotic system exists. However, the chaotic secure communication method proposed in this paper still has some limitations. Since conventional amplifiers and current conveyors have frequency limitations, they have limited performance in the implementation of nonlinear circuits. And another important problem is how to improve the unpredictability of chaotic communication system. If the chaotic oscillator has higher positive Lyapunov exponents, those designs can be improved because it determines the unpredictability grade of chaotic oscillators.

That way, our future research will focus on the optimization of Lyapunov exponents and circuit implementation using embedded systems like FPGA, which can lead us to observe complex attractors with high Lyapunov exponent values.

Conflicts of Interest

The authors have declared that no conflicts of interest exist.

Acknowledgments

The authors are greatly thankful for the help and support from the Open Project of State Key Laboratory of ASIC & System (Grant no. 2016KF004).

References

[1] E. N. Lorenz, "Deterministic nonperiodic flow," *Journal of the Atmospheric Sciences*, vol. 20, no. 2, pp. 130–141, 1963.

[2] K. M. Cuomo and A. V. Oppenheim, "Circuit implementation of synchronized chaos with applications to communications," *Physical Review Letters*, vol. 71, no. 1, pp. 65–68, 1993.

[3] L.-H. Yu and J.-C. Fang, "Synchronization of chaotic neural networks based on adaptive inverse control and its applications in secure communications," *Acta Physica Sinica*, vol. 54, no. 9, pp. 4012–4018, 2005.

[4] B. Muthuswamy and L. O. Chua, "Simplest chaotic circuit," *International Journal of Bifurcation and Chaos*, vol. 20, no. 5, pp. 1567–1580, 2010.

[5] Y. Liu and Q. Yang, "Dynamics of a new Lorenz-like chaotic system," *Nonlinear Analysis: Real World Applications*, vol. 11, no. 4, pp. 2563–2572, 2010.

[6] X. G. Zhang, H. T. Sun, J. L. Zhao et al., "Equivalent circuit in function and topology to Chuas circuit and the design methods of these circuits," *Acta Physica Sinica*, vol. 63, no. 20, pp. 1–8, 2014.

[7] G. A. Leonov and N. V. Kuznetsov, "On differences and similarities in the analysis of Lorenz, Chen, and LU systems," *Applied Mathematics and Computation*, vol. 256, pp. 334–343, 2015.

[8] G. M. Mahmoud, M. E. Ahmed, and E. E. Mahmoud, "Analysis of hyperchaotic complex Lorenz systems," *International Journal of Modern Physics C*, vol. 19, no. 10, pp. 1477–1494, 2008.

[9] G. M. Mahmoud and E. E. Mahmoud, "Synchronization and control of hyperchaotic complex Lorenz system," *Mathematics*

and Computers in Simulation, vol. 80, no. 12, pp. 2286–2296, 2010.

[10] A. M. El-Sayed, H. M. Nour, A. Elsaid, A. E. Matouk, and A. Elsonbaty, "Circuit realization, bifurcations, chaos and hyperchaos in a new 4D system," *Applied Mathematics and Computation*, vol. 239, pp. 333–345, 2014.

[11] L. Merah, A. Ali-Pacha, N. H. Said, and M. Mamat, "Design and FPGA implementation of Lorenz chaotic system for information security issues," *Applied Mathematical Sciences*, vol. 7, no. 5-8, pp. 237–246, 2013.

[12] M. Halimi, K. Kemih, and M. Ghanes, "Circuit simulation of an analog secure communication based on synchronized Chaotic Chua's system," *Applied Mathematics & Information Sciences*, vol. 8, no. 4, pp. 1509–1516, 2014.

[13] M. Zapateiro, Y. Vidal, and L. Acho, "A secure communication scheme based on chaotic Duffing oscillators and frequency estimation for the transmission of binary-coded messages," *Communications in Nonlinear Science and Numerical Simulation*, vol. 19, no. 4, pp. 991–1003, 2014.

[14] E. Tlelo-Cuautle, V. H. Carbajal-Gomez, P. J. Obeso-Rodelo, J. J. Rangel-Magdaleno, and J. C. Núñez-Pérez, "FPGA realization of a chaotic communication system applied to image processing," *Nonlinear Dynamics*, vol. 82, no. 4, pp. 1879–1892, 2015.

[15] T.-C. Lin, F.-Y. Huang, Z. Du, and Y.-C. Lin, "Synchronization of fuzzy modeling chaotic time delay memristor-based Chua's circuits with application to secure communication," *International Journal of Fuzzy Systems*, vol. 17, no. 2, pp. 206–214, 2015.

[16] H.-C. Chen, B.-Y. Liau, and Y.-Y. Hou, "Hardware implementation of lorenz circuit systems for secure chaotic communication applications," *Sensors*, vol. 13, no. 2, pp. 2494–2505, 2013.

[17] W. Shen, Z. Zeng, and L. Wang, "Stability analysis for uncertain switched neural networks with time-varying delay," *Neural Networks*, vol. 83, pp. 32–41, 2016.

[18] Y. Cao, S. Wen, M. Z. Q. Chen, T. Huang, and Z. Zeng, "New results on anti-synchronization of switched neural networks with time-varying delays and lag signals," *Neural Networks*, vol. 81, pp. 52–58, 2016.

[19] C. Feng, L. Cai, Q. Kang, S. Wang, and H. Zhang, "Novel hyperchaotic system and its circuit implementation," *Journal of Computational and Nonlinear Dynamics*, vol. 10, no. 6, Article ID 4029227, 2015.

[20] E. E. Mahmoud, "Complex complete synchronization of two nonidentical hyperchaotic complex nonlinear systems," *Mathematical Methods in the Applied Sciences*, vol. 37, no. 3, pp. 321–328, 2014.

[21] E. E. Mahmoud, "Dynamics and synchronization of new hyperchaotic complex Lorenz system," *Mathematical and Computer Modelling*, vol. 55, no. 7-8, pp. 1951–1962, 2012.

[22] G. M. Mahmoud and E. E. Mahmoud, "Complete synchronization of chaotic complex nonlinear systems with uncertain parameters," *Nonlinear Dynamics*, vol. 62, no. 4, pp. 875–882, 2010.

[23] V. Sundarapandian and I. Pehlivan, "Analysis, control, synchronization, and circuit design of a novel chaotic system," *Mathematical and Computer Modelling*, vol. 55, no. 7-8, pp. 1904–1915, 2012.

[24] I. Pehlivan, I. M. Moroz, and S. Vaidyanathan, "Analysis, synchronization and circuit design of a novel butterfly attractor," *Journal of Sound and Vibration*, vol. 333, no. 20, pp. 5077–5096, 2014.

[25] L. Wang, Z. Zeng, J. Hu, and X. Wang, "Controller design for global fixed-time synchronization of delayed neural networks with discontinuous activations," *Neural Networks*, vol. 87, pp. 122–131, 2017.

[26] P. S. Swathy and K. Thamilmaran, "Hyperchaos in SC-CNN based modified canonical Chua's circuit," *Nonlinear Dynamics*, vol. 78, no. 4, pp. 2639–2650, 2014.

[27] G. A. Leonov, N. V. Kuznetsov, and T. N. Mokaev, "Hidden attractor and homoclinic orbit in Lorenz-like system describing convective fluid motion in rotating cavity," *Communications in Nonlinear Science and Numerical Simulation*, vol. 28, no. 1-3, pp. 166–174, 2015.

[28] J. Ma, F. Wu, G. Ren, and J. Tang, "A class of initials-dependent dynamical systems," *Applied Mathematics and Computation*, vol. 298, pp. 65–76, 2017.

[29] R. Trejo-Guerra, E. Tlelo-Cuautle, J. Jimenez-Fuentes et al., "Integrated circuit generating 3- and 5-scroll attractors," *Communications in Nonlinear Science and Numerical Simulation*, vol. 17, no. 11, pp. 4328–4335, 2012.

[30] F. Li and C. Yao, "The infinite-scroll attractor and energy transition in chaotic circuit," *Nonlinear Dynamics*, vol. 84, no. 4, pp. 2305–2315, 2016.

[31] D. A. Prousalis, C. K. Volos, I. N. Stouboulos, and I. M. Kyprianidis, "A novel 4-D hyperchaotic four-wing memristive system," in *Proceedings of the 5th International Conference on Modern Circuits and Systems Technologies, MOCAST 2016*, grc, May 2016.

[32] J. M. Muñoz-Pacheco, E. Tlelo-Cuautle, I. Toxqui-Toxqui, C. Sánchez-López, and R. Trejo-Guerra, "Frequency limitations in generating multi-scroll chaotic attractors using CFOAs," *International Journal of Electronics*, vol. 101, no. 11, pp. 1559–1569, 2014.

[33] R. L. Filali, M. Benrejeb, and P. Borne, "On observer-based secure communication design using discrete-time hyperchaotic systems," *Communications in Nonlinear Science and Numerical Simulation*, vol. 19, no. 5, pp. 1424–1432, 2014.

[34] X. Li, Y.-J. Lu, Y.-F. Zhang, X.-G. Zhang, and P. Gupta, "Design and hardware implementation of a new chaotic secure communication technique," *PLoS ONE*, vol. 11, no. 8, Article ID e0158348, 2016.

Hindawi
Complexity
Volume 2017, Article ID 6853826, 16 pages
https://doi.org/10.1155/2017/6853826

Research Article

Adaptive Fuzzy Synchronization of Fractional-Order Chaotic (Hyperchaotic) Systems with Input Saturation and Unknown Parameters

Heng Liu,[1] Ye Chen,[2] Guanjun Li,[1] Wei Xiang,[1] and Guangkui Xu[1]

[1]*Department of Applied Mathematics, Huainan Normal University, Huainan 232038, China*
[2]*College of Mathematics and Information Science, Shaanxi Normal University, Xi'an 710119, China*

Correspondence should be addressed to Heng Liu; liuheng122@gmail.com

Received 20 July 2017; Accepted 4 October 2017; Published 2 November 2017

Academic Editor: Abdelalim Elsadany

We investigate the synchronization problem of fractional-order chaotic systems with input saturation and unknown external disturbance by means of adaptive fuzzy control. An adaptive controller, accompanied with fractional adaptation law, is established, fuzzy logic systems are used to approximate the unknown nonlinear functions, and the fractional Lyapunov stability theorem is used to analyze the stability. This control method can realize the synchronization of two fractional-order chaotic or hyperchaotic systems and the synchronization error tends to zero asymptotically. Finally, we show the effectiveness of the proposed method by two simulation examples.

1. Introduction

Recent studies showed that a large number of physical phenomena of nature and chemical processes, such as viscosity systems, colored noise, electrolyte electrode polarization, electromagnetic waves, and many actual systems can be described by fractional-order differential equations, making the slowly developed fractional calculus be a resurgence of interest [1–10]. Today, fractional-order systems described by fractional operators play a very important role in control fields [11–13]. Using the traditional integer-order differential equations as a method of describing dynamic system models has great limitation in biological engineering, cell engineering, neural network engineering, and some other emerging fields. However, the models established by fractional calculus can often achieve more satisfying and unexpected results [9, 14, 15]. Actually, the physical models established by the theory of fractional-order calculus are more concise and accurate in presentation when describing the complex problems of physics. In addition, the fractional controller not only can expand the freedom of the controlled system but also is able to obtain better control performance. Furthermore, the feature that fractional calculus has the function of memory makes the system's states in the future be related to the previous and current states. Thus the memory and genetic characteristics of certain processes and materials can be expressed more accurately, which is conducive to improving the control effect of the systems [16, 17].

It is well known that chaos has potential application values and great prospect in secure communication and other areas [18–22]. Recently, fractional-order chaotic systems and hyperchaotic systems have been studied in a widespread way and have been payed close attention with the deepening of theoretical research of fractional-order systems [23–26]. Many scholars have studied the synchronization control problems for fractional-order chaotic systems. So far, there are many control methods for fractional-order nonlinear chaotic systems (such as drive-response method, finite-time synchronization, nonlinear feedback method, adaptive synchronization control method, nonlinear disturbance observer method, nonlinear coupling method, sliding method, PC method, Lyapunov function activated method,

and synchronization control method [27–33]). It is worth noting that the above literatures which study the problem of fractional-order chaotic systems synchronization have a basic assumption that the controller does not have any restrictions. However, almost all actuators in actual control systems have full amplitude or amplitude constraint problem (the amplitude of the output of the controller is limited artificially for reliability [34]). In addition, the presence of the input saturation of the control systems tends to attenuate the good performance of the system and even leads to instability of the closed-loop system. So many scholars have conducted extensive research in integer-order systems with input saturation in the recent years (literatures [35–37], etc.). Little work has been done to study the synchronous control of fractional-order nonlinear chaotic systems with input saturation.

In this paper, the adaptive fuzzy synchronization of uncertain fractional-order nonlinear systems with input saturation and external disturbance is investigated on the basis of the above discussions. Fuzzy logic systems are used to approximate the fully unknown nonlinear functions of the systems. A fractional adaptive fuzzy synchronization controller is designed, and we prove the stability of the chaotic systems according to the fractional Lyapunov stability criterion. The main work of this paper can be concluded as follows: (1) The synchronization of fractional-order chaotic systems with input saturation and external disturbance is discussed in this paper. (2) An adaptive fuzzy synchronization controller is designed and fractional adaptive laws are designed to update the values of the parameters online.

2. Preliminaries

2.1. Preliminaries of Fractional Calculus. With the history of more than 300 years, there are many definitions of fractional calculus. But the most commonly used definitions are Grünwald-Letnikov, Caputo, and Riemann-Liouville definitions [11]. We choose Caputo's derivative in this paper as its Laplace transform requires the initial values of the classical integer-order systems.

The αth fractional integral operator is defined as

$$\mathscr{J}_\tau^{-\alpha} f(\tau) = {}_0D_\tau^{-\alpha} f(\tau) = \frac{1}{\Gamma(\alpha)} \int_0^\tau (\tau-\nu)^{\alpha-1} f(\nu)\, d\nu, \quad (1)$$

where $\Gamma(z) = \int_0^\infty \tau^{z-1} e^{-\tau} d\tau$ represents Euler's Gamma function. The αth fractional derivative operator is given as

$$D_t^\alpha f(\tau) = \frac{1}{\Gamma(n-\alpha)} \int_0^\tau (\tau-\nu)^{n-\alpha-1} f^{(n)}(\nu)\, d\nu, \quad (2)$$

where $n-1 \leq \alpha < n$ and n is an integer. And the Laplace transform of the formed formula (2) is

$$\int_0^\infty e^{-st} D_\tau^\alpha f(\tau)\, d\tau = s^\alpha F(s) - \sum_{k=0}^{n-1} s^{\alpha-k-1} f^{(k)}(0). \quad (3)$$

The following properties of fractional calculus hold.

Property 1 (see [38]). Suppose that $x(\tau) \in C^1[0,T]$, $T > 0$; then

$$D_\tau^{\alpha_1} D_\tau^{\alpha_2} x(\tau) = D_\tau^{\alpha_1+\alpha_2} x(\tau), \quad (4)$$

where $\alpha_1, \alpha_2 > 0$ and $\alpha_1 + \alpha_2 \leqslant 1$.

Property 2 (see [38]). The linearity of the Caputo fractional operator is as follows:

$$D_\tau^\alpha \left(\lambda x(\tau) + \omega y(\tau)\right) = \lambda D_\tau^\alpha x(\tau) + \omega D_\tau^\alpha y(\tau), \quad (5)$$

where λ and ω are two real constants.

Remark 1. If c is a constant, then its Caputo derivative is 0. Namely, $D_\tau^\alpha c = 0$. Particularly, we have $D_\tau^\alpha 0 = 0$.

Property 3 (see [11]). Let $x(\tau) \in C^1[0,T]$ and $0 < \alpha < 1$; then

$$\begin{aligned} D_\tau^{-\alpha} D_\tau^\alpha x(\tau) &= x(\tau) - x(0), \\ D_\tau^\alpha D_\tau^{-\alpha} x(\tau) &= x(\tau). \end{aligned} \quad (6)$$

Note that the above properties hold if and only if $0 < \alpha < 1$. Consequently, only the case where $0 < \alpha < 1$ is involved in the controller design and stability analysis. For convenience, in the rest of this paper, we always assume that $\alpha \in (0,1)$.

2.2. Fuzzy Logic Systems. A fuzzy logic system (FLS) consists of four parts (cf. [8, 9, 39–44]): the knowledge base, the fuzzifier, the fuzzy inference engine working on the fuzzy rules, and the defuzzifier. Usually, a fuzzy logic system is modeled by

$$\widehat{y} = \frac{\sum_{j\in J} w_j(t)\, \mu_j(x(t))}{\sum_{j\in J} \mu_j(x(t))}, \quad (7)$$

where $\widehat{y}$ (a Lipschitz continuous mapping from a compact subset $\Omega \subseteq \mathscr{R}^n$ to the real line $\mathscr{R}$) is called the output of the fuzzy logic system, $x = [x_1, \ldots, x_n]^T \in C^1[\mathscr{I}, \Omega]$ (the set of all continuous mappings from $\mathscr{I} = [0, +\infty) \subseteq \mathscr{R}$ to Ω which have continuous derivatives) is called the input vector which is defined by $x(t) = [x_1(t), \ldots, x_n(t)]^T$ ($\forall t \in \mathscr{I}$), $J = \prod_{i=1}^n \mathscr{F}_i$, $\mathscr{F}_i$ consists of N_i fuzzy sets ($1 \leq i \leq n$), μ_j (a mapping from $\mathscr{R}^n$ to the closed unit interval $[0,1] \subseteq \mathscr{R}$) is called the membership function of rule j ($j \in J$), and w_j (a mapping from $\mathscr{I}$ to $\mathscr{R}$) is called the centroid of the jth consequent set ($j \in J$); we may identify J with $\{1, 2, \ldots, N\}$ for the sake of convenience. Write $\mathscr{W}(t) = [w_1(t), \ldots, w_N(t)]^T$ and $\varphi(x(t)) = [q_1(x(t)), q_2(x(t)), \ldots, q_N(x(t))]^T$, where q_j (called the jth fuzzy basis function, $j \in J$) is a continuous mapping (and thus $\varphi\Omega \to \mathscr{R}^N$ is continuous) defined by

$$q_j(x(t)) = \frac{w_j(t)}{\sum_{s\in J} \mu_s(x(t))}. \quad (8)$$

Then system (7) can be rewritten as

$$y = \mathscr{W}^T \varphi(X). \quad (9)$$

In contrast to conventional control techniques, fuzzy logic systems are best utilized in complex ill-defined processes that can be controlled by a skilled human operator without much knowledge of their underlying dynamics. The basic idea behind fuzzy logic systems is to incorporate the "expert experience" of a human operator in the design of the controller in controlling a process whose input-output relationship is described by a collection of fuzzy control rules involving linguistic variables rather than a complicated dynamic model.

The fuzzy logic system (9) is employed to approximate the unknown nonlinear function $f(\mu)$ in this paper. It can be expressed as

$$f(\mu) = \mathscr{W}^{*T}\varphi(\mu) + \epsilon(\mu), \tag{10}$$

where $\epsilon(\mu)$ is the ideal vector of the approximation error. $\mathscr{W}^*$ is the ideal weight matrix which can be expressed as

$$\mathscr{W}^* = \arg\min_{\mathscr{W}} \left[\sup\left|\widehat{f}(\mu) - f(\mu)\right|\right], \tag{11}$$

where $\widehat{f}(\mu)$ is the estimation of $f(\mu)$.

3. Adaptive Fuzzy Synchronization Controller Design and Stability Analysis

3.1. Problem Statement. Consider the following fractional-order chaotic systems:

$$D_t^\alpha x(t) = Ax(t) + f(x(t)), \tag{12}$$

$$D_t^\alpha y(t) = Cy(t) + g(y(t)) + \mathrm{sat}(u) + d(t), \tag{13}$$

where $x(t) = [x_1(t), \ldots, x_n(t)]^T \in R^n$ is the state vector of the drive system (12) and $y(t) = [y_1(t), \ldots, y_n(t)]^T \in R^n$ is the state vector of the response system (13). $f_i(\cdot)$ and $g_i(\cdot)$, $i = 1, 2, \ldots, n$, are two unknown nonlinear functions, A and $C \in R^{n\times n}$ are two constant matrices, $d(t) \in R^n$ is the external disturbance, $\mathrm{sat}(u) \in R^n$ represents the input saturation, and $u(t) \in R^n$ is the control input.

Remark 2. In theoretical analysis, one often hopes that the input value and the output value can keep proportionally synchronized change when the former is relatively small. However, when the input value increases to a certain extent due to the system limitation factor, the output value of the actual conditions is no longer increasing but tends to or stays at a certain value in practical systems. This is said to be "saturation" phenomenon which is shown in Figure 1.

Definition 3 (see [45, 46]). A mapping from R^n to R^n sat : $\nu \to \mathrm{sat}(\nu)$ is called a saturator, where $\nu = [\nu_1, \nu_2, \ldots, \nu_n]^T \in R^n$ and $\mathrm{sat}(\nu) = [\mathrm{sat}(\nu_1), \mathrm{sat}(\nu_2), \ldots, \mathrm{sat}(\nu_n)]^T$. The definition of $\mathrm{sat}(u)$ is as follows:

$$\mathrm{sat}(u(t)) = \begin{cases} u_r, & u(t) \geq u_r \\ u(t), & u_l < u(t) < u_r \\ u_l, & u(t) \leqslant u_l. \end{cases} \tag{14}$$

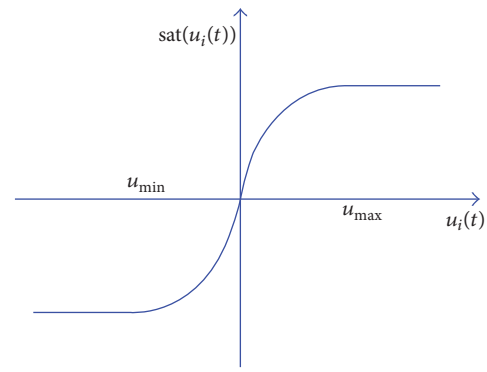

Figure 1: The phenomenon of saturation.

Suppose that the part that exceeds the saturation limiter is referred to as $\delta(t)$; then one has

$$\delta(t) = \begin{cases} u_r - u(t), & u(t) \geq u_r \\ 0, & u_l < u(t) < u_r \\ u_l - u(t), & u(t) \leqslant u_l, \end{cases} \tag{15}$$

where u_r and u_l are called saturated amplitude satisfying $u_l < 0$ and $u_r > 0$.

Assumption 4. The external disturbance $d_i(\cdot)$ is a bounded continuous function. Namely, there exists an unknown constant $\rho_i > 0$ such that

$$\left|d_i(\cdot)\right| \leqslant \rho_i, \quad (i = 1, 2, \ldots, n). \tag{16}$$

Remark 5. It should be pointed out that Assumption 4 is reasonable. We just need the boundaries of the external disturbances, and their exact values are not needed in the process of designing the controller.

The objective of our work is to design an appropriate adaptive fuzzy controller such that the synchronization error $e(t) = y(t) - x(t)$ tends to zero asymptotically (namely, $\lim_{t\to\infty}\|e(t)\| = 0$).

3.2. Controller Design. The dynamical equation of the synchronization error can be described as

$$\begin{aligned} D_t^\alpha e(t) = {} & Ce(t) + (C - A)x(t) + g(y(t)) - f(x(t)) \\ & + \mathrm{sat}(u) + d(t). \end{aligned} \tag{17}$$

Based on the definition of $\mathrm{sat}(u)$, we can obtain that

$$\mathrm{sat}(u) = u(t) + \delta(t). \tag{18}$$

Then (17) can be rewritten as

$$\begin{aligned} D_t^\alpha e(t) = {} & Ce(t) + (C - A)x(t) + g(y(t)) - f(x(t)) \\ & + u(t) + \delta(t) + d(t). \end{aligned} \tag{19}$$

Consider

$$h(x(t), y(t)) = h(t) = (C - A)x(t) + g(y(t)) - f(x(t)) + \delta(t). \quad (20)$$

Nothing that the nonlinear function $h(t)$ is unknown, it can be approximated, through the fuzzy logic system (9), as

$$\widehat{h}_i(t) = \mathscr{W}_i^T(t)\varphi_i(x), \quad (21)$$

where $\mathscr{W}_i^* = \arg\min_{\mathscr{W}_i(t)}[\sup|h_i(t) - \widehat{h}_i(t, \mathscr{W}_i(t))|]$. Let the unknown constant estimation error of the fuzzy logic systems and the approximation error, respectively, be

$$\widetilde{\mathscr{W}}_i(t) = \mathscr{W}_i(t) - \mathscr{W}_i^*, \quad \epsilon_i(t) = h_i(t) - \widehat{h}_i(t, \mathscr{W}_i^*). \quad (22)$$

The following assumption is needed in the controller design.

Assumption 6. Suppose that the estimation error $\epsilon_i(t)$ is bounded; namely, $|\epsilon_i| \leqslant \epsilon_i{}^*$, where $\epsilon_i{}^* > 0$ is an unknown constant ($i = 1, 2, \ldots, n$).

Then the estimated error of unknown nonlinear function $h(t)$ can be written as

$$\begin{aligned}\widehat{h}(t, \mathscr{W}) - h(t) &= \widehat{h}(t, \mathscr{W}) - \widehat{h}(t, \mathscr{W}^*) + \widehat{h}(t, \mathscr{W}^*) - h(t) \\ &= \widehat{h}(t, \mathscr{W}) - \widehat{h}(t, \mathscr{W}^*) - \epsilon(t) \\ &= \widetilde{\mathscr{W}}^T(t)\varphi(x) - \epsilon(t),\end{aligned} \quad (23)$$

where $\mathscr{W}^* = [\mathscr{W}_1^*, \mathscr{W}_2^*, \ldots, \mathscr{W}_m^*]^T$.

Based on the above discussion, the synchronization controller $u(t)$ can be designed as

$$u(t) = -Ke(t) - \mathscr{W}^T(t)\varphi(x) - H\ \mathrm{sign}(e(t)) - \widehat{\rho}\ \mathrm{sign}(e(t)), \quad (24)$$

where $K = \mathrm{diag}[k_1, k_2, \ldots, k_n] \in R^{n\times n}$ and $k_i > 0$ is the designed parameter. $H = \mathrm{diag}[\epsilon_1^*, \ldots, \epsilon_n^*]$, $\widehat{\rho} = \mathrm{diag}[\widehat{\rho}_1, \widehat{\rho}_2, \ldots, \widehat{\rho}_n] \in R^{n\times n}$, and $\widehat{\rho}_i$ is the estimation of ρ_i ($i = 1, 2, \ldots, n$). The fuzzy parameters and $\widehat{\rho}_i(t)$ are, respectively, updated by

$$D_t^\alpha \mathscr{W}_i(t) = \mu_i e_i(t)\varphi_i(x), \quad (25)$$

$$D_t^\alpha \widehat{\rho}_i(t) = \gamma_i |e_i(t)|, \quad (26)$$

where $\mu_i, \gamma_i > 0$ are positive design parameters.

Remark 7. The above fractional adaptive laws are used to update the adjustable parameters. Notice that (26) can also be written as the following equation:

$$\widehat{\rho}_i(\nu) = \widehat{\rho}_i(0) + \frac{1}{\Gamma(\alpha)}\int_0^\nu \gamma_i(\nu - \tau)^{\alpha-1}|e_i(\tau)|\,d\tau. \quad (27)$$

Definition 8 (see [11]). Mittag-Leffler functions (M-L functions) with one parameter and two parameters are, respectively, defined as

$$E_\alpha(t) = \sum_{k=0}^{\infty}\frac{t^k}{\Gamma(\alpha k + 1)}, \quad (28)$$

$$E_{\alpha,\beta}(t) = \sum_{k=0}^{\infty}\frac{t^k}{\Gamma(\alpha k + \beta)}, \quad (29)$$

where $\alpha, \beta > 0$. The Laplace transform of (29) is expressed as

$$\mathscr{L}\left(t^{\beta-1}E_{\alpha,\beta}(-\lambda t^\alpha)\right) = \frac{s^{\alpha-\beta}}{s^\alpha + \lambda}, \quad \left(\mathrm{Re}(s) > |\lambda|^{1/\alpha}\right), \quad (30)$$

where $t \geq 0$ and $\lambda \in R$.

Lemma 9 (fractional Lyapunov second method [11]). *Let the origin be the equilibrium point of the following system:*

$$D_t^\alpha x(t) = f(t, x(t)), \quad (31)$$

where $x(t) \in R^n$ is the system variable and $f(t, x(t)) \in R^n$ is nonlinear function that satisfies the local Lipschitz condition. If there exists Lyapunov function $\mathscr{V}(t, x(t))$ and positive parameters h_1, h_2, and h_3 such that

$$h_1\|x(t)\| \leq \mathscr{V}(t, x(t)) \leq h_2\|x(t)\|, \quad D_t^\alpha \mathscr{V}(t, x(t)) \leq -h_3\|x(t)\|, \quad (32)$$

then system (31) is asymptotically stable.

Lemma 10 (see [47]). *Suppose that $x(t) \in R^n$ is a continuously differentiable function; then one has*

$$\frac{1}{2}D_t^\alpha x^T(t)x(t) \leq x^T(t)D_t^\alpha x(t). \quad (33)$$

Lemma 11 (fractional monotonic principle [47]). *If $D_t^\alpha x(t) \geq 0$, then $x(t)$ is monotonically increasing in $[0, +\infty)$. If $D_t^\alpha x(t) \leqslant 0$, then $x(t)$ is monotonically decreasing in $[0, +\infty]$.*

Lemma 12 (see [9, 47]). *Let $V_1(t) = (1/2)x^2(t) + (1/2)y^2(t)$; $x(t)$ and $y(t) \in R$ are two continuous functions. If there exists a positive constant k satisfying*

$$D_t^\alpha V_1(t) \leqslant -kx^2(t), \quad (34)$$

then one has the following inequality:

$$x^2(t) \leqslant 2V_1(0)E_\alpha(-2kt^\alpha). \quad (35)$$

Lemma 13. *Suppose that $V(t) = (1/2)x^T(t)x(t) + (1/2)y^T(t)y(t)$, where $x(t), y(t) \in R^n$ have continuous derivative. If there exists a constant $h > 0$ such that*

$$D_t^\alpha V(t) \leqslant -hx^T(t)x(t), \quad (36)$$

then $\|x(t)\|$ and $\|y(t)\|$ are bounded for all $t > 0$, and $x(t)$ converges to zero asymptotically.

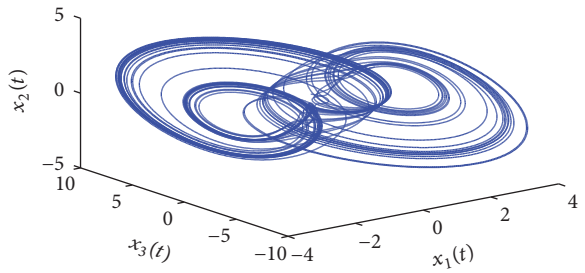

Figure 2: Fractional-order Arneodo system.

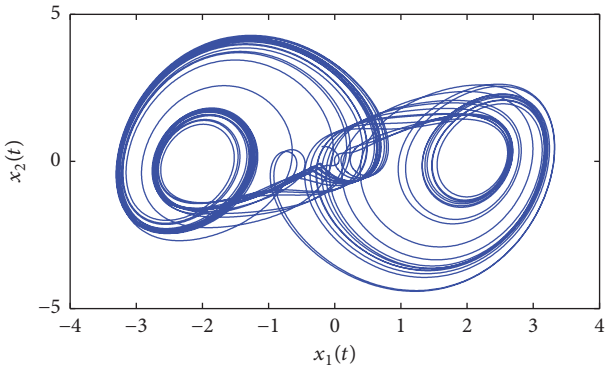

Figure 3: The chaotic behavior of fractional-order Arneodo system in x_1-x_2 plane.

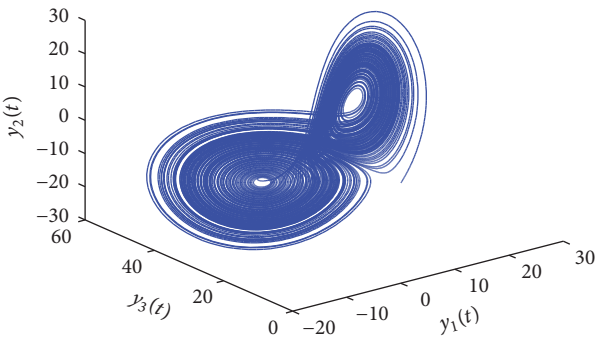

Figure 4: Fractional-order Lorenz system.

Proof. From (36), we have

$$D_t^{\alpha} V_2(t) \leqslant -h x^T(t)\, x(t) \leqslant 0. \tag{37}$$

Based on Lemma 11, we know that $V_2(t)$ is monotonically decreasing in $[0, +\infty]$. Then

$$V_2(t) \leqslant V_2(0). \tag{38}$$

Thus, $\|x(t)\| \leqslant \sqrt{2V_2(0)}$ and $\|y(t)\| \leqslant \sqrt{2V_2(0)}$; namely, $\|x(t)\|$ and $\|y(t)\|$ are bounded. Next we will prove that $x(t)$ tends to 0 asymptotically. Taking αth integral on both sides of (37), we have

$$V_2(t) - V_2(0) \leqslant -h D_t^{-\alpha} x^T(t)\, x(t). \tag{39}$$

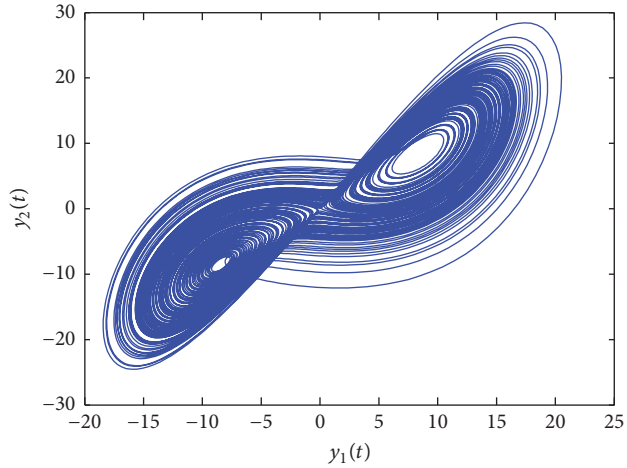

Figure 5: The chaotic behavior of fractional-order Lorenz system in y_1-y_2 plane.

Noting that $V_2(t) = (1/2)x^T(t)x(t) + (1/2)y^T(t)y(t)$, we have $x^T(t)x(t) \leqslant 2V_2(t)$. Consequently,

$$x^T(t)\, x(t) \leqslant 2V_2(0) - 2h D_t^{-\alpha} x^T(t)\, x(t). \tag{40}$$

Thus, we can find a nonnegative function $Z(t)$ such that

$$x^T(t)\, x(t) + Z(t) = 2V_2(0) - 2h D_t^{-\alpha} x^T(t)\, x(t). \tag{41}$$

Taking *Laplace* transform on both sides of (41), we have

$$X^T(s)\, X(s) = 2V_2(0)\, \frac{s^{\alpha-1}}{s^{\alpha} + 2h} - \frac{s^{\alpha}}{s^{\alpha} + 2h} Z(s). \tag{42}$$

According to (30), the solution of (42) is

$$\begin{aligned} x^T(t)\, x(t) = {} & 2V_2(0)\, E_{\alpha,0}\left(-2ht^{\alpha}\right) - Z(t) \\ & * \left[t^{-1} E_{\alpha,0}\left(-2ht^{\alpha}\right)\right], \end{aligned} \tag{43}$$

where $*$ is convolution. Because t^{-1} and $E_{\alpha,0}(-2ht^{\alpha})$ are nonnegative functions, it follows from Lemma 12 that $x(t)$ converges to zero asymptotically. This completes the proof of Lemma 13. □

Remark 14. If $x^T(t)x(t) \leqslant 2V_2(0)E_{\alpha}(-2ht^{\alpha})$, we know that $x(t)$ will tend to 0 asymptotically according to the results in [48]. Namely, $\lim_{t\to\infty}\|x(t)\| = 0$.

3.3. Stability Analysis

Theorem 15. *If $d(t) = 0$, we can realize the synchronization of system (12) and (13) under the effect of the adaptive controller (24) and the fractional-order adaptive law (25). And all the variables in the closed-loop system remain bounded.*

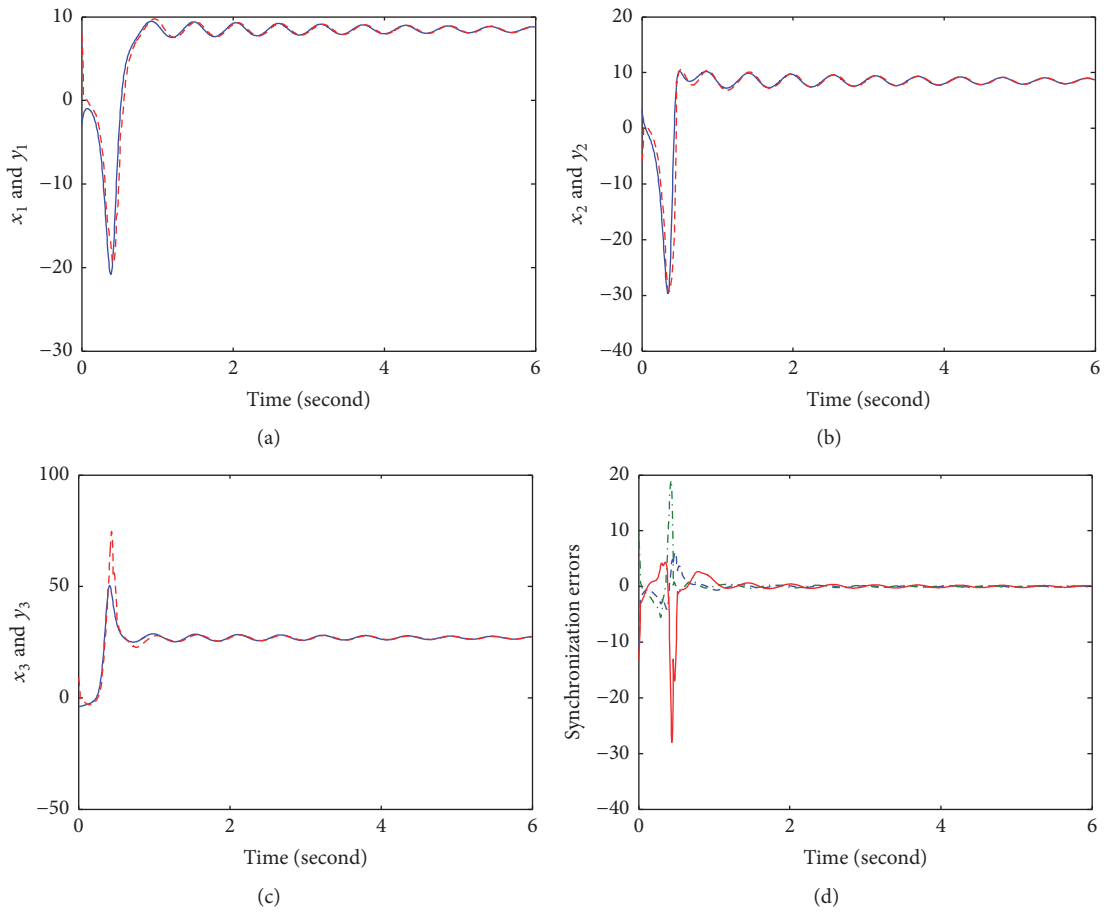

FIGURE 6: Synchronization results: (a) $x_1(t)$ (solid line) and $y_1(t)$ (dashed-dotted line); (b) $x_2(t)$ (solid line) and $y_2(t)$ (dashed-dotted line); and (c) $x_3(t)$ (solid line) and $y_3(t)$ (dashed-dotted line). (d) Synchronization errors: $e_1(t)$ (dashed line), $e_2(t)$ (dashed-dotted line), and $e_3(t)$ (solid line).

Proof. Substituting the synchronization controllers (24) and (23) into the error dynamical equation (19), we have

$$\begin{aligned} D_t^\alpha e(t) &= Ce(t) + h(t) - Ke(t) - \mathscr{W}^T \varphi(x) \\ &\quad - H\ \mathrm{sign}(e(t)) \\ &= -(K-C)\, e(t) + \epsilon(t) - \widetilde{\mathscr{W}}^T \varphi(x) \\ &\quad - H\ \mathrm{sign}(e(t)) \\ &= -Pe(t) + \epsilon(t) - \widetilde{\mathscr{W}}^T \varphi(x) - H\ \mathrm{sign}(e(t)), \end{aligned} \tag{44}$$

where $P = K - C$. We can choose an appropriate gain matrix K such that P is a positive definite matrix. Multiplying $e^T(t)$ on both sides of (44) yields

$$\begin{aligned} e^T(t)\, D_t^\alpha e(t) &= -e^T(t)\, Pe(t) + e^T(t)\, \epsilon(t) \\ &\quad - e^T(t)\, \widetilde{\mathscr{W}}^T \varphi(x) \\ &\quad - e^T(t)\, H\ \mathrm{sign}(e(t)) \\ &\leqslant -e^T(t)\, Pe(t) + \sum_{i=1}^{n} |e_i(t)|\, \epsilon_i^*(t) \\ &\quad - \sum_{i=1}^{n} e_i(t)\, \widetilde{\mathscr{W}}_i^T \varphi_i(x) \\ &\quad - \sum_{i=1}^{n} |e_i(t)|\, \epsilon_i^*(t) \\ &\leqslant -e^T(t)\, Pe(t) - \sum_{i=1}^{n} e_i(t)\, \widetilde{\mathscr{W}}_i^T \varphi_i(x). \end{aligned} \tag{45}$$

Consider the following Lyapunov function:

$$V(t) = \frac{1}{2} e^T(t)\, e(t) + \frac{1}{2} \sum_{i=1}^{n} \frac{1}{\mu_i} \widetilde{\mathscr{W}}_i^T \widetilde{\mathscr{W}}_i. \tag{46}$$

Because the αth Caputo derivative of a constant is 0, we have $D_t^\alpha \widetilde{W}_i = D_t^\alpha W_i$. Taking αth derivative of $V(t)$ based on Lemma 10 gives

$$D_t^\alpha V(t) \leqslant e^T(t)\, D_t^\alpha e(t) + \sum_{i=1}^{n} \frac{1}{\mu_i} \widetilde{\mathscr{W}}_i^T D_t^\alpha \mathscr{W}_i. \tag{47}$$

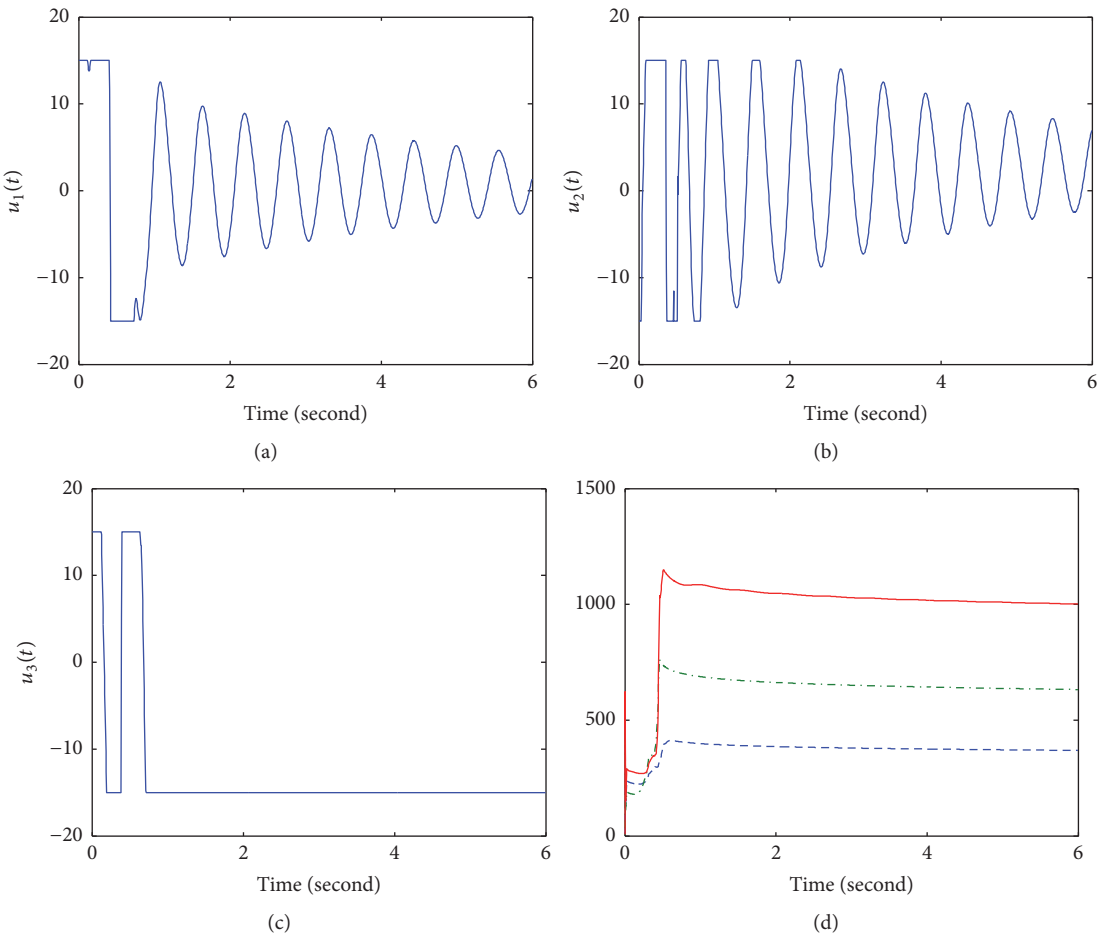

FIGURE 7: Control inputs and parameters: (a) $u_1(t)$; (b) $u_2(t)$; (c) $u_3(t)$; and (d) $\|W_1(t)\|$ (dashed line), $\|W_2(t)\|$ (dashed-dotted line), and $\|W_3(t)\|$ (solid line).

Substituting (45) and (25) into (47), we have

$$\begin{aligned} D_t^\alpha V(t) &\leqslant -e^T(t) Pe(t) - \sum_{i=1}^{n} e_i(t) \widetilde{\mathscr{W}}_i^T \varphi_i(x) \\ &\quad + \sum_{i=1}^{n} \frac{1}{\mu_i} \widetilde{\mathscr{W}}^T{}_i D_t^\alpha \mathscr{W}_i \\ &\leqslant -e^T(t) Pe(t) - \sum_{i=1}^{n} e_i(t) \widetilde{\mathscr{W}}_i^T \varphi_i(x) \\ &\quad + \sum_{i=1}^{n} e_i(t) \widetilde{\mathscr{W}}_i^T \varphi_i(x) \leqslant -e^T(t) Pe(t) \\ &\leqslant -\lambda_{\min} e^T(t) e(t), \end{aligned} \tag{48}$$

where $\lambda_{\min}$ is the minimum eigenvalue of matrix P. From (48) and Lemma 13, we know that the synchronization error $e(t)$ tends to 0 asymptotically; namely, $\lim_{t\to\infty}\|e(t)\| = 0$. □

Theorem 16. *We can realize the synchronization of system (12) and (13) under the effect of the adaptive controller (24) and the fractional-order adaptive laws (see (25) and (26)). And all variables in the closed-loop system remain bounded when* $d(t) \neq 0$.

Proof. Substituting (23) and (24) into the error dynamical equation (19), we obtain

$$\begin{aligned} D_t^\alpha e(t) &= Ce(t) + h(t) + d(t) - Ke(t) - \mathscr{W}^T \varphi(x) \\ &\quad - H \operatorname{sign}(e(t)) - \widehat{\rho} \operatorname{sign}(e(t)) \\ &= -(K - C) e(t) + d(t) + \epsilon(t) - \widetilde{\mathscr{W}}^T \varphi(x) \\ &\quad - H \operatorname{sign}(e(t)) - \widehat{\rho} \operatorname{sign}(e(t)) \\ &\leqslant -Pe(t) + \epsilon(t) - \widetilde{\mathscr{W}}^T \varphi(x) - H \operatorname{sign}(e(t)) \\ &\quad - \widetilde{\rho} \operatorname{sign}(e(t)), \end{aligned} \tag{49}$$

where $P = K - C$ is a positive matrix.

$$\widetilde{\rho}_i(t) = \widehat{\rho}_i(t) - \rho_i. \tag{50}$$

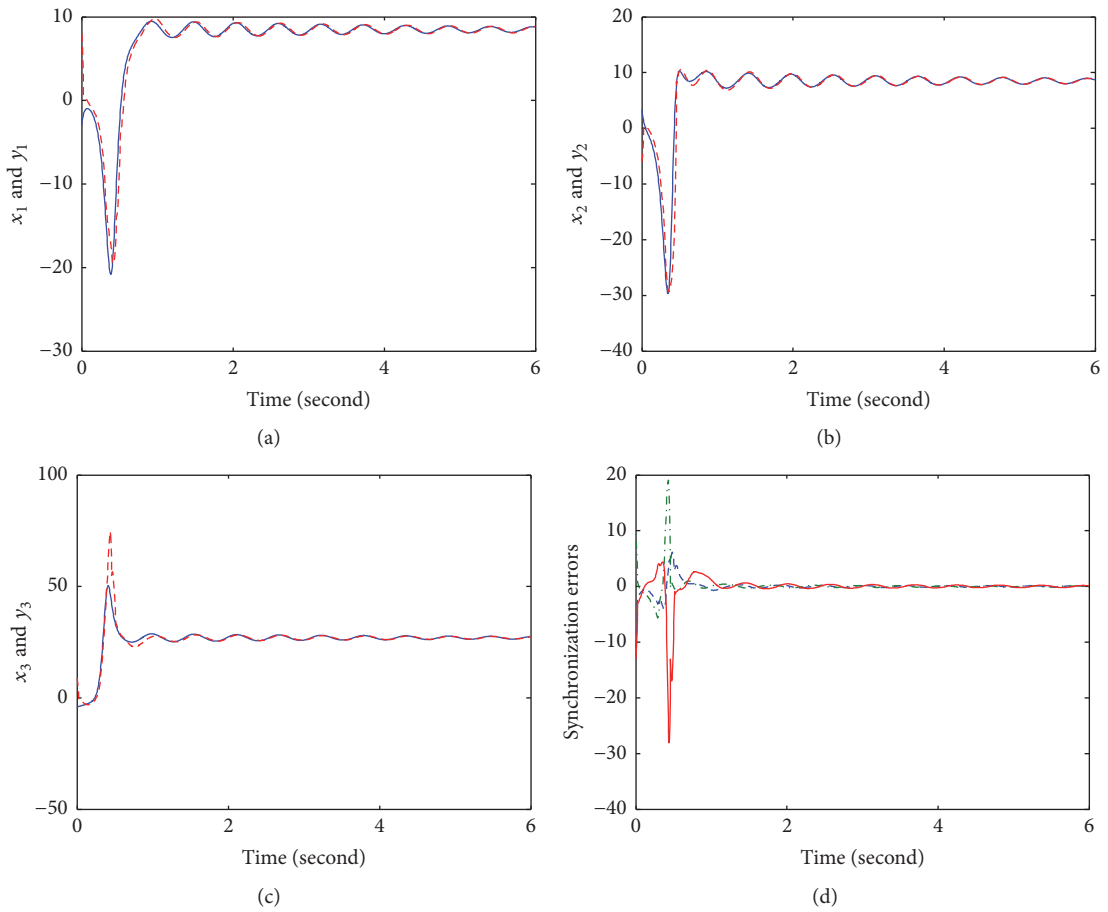

FIGURE 8: Synchronization results: (a) $x_1(t)$ (solid line) and $y_1(t)$ (dashed-dotted line); (b) $x_2(t)$ (solid line) and $y_2(t)$ (dashed-dotted line); and (c) $x_3(t)$ (solid line) and $y_3(t)$ (dashed-dotted line). (d) Synchronization errors: $e_1(t)$ (dashed line), $e_2(t)$ (dashed-dotted line), and $e_3(t)$ (solid line).

Multiplying $e^T(t)$ on both sides of (50) gives

$$\begin{aligned} e^T(t) D_t^\alpha e(t) &= -e^T(t) Pe(t) + e^T(t) \epsilon(t) \\ &\quad - e^T(t) \widetilde{\mathscr{W}}^T \varphi(x) \\ &\quad - e^T(t) H \ \mathrm{sign}(e(t)) \\ &\quad - e^T(t) \tilde{\rho} \ \mathrm{sign}(e(t)) \\ &\leqslant -e^T(t) Pe(t) + \sum_{i=1}^{n} |e_i(t)| \epsilon_i^*(t) \\ &\quad - \sum_{i=1}^{n} e_i(t) \widetilde{\mathscr{W}}_i^T \varphi_i(x) - \sum_{i=1}^{n} \epsilon_i^*(t) |e_i(t)| \\ &\quad - \sum_{i=1}^{n} \tilde{\rho}_i(t) |e_i(t)| \\ &\leqslant -e^T(t) Pe(t) - \sum_{i=1}^{n} e_i(t) \widetilde{\mathscr{W}}_i^T \varphi_i(x) \\ &\quad - \sum_{i=1}^{n} \tilde{\rho}_i(t) |e_i(t)|. \end{aligned} \tag{51}$$

Consider the following Lyapunov function:

$$V(t) = \frac{1}{2} e^T(t) e(t) + \frac{1}{2} \sum_{i=1}^{n} \frac{1}{\mu_i} \widetilde{\mathscr{W}}_i^T \widetilde{\mathscr{W}}_i + \frac{1}{2} \sum_{i=1}^{n} \frac{1}{\gamma_i} \tilde{\rho}_i^2(t). \tag{52}$$

Taking αth derivative of $V(t)$ based on Lemma 10, we have

$$\begin{aligned} D_t^\alpha V(t) &\leqslant e^T(t) D_t^\alpha e(t) + \sum_{i=1}^{n} \frac{1}{\mu_i} \widetilde{\mathscr{W}}_i^T D_t^\alpha \mathscr{W}_i \\ &\quad + \sum_{i=1}^{n} \frac{1}{\gamma_i} \tilde{\rho}_i(t) D_t^\alpha \rho_i(t). \end{aligned} \tag{53}$$

Substituting (45), (25), and (26) into (53), we have

$$\begin{aligned} D_t^\alpha V(t) &\leqslant -e^T(t) Pe(t) - \sum_{i=1}^{n} e_i(t) \widetilde{\mathscr{W}}_i^T \varphi_i(x) \\ &\quad - \sum_{i=1}^{n} \tilde{\rho}_i(t) |e_i(t)| + \sum_{i=1}^{n} \frac{1}{\mu_i} \widetilde{\mathscr{W}}_i^T D_t^\alpha \mathscr{W}_i \\ &\quad + \sum_{i=1}^{n} \frac{1}{\gamma_i} \tilde{\rho}_i(t) D_t^\alpha \rho_i(t) \end{aligned}$$

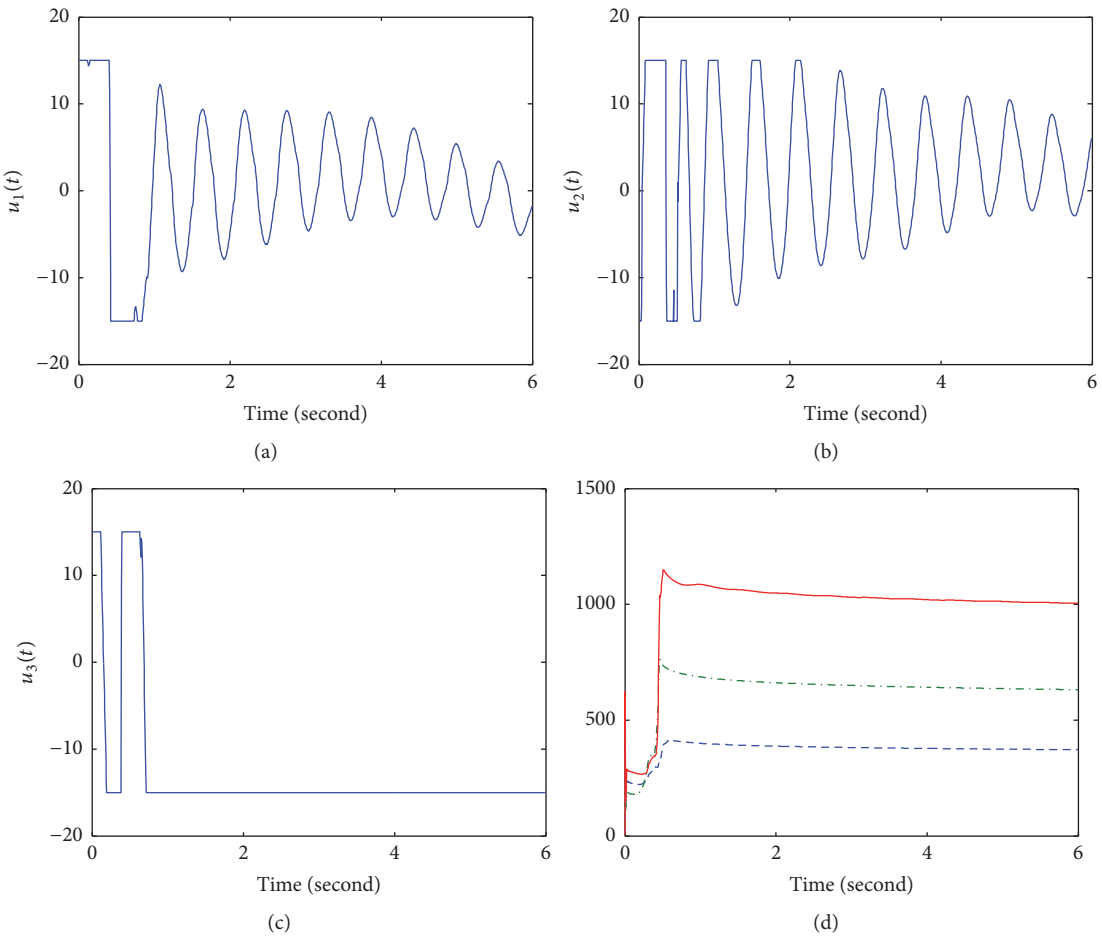

FIGURE 9: Control inputs and parameters: (a) $u_1(t)$; (b) $u_2(t)$; (c) $u_3(t)$; and (d) $\|W_1(t)\|$ (dashed line), $\|W_2(t)\|$ (dotted dashed line), and $\|W_3(t)\|$ (solid line).

$$\begin{aligned}
&\leqslant -e^T(t)\,Pe(t) - \sum_{i=1}^{n} e_i(t)\,\widetilde{\mathscr{W}}_i^T\varphi_i(x) \\
&\quad - \sum_{i=1}^{n}\widetilde{\rho}_i(t)\,|e_i(t)| + \sum_{i=1}^{n} e_i(t)\,\widetilde{\mathscr{W}}_i^T\varphi_i(x) \\
&\quad + \sum_{i=1}^{n}\widetilde{\rho}_i(t)\,|e_i(t)| \leqslant -e^T(t)\,Pe(t) \\
&\leqslant -\lambda_{\min} e^T(t)\,e(t),
\end{aligned} \tag{54}$$

where $\lambda_{\min}$ is the minimum eigenvalue of matrix P. From (54) and Lemma 13, we know that the synchronization error $e(t)$ tends to 0 asymptotically; namely, $\lim_{t\to\infty}\|e(t)\| = 0$. □

4. Simulation Studies

In this section, two fractional-order chaotic systems and two fractional-order hyperchaotic systems will be synchronized to show the validity of the above method.

4.1. Example 1. Choose the frequently used fractional-order Arneodo system [49] in literature as the drive system:

$$\begin{aligned}
D_t^\alpha x_1(t) &= x_2(t) \\
D_t^\alpha x_2(t) &= x_3(t) \\
D_t^\alpha x_3(t) &= a x_1(t) - b x_2(t) - c x_3(t) + d x_1^3(t).
\end{aligned} \tag{55}$$

When $a = -5.5$, $b = 3.5$, $c = 0.4$, $d = -1$, and $\alpha = 0.9$, the fractional-order Arneodo system shows chaotic phenomenon, which is indicated in Figures 2 and 3.

Let the response system be the following fractional-order Lorenz system [50]:

$$\begin{aligned}
D_t^\alpha y_1(t) &= \sigma\left(y_2(t) - y_1(t)\right) \\
D_t^\alpha y_2(t) &= y_1(t)\left(\rho - y_3(t)\right) - y_2(t) \\
D_t^\alpha y_3(t) &= y_1(t)\,y_2(t) - \beta y_3(t).
\end{aligned} \tag{56}$$

When $\sigma = 10$, $\rho = 28$, $\beta = 8/3$, and $\alpha = 0.99$, the chaotic behavior of system (56) is included in Figures 4 and 5.

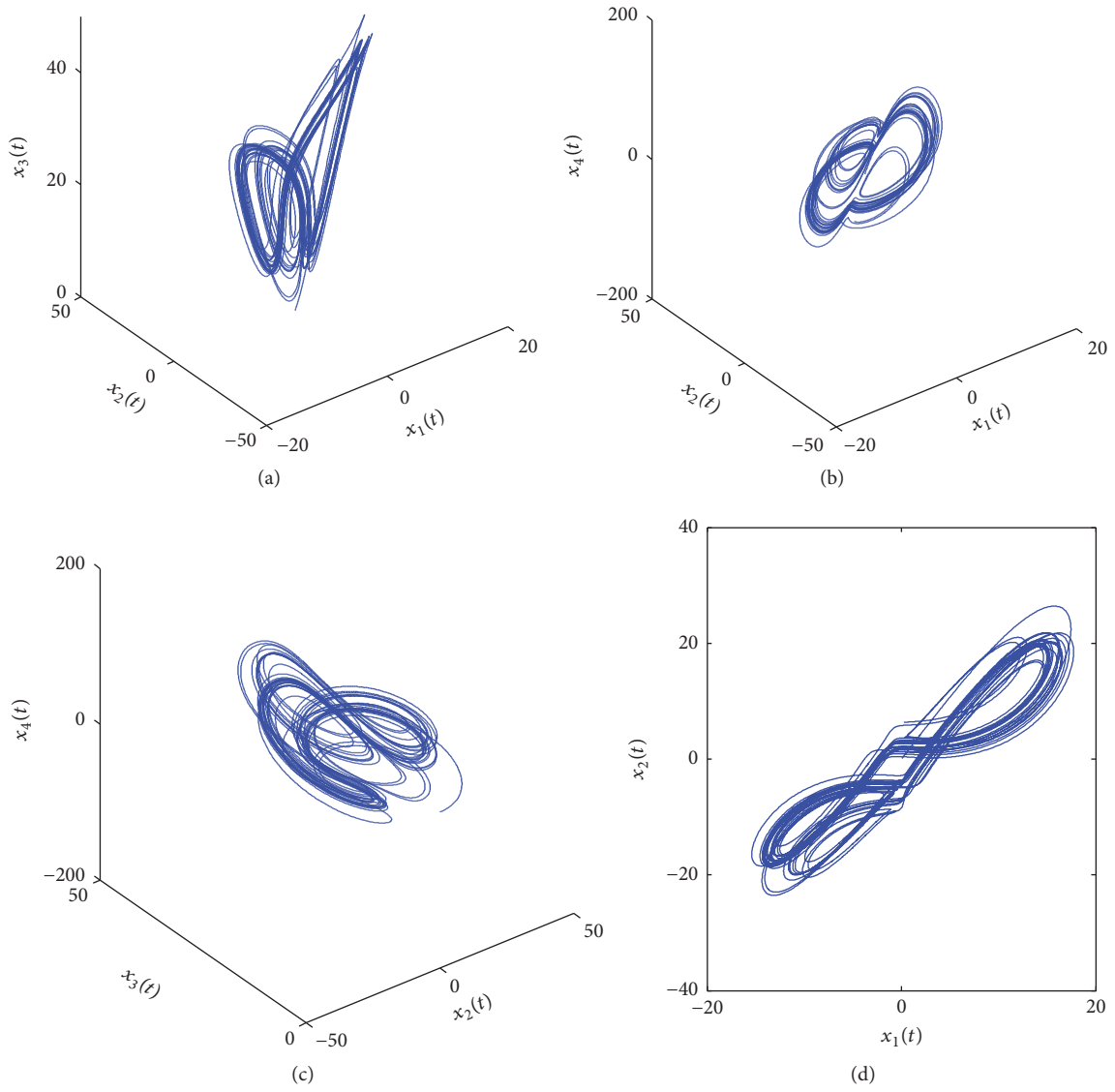

Figure 10: Fractional-order hyperchaotic Lorenz system (58).

It follows from (55) and (56) that

$$A = \begin{pmatrix} 0 & 0 & 0 \\ 0 & 0 & 1 \\ a & -b & -c \end{pmatrix}$$
$$C = \begin{pmatrix} -\sigma & \sigma & 0 \\ \rho & -1 & 0 \\ 0 & 0 & -\beta \end{pmatrix}. \quad (57)$$

Firstly, we consider the synchronization of system (55) and system (56) in the absence of external disturbance (namely, $d(t) = 0$). In the simulation, we choose $\sigma = 0.8$, $\alpha = 0.96$, and $k_1 = k_2 = k_3 = 3$. The initial condition of system (55) is $x(0) = [-3, 3.4, -4]^T$, and the initial condition of system (56) is $y(0) = [8, -6, 9]^T$. With respect to the fuzzy logic system, we define 6 Gaussian membership functions uniformly distributed on $[-20\ 20]$. The initial condition of the fuzzy parameter is chosen as zero vector. The input saturation limiter $u_r = -u_l = 5$. The simulation results are depicted in Figures 6 and 7.

Then we study the synchronization of system (55) and system (56) with the external disturbance. In simulation, we select $\sigma = 0.8$, $\alpha = 0.96$, and $k_1 = k_2 = k_3 = 3$. The initial conditions are $x(0) = [-3, 3.4, -4]^T$ and $y(0) = [8, -6, 9]^T$. Let $d(t) = [0.15\sin(t), 0.05\cos(t), 0.1\cos(t)]^T$ and let the input saturation limiter be $u_r = -u_l = 5$. The simulation results are as shown in Figures 8 and 9.

4.2. Example 2. Choose the fractional-order hyperchaotic Lorenz system [50] as the drive system:

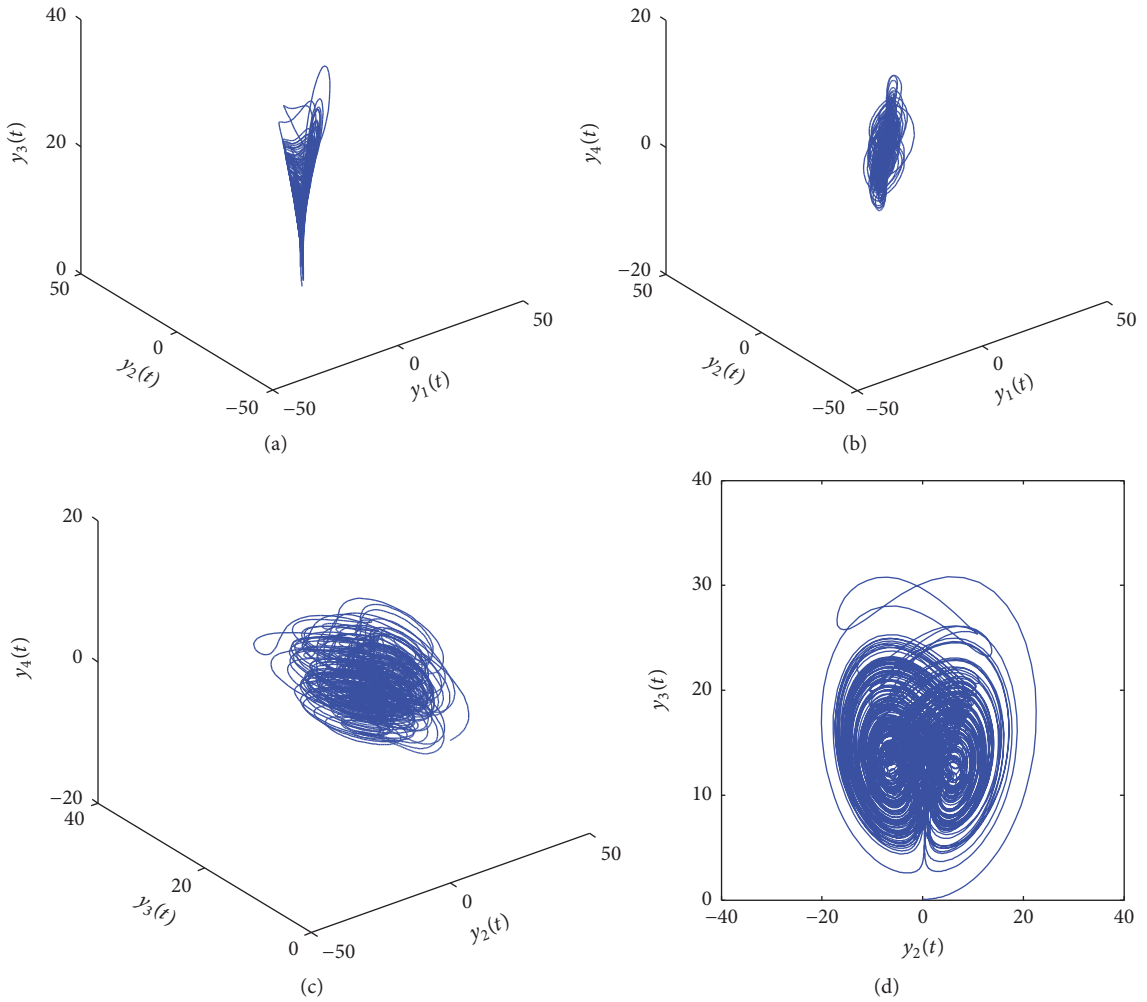

Figure 11: Fractional-order hyperchaotic system (59).

$$
\begin{aligned}
D_t^{\alpha} x_1(t) &= a\left(x_2(t) - x_1(t)\right) + x_4(t) \\
D_t^{\alpha} x_2(t) &= c x_1(t) - x_2(t) - x_1(t)\, x_3(t) \\
D_t^{\alpha} x_3(t) &= x_1(t)\, x_2(t) - b x_3(t) \\
D_t^{\alpha} x_4(t) &= -x_1(t)\, x_3(t) + \gamma x_4(t).
\end{aligned} \tag{58}
$$

When $a = 10$, $b = 8/3$, $c = 28$, $\gamma = -1$, and $\alpha = 0.93$, the fractional-order hyperchaotic Lorenz system (58) has chaotic attractors, as shown in Figure 10.

The response system is the following fractional-order hyperchaotic system:

$$
\begin{aligned}
D_t^{\alpha} y_1(t) &= a\left(y_2(t) - y_1(t)\right) \\
D_t^{\alpha} y_2(t) &= d y_1(t) - y_1(t)\, y_3(t) + c y_2(t) - y_4(t) \\
D_t^{\alpha} y_3(t) &= y_1(t)\, y_2(t) - b y_3(t) \\
D_t^{\alpha} y_4(t) &= y_1(t) + k.
\end{aligned} \tag{59}
$$

When $a = 36.01$, $b = 3.00$, $c = 28.00$, $d = -16.00$, $k = 0.50$, and $\alpha = 0.95$, the chaotic behavior of system (59) is given in Figure 11.

Firstly, we consider the synchronization of system (58) and system (59) when $d(t) = 0$. In the simulation, we choose the control parameters as $\sigma = 0.8$, $\alpha = 0.95$, and $k_1 = k_2 = k_3 = k_4 = 3$. The initial conditions are $x(0) = [-6, 2.4, -4, -6]^T$ and $y(0) = [9.6, -6, 9, 5]^T$. The input saturation limiter $u_{r1} = -u_{l1} = 12$ and $u_{ri} = -u_{li} = 14$, $i = 2, 3, 4$. The simulation results are presented in Figures 12–15.

Then, we consider the synchronization of system (58) and system (59) with external disturbance. In the simulation, let $\sigma = 0.8$, $\alpha = 0.95$, $k_1 = k_2 = k_3 = k_4 = 3$, and $d(t) = [0.15\sin(t), 0.05\cos(t), 0.1\cos(t), 0.5\sin(t)\cos(t)]^T$. The initial conditions are $x(0) = [-3, 3.4, -4, -6]^T$ and $y(0) = [9.6, -6, 9, 5]^T$. The input saturation limiter is $u_{r1} = -u_{l1} = 12$ and $u_{ri} = -u_{li} = 14$, $i = 2, 3, 4$. The simulation results are depicted in Figures 16–19.

5. Conclusions

In this paper, we investigate the synchronization for two uncertain fractional-order nonlinear chaotic systems with saturated input and external disturbances in accordance with

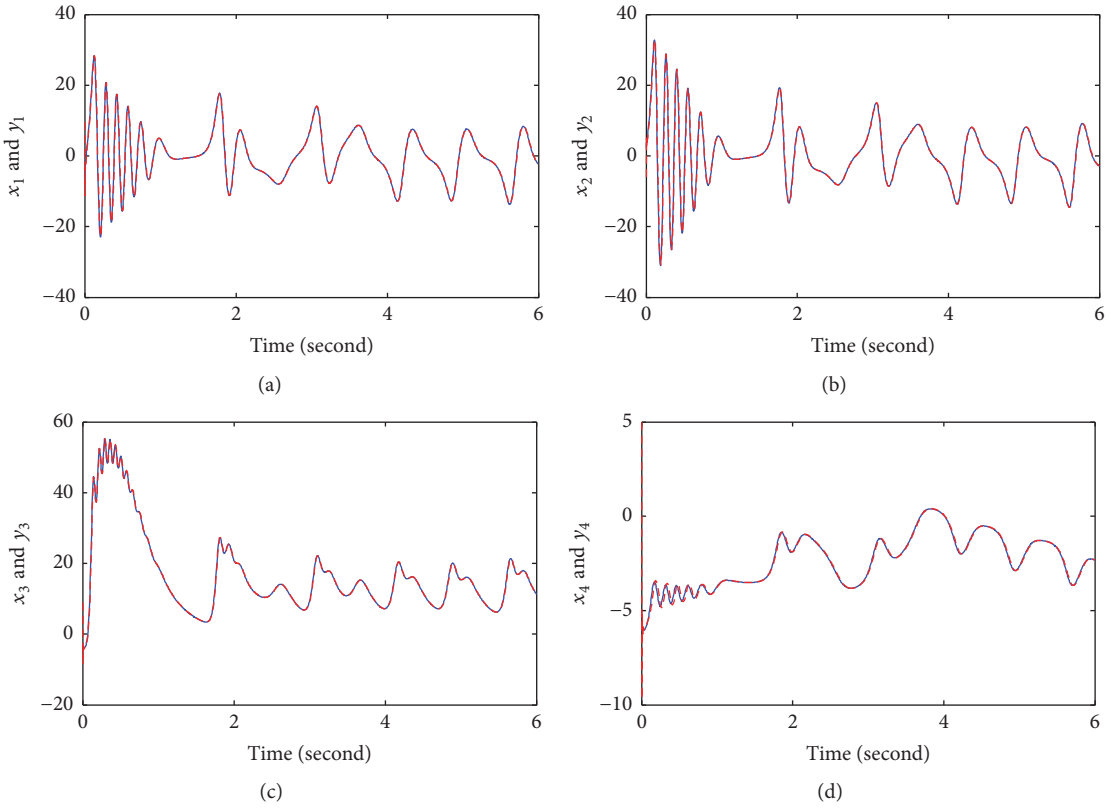

FIGURE 12: Synchronization results: (a) $x_1(t)$ (solid line) and $y_1(t)$ (dashed line); (b) $x_2(t)$ (solid line) and $y_2(t)$ (dashed line); (c) $x_3(t)$ (solid line) and $y_3(t)$ (dashed line); and (d) $x_4(t)$ (solid line) and $y_4(t)$ (dashed line).

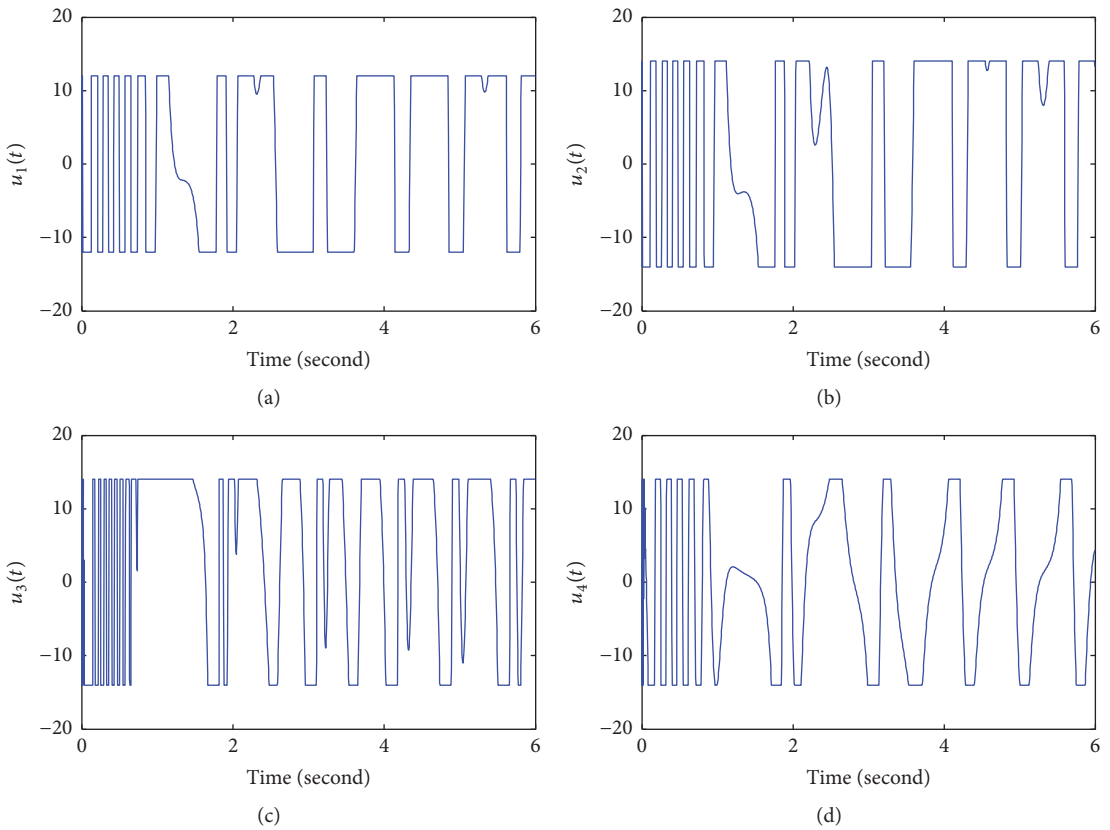

FIGURE 13: Control inputs: (a) $u_1(t)$; (b) $u_2(t)$; (c) $u_3(t)$; and (d) $u_4(t)$.

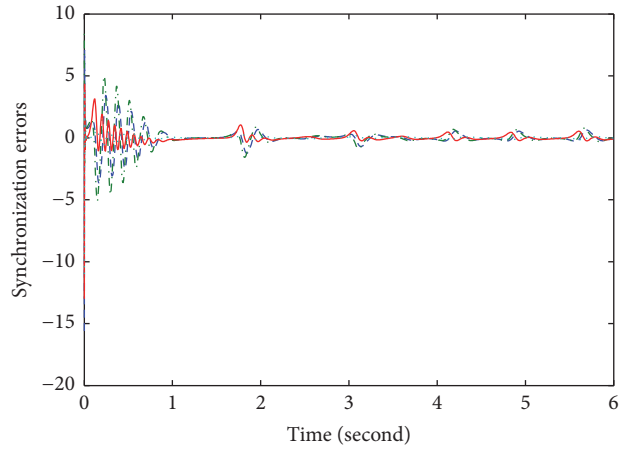

FIGURE 14: Synchronization errors: $e_1(t)$ (dotted line), $e_2(t)$ (dotted dashed line), $e_3(t)$ (solid line), and $e_4(t)$ (dashed line).

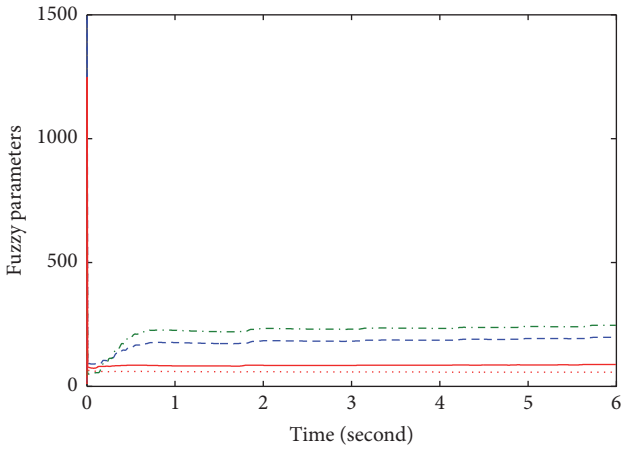

FIGURE 15: Parameters: $\|W_1(t)\|$ (dotted line), $\|W_2(t)\|$ (dotted dashed line), $\|W_3(t)\|$ (solid line), and $|W_4(t)|$ (dashed line).

the fractional Lyapunov stability theory and adaptive fuzzy control method. A fractional-order adaptive controller that can guarantee that the synchronization error tends to a small region of origin and fractional parameters adaptive laws are designed. Based on the proposed method, we can achieve synchronization of many fractional-order chaotic systems and hyperchaotic systems. It should be mentioned that the proposed controller can guarantee that the synchronization errors converge to a small region of the origin eventually. How to design an adaptive fuzzy controller such that the dynamical system is asymptotic stable is one of our future research directions.

Conflicts of Interest

The authors declare that there are no conflicts of interest regarding the publication of this paper.

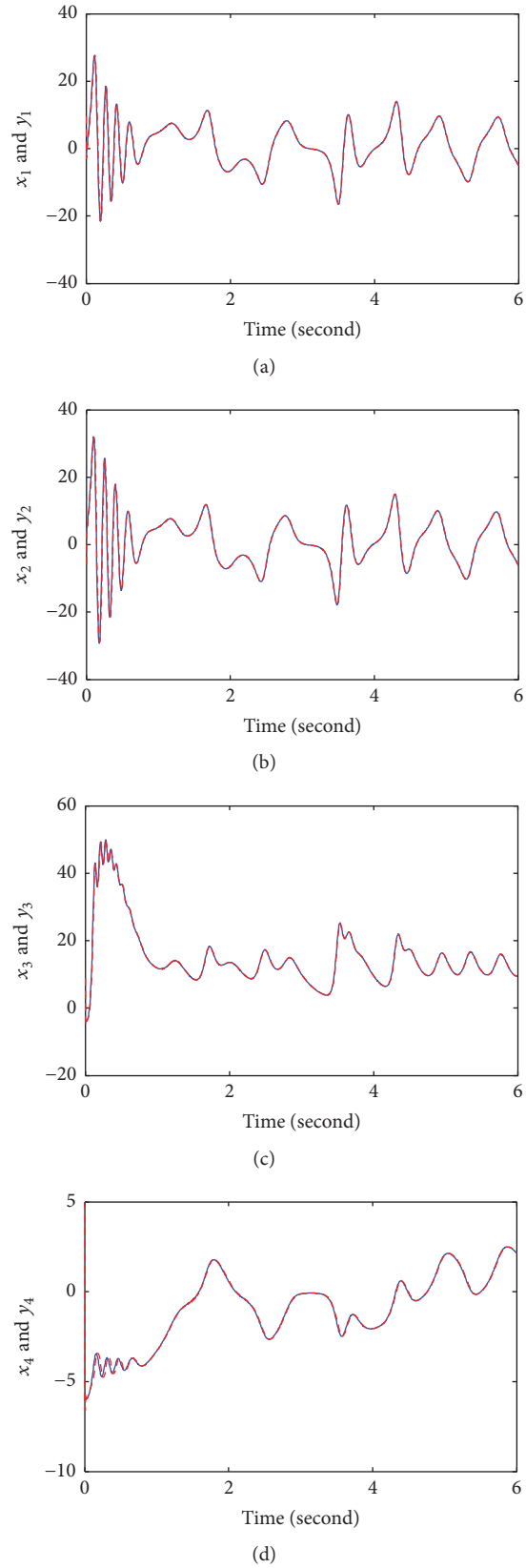

FIGURE 16: Synchronization results: (a) $x_1(t)$ (solid line) and $y_1(t)$ (dashed line); (b) $x_2(t)$ (solid line) and $y_2(t)$ (dashed line); (c) $x_3(t)$ (solid line) and $y_3(t)$ (dashed line); and (d) $x_4(t)$ (solid line) and $y_4(t)$ (dashed line).

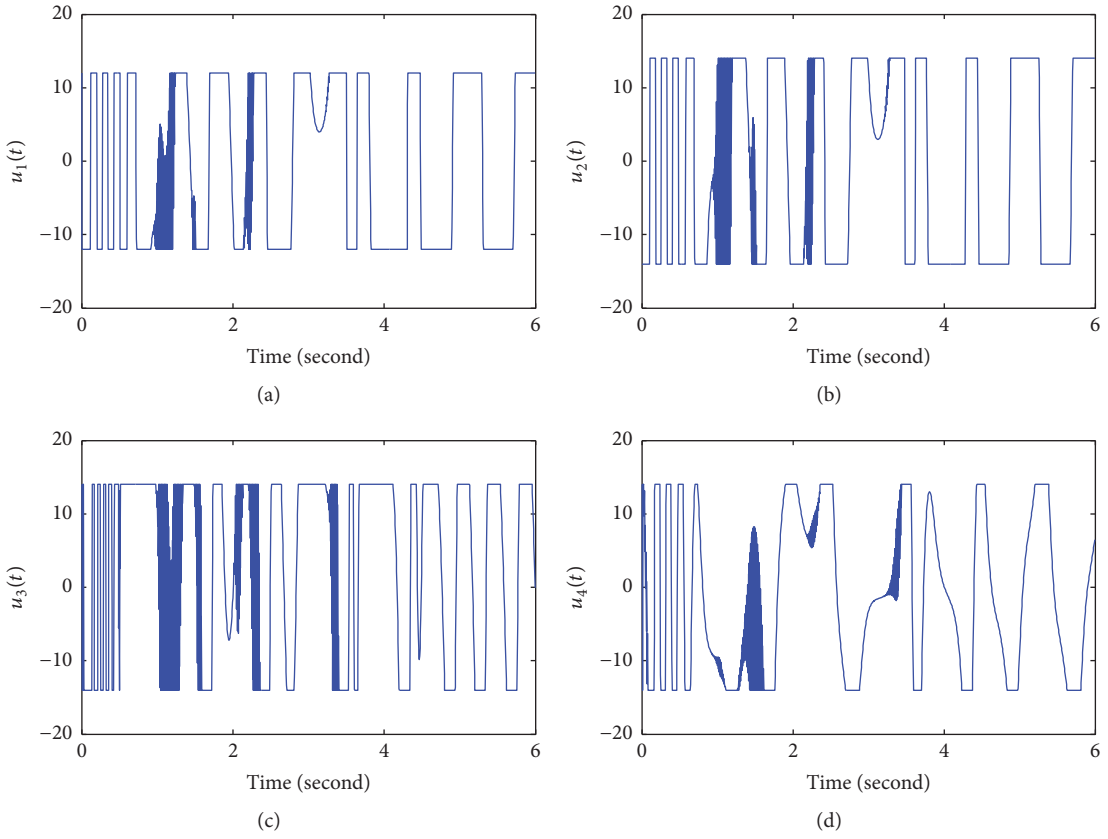

FIGURE 17: Control inputs: (a) $u_1(t)$; (b) $u_2(t)$; (c) $u_3(t)$; and (d) $u_4(t)$.

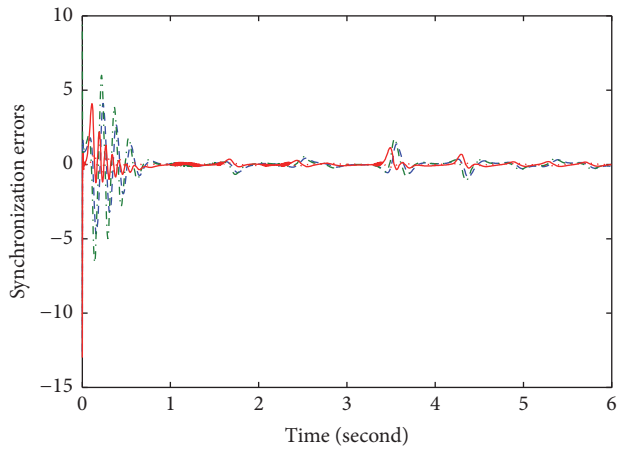

FIGURE 18: Synchronization errors: $e_1(t)$ (dotted line), $e_2(t)$ (dot dash line), $e_3(t)$ (solid line), and $e_4(t)$ (dashed line).

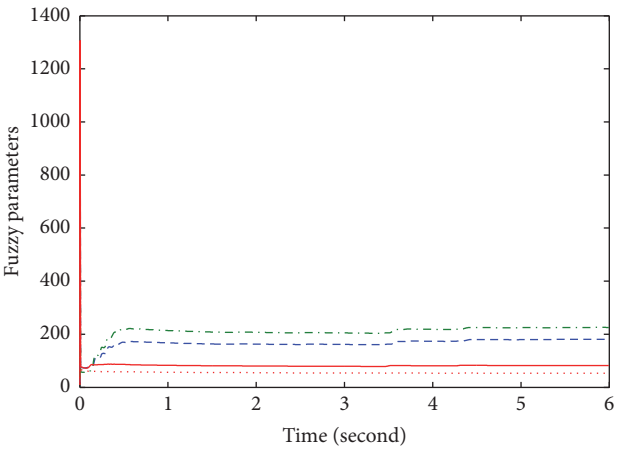

FIGURE 19: Parameters: $\|W_1(t)\|$ (dotted line), $\|W_2(t)\|$ (dotted dashed line), $\|W_3(t)\|$ (solid line), and $\|W_4(t)\|$ (dashed line).

Acknowledgments

This work is supported by the National Natural Science Foundation of China (Grants nos. 11771263 and 11601177), the Natural Science Foundation of Anhui Province of China (Grant no. 1508085QA16), and the Foundation for Distinguished Young Talents in Higher Education of Anhui Province of China (Grant no. GXYQZD2016257).

References

[1] A. Elsaid, "Homotopy analysis method for solving a class of fractional partial differential equations," *Communications in*

Nonlinear Science and Numerical Simulation, vol. 16, no. 9, pp. 3655–3664, 2011.

[2] P. Han and M. E. Schonbek, "Large time decay properties of solutions to a viscous Boussinesq system in a half space," *Advances in Differential Equations*, vol. 19, no. 1-2, pp. 87–132, 2014.

[3] R. M. Balan and C. A. Tudor, "Stochastic heat equation with multiplicative fractional-colored noise," *Journal of Theoretical Probability*, vol. 23, no. 3, pp. 834–870, 2010.

[4] A. Elsaid, "Fractional differential transform method combined with the Adomian polynomials," *Applied Mathematics and Computation*, vol. 218, no. 12, pp. 6899–6911, 2012.

[5] G. S. Frederico and D. F. Torres, "Necessary optimality conditions for fractional action-like problems with intrinsic and observer times," *WSEAS Transactions on Mathematics*, vol. 7, no. 1, pp. 6–11, 2008.

[6] A. Hussain, M. Faryad, and Q. A. Naqvi, "Fractional curl operator and fractional Chiro-waveguide," *Journal of Electromagnetic Waves and Applications*, vol. 21, no. 8, pp. 1119–1129, 2007.

[7] M. Zubair, M. J. Mughal, and Q. A. Naqvi, "An exact solution of the spherical wave equation in D-dimensional fractional space," *Journal of Electromagnetic Waves and Applications*, vol. 25, no. 10, pp. 1481–1491, 2011.

[8] H. Liu, Y. Pan, S. Li, and Y. Chen, "Adaptive Fuzzy Backstepping Control of Fractional-Order Nonlinear Systems," *IEEE Transactions on Systems, Man, and Cybernetics: Systems*, vol. 47, no. 8, pp. 2209–2217, 2017.

[9] H. Liu, S. Li, J. D. Cao, A. G. Alsaedi, and F. E. Alsaadi, "Adaptive fuzzy prescribed performance controller design for a class of uncertain fractional-order nonlinear systems with external disturbances," *Neurocomputing*, vol. 219, pp. 422–430, 2017.

[10] H. Liu, S. Li, G. Li, and H. Wang, "Robust adaptive control for fractional-order financial chaotic systems with system uncertainties and external disturbances," *Information Technology and Control*, vol. 46, no. 2, 2017.

[11] I. Podlubny, *Fractional Differential Equations*, vol. 198 of *Mathematics in Science and Engineering*, Academic Press, San Diego, Calif, USA, 1998.

[12] R. Hilfer, *Applications of Fractional Calculus in Physics*, World Scientific, Singapore, 2000.

[13] H. Bao, J. H. Park, and J. Cao, "Synchronization of fractional-order complex-valued neural networks with time delay," *Neural Networks*, vol. 81, pp. 16–28, 2016.

[14] L. Geng, Y. Yu, and S. Zhang, "Function projective synchronization between integer-order and stochastic fractional-order nonlinear systems," *ISA Transactions®*, vol. 64, pp. 34–46, 2016.

[15] A. J. Muñoz-Vázquez, V. Parra-Vega, and A. Sánchez-Orta, "Continuous fractional-order sliding PI control for nonlinear systems subject to non-differentiable disturbances," *Asian Journal of Control*, vol. 19, no. 1, pp. 279–288, 2017.

[16] A. A. Khamzin, R. R. Nigmatullin, and I. . Popov, "Justification of the empirical laws of the anomalous dielectric relaxation in the framework of the memory function formalism," *Fractional Calculus and Applied Analysis An International Journal for Theory and Applications*, vol. 17, no. 1, pp. 247–258, 2014.

[17] C. W. Granger and R. Joyeux, "An introduction to long-memory time series models and fractional differencing," *Journal of Time Series Analysis*, vol. 1, no. 1, pp. 15–29, 1980.

[18] S. Bhalekar, V. Daftardar-Gejji, D. Baleanu, and R. Magin, "Transient chaos in fractional Bloch equations," *Computers & Mathematics with Applications*, vol. 64, no. 10, pp. 3367–3376, 2012.

[19] A. Elsonbaty, S. F. Hegazy, and S. S. A. Obayya, "Simultaneous Suppression of Time-Delay Signature in Intensity and Phase of Dual-Channel Chaos Communication," *IEEE Journal of Quantum Electronics*, vol. 51, no. 9, 2015.

[20] A. A. Elsadany and A. E. Matouk, "Dynamical behaviors of fractional-order Lotka-Volterra predator-prey model and its discretization," *Applied Mathematics and Computation*, vol. 49, no. 1-2, pp. 269–283, 2015.

[21] A. E. Matouk and A. A. Elsadany, "Dynamical analysis, stabilization and discretization of a chaotic fractional-order GLV model," *Nonlinear Dynamics*, vol. 85, no. 3, pp. 1597–1612, 2016.

[22] A. Elsadany, A. Matouk, A. Abdelwahab, and H. Abdallah, "Dynamical analysis, linear feedback control and synchronization of a generalized Lotka-Volterra system," in *International Journal of Dynamics and Control*, vol. 111, pp. 1–11, 2017.

[23] Y. Pan and H. Yu, "Biomimetic hybrid feedback feedforward neural-network learning control," *IEEE Transactions on Neural Networks and Learning Systems*, vol. 28, no. 6, pp. 1481–1487, 2017.

[24] A. Sambas, S. Vaidyanathan, M. Mamat, W. S. M. Sanjaya, and D. S. Rahayu, "A 3-D novel jerk chaotic system and its application in secure communication system and mobile robot navigation," *Studies in Computational Intelligence*, vol. 636, pp. 283–310, 2016.

[25] S. Vaidyanathan, C. K. Volos, V.-T. Pham, and A. T. Azar, "Hyperchaos, control, synchronization and circuit simulation of a novel 4-d hyperchaotic system with three quadratic nonlinearities," *Studies in Fuzziness and Soft Computing*, vol. 337, pp. 297–325, 2016.

[26] Z. Cheng, D. Li, and J. Cao, "Stability and Hopf bifurcation of a three-layer neural network model with delays," *Neurocomputing*, vol. 175, pp. 355–370, 2015.

[27] A. Boulkroune, "A fuzzy adaptive control approach for nonlinear systems with unknown control gain sign," *Neurocomputing*, vol. 179, pp. 318–325, 2016.

[28] Y. Pan, T. Sun, and H. Yu, "Peaking-free output-feedback adaptive neural control under a nonseparation principle," *IEEE Transactions on Neural Networks and Learning Systems*, vol. 26, no. 12, pp. 3097–3108, 2015.

[29] G. Velmurugan, R. Rakkiyappan, and J. Cao, "Finite-time synchronization of fractional-order memristor-based neural networks with time delays," *Neural Networks*, vol. 73, pp. 36–46, 2016.

[30] N. Bounar, A. Boulkroune, F. Boudjema, M. M'Saad, and M. Farza, "Adaptive fuzzy vector control for a doubly-fed induction motor," *Neurocomputing*, vol. 151, no. 2, pp. 756–769, 2015.

[31] Y. Pan, H. Yu, and M. J. Er, "Adaptive neural PD control with semiglobal asymptotic stabilization guarantee," *IEEE Transactions on Neural Networks and Learning Systems*, vol. 25, no. 12, pp. 2264–2274, 2014.

[32] C. Yin, S.-m. Zhong, and W.-f. Chen, "Design of sliding mode controller for a class of fractional-order chaotic systems," *Communications in Nonlinear Science and Numerical Simulation*, vol. 17, no. 1, pp. 356–366, 2012.

[33] A. Boulkroune, M. Tadjine, M. M'Saad, and M. Farza, "A unified approach for design of indirect adaptive output-feedback fuzzy controller," *International Journal of Intelligent Systems Technologies and Applications*, vol. 5, no. 1-2, pp. 83–103, 2008.

[34] W. S. Leaney, Methods and systems for processing microseismic data, 2016.

[35] N. Kapoor, A. R. Teel, and P. Daoutidis, "An anti-windup design for linear systems with input saturation," *Automatica*, vol. 34, no. 5, pp. 559–574, 1998.

[36] K. Yakoubi and Y. Chitour, "Linear systems subject to input saturation and time delay: global asymptotic stabilization," *Institute of Electrical and Electronics Engineers Transactions on Automatic Control*, vol. 52, no. 5, pp. 874–879, 2007.

[37] G. Cui, S. Xu, F. L. Lewis, B. Zhang, and Q. Ma, "Distributed consensus tracking for non-linear multi-agent systems with input saturation: a command filtered backstepping approach," *IET Control Theory & Applications*, vol. 10, no. 5, pp. 509–516, 2016.

[38] C. Li and W. Deng, "Remarks on fractional derivatives," *Applied Mathematics and Computation*, vol. 187, no. 2, pp. 777–784, 2007.

[39] Y. Li and S. Tong, "Adaptive Fuzzy Output-Feedback Control for Switched Nonlinear Systems with Arbitrary Switchings," *Circuits, Systems and Signal Processing*, vol. 35, no. 9, pp. 3152–3171, 2016.

[40] Y.-J. Liu, S. Tong, D.-J. Li, and Y. Gao, "Fuzzy adaptive control with state observer for a class of nonlinear discrete-time systems with input constraint," *IEEE Transactions on Fuzzy Systems*, vol. 24, no. 5, pp. 1147–1158, 2015.

[41] Y.-J. Liu, Y. Gao, S. Tong, and Y. Li, "Fuzzy approximation-based adaptive backstepping optimal control for a class of nonlinear discrete-time systems with dead-zone," *IEEE Transactions on Fuzzy Systems*, vol. 24, no. 1, pp. 16–28, 2016.

[42] Y. M. Li, S. C. Tong, and T. S. Li, "Hybrid fuzzy adaptive output feedback control design for uncertain MIMO nonlinear systems with time-varying delays and input saturation," *IEEE Transactions on Fuzzy Systems*, vol. 24, no. 4, pp. 841–853, 2015.

[43] H. Y. Li, C. W. Wu, L. G. Wu, H. K. Lam, and Y. B. Gao, "Filtering of interval type-2 fuzzy systems with intermittent measurements," *IEEE Transactions on Cybernetics*, vol. 46, no. 3, pp. 668–678, 2015.

[44] H. Li, C. W. Wu, S. Yin, and H. K. Lam, "Observer-based fuzzy control for nonlinear networked systems under unmeasurable premise variables," *IEEE Transactions on Fuzzy Systems*, vol. 24, no. 5, pp. 1233–1245, 2016.

[45] X. Yin, D. Yue, and S. Hu, "Adaptive periodic event-triggered consensus for multi-agent systems subject to input saturation," *International Journal of Control*, vol. 89, no. 4, pp. 653–667, 2016.

[46] M. K. Talkhoncheh, M. Shahrokhi, and M. R. Askari, "Observer-Based adaptive neural network controller for uncertain nonlinear systems with unknown control directions subject to input time delay and saturation," *Information Sciences*, vol. 418-419, pp. 717–737, 2017.

[47] H. Liu, S. Li, H. Wang, Y. Huo, and J. Luo, "Adaptive synchronization for a class of uncertain fractional-order neural networks," *Entropy. An International and Interdisciplinary Journal of Entropy and Information Studies*, vol. 17, no. 10, pp. 7185–7200, 2015.

[48] Y. Li, Y. Chen, and I. Podlubny, "Mittag-Leffler stability of fractional order nonlinear dynamic systems," *Automatica*, vol. 45, no. 8, pp. 1965–1969, 2009.

[49] J. G. Lu, "Chaotic dynamics and synchronization of fractional-order Arneodos systems," *Chaos, Solitons & Fractals*, vol. 26, no. 4, pp. 1125–1133, 2005.

[50] X. Y. Wang and J. M. Song, "Synchronization of the fractional order hyperchaos Lorenz systems with activation feedback control," *Communications in Nonlinear Science and Numerical Simulation*, vol. 14, no. 8, pp. 3351–3357, 2009.

Hindawi
Complexity
Volume 2017, Article ID 3720471, 7 pages
https://doi.org/10.1155/2017/3720471

Research Article

Fundamental Results of Conformable Sturm-Liouville Eigenvalue Problems

Mohammed Al-Refai[1] and Thabet Abdeljawad[2]

[1]*Department of Mathematical Sciences, UAE University, P.O. Box 15551, Al Ain, Abu Dhabi, UAE*
[2]*Department of Mathematics and General Sciences, Prince Sultan University, P.O. Box 66833, Riyadh 11586, Saudi Arabia*

Correspondence should be addressed to Mohammed Al-Refai; m_alrefai@uaeu.ac.ae

Received 7 May 2017; Accepted 6 August 2017; Published 14 September 2017

Academic Editor: Abdelalim Elsadany

We suggest a regular fractional generalization of the well-known Sturm-Liouville eigenvalue problems. The suggested model consists of a fractional generalization of the Sturm-Liouville operator using conformable derivative and with natural boundary conditions on bounded domains. We establish fundamental results of the suggested model. We prove that the eigenvalues are real and simple and the eigenfunctions corresponding to distinct eigenvalues are orthogonal and we establish a fractional Rayleigh Quotient result that can be used to estimate the first eigenvalue. Despite the fact that the properties of the fractional Sturm-Liouville problem with conformable derivative are very similar to the ones with the classical derivative, we find that the fractional problem does not display an infinite number of eigenfunctions for arbitrary boundary conditions. This interesting result will lead to studying the problem of completeness of eigenfunctions for fractional systems.

1. Introduction and Preliminaries

Fractional calculus is old as the Newtonian calculus [1–3]. The name fractional was given to express the integration and differentiation up to arbitrary order. Traditionally, there are two approaches to define the fractional derivative. The first approach, Riemann-Liouville approach, is to iterate the integral with respect to certain weight function and replace the iterated integral by single integral through Leibniz-Cauchy formula and then replace the factorial function by the Gamma function. In this approach, the arbitrary order Riemann-Liouville results from the integrating measure dt and the Hadamard fractional integral results from the integrating measure dt/t. The second approach, Grünwald-Letinkov approach, is to iterate the limit definition of the derivative to get a quantity with certain binomial coefficient and then fractionalize by using the Gamma function instead of the factorial in the binomial coefficient. In case of the Riemann-Liouville and Caputo fractional derivatives, a singular kernel of the form $(t-s)^{-\alpha}$ is generated for $0 < \alpha < 1$ to reflect the nonlocality and the memory in the fractional operator. Through history, hundreds of researchers did their best to develop the theory of fractional calculus and generalize it, either by obtaining more general fractional derivatives with different kernels or by defining the fractional operator on different time scales such as the discrete fractional difference operators (see [4–7] and the references therein) and q-fractional operators (see [8] and the references therein).

In 2014 [9], Khalil et al. introduced the so-called conformable fractional derivative by modifying the limit definition of the derivative by inserting the multiple $t^{1-\alpha}$, $0 < \alpha < 1$ inside the definition. The word fractional there was used to express the derivative of arbitrary order although no memory effect exists inside the corresponding integral inverse operator. This conformable (fractional) derivative seems to be kind of local derivative without memory. An interesting application of the conformable fractional derivative in Physics was discussed in [10], where it has been used to formulate an Action Principle for particles under frictional forces. Despite the many nice properties the conformable derivative has, it has the drawbacks that when α tends to zero we do not obtain the original function and the conformable integrals inverse operators are free of memory

and do not have a semigroup property. It is most likely to call them conformable derivatives or local derivatives of arbitrary order. In connection with this, at the end of reference [11], the author asked whether it is possible to fractionalize the conformable (fractional) derivative by using conformable (fractional) integrals of order $0 < \alpha \leq 1$ or by iterating the conformable derivative. The first part, Riemann-Liouville approach, was answered in [12, 13], where the author iterated the (conformable) integral with weight $t^{\rho-1}$, $\rho \neq 0$ to define generalized fractional integrals and derivatives that unify Riemann-Liouville fractional integrals ($\rho = 1$) and derivatives together with Hadamard fractional integrals and derivatives. Actually, the limiting case of that generalization is when $\rho \to 0^+$ leads to Hadamard type. However, the Grünwald-Letinkov approach for conformable derivatives is still open. The conformable time-scale fractional calculus of order $0 < \alpha < 1$ is introduced in [14] and has been used to develop the fractional differentiation and fractional integration. After then, many authors got interested in this type of derivatives for their many nice behaviors [10, 15–18]. Motivated by the need of some new fractional derivatives with nice properties and that can be applied to more real world modeling, some authors introduced very recently new kinds of fractional derivatives whose kernel is nonsingular. For the fractional derivatives with exponential kernels we refer to [19]. For fractional derivatives of nonsingular Mittag-Leffler functions we refer to [20–22].

Motivated, as mentioned above, with the need of new fractional derivatives with nice properties we study in this article the eigenvalue problems of Sturm-Liouville into conformable (fractional) calculus. Recently, there are several analytical studies devoted to fractional Sturm-Liouville eigenvalue problems; see [23–27]. In these studies some of the well-known results of the Sturm-Liouville problems are extended to the fractional ones with left- and right-sided fractional derivatives of Riemann-Liouville and Caputo and Riesz derivatives. These results include orthogonality and completeness of eigenfunctions and countability of the real eigenvalues. Another class of fractional eigenvalue problem with Caputo fractional derivative has been studied in [28] using maximum principles and method of upper and lower solutions.

For a function $f : (0, \infty) \to \mathbb{R}$ the (conformable) fractional derivative of order $0 < \alpha \leq 1$ of f at $t > 0$ was defined by

$$D_a^\alpha f(t) = \lim_{\epsilon \to 0} \frac{f\left(t + \epsilon (t-a)^{1-\alpha}\right) - f(t)}{\epsilon}, \tag{1}$$

and the fractional derivative at a is defined as $(D_a^\alpha f)(a) = \lim_{t \to a^+} (D_a^\alpha f)(t)$. The corresponding conformable (fractional) integral of order $0 < \alpha < 1$ and starting from a is defined by

$$\left(I_a^\alpha f\right)(x) = \int_a^x f(t)\, d\alpha(t) = \int_a^x f(t)\,(t-a)^{\alpha-1}\, dt. \tag{2}$$

It is to be noted that the author used this modified conformable integral in order to extend it to left-right concept and confirm it by the Q-operator and obtain a left-right integration by parts version. Otherwise the integral can be given by $(I_a^\alpha f)(x) = \int_a^x f(t) t^{\alpha-1} dt$. It was shown in [9, 11] that $(I_a^\alpha D_a^\alpha f)(x) = f(x) - f(a)$ and $(D_a^\alpha I_a^\alpha f)(x) = f(x)$. For the higher order case and other details such as the product rule, chain rule, and integration by parts, we refer the reader to [9, 11].

2. Main Results

In this paper we consider the fractional extension of the Sturm-Liouville eigenvalue problem

$$D_a^\alpha \left(p(x) D_a^\alpha y\right) + q(x) y = -\lambda w(x) y, \quad \frac{1}{2} < \alpha \leq 1,\ a < x < b, \tag{3}$$

where $p, D_a^\alpha p, q$ and the weight functions w are continuous on (a, b), $p(x) > 0$, and $w(x) > 0$, on $[a, b]$, and the fractional derivative D_a^α is the conformable fractional derivative. We discuss (3) with boundary conditions

$$\begin{aligned} c_1 y(a) + c_2 y'(a) &= 0, \quad c_1^2 + c_2^2 > 0, \\ r_1 y(b) + r_2 y'(b) &= 0, \quad r_1^2 + r_2^2 > 0. \end{aligned} \tag{4}$$

We say that y is 2α-continuously differentiable on $[a, b]$, if $D_a^\alpha D_a^\alpha y$ is continuous on $[a, b]$, and $y \in C^{2\alpha}[a, b]$, if $y \in C^1[a, b]$ and is 2α-continuously differentiable on $[a, b]$.

Let

$$L(y, \alpha) = D_a^\alpha \left(p(x) D_a^\alpha y\right) + q(x) y; \tag{5}$$

then the fractional Sturm-Liouville eigenvalue problem (3) can be written as

$$L(y, \alpha) = -\lambda w(x) y. \tag{6}$$

The following is a generalized result of the well-known Lagrange identity.

Theorem 1 (fractional Lagrange identity). *Letting y_1, y_2 be 2α-continuously differentiable on $[a, b]$, then the following holds true:*

$$\begin{aligned} &\int_a^b \left(y_2 L(y_1, \alpha) - y_1 L(y_2, \alpha)\right) d\alpha(x) \\ &\quad = \left[p(x)\left(y_2 D_a^\alpha y_1 - y_1 D_a^\alpha y_2\right)\right]\Big|_a^b. \end{aligned} \tag{7}$$

Proof. We have

$$\begin{aligned} &y_2 L(y_1, \alpha) - y_1 L(y_2, \alpha) \\ &\quad = y_2 D_a^\alpha \left(p(x) D_a^\alpha y_1\right) + q(x) y_1 y_2 \\ &\qquad - y_1 D_a^\alpha \left(p(x) D_a^\alpha y_2\right) - q(x) y_1 y_2 \\ &\quad = y_2 D_a^\alpha \left(p(x) D_a^\alpha y_1\right) - y_1 D_a^\alpha \left(p(x) D_a^\alpha y_2\right). \end{aligned} \tag{8}$$

Using the integration by parts formula of the conformable fractional derivative [11], we have

$$\begin{aligned}\int_a^b &\left(y_2 D_a^\alpha \left(p\left(x\right) D_a^\alpha y_1\right) - y_1 D_a^\alpha \left(p\left(x\right) D_a^\alpha y_2\right)\right) d\alpha\left(x\right)\\ &= p\left(x\right) y_2 D_a^\alpha y_1\Big|_a^b - \int_a^b p\left(x\right) D_a^\alpha y_1 D_a^\alpha y_2 d\alpha\left(x\right)\\ &\quad - p\left(x\right) y_1 D_a^\alpha y_2\Big|_a^b + \int_a^b p\left(x\right) D_a^\alpha y_1 D_a^\alpha y_2 d\alpha\left(x\right)\\ &= \left[p\left(x\right)\left(y_2 D_a^\alpha y_1 - y_1 D_a^\alpha y_2\right)\right]\Big|_a^b,\end{aligned} \tag{9}$$

which proves the result. □

Proposition 2. *If $y \in C^1[0,1]$ and $y'(x_0) = 0$, for some $x_0 \in [a,b]$, then $(D_a^\alpha y)(x_0) = 0$.*

Proof. Since $y \in C^1[0,1]$, then $(D_a^\alpha y)(x) = (x-a)^{1-\alpha} y'(x)$, and the result follows for $a < x_0 \leq b$. If $x_0 = a$, we have $(D_a^\alpha y)(a) = \lim_{x\to a^+}(x-a)^{1-\alpha} y'(x) = 0$. □

Proposition 3. *Let y_1 and y_2 in $C^1[a,b]$, which satisfy the boundary conditions (4); then it holds that*

$$\left[p\left(x\right)\left(y_2 D_a^\alpha y_1 - y_1 D_a^\alpha y_2\right)\right]\Big|_a^b = 0. \tag{10}$$

Proof. Since $y_1 \in C^1[a,b]$, then $D_a^\alpha y_1 = (x-a)^{1-\alpha} y_1'(x)$. Similarly, $D_a^\alpha y_2 = (x-a)^{1-\alpha} y_2'(x)$. We have

$$\begin{aligned}&\left[p\left(x\right)\left(y_2 D_a^\alpha y_1 - y_1 D_a^\alpha y_2\right)\right]\Big|_a^b\\ &= p\left(b\right)\left(y_2\left(b\right)\left(D_a^\alpha y_1\right)\left(b\right) - y_1\left(b\right)\left(D_a^\alpha y_2\right)\left(b\right)\right)\\ &\quad - p\left(a\right)\left(y_2\left(a\right)\left(D_a^\alpha y_1\right)\left(a\right) - y_1\left(a\right)\left(D_a^\alpha y_2\right)\left(a\right)\right).\end{aligned} \tag{11}$$

Since $c_1^2 + c_2^2 > 0$, and $r_1^2 + r_2^2 > 0$, we first assume that, without loss of generality, $c_1 \neq 0$ and $r_1 \neq 0$, and the proof of other cases will be obtained analogously. We have

$$\begin{aligned}y\left(a\right) &= -\frac{c_2}{c_1} y'\left(a\right),\\ y\left(b\right) &= -\frac{r_2}{r_1} y'\left(b\right).\end{aligned} \tag{12}$$

Thus,

$$\begin{aligned}y_2\left(b\right)\left(D_a^\alpha y_1\right)\left(b\right) &- y_1\left(b\right)\left(D_a^\alpha y_2\right)\left(b\right) = -\frac{r_2}{r_1} y_2'\left(b\right)\\ &\cdot \left(D_a^\alpha y_1\right)\left(b\right) + \frac{r_2}{r_1} y_1'\left(b\right)\left(D_a^\alpha y_2\left(b\right)\right)\\ &= -\frac{r_2}{r_1}\left(y_2'\left(b\right)\left(b-a\right)^{1-\alpha} y_1\left(b\right)\right.\\ &\quad \left. - y_1'\left(b\right)\left(b-a\right)^{1-\alpha} y_2'\left(b\right)\right) = 0.\end{aligned} \tag{13}$$

Analogously,

$$y_2\left(a\right)\left(D_a^\alpha y_1\right)\left(a\right) - y_1\left(a\right)\left(D_a^\alpha y_2\right)\left(a\right) = 0, \tag{14}$$

which proves the result. □

Definition 4. We say that f and g are α-orthogonal with respect to the weight function $\mu(x) \geq 0$, if

$$\int_a^b \mu\left(x\right) f\left(x\right) g\left(x\right) d\alpha\left(x\right) = 0. \tag{15}$$

Theorem 5. *The eigenfunctions of the fractional eigenvalue problem (3)-(4) corresponding to distinct eigenvalues are α-orthogonal with respect to the weight function $w(x)$.*

Proof. Let λ_1 and λ_2 be two distinct eigenvalues and y_1 and y_2 are the corresponding eigenfunctions. We have

$$L\left(y_1, \alpha\right) = -\lambda_1 w\left(x\right) y_1, \tag{16}$$

$$L\left(y_2, \alpha\right) = -\lambda_2 w\left(x\right) y_2. \tag{17}$$

Multiplying (16) by y_2 and (17) by y_1 and subtracting the two equations yield

$$y_2 L\left(y_1, \alpha\right) - y_1 L\left(y_2, \alpha\right) = -\left(\lambda_1 - \lambda_2\right) w\left(x\right) y_1 y_2. \tag{18}$$

Performing the fractional integral I_a^α and using the fractional Lagrange identity we have

$$\begin{aligned}&-\left(\lambda_1 - \lambda_2\right)\int_a^b w\left(x\right) y_1 y_2 d\alpha\left(x\right)\\ &= \int_a^b \left(y_2 L\left(y_1, \alpha\right) - y_1 L\left(y_2, \alpha\right)\right) d\alpha\left(x\right)\\ &= \left[p\left(x\right)\left(y_2 D_a^\alpha y_1 - y_1 D_a^\alpha y_2\right)\right]\Big|_a^b = 0,\end{aligned} \tag{19}$$

by virtue of Proposition 3. Since $\lambda_1 \neq \lambda_2$, we have $\int_a^b w(x) y_1 y_2 d\alpha(x) = 0$, and the result is obtained. □

Theorem 6. *The eigenvalues of the fractional eigenvalue problem (3)-(4) are real.*

Proof. Let y be a solution to the fractional Sturm-Liouville eigenvalue problem (3)-(4). Taking the complex conjugate of (3)-(4) and using the fact that $p(x), q(x)$ and $w(x)$ are real valued functions, we have

$$\begin{aligned}L\left(\overline{y}, \alpha\right) &= D_a^\alpha\left(p\left(x\right)\overline{D_a^\alpha y}\right) + q\left(x\right)\overline{y}\\ &= -\lambda w\left(x\right)\overline{y},\\ c_1\overline{y}\left(a\right) + c_2\overline{y'}\left(a\right) &= 0,\\ r_1\overline{y}\left(b\right) + r_2\overline{y'}\left(b\right) &= 0.\end{aligned} \tag{20}$$

Applying analogous steps to the proofs of Theorem 5 and Proposition 3 with $y_1 = y$ and $y_2 = \overline{y}$, we have

$$\begin{aligned}&-\left(\lambda - \overline{\lambda}\right)\int_a^b w\left(x\right)\left|y\left(x\right)\right|^2 d\alpha\left(x\right)\\ &= \int_a^b \left(\overline{y} L\left(y, \alpha\right) - y L\left(\overline{y}, \alpha\right)\right) dx\left(\alpha\right)\\ &= \left[p\left(x\right)\left(\overline{y} D_a^\alpha y - y\overline{D_a^\alpha y}\right)\right]\Big|_a^b = 0,\end{aligned} \tag{21}$$

and thus $\lambda = \overline{\lambda}$ which completes the proof. □

Definition 7. Let f and g be α-differentiable; the fractional Wronskian function is defined by

$$W_\alpha(f,g) = fD_a^\alpha g - gD_a^\alpha f. \tag{22}$$

Theorem 8. *Let y_1 and y_2 be 2α-continuously differentiable on $[a,b]$, and they are linearly independent solutions of (3); then*

$$W_\alpha(y_1,y_2) = \frac{W_\alpha(y_1,y_2)(a)\,p(a)}{p(x)}. \tag{23}$$

Proof. Applying the product rule one can easily verify that

$$D_a^\alpha W_\alpha(y_1,y_2) = y_1 D_a^\alpha D_a^\alpha y_2 - y_2 D_a^\alpha D_a^\alpha y_1. \tag{24}$$

Analogously, applying the product rule to (3) yields

$$D_a^\alpha D_a^\alpha y = -\frac{1}{p}\left(D_a^\alpha p D_a^\alpha y + (q+\lambda w)\,y\right). \tag{25}$$

Substituting the last equation in (24) yields

$$\begin{aligned} D_a^\alpha W_\alpha(y_1,y_2) &= -\frac{y_1}{p}\left(D_a^\alpha p D_a^\alpha y_2 + (q+\lambda w)\,y_2\right) \\ &\quad + \frac{y_2}{p}\left(D_a^\alpha p D_a^\alpha y_1 + (q+\lambda w)\,y_1\right) \\ &= \frac{D_a^\alpha p}{p}\left(y_2 D_a^\alpha y_1 - y_1 D_a^\alpha y_2\right) \\ &= -\frac{D_a^\alpha p}{p} W_\alpha(y_1,y_2). \end{aligned} \tag{26}$$

One can easily verify that the solution of the above fractional differential equation is

$$W_\alpha(y_1,y_2) = \frac{c}{p}, \tag{27}$$

where c is constant. Now, $W_\alpha(y_1,y_2)(a) = c/p(a)$, and thus $c = W_\alpha(y_1,y_2)(a)p(a)$, and hence the result. □

Theorem 9. *The eigenvalues of the fractional eigenvalue problem (3)-(4) are simple.*

Proof. Let y_1 and y_2 be two eigenfunctions for the same eigenvalue λ. From (18) we have

$$\begin{aligned} 0 &= y_2 L(y_1,\alpha) - y_1 L(y_2,\alpha) \\ &= y_2 D_a^\alpha\left(p(x) D_a^\alpha y_1\right) - y_1 D_a^\alpha\left(p(x) D_a^\alpha y_2\right) \\ &= y_2\left(D_a^\alpha p D_a^\alpha y_1 + p D_a^\alpha D_a^\alpha y_1\right) \\ &\quad - y_1\left(D_a^\alpha p D_a^\alpha y_2 + p D_a^\alpha D_a^\alpha y_2\right) \\ &= p\left(y_2 D_a^\alpha D_a^\alpha y_1 - y_1 D_a^\alpha D_a^\alpha y_2\right) \\ &\quad + D_a^\alpha p\left(y_2 D_a^\alpha y_1 - y_1 D_a^\alpha y_2\right) \\ &= D_a^\alpha\left(p\left[y_2 D_a^\alpha y_1 - y_1 D_a^\alpha y_2\right]\right). \end{aligned} \tag{28}$$

Thus

$$p\left[y_2 D_a^\alpha y_1 - y_1 D_a^\alpha y_2\right] = c, \tag{29}$$

and since y_1 and y_2 satisfy the same boundary conditions, we have $c = 0$ and

$$y_2 D_a^\alpha y_1 - y_1 D_a^\alpha y_2 = 0. \tag{30}$$

Since $W_\alpha(y_1,y_2) = 0$, and y_1 and y_2 are both solutions to the fractional eigenvalue problem (3)-(4), then they are linearly dependent. □

Theorem 10 (fractional Rayleigh Quotient). *The eigenvalues λ of problem (3) satisfy*

$$\lambda = \frac{\int_a^b p\left(D_a^\alpha y\right)^2 d\alpha(x) - \int_a^b q y^2 d\alpha(x) - p y D_a^\alpha y\big|_a^b}{\int_a^b w y^2 d\alpha(x)} \tag{31}$$

Proof. Multiplying (3) by y and integrating yields

$$\begin{aligned} &\int_a^b y D_a^\alpha\left(p(x) D_a^\alpha y\right) d\alpha(x) + \int_0^1 q(x)\,y^2 d\alpha(x) \\ &\quad = -\lambda\int_a^b w(x)\,y^2 d\alpha(x). \end{aligned} \tag{32}$$

Integrating the first integral by parts we have

$$\begin{aligned} &p y D_a^\alpha y\big|_a^b - \int_a^b p\left(D_a^\alpha y\right)^2 d\alpha(x) + \int_a^b q(x)\,y^2 d\alpha(x) \\ &\quad = -\lambda\int_a^b w(x)\,y^2 d\alpha(x) \end{aligned} \tag{33}$$

which proves the result. □

Corollary 11. *Letting $y \in C^1[a,b]$ and $q(x) \le 0$, then the eigenvalues of (3) associated with homogeneous boundary conditions of Dirichlet or Neumann type are nonnegative.*

Proof. Since the boundary conditions are of Dirichlet or Neumann type then it holds that

$$y D_a^\alpha y\big|_a^b = 0. \tag{34}$$

Then the result is directly obtained from the fractional Rayleigh Quotient as $q(x) \le 0$. □

Now if y is a stationary function for

$$\begin{aligned} J_a^\alpha(y) &= \int_a^b F\left(y, D_a^\alpha y, x\right) dx(\alpha) \\ &= \int_a^b F\left(y, D_a^\alpha y, x\right)(x-a)^{\alpha-1}\,dx, \end{aligned} \tag{35}$$

then it holds that, see [10],

$$\frac{\partial F}{\partial y}\left(y, D_a^\alpha y, x\right) - D_a^\alpha\left(\frac{\partial F}{\partial y^\alpha}\left(y, D_a^\alpha y, x\right)\right) = 0, \tag{36}$$

the fractional Euler equation. We remark here that the above equation is a necessary condition for a stationary point and not sufficient. In the following we show that the fractional Sturm-Liouville eigenvalue problem (3)-(4) is equivalent to the following:

(i) Finding the stationary function $y(x)$ of

$$F[y] = \int_a^b \left(p\left(D_a^\alpha y\right)^2 - qy^2\right)(x-a)^{\alpha-1}\,dx, \tag{37}$$

subject to $G[y] = 1$, where

$$G[y] = \int_a^b wy^2\,(x-a)^{\alpha-1}\,dx. \tag{38}$$

To find the stationary of $F[y]$ subject to $G[y] = 1$, we first find the stationary value y of $K[y] = F[y] - \lambda G[y]$ and then eliminate λ using $G[y] = 1$. Applying the fractional Euler Equation (36) to $K[y]$ yields

$$-2qy - 2\lambda wy - D_a^\alpha\left(2pD_a^\alpha y\right) = 0, \tag{39}$$

or

$$D_a^\alpha\left(pD_a^\alpha y\right) + qy = \lambda wy, \tag{40}$$

which is the fractional Sturm-Liouville problem. Moreover, multiplying (3) by y and integrating yields

$$\begin{aligned}&\int_a^b yD_a^\alpha\left(pD_a^\alpha y\right)(x-a)^{\alpha-1}\,dx + \int_a^b qy^2\,(x-a)^{\alpha-1}\,dx\\ &\quad = -\lambda\int_a^b wy^2\,(x-a)^{\alpha-1}\,dx.\end{aligned} \tag{41}$$

Performing integration by parts of the first integral yields

$$\begin{aligned}&pyD_a^\alpha y\big|_a^b - \int_a^b p\left(D_a^\alpha y\right)^2(x-a)^{\alpha-1}\,dx\\ &\quad + \int_a^b qy^2\,(x-a)^{\alpha-1}\,dx\\ &\quad = -\lambda\int_a^b wy^2\,(x-a)^{\alpha-1}\,dx.\end{aligned} \tag{42}$$

Since

$$yD_a^\alpha y\big|_a^b = 0, \tag{43}$$

we have

$$\begin{aligned}&\lambda\int_a^b wy^2\,(x-a)^{\alpha-1}\,dx\\ &\quad = \int_a^b\left(p\left(D_a^\alpha y\right)^2 - qy^2\right)(x-a)^{\alpha-1}\,dx.\end{aligned} \tag{44}$$

Since $\int_a^b wy^2(x-a)^{\alpha-1}dx = 1$, we have

$$\lambda = \int_a^b\left(p\left(D_a^\alpha y\right)^2 - qy^2\right)(x-a)^{\alpha-1}\,dx. \tag{45}$$

That is, λ is determined by $F[y]$ in (37).

The problem in (i) is equivalent to the problem of finding the stationary function of (ii) $A[y] = F[y]/G[y]$. Thus the eigenvalues of the fractional Sturm-Liouville eigenvalue problem are the values given by $A[y]$. The proof of (i) being equivalent to (ii) is well-known in the literature and we present it here for the sake of completeness.

We have

$$\delta A = \frac{G\delta F - F\delta G}{G^2}, \tag{46}$$

and $\delta A = 0$ if and only if $G\delta F - F\delta G = 0$, or

$$\delta F - \frac{F}{G}\delta G = \delta F - AG = 0, \tag{47}$$

which is the same as δK.

Using the above results and the fractional Rayleigh Quotient result we have the following.

Lemma 12. *For the fractional eigenvalue problem (3)-(4) it holds that*

$$\lambda = \frac{\int_a^b p\left(D_a^\alpha y\right)^2 d\alpha(x) - \int_a^b qy^2 d\alpha(x)}{\int_a^b wy^2 d\alpha(x)} \tag{48}$$

and the eigenfunction y is a stationary (minimum) value of the above ratio.

Remark 13. Assuming that the eigenvalues of (3)-(4) are ordered, $\lambda_1 < \lambda_2 \cdots < \lambda_n \cdots$, then the above result can be used to give an upper estimate value of the first eigenvalue λ_1, by choosing arbitrary function ψ that satisfies the same boundary conditions, and computing the ratio in (48) for ψ.

3. Illustrative Examples

Example 1. Consider the fractional eigenvalue problem (3)-(4) with $p = 1, q = 0, w = 1$, $0 < x < 1$ and with Dirichlet boundary condition $y(0) = y(1) = 0$. The eigenfunctions are $\phi_n = \sin(n\pi x^\alpha)$ and the corresponding eigenvalues are $\lambda_n = n^2\alpha^2\pi^2$.

In the following we apply the fractional Rayleigh Quotient to obtain lower estimates of the first eigenvalue. We start with the atrial function $\psi(x) = x^\alpha - x^{2\alpha}$, which satisfies the homogenous boundary conditions $\psi(0) = \psi(1) = 0$. We have $D_0^\alpha\psi = \alpha(1-2x^\alpha)$, and thus

$$\begin{aligned}\lambda_1 &\le \frac{\int_0^1\left(D_0^\alpha\psi\right)^2 x^{\alpha-1}dx}{\int_0^1\psi^2 x^{\alpha-1}dx} = \frac{\int_0^1\alpha^2\left(1-2x^\alpha\right)^2 x^{\alpha-1}dx}{\int_0^1\left(x^\alpha - x^{2\alpha}\right)^2 x^{\alpha-1}dx}\\ &= 10\alpha^2.\end{aligned} \tag{49}$$

So, we obtain an upper estimate $\overline{\lambda_1} = 10\alpha^2$, which is comparable with the exact eigenvalue $\lambda_1 = \pi^2\alpha^2$. However, this upper bound can be improved by choosing a trial function

$$\psi(x) = x^\alpha\left(1 - x^\alpha\right) + a\left(x^\alpha\left(1 - x^\alpha\right)\right)^2, \tag{50}$$

with parameter a and then choosing a to minimize the fractional Rayleigh Quotient. Direct calculations show that

$$\begin{aligned}\int_0^1 \left(D_0^\alpha\psi\right)^2 x^{\alpha-1}dx &= \frac{\alpha}{105}\left(35 + 2a\left(a+7\right)\right),\\ \int_0^1 \psi^2 x^{\alpha-1}dx &= \frac{21 + a\left(a+9\right)}{630a}.\end{aligned} \tag{51}$$

Thus, the fractional Rayleigh Quotient will produce

$$\mathrm{FR}(a,\alpha) = \alpha^2\frac{630}{105}\frac{35 + a\left(a+7\right)}{21 + a\left(a+9\right)}. \tag{52}$$

The minimum value of

$$R(a) = \frac{630}{105}\frac{35 + a\left(a+7\right)}{21 + a\left(a+9\right)} \tag{53}$$

is 9.86975 and occurs at $a = 1.13314\cdots$. Hence, an upper estimate $\overline{\lambda_1} = 9.86975\alpha^2$ is obtained which is very close to the exact one.

Example 2. Consider the fractional eigenvalue problem (3)-(4) with $p = 1, q = 0, w = 1$, $0 < x < 1$ and with boundary condition $y(0) - y'(0) = 0$, $y'(1) = 0$. The eigenfunctions are

$$\phi_n = a_n\sin\left(\lambda_n x^\alpha\right) + b_n\cos\left(\lambda_n x^\alpha\right). \tag{54}$$

We choose $a_n = 0$, so that $\phi_n' = \lambda_n\alpha x^{\alpha-1}a_n\cos(\lambda_n x^\alpha) - \lambda_n\alpha x^{\alpha-1}b_n\sin(\lambda_n x^\alpha)$ is defined at $x = 0$. Thus, $\phi_n = b_n\cos(\lambda_n x^\alpha)$, and applying the boundary conditions we have $\phi_n = 0$. That is, the problem possesses no eigenfunctions for $1/2 < \alpha < 1$.

Remark 3. It is well-known that the regular Sturm-Liouville eigenvalue problem with integer derivative possesses an infinite number of eigenvalues. This result is not valid for the fractional one as shown in the previous example. However, the fractional Sturm-Liouville equation in (3) can be discussed with fractional boundary conditions of the type

$$\begin{aligned}c_1 y(a) + c_2\left(D_a^\alpha y\right)(a) &= 0, \quad c_1^2 + c_2^2 > 0,\\ r_1 y(b) + r_2\left(D_a^\alpha y\right)(b) &= 0, \quad r_1^2 + r_2^2 > 0.\end{aligned} \tag{55}$$

We believe that the above fractional eigenvalue problem possesses an infinite number of eigenvalues and we left it for a future work.

4. Conclusion

We have considered a regular conformable fractional Sturm-Liouville eigenvalue problem. We proved that the eigenvalues are real and simple and the eigenfunctions are orthogonal. We also established the fractional Wronskian result for any two linearly independent solutions of the problem. We obtained a fractional Rayleigh Quotient and applied a fractional variational principle to show that the minimum value of the Quotient is obtained at an eigenfunction. This result is used to estimate the first eigenvalue and the presented example illustrates the efficiency of the result. We illustrated by an example that the existence of eigenfunctions is not guaranteed unlike the result for the regular Sturm-Liouville eigenvalue problem. Most of the obtained results are analogous for the ones of regular Sturm-Liouville eigenvalue problems and they open the door for establishing other results such as the countability of eigenfunctions and completeness of eigenfunctions which are essential in solving fractional differential equations by fractional eigenfunction expansion.

Conflicts of Interest

The authors declare that they have no conflicts of interest.

Acknowledgments

The first author gratefully acknowledges the support of the United Arab Emirates University under the Grant 31S239-UPAR(1) 2016.

References

[1] S. G. Samko, A. A. Kilbas, and O. I. Marichev, *Fractional Integrals and Derivatives, Theory and Applications*, Gordon and Breach, Yverdon, Switzerland, 1993.

[2] I. Podlubny, *Fractional Differential Equations*, vol. 198 of *Mathematics in Science and Engineering*, Academic Press, San Diego, Calif, USA, 1999.

[3] A. A. Kilbas, H. M. Srivastava, and J. J. Trujillo, "Preface," *North-Holland Mathematics Studies*, vol. 204, no. C, pp. vii–x, 2006.

[4] K. S. Miller and B. Ross, "Fractional difference calculus," in *Proceedings of the International Symposium on Univalent Functions, Fractional Calculus and Their Applications*, pp. 139–152, Nihon University, Koriyama, Japan, 1989.

[5] F. M. Atici and P. W. Eloe, "Initial value problems in discrete fractional calculus," *Proceedings of the American Mathematical Society*, vol. 137, no. 3, pp. 981–989, 2009.

[6] T. Abdeljawad and F. M. Atici, "On the definitions of nabla fractional operators," *Abstract and Applied Analysis*, vol. 2012, Article ID 406757, 13 pages, 2012.

[7] T. Abdeljawad, "Dual identities in fractional difference calculus within Riemann," *Advances in Difference Equations*, vol. 2013, no. 36, 2013.

[8] M. H. Annaby and Z. S. Mansour, *q-Fractional Calculus and Equations*, vol. 2056 of *Lecture Notes in Mathematics*, Springer, Berlin, Germany, 2012.

[9] R. Khalil, M. Al Horani, A. Yousef, and M. Sababheh, "A new definition of fractional derivative," *Journal of Computational and Applied Mathematics*, vol. 264, pp. 65–70, 2014.

[10] M. J. Lazo and D. F. Torres, "Variational calculus with conformable fractional derivatives," *IEEE/CAA Journal of Automatica Sinica*, vol. 4, no. 2, pp. 340–352, 2017.

[11] T. Abdeljawad, "On conformable fractional calculus," *Journal of Computational and Applied Mathematics*, vol. 279, pp. 57–66, 2015.

[12] U. N. Katugampola, "New approach to a generalized fractional integral," *Applied Mathematics and Computation*, vol. 218, no. 3, pp. 860–865, 2011.

[13] U. N. Katugampola, "A new approach to generalized fractional derivatives," *Bulletin of Mathematical Analysis and Applications*, vol. 6, no. 4, pp. 1–15, 2014.

[14] N. Benkhettou, S. Hassani, and D. F. M. Torres, "A conformable fractional calculus on arbitrary time scales," *Journal of King Saud University-Science*, vol. 28, no. 1, pp. 93–98, 2016.

[15] T. Abdeljawad, M. Al Horani, and R. Khali, "Conformable fractional semigroup operators," *Journal of Semigroup Theory and Applications*, vol. 2015, article 7, 2015.

[16] E. Ünal, A. an, and E. Çelik, "Solutions of Sequential Conformable Fractional Differential Equations around an Ordinary Point and Conformable Fractional Hermite Differential Equation," *British Journal of Applied Science & Technology*, vol. 10, no. 2, pp. 1–11, 2015.

[17] R. Khalil, M. Al Horania, and Douglas A., "Undetermined coefficients for local fractional differential equations," *Journal of Mathematics and Computer Science*, vol. 16, pp. 140–146, 2016.

[18] Y. Çenesiz, D. Baleanu, A. Kurt, and O. Tasbozan, "New exact solutions of Burgers' type equations with conformable derivative," *Waves in Random and Complex Media. Propagation, Scattering and Imaging*, vol. 27, no. 1, pp. 103–116, 2017.

[19] M. Caputo and M. Fabrizio, "A new definition of fractional derivative without singular kernel," *Progress in Fractional Differentiation and Applications*, vol. 1, no. 2, pp. 73–85, 2015.

[20] A. Atangana and D. Baleanu, "New fractional derivatives with nonlocal and non-singular kernel: theory and application to heat transfer model," *Thermal Science*, vol. 20, no. 2, pp. 763–769, 2016.

[21] T. Abdeljawad and D. Baleanu, "Discrete fractional differences with nonsingular discrete Mittag-Leffler kernels," *Advances in Difference Equations*, vol. 232, 2016.

[22] T. Abdeljawad and D. Baleanu, "On fractional derivatives with exponential kernel and their discrete versions," *Reports on Mathematical Physics*, vol. 80, no. 1, pp. 11–27, 2017.

[23] M. Klimek and O. P. Agrawal, "Fractional Sturm-Liouville problem," *Computers & Mathematics with Applications*, vol. 66, no. 5, pp. 795–812, 2013.

[24] M. Klimek, "Fractional Sturm-Liouville problem in terms of Riesz derivatives, Theoretical development and applications of non-integer order systems," in *Proceeding of the 7th Conference on Non-Integer Order Calculus and its Applications*, Szczecin, Ploand, 2015.

[25] J. Li and J. Qi, "Spectral problems for fractional differential equations from nonlocal continuum mechanics," *Advances in Difference Equations*, vol. 85, 2014.

[26] M. Al-Refai, "Basic results on nonlinear eigenvalue problems of fractional order," *Electronic Journal of Differential Equations*, vol. 2012, no. 91, pp. 1–12, 2012.

[27] M. Zayernouri and G. E. Karniadakis, "Fractional Sturm-Liouville eigen-problems: theory and numerical approximation," *Journal of Computational Physics*, vol. 252, pp. 495–517, 2013.

[28] M. Al-Refai, "Basic results on nonlinear eigenvalue problems of fractional order," *Electronic Journal of Differential Equations*, vol. 2012, no. 191, pp. 1–12, 2012.

Hindawi
Complexity
Volume 2017, Article ID 6875874, 13 pages
https://doi.org/10.1155/2017/6875874

Research Article

Existence and Globally Asymptotic Stability of Equilibrium Solution for Fractional-Order Hybrid BAM Neural Networks with Distributed Delays and Impulses

Hai Zhang,[1] Renyu Ye,[1,2] Jinde Cao,[3,4] and Ahmed Alsaedi[5]

[1] *School of Mathematics and Computation Science, Anqing Normal University, Anqing 246133, China*
[2] *College of Science, Nanjing University of Aeronautics and Astronautics, Nanjing 211106, China*
[3] *School of Mathematics and Research Center for Complex Systems and Network Sciences, Southeast University, Nanjing 210096, China*
[4] *Department of Mathematics, Faculty of Science, King Abdulaziz University, Jeddah 21589, Saudi Arabia*
[5] *Nonlinear Analysis and Applied Mathematics (NAAM) Research Group, Department of Mathematics, King Abdulaziz University, Jeddah 21589, Saudi Arabia*

Correspondence should be addressed to Jinde Cao; jdcao@seu.edu.cn

Received 7 May 2017; Revised 10 July 2017; Accepted 20 July 2017; Published 13 September 2017

Academic Editor: Amr Elsonbaty

This paper investigates the existence and globally asymptotic stability of equilibrium solution for Riemann-Liouville fractional-order hybrid BAM neural networks with distributed delays and impulses. The factors of such network systems including the distributed delays, impulsive effects, and two different fractional-order derivatives between the U-layer and V-layer are taken into account synchronously. Based on the contraction mapping principle, the sufficient conditions are derived to ensure the existence and uniqueness of the equilibrium solution for such network systems. By constructing a novel Lyapunov functional composed of fractional integral and definite integral terms, the globally asymptotic stability criteria of the equilibrium solution are obtained, which are dependent on the order of fractional derivative and network parameters. The advantage of our constructed method is that one may directly calculate integer-order derivative of the Lyapunov functional. A numerical example is also presented to show the validity and feasibility of the theoretical results.

1. Introduction

Since fractional derivatives are nonlocal and have weakly singular kernels, the subject of fractional calculus has been attracting attention and interest in various fields of diffusion [1], physics [2], market dynamics [3], engineering [4], control system [5], biological system [6], financial system [7], epidemic model [8], and so on. At the same time, fractional-order differential equations have been proved to be an excellent tool in the modelling of many phenomena [9–11]. Recently, some important advances on dynamical behaviors such as chaos phenomena, Hopf bifurcation, synchronization control, and stabilization problems for fractional-order systems or fractional-order practical models have been reported in [12–16]. These proposed results show the superiority and importance of fractional calculus and effectively motivate the development of new applied fields.

Note that various classes of neural networks such as Hopfield neural networks [17, 18], recurrent neural networks [19, 20], cellular neural networks [21], Cohen-Grossberg neural networks [22], and bidirectional associative memory (BAM) neural networks [23–25] have been widely used in solving some signal processing, optimization, and image processing problems. In the last few years, some researchers have introduced fractional operators to neural networks to form fractional-order neural models [26–30], which could better describe the dynamical behaviors of the neurons. As an important dynamic behavior, stability is one of the most concerned problems for any dynamic system. For example, Song and Cao [26] have established some sufficient conditions to

ensure the existence and uniqueness of the nontrivial solution by using the contraction mapping principle, Krasnoselskii fixed point theorem, and the inequality technique, in which uniform stability conditions of fractional-order neural networks are also derived in fixed time-intervals. Note that time-delay (see [23–25, 31–37]) is a common phenomenon and is inevitable in practice, which often exists in almost every neural network and has an important effect on the stability and performance of system.

There are also several recent results discussing the topics including stability analysis for fractional-order dynamical systems in [38, 39]. For instance, the stability problems of main concern for control theory in finite-dimensional linear fractional-order systems have been considered [38], in which both internal and external stabilities for fractional-order differential systems in state-space form have been studied. For fractional-order differential systems in polynomial representation, the external stability has been thoroughly discussed. In [39], Matouk has investigated the stability conditions of a class of fractional-order hyperchaotic systems; then the stability conditions have been applied to a novel fractional-order hyperchaotic system. Based on the Routh-Hurwitz theorem, the conditions for controlling hyperchaos via feedback control approach have also been derived. At the same time, the various kinds of stability of delayed fractional-order neural networks have been extensively investigated. For example, Mittag-Leffler stability of fractional-order delayed neural networks has been investigated by applying fractional Lyapunov direct method [28, 30, 32]. The finite-time stability of Caputo fractional-order delayed neural networks has been studied by applying Gronwall's inequality approach and inequality scaling techniques [33, 34]. The delay-independent stability criteria of Riemann-Liouville fractional-order neutral-type delayed neural networks have been proposed based on classical Lyapunov functional method [35]. The uniform stability and global stability of fractional neural networks with delay are considered based on the fractional calculus theory and analytical techniques [36]. Global $o(t^{-\alpha})$ stability and global asymptotical periodicity for a class of fractional-order complex-valued neural networks with time-varying delays are discussed by using the fractional Lyapunov method and a Leibniz rule for fractional differentiation [37].

Although most dynamical systems are analyzed in either the continuous-time or discrete-time domain, many real systems in physics, engineering, chemistry, biology, and information science may experience abrupt changes as certain instants during the continuous dynamical processes. This kind of impulsive behaviors can be modelled by impulsive systems [23, 25, 29, 32, 40–42]. On the other hand, bidirectional associative memory (BAM) neural networks attract many studies due to its extensive applications in many fields [22–25, 43–46]. In [43], Kosko first introduced hybrid BAM neural network models. The remarkable feature of the proposed BAM neural networks lies in the close relation of the neurons between the U-layer and V-layer. That is, the neurons in one layer are fully interconnected to the one in the other layer, but there are not any interconnections among neurons in the same layer. It is worth mentioning that many contributions have been made concerning the dynamics of fractional-order BAM delayed neural networks (see [44–46]) including finite-time stability [44] and Mittag-Leffler synchronization [45]. In [46], globally asymptotic stability problem of impulsive fractional-order neural networks with discrete delays has been studied, yet the existence of the equilibrium solution for fractional-order BAM neural networks has not been taken into account. On the other hand, it should be pointed out that the finite-time stability and asymptotic stability in the sense of Lyapunov are different concepts, because finite-time stability does not contain Lyapunov asymptotic stability and vice versa [34, 47]. Although the signal transmission is sometimes instantaneous modelling with discrete delays, it may be sometimes a distribution propagation delay over a period of time so that distributed delays (see [20, 23, 25]) should not be ignored in the model. Compared to the advances of integer-order neural networks with or without time delays, the research on the stability of fractional-order BAM delayed neural networks is still at the stage of exploiting and developing [44–46]. To the best of our knowledge, there are few papers on investigating the global stability of the fractional-order hybrid BAM neural networks with both impulse and distributed delay in the current literature.

Motivated by the above discussions, this paper investigates the existence and globally asymptotic stability of equilibrium solution for impulsive Riemann-Liouville fractional-order hybrid BAM neural networks with distributed delays. The factors of such network systems including the distributed delays, impulses, and two different fractional-order derivatives between the U-layer and V- layer are taken into account synchronously. Based on the contraction mapping principle, the sufficient conditions are presented for the existence and uniqueness of the equilibrium solution for such network systems. By constructing a suitable Lyapunov functional associated with fractional integral terms, the globally asymptotic stability criteria of the equilibrium point are derived. The advantage of constructing the Lyapunov functional is that one can directly calculate its first-order derivative to check global stability. A numerical example is also given to show the validity and feasibility of the theoretical results.

This paper is organized as follows. In Section 2, we recall some definitions concerning fractional calculus and describe impulsive Riemann-Liouville fractional-order BAM neural networks with distributed delays. In Section 3, the existence and uniqueness of the equilibrium solution for such network systems are discussed based on the contraction mapping principle. In Section 4, the globally asymptotic stability criteria of the equilibrium solution are derived. An illustrative example is given to show the effectiveness and applicability of the proposed results in Section 5. Finally, some concluding remarks are drawn in Section 6.

2. Preliminaries and Model Description

In this section, we recall the definitions of fractional calculus and several basic lemmas. Moreover, we describe a class of impulsive fractional-order hybrid BAM neural network models with distributed delays.

Definition 1 (see [10]). The Riemann-Liouville fractional integral of order q for a function f is defined as

$$ {}_{t_0}D_t^{-q} f(t) = \frac{1}{\Gamma(q)} \int_{t_0}^{t} (t-s)^{q-1} f(s)\, ds, \tag{1} $$

where $q > 0$, $t \geqslant t_0$. The Gamma function $\Gamma(q)$ is defined by the integral

$$ \Gamma(z) = \int_0^{+\infty} s^{z-1} e^{-s} ds, \quad (\mathfrak{Re}(z) > 0). \tag{2} $$

Currently, there exist several definitions about the fractional derivative of order $q > 0$ including Grünwald-Letnikov (GL) definition, Riemann-Liouville (RL) definition, and Caputo definition [9–11]. In this paper, our consideration is the fractional-order neural networks with Riemann-Liouville derivative, whose definition and properties are given below.

Definition 2 (see [10]). The Riemann-Liouville fractional derivative of order q for a function f is defined as

$$ \begin{aligned} {}^{\mathrm{RL}}_{t_0}D_t^q f(t) &= \frac{d^m}{dt^m}\left[{}_{t_0}D_t^{-(m-q)} f(t) \right] \\ &= \frac{1}{\Gamma(m-q)} \frac{d^m}{dt^m} \int_{t_0}^{t} (t-s)^{m-q-1} f(s)\, ds, \end{aligned} \tag{3} $$

where $0 \leqslant m-1 < q < m$, $m \in \mathbb{Z}^+$.

In particular, for $\alpha \in (0,1)$ case, the Riemann-Liouville fractional derivative of order α for a constant x^* is

$$ {}^{\mathrm{RL}}_{0}D_t^{\alpha} x^* = \frac{t^{-\alpha}}{\Gamma(1-\alpha)} x^*. \tag{4} $$

Lemma 3 (see [10]). *If $f(t)$, $g(t) \in \mathbf{C}^m[t_0, b]$, and $m-1 \leqslant p < m \in \mathbb{Z}^+$, then*

(1) ${}^{\mathrm{RL}}_{t_0}D_t^q (L_1 f(t) + L_2 g(t)) = L_1 {}^{\mathrm{RL}}_{t_0}D_t^q f(t) + L_2 {}^{\mathrm{RL}}_{t_0}D_t^q g(t)$, $L_1, L_2 \in \mathbb{R}$, $q > 0$;

(2) ${}_{t_0}D_t^{-p}({}_{t_0}D_t^{-q} f(t)) = {}_{t_0}D_t^{-(p+q)} f(t)$, $p, q > 0$;

(3) ${}^{\mathrm{RL}}_{t_0}D_t^{p}({}_{t_0}D_t^{-q} f(t)) = {}^{\mathrm{RL}}_{t_0}D_t^{p-q} f(t)$, $p > q > 0$;

(4) ${}^{\mathrm{RL}}_{t_0}D_t^{p}({}_{t_0}D_t^{-q} f(t)) = {}_{t_0}D_t^{-(q-p)} f(t)$, $q > p > 0$.

The following lemmas will be used in the proof of our main results.

Lemma 4 (contraction mapping principle [48]). *Suppose that (X, ρ) is a complete metric space, $\Phi : X \to X$, and there is some real number $0 < k < 1$ such that*

$$ \rho(\Phi(x), \Phi(y)) \leqslant k\rho(x, y), \quad \forall x, y \in X; \tag{5} $$

then there is a unique point $x_0 \in X$ such that $\Phi(x_0) = x_0$.

Lemma 5 (fractional Barbalat lemma [42]). *If $\int_{t_0}^{t} w(s)ds$ has a finite limit as $t \to +\infty$, and ${}^{\mathrm{RL}}_{t_0}D_t^{\alpha} w(t)$ is bounded, then $w(t) \to 0$ as $t \to +\infty$, where $0 < \alpha < 1$.*

In this paper, we consider the Riemann-Liouville fractional-order hybrid BAM neural network models with distributed delay and impulsive effects described by the following states equations:

$$ \begin{aligned} {}^{\mathrm{RL}}_{0}D_t^{\alpha} x_i(t) &= -a_i x_i(t) + \sum_{j=1}^{m} b_{ij} f_j\left(y_j(t)\right) \\ &\quad + \sum_{j=1}^{m} \int_0^{\tau} r_{ij}(s)\, f_j\left(y_j(t-s)\right) ds + I_i, \\ &\qquad t > 0,\ t \neq t_k, \\ \Delta x_i(t_k) &= \gamma_k^{(1)}(x_i(t_k)), \\ &\qquad i = 1, 2, \ldots, n;\ k = 1, 2, \ldots, \\ {}^{\mathrm{RL}}_{0}D_t^{\beta} y_j(t) &= -c_j y_j(t) + \sum_{i=1}^{n} d_{ji} g_i(x_i(t)) \\ &\quad + \sum_{i=1}^{n} \int_0^{\tau} p_{ji}(s)\, g_i(x_i(t-s))\, ds + J_j, \\ &\qquad t > 0,\ t \neq t_k, \\ \Delta y_j(t_k) &= \gamma_k^{(2)}\left(y_j(t_k)\right), \\ &\qquad j = 1, 2, \ldots, m;\ k = 1, 2, \ldots, \end{aligned} \tag{6} $$

where $U = \{x_1, x_2, \ldots, x_n\}$ and $V = \{y_1, y_2, \ldots, y_m\}$ are two layers in the BAM model (6); $x_i(t)$ and $y_j(t)$ are state variables of ith neuron in the U-layer and jth neuron in the V-layer, respectively; ${}^{\mathrm{RL}}_{0}D_t^{\alpha} x_i(\cdot)$ and ${}^{\mathrm{RL}}_{0}D_t^{\beta} y_j(\cdot)$ denote an α and a β order Riemann-Liouville fractional-order derivative of $x_i(\cdot)$ and $y_j(\cdot)$, respectively; the constants α and β satisfy $0 < \alpha < 1$, $0 < \beta < 1$. $a_i > 0$ and $c_j > 0$ denote decay coefficients of signals from neurons x_i to y_j, respectively; f_i and g_j are the neuron activation functions; b_{ij}, d_{ji}, $r_{ij}(t)$ and $p_{ji}(t)$ represent the weight coefficients of the neurons; I_i and J_j denote the external inputs of U-layer and V-layer, respectively; $\tau > 0$ denotes the maximum possible transmission delay from neuron to another. Moreover, impulsive moments $\{t_k \mid k = 1, 2, \ldots\}$ satisfy $0 = t_0 < t_1 < t_2 < \cdots < t_k < \cdots$, $t_k \to +\infty$ as $k \to +\infty$, and

$$ \begin{aligned} \Delta x_i(t_k) &= x_i(t_k^+) - x_i(t_k^-), \\ x_i(t_k^+) &= \lim_{\varepsilon \to 0^+} x_i(t_k + \varepsilon),\ x_i(t_k^-) = x_i(t_k), \\ \Delta y_j(t_k) &= y_j(t_k^+) - y_j(t_k^-), \\ y_j(t_k^+) &= \lim_{\varepsilon \to 0^+} y_j(t_k + \varepsilon),\ y_j(t_k^-) = y_j(t_k), \end{aligned} \tag{7} $$

where $x_i(t_k^+)$ and $x_i(t_k^-)$ represent the right and left limits of $x_i(t)$ at $t = t_k$, respectively; $x_i(t_k^-) = x_i(t_k)$ and $y_j(t_k^-) = y_j(t_k)$ imply that $x_i(t)$ and $y_j(t)$ are both left continuous at $t = t_k$. The initial conditions associated with Riemann-Liouville

fractional-order network system (6) can be expressed as (see [9–11])

$$
\begin{aligned}
&{}_0D_t^{-(1-\alpha)} x_i(t) = \varphi_i(t),\\
&{}_0D_t^{-(1-\alpha)} y_j(t) = \psi_j(t),\\
&\qquad i = 1,2,\ldots,n;\ \ j = 1,2,\ldots,m,\ \ t \in [-\tau, 0].
\end{aligned}
\tag{8}
$$

Throughout this paper, we assume that the neuron activation functions f_j, g_i and impulsive operators $\gamma_k^{(1)}(x_i(t_k))$, $\gamma_k^{(2)}(y_j(t_k))$ satisfy the following conditions:

(**H1**) For $i = 1,2,\ldots,n$; $j = 1,2,\ldots,m$, the functions $r_{ij}(\cdot)$ and $p_{ji}(\cdot)$ are continuous on $[0,\tau]$. Thus, there exist positive constants $R_{ij}, P_{ji} \in \mathbb{R}^+$ such that

$$
\begin{aligned}
&\left|r_{ij}(s)\right| \leqslant R_{ij},\\
&\left|p_{ji}(s)\right| \leqslant P_{ji},\\
&\qquad \forall s \in [0,\tau].
\end{aligned}
\tag{9}
$$

(**H2**) The neuron activation functions $f_j(\cdot), g_i(\cdot)$ ($i = 1,2,\ldots,n$; $j = 1,2,\ldots,m$) are Lipschitz continuous. That is, there exist positive constants $F_j, G_j \in \mathbb{R}^+$ such that

$$
\begin{aligned}
&\left|f_j(x) - f_j(y)\right| \leqslant F_j\left|x - y\right|,\\
&\left|g_i(x) - g_i(y)\right| \leqslant G_i\left|x - y\right|,\\
&\qquad \forall x, y \in \mathbb{R}.
\end{aligned}
\tag{10}
$$

(**H3**) The impulsive operators $\gamma_k^{(1)}(x_i(t_k))$ and $\gamma_k^{(2)}(y_j(t_k))$ satisfy

$$
\begin{aligned}
&\gamma_k^{(1)}\left(x_i(t_k)\right) = -\lambda_{ik}^{(1)}\left(x_i(t_k) - x_i^*\right),\\
&\qquad i = 1,2,\ldots,n;\ \ k = 1,2,\ldots,\\
&\gamma_k^{(2)}\left(y_j(t_k)\right) = -\lambda_{jk}^{(2)}\left(y_j(t_k) - y_j^*\right),\\
&\qquad j = 1,2,\ldots,m;\ \ k = 1,2,\ldots,
\end{aligned}
\tag{11}
$$

where $\lambda_{ik}^{(1)} \in (0,2)$ ($i = 1,2,\ldots,n$; $k = 1,2,\ldots$), and $\lambda_{jk}^{(2)} \in (0,2)$ ($j = 1,2,\ldots,m$; $k = 1,2,\ldots$).

Remark 6. The purpose of this paper is to investigate the existence and globally asymptotic stability conditions of the equilibrium solution for fractional-order BAM network model (6). In discussing the stability of neural networks, the neuron activation functions are usually assumed to be bounded, monotonic [23], and differential [36, 37]. In system (6), the neuron activation functions are not necessarily bounded, monotonic, and differential. Therefore, the globally asymptotic stability criteria are more general and less conservative in this paper.

3. Existence of Equilibrium Solution

In this section, the sufficient conditions for the existence and uniqueness of the equilibrium solution of system (6) are derived based on the contraction mapping principle [48].

Similar to integer-order differential systems, we first define the equilibrium solution of fractional-order network systems. It should be pointed out that Riemann-Liouville fractional-order derivative of a nonzero constant is not equal to zero, which leads to the remarkable difference of the equilibrium solution between integer-order systems and Riemann-Liouville fractional-order systems.

Definition 7. A constant vector $(x^{*T}, y^{*T})^T = (x_1^*, x_2^*, \ldots, x_n^*, y_1^*, y_2^*, \ldots, y_m^*)^T \in \mathbb{R}^{n+m}$ is an equilibrium solution of system (6) if and only if $x^* = (x_1^*, x_2^*, \ldots, x_n^*)^T$ and $y^* = (y_1^*, y_2^*, \ldots, y_m^*)^T$ satisfy the following equations:

$$
\begin{aligned}
{}^{\mathrm{RL}}_0D_t^{\alpha}\left\{x_i^*\right\} &= -a_i x_i^* + \sum_{j=1}^{m} b_{ij} f_j\left(y_j^*\right)\\
&\quad + \sum_{j=1}^{m}\int_0^{\tau} r_{ij}(s)\, f_j\left(y_j^*\right) ds + I_i,\\
&\qquad i = 1,2,\ldots,n,\\
{}^{\mathrm{RL}}_0D_t^{\beta}\left\{y_j^*\right\} &= -c_j y_j^* + \sum_{i=1}^{n} d_{ji} g_i\left(x_i^*\right)\\
&\quad + \sum_{i=1}^{n}\int_0^{\tau} p_{ji}(s)\, g_i\left(x_i^*\right) ds + J_j,\\
&\qquad j = 1,2,\ldots,m,
\end{aligned}
\tag{12}
$$

and the impulsive jumps $\gamma_k^{(1)}(x_i(t_k))$ and $\gamma_k^{(2)}(y_j(t_k))$ are assumed to satisfy

$$
\begin{aligned}
&\gamma_k^{(1)}\left(x_i^*\right) = 0,\\
&\gamma_k^{(2)}\left(y_j^*\right) = 0,\\
&\qquad i = 1,2,\ldots,n;\ \ j = 1,2,\ldots,m;\ \ k = 1,2,\ldots.
\end{aligned}
\tag{13}
$$

In what follows, we use the following vector norm of $\mathbb{R}^{n+m}$:

$$
\|u\| = \sum_{i=1}^{n+m}\left|u_i\right|, \quad u = \left(u_1, u_2, \ldots, u_{n+m}\right)^T \in \mathbb{R}^{n+m}. \tag{14}
$$

Theorem 8. *Suppose that conditions (**H1**)–(**H3**) hold; then there exists a unique equilibrium solution for system (6), if the following inequalities simultaneously hold for a small enough constant $\varepsilon > 0$*

$$
\begin{aligned}
\omega_1 &= \max_{1\leqslant i\leqslant n}\left\{\frac{\varepsilon}{\Gamma(1-\alpha)}\cdot\frac{1}{a_i} + \frac{G_i}{a_i}\sum_{j=1}^{m}\left[\left|d_{ji}\right| + \tau P_{ji}\right]\right\}\\
&< 1,
\end{aligned}
$$

$$\omega_2 = \max_{1\leqslant j\leqslant m}\left\{\frac{\varepsilon}{\Gamma(1-\beta)}\cdot\frac{1}{c_j}+\frac{F_j}{c_j}\sum_{i=1}^{n}\left[\left|b_{ij}\right|+\tau R_{ij}\right]\right\} < 1. \tag{15}$$

Proof. According to Definition 2, for $\alpha,\beta \in (0,1)$, the Riemann-Liouville fractional-order derivatives of the constants u_i^* and v_j^* can be written as the following forms:

$$\begin{aligned} {}^{\mathrm{RL}}_{0}D_t^{\alpha}u_i^* &= \frac{t^{-\alpha}}{\Gamma(1-\alpha)}u_i^*,\\ {}^{\mathrm{RL}}_{0}D_t^{\beta}v_j^* &= \frac{t^{-\beta}}{\Gamma(1-\beta)}v_j^*, \end{aligned} \tag{16}$$

$$i = 1,2,\ldots,n;\ \ j = 1,2,\ldots,m.$$

Define a mapping $\Phi:\mathbb{R}^{n+m}\to\mathbb{R}^{n+m}$, where $\mathbf{u} = (u_1,\ldots,u_n, v_1,\ldots,v_m)^T \in \mathbb{R}^{n+m}$ and

$$\Phi(\mathbf{u}) = \begin{bmatrix} \sum_{j=1}^{m} b_{1j} f_j\left(\frac{v_j}{c_j}\right) + \sum_{j=1}^{m}\int_0^{\tau} r_{1j}(s)\, f_j\left(\frac{v_j}{c_j}\right)ds + I_1 - \frac{t^{-\alpha}}{\Gamma(1-\alpha)}\frac{u_1}{a_1} \\ \vdots \\ \sum_{j=1}^{m} b_{nj} f_j\left(\frac{v_j}{c_j}\right) + \sum_{j=1}^{m}\int_0^{\tau} r_{nj}(s)\, f_j\left(\frac{v_j}{c_j}\right)ds + I_n - \frac{t^{-\alpha}}{\Gamma(1-\alpha)}\frac{u_n}{a_n} \\ \sum_{i=1}^{n} d_{1i} g_i\left(\frac{u_i}{a_i}\right) + \sum_{i=1}^{n}\int_0^{\tau} p_{1i}(s)\, g_i\left(\frac{u_i}{a_i}\right)ds + J_1 - \frac{t^{-\beta}}{\Gamma(1-\beta)}\frac{v_1}{c_1} \\ \vdots \\ \sum_{i=1}^{n} d_{mi} g_i\left(\frac{u_i}{a_i}\right) + \sum_{i=1}^{n}\int_0^{\tau} p_{mi}(s)\, g_i\left(\frac{u_i}{a_i}\right)ds + J_m - \frac{t^{-\beta}}{\Gamma(1-\beta)}\frac{v_{\mathrm{m}}}{c_m} \end{bmatrix}. \tag{17}$$

Consider $\forall\overline{\mathbf{u}} = (\overline{u}_1,\ldots,\overline{u}_n,\overline{v}_1,\ldots,\overline{v}_m)^T \in \mathbb{R}^{n+m}$; then it follows from (14) that

$$\begin{aligned} \|\Phi(\mathbf{u})-\Phi(\overline{\mathbf{u}})\| \leqslant{}& \sum_{i=1}^{n}\left|\sum_{j=1}^{m}\left\{b_{ij}\left[f_j\left(\frac{v_j}{c_j}\right)-f_j\left(\frac{\overline{v}_j}{c_j}\right)\right]+\int_0^{\tau} r_{ij}(s)\left[f_j\left(\frac{v_j}{c_j}\right)-f_j\left(\frac{\overline{v}_j}{c_j}\right)\right]ds\right\}\right| \\ &+\sum_{j=1}^{m}\left|\sum_{i=1}^{n}\left\{d_{ji}\left[g_i\left(\frac{u_i}{a_i}\right)-g_i\left(\frac{\overline{u}_i}{a_i}\right)\right]+\int_0^{\tau} p_{ji}(s)\left[g_i\left(\frac{u_i}{a_i}\right)-g_i\left(\frac{\overline{u}_i}{a_i}\right)\right]ds\right\}\right| \\ &+\sum_{i=1}^{n}\left|\frac{t^{-\alpha}}{\Gamma(1-\alpha)}\left[\frac{u_i}{a_i}-\frac{\overline{u}_i}{a_i}\right]\right|+\sum_{j=1}^{m}\left|\frac{t^{-\beta}}{\Gamma(1-\beta)}\left[\frac{v_j}{c_j}-\frac{\overline{v}_j}{c_j}\right]\right|. \end{aligned} \tag{18}$$

According to (**H1**)-(**H2**), one has

$$\begin{aligned} \|\Phi(\mathbf{u})-\Phi(\overline{\mathbf{u}})\| \leqslant{}& \sum_{i=1}^{n}\sum_{j=1}^{m}\left\{\left|b_{ij}\right|F_j\left|\frac{v_j-\overline{v}_j}{c_j}\right| \right. \\ &+\left.\int_0^{\tau}\left|r_{ij}(s)\right|F_j\left|\frac{v_j-\overline{v}_j}{c_j}\right|ds\right\} \\ &+\sum_{j=1}^{m}\sum_{i=1}^{n}\left\{\left|d_{ji}\right|G_i\left|\frac{u_i-\overline{u}_i}{a_i}\right| \right. \\ &+\left.\int_0^{\tau}\left|p_{ji}(s)\right|G_i\left|\frac{u_i-\overline{u}_i}{a_i}\right|ds\right\}+\frac{t^{-\alpha}}{\Gamma(1-\alpha)} \\ &\cdot\max_{1\leqslant i\leqslant n}\left\{\frac{1}{a_i}\right\}\cdot\sum_{i=1}^{n}\left|u_i-\overline{u}_i\right|+\frac{t^{-\beta}}{\Gamma(1-\beta)}\cdot\max_{1\leqslant j\leqslant m}\left\{\frac{1}{c_j}\right\} \\ &\cdot\sum_{j=1}^{m}\left|v_j-\overline{v}_j\right|, \end{aligned} \tag{19}$$

For $\alpha,\beta\in(0,1)$, we have $\lim_{t\to+\infty}t^{-\alpha}=0$, $\lim_{t\to+\infty}t^{-\beta}=0$. Therefore, there exists a small enough constant $\varepsilon>0$ such that $t^{-\alpha}<\varepsilon$, $t^{-\beta}<\varepsilon$. Thus, it follows from (19) that

$$\begin{aligned} \|\Phi(\mathbf{u})-\Phi(\overline{\mathbf{u}})\| \leqslant{}& \sum_{i=1}^{n}\sum_{j=1}^{m}\left[\frac{\left|b_{ij}\right|+\tau R_{ij}}{c_j}F_j\left|v_j-\overline{v}_j\right|\right] \\ &+\sum_{j=1}^{m}\sum_{i=1}^{n}\left[\frac{\left|d_{ji}\right|+\tau P_{ji}}{a_i}G_i\left|u_i-\overline{u}_i\right|\right]+\frac{\varepsilon}{\Gamma(1-\alpha)} \end{aligned}$$

$$\cdot \max_{1\leqslant i\leqslant n}\left\{\frac{1}{a_i}\right\}\cdot\sum_{i=1}^{n}\left|u_i-\overline{u}_i\right|+\frac{\varepsilon}{\Gamma(1-\beta)}\cdot\max_{1\leqslant j\leqslant m}\left\{\frac{1}{c_j}\right\}$$
$$\cdot\sum_{j=1}^{m}\left|v_j-\overline{v}_j\right|$$
$$\leqslant \max_{1\leqslant j\leqslant m}\left\{\frac{\varepsilon}{\Gamma(1-\beta)}\cdot\frac{1}{c_j}+\frac{F_j}{c_j}\sum_{i=1}^{n}\left[\left|b_{ij}\right|+\tau R_{ij}\right]\right\}$$
$$\cdot\sum_{j=1}^{m}\left|v_j-\overline{v}_j\right|$$
$$+\max_{1\leqslant i\leqslant n}\left\{\frac{\varepsilon}{\Gamma(1-\alpha)}\cdot\frac{1}{a_i}+\frac{G_i}{a_i}\sum_{j=1}^{m}\left[\left|d_{ji}\right|+\tau P_{ji}\right]\right\}$$
$$\cdot\sum_{i=1}^{n}\left|u_i-\overline{u}_i\right|. \tag{20}$$

Let $k=\max\{\omega_1,\omega_2\}$, where ω_1 and ω_2 are defined in (15). Hence, we have

$$\begin{aligned}\left\|\Phi(\mathbf{u})-\Phi(\overline{\mathbf{u}})\right\| &\leqslant k\left[\sum_{i=1}^{n}\left|u_i-\overline{u}_i\right|+\sum_{j=1}^{m}\left|v_j-\overline{v}_j\right|\right]\\ &= k\left\|\mathbf{u}-\overline{\mathbf{u}}\right\|.\end{aligned} \tag{21}$$

Thus, it follows from (15) that $0<k<1$, which implies that $\Phi:\mathbb{R}^{n+m}\to\mathbb{R}^{n+m}$ is a contraction mapping. Therefore, from Lemma 4, there exists a unique fixed point of the map $\Phi:\mathbb{R}^{n+m}\to\mathbb{R}^{n+m}$, such that $\Phi(\mathbf{u}^*)=\mathbf{u}^*$. Thus, from (17), we get

$$\begin{aligned}&\sum_{j=1}^{m}b_{ij}f_j\left(\frac{v_j^*}{c_j}\right)+\sum_{j=1}^{m}\int_0^{\tau}r_{ij}(s)\,f_j\left(\frac{v_j^*}{c_j}\right)ds+I_i\\ &\quad-\frac{t^{-\alpha}}{\Gamma(1-\alpha)}\frac{u_i^*}{a_i}=u_i^*,\quad i=1,2,\ldots,n,\\ &\sum_{i=1}^{n}d_{ji}g_i\left(\frac{u_i^*}{a_i}\right)+\sum_{i=1}^{n}\int_0^{\tau}p_{ji}(s)\,g_i\left(\frac{u_i^*}{a_i}\right)ds+J_j\\ &\quad-\frac{t^{-\beta}}{\Gamma(1-\beta)}\frac{v_j^*}{c_j}=v_j^*,\quad j=1,2,\ldots,m.\end{aligned} \tag{22}$$

Let $x_i^*=u_i^*/a_i$, $y_j^*=v_j^*/c_j$; then it follows from (22) that

$$\begin{aligned}&\sum_{j=1}^{m}b_{ij}f_j\left(y_j^*\right)+\sum_{j=1}^{m}\int_0^{\tau}r_{ij}(s)\,f_j\left(y_j^*\right)ds+I_i\\ &\quad-\frac{t^{-\alpha}}{\Gamma(1-\alpha)}x_i^*=a_ix_i^*,\quad i=1,2,\ldots,n,\\ &\sum_{i=1}^{n}d_{ji}g_i\left(x_i^*\right)+\sum_{i=1}^{n}\int_0^{\tau}p_{ji}(s)\,g_i\left(x_i^*\right)ds+J_j\\ &\quad-\frac{t^{-\beta}}{\Gamma(1-\beta)}y_j^*=c_jy_j^*,\quad j=1,2,\ldots,m;\end{aligned} \tag{23}$$

that is

$$\begin{aligned}&\sum_{j=1}^{m}b_{ij}f_j\left(y_j^*\right)+\sum_{j=1}^{m}\int_0^{\tau}r_{ij}(s)\,f_j\left(y_j^*\right)ds+I_i-a_ix_i^*\\ &\quad={}_0^{\mathrm{RL}}D_t^{\alpha}\left\{x_i^*\right\},\quad i=1,2,\ldots,n,\\ &\sum_{i=1}^{n}d_{ji}g_i\left(x_i^*\right)+\sum_{i=1}^{n}\int_0^{\tau}p_{ji}(s)\,g_i\left(x_i^*\right)ds+J_j-c_jy_j^*\\ &\quad={}_0^{\mathrm{RL}}D_t^{\beta}\left\{y_j^*\right\},\quad j=1,2,\ldots,m.\end{aligned} \tag{24}$$

According to (**H3**), we know that

$$\begin{aligned}&\gamma_k^{(1)}\left(x_i^*\right)=0,\\ &\gamma_k^{(2)}\left(y_j^*\right)=0,\\ &\qquad i=1,2,\ldots,n;\ \ j=1,2,\ldots,m;\ \ k=1,2,\ldots.\end{aligned} \tag{25}$$

Thus, it follows from Definition 7 that $(x_1^*,x_2^*,\ldots,x_n^*,y_1^*,y_2^*,\ldots,y_m^*)^T\in\mathbb{R}^{n+m}$ is a unique equilibrium solution for system (6). The proof is complete. □

The following corollary is the direct result of Theorem 8.

Corollary 9. *Suppose that conditions (**H1**)–(**H3**) hold; then there exists a unique equilibrium solution for system (6), if the following inequalities simultaneously hold for a small enough constant $\varepsilon>0$*

$$\begin{aligned}&\min_{1\leqslant i\leqslant n}\left\{a_i-\frac{\varepsilon}{\Gamma(1-\alpha)}-G_i\sum_{j=1}^{m}\left[\left|d_{ji}\right|+\tau P_{ji}\right]\right\}>0,\\ &\min_{1\leqslant j\leqslant m}\left\{c_j-\frac{\varepsilon}{\Gamma(1-\beta)}-F_j\sum_{i=1}^{n}\left[\left|b_{ij}\right|+\tau R_{ij}\right]\right\}>0.\end{aligned} \tag{26}$$

Remark 10. Theorem 8 and Corollary 9 reveal that the conditions of existence and uniqueness of the equilibrium solution for system (6) are based on the contraction mapping principle, which can be expressed in terms of the algebraic inequalities. The conditions of existence and uniqueness of the equilibrium point for system (6) reflect the close relation between the coefficients, neuron activation functions, and time-delay of network parameters, which are also dependent on the orders α and β of Riemann-Liouville derivatives. On the other hand, if we only assume that (**H1**)–(**H3**) hold, then there exists at least an equilibrium solution for system (6) by applying Schauder fixed point theorem, whose proof is omitted here.

4. Globally Asymptotic Stability Criteria

In this section, by constructing a novel Lyapunov functional, we obtain the sufficient conditions to ensure the globally asymptotic stability of the equilibrium solution for system (6) based on fractional Barbalat theorem and classical Lyapunov stability theory.

Theorem 11. *Suppose that conditions (**H1**)–(**H3**) hold; then a unique equilibrium solution for system (6) is globally asymptotically stable, if the following inequalities simultaneously hold for a small enough constant $\varepsilon > 0$*

$$\eta_1 = \min_{1\leqslant i\leqslant n}\left\{a_i - G_i\sum_{j=1}^{m}\left[\left|d_{ji}\right| + \tau P_{ji}\right]\right\} > \frac{\varepsilon}{\Gamma(1-\alpha)},$$
$$\eta_2 = \min_{1\leqslant j\leqslant m}\left\{c_j - F_j\sum_{i=1}^{n}\left[\left|b_{ij}\right| + \tau R_{ij}\right]\right\} > \frac{\varepsilon}{\Gamma(1-\beta)}. \tag{27}$$

Proof. From Corollary 9, there exists a unique equilibrium solution $(x^{*T}, y^{*T})^T$ for system (6). By using the variable transformation method, we can shift the equilibrium point to the origin. Let $u_i(t) = x_i(t) - x_i^*$, $v_j(t) = y_j(t) - y_j^*$; then system (6) is transformed into

$$\begin{aligned}
&{}^{\mathrm{RL}}_{0}D_t^{\alpha}u_i(t)\\
&\quad = -a_iu_i(t) + \sum_{j=1}^{m}b_{ij}\left[f_j\left(y_j(t)\right) - f_j\left(y_j^*\right)\right]\\
&\qquad + \sum_{j=1}^{m}\int_0^{\tau}r_{ij}(s)\left[f_j\left(y_j(t-s)\right) - f_j\left(y_j^*\right)\right]ds,\\
&\qquad\qquad t \neq t_k,\\
&u_i\left(t_k^+\right) = \left(1-\lambda_{ik}^{(1)}\right)u_i\left(t_k^-\right),\\
&\qquad\qquad i = 1,2,\ldots,n;\ k = 1,2,\ldots,\\
&{}^{\mathrm{RL}}_{0}D_t^{\beta}v_j(t)\\
&\quad = -c_jv_j(t) + \sum_{i=1}^{n}d_{ji}\left[g_i\left(x_i(t)\right) - g_i\left(x_i^*\right)\right]\\
&\qquad + \sum_{i=1}^{n}\int_0^{\tau}p_{ji}(s)\left[g_ix_i(t-s) - g_i\left(x_i^*\right)\right]ds,\\
&\qquad\qquad t \neq t_k,\\
&v_j\left(t_k^+\right) = \left(1-\lambda_{jk}^{(2)}\right)v_j\left(t_k^-\right),\\
&\qquad\qquad j = 1,2,\ldots,m;\ k = 1,2,\ldots.
\end{aligned} \tag{28}$$

Construct a novel Lyapunov functional composed of fractional-order integral and definite integral terms:

$$\begin{aligned}
V(t) = {}& {}_0D_t^{-(1-\alpha)}\left[\sum_{i=1}^{n}\left|u_i(t)\right|\right]\\
&+ {}_0D_t^{-(1-\beta)}\left[\sum_{j=1}^{m}\left|v_j(t)\right|\right]\\
&+ \sum_{i=1}^{n}\sum_{j=1}^{m}F_j\left|b_{ij}\right|\int_{t-\tau}^{t}\left|v_j(s)\right|ds\\
&+ \sum_{j=1}^{m}\sum_{i=1}^{n}G_i\left|d_{ji}\right|\int_{t-\tau}^{t}\left|u_i(s)\right|ds\\
&+ \sum_{i=1}^{n}\sum_{j=1}^{m}F_jR_{ij}\int_0^{\tau}\int_{t-s}^{t}\left|v_j(\eta)\right|d\eta\,ds\\
&+ \sum_{j=1}^{m}\sum_{i=1}^{n}G_iP_{ji}\int_0^{\tau}\int_{t-s}^{t}\left|u_i(\eta)\right|d\eta\,ds.
\end{aligned} \tag{29}$$

The time derivative of $V(t)$ along the trajectories of system (6) can be calculated, which are carried out for the following cases.

Case 1. For $t \neq t_k$, from Lemma 3, we obtain

$$\begin{aligned}
\frac{d^+V(t)}{dt} = {}& {}^{\mathrm{RL}}_{0}D_t^{\alpha}\left[\sum_{i=1}^{n}\left|u_i(t)\right|\right] + {}^{\mathrm{RL}}_{0}D_t^{\beta}\left[\sum_{j=1}^{m}\left|v_j(t)\right|\right]\\
&+ \sum_{i=1}^{n}\sum_{j=1}^{m}F_j\left|b_{ij}\right|\left[\left|v_j(t)\right| - \left|v_j(t-\tau)\right|\right]\\
&+ \sum_{j=1}^{m}\sum_{i=1}^{n}G_i\left|d_{ji}\right|\left[\left|u_i(t)\right| - \left|u_i(t-\tau)\right|\right]\\
&+ \sum_{i=1}^{n}\sum_{j=1}^{m}F_jR_{ij}\int_0^{\tau}\left[\left|v_j(t)\right| - \left|v_j(t-s)\right|\right]ds\\
&+ \sum_{j=1}^{m}\sum_{i=1}^{n}G_iP_{ji}\int_0^{\tau}\left[\left|u_i(t)\right| - \left|u_i(t-s)\right|\right]ds.
\end{aligned} \tag{30}$$

An application of Definition 2 yields

$$\begin{aligned}
{}^{\mathrm{RL}}_{0}D_t^{\alpha}\left|u_i(t)\right| &= \mathrm{sgn}\left(u_i(t)\right)\cdot\left({}^{\mathrm{RL}}_{0}D_t^{\alpha}u_i(t)\right),\\
{}^{\mathrm{RL}}_{0}D_t^{\beta}\left|v_j(t)\right| &= \mathrm{sgn}\left(v_j(t)\right)\cdot\left({}^{\mathrm{RL}}_{0}D_t^{\beta}v_j(t)\right),
\end{aligned} \tag{31}$$

where sgn(·) denotes the standard signum function. Thus, (30) can be rewritten as

$$\begin{aligned}
\frac{d^+V(t)}{dt} = {}& \sum_{i=1}^{n}\mathrm{sgn}\left(u_i(t)\right)\left[{}^{\mathrm{RL}}_{0}D_t^{\alpha}\left(u_i(t)\right)\right]\\
&+ \sum_{j=1}^{m}\mathrm{sgn}\left(v_j(t)\right)\left[{}^{\mathrm{RL}}_{0}D_t^{\beta}\left(v_j(t)\right)\right]\\
&+ \sum_{i=1}^{n}\sum_{j=1}^{m}F_j\left|b_{ij}\right|\left[\left|v_j(t)\right| - \left|v_j(t-\tau)\right|\right]
\end{aligned}$$

$$+\sum_{j=1}^{m}\sum_{i=1}^{n}G_i\left|d_{ji}\right|\left[\left|u_i(t)\right|-\left|u_i(t-\tau)\right|\right]$$
$$+\sum_{i=1}^{n}\sum_{j=1}^{m}F_jR_{ij}\int_0^{\tau}\left[\left|v_j(t)\right|-\left|v_j(t-s)\right|\right]ds$$
$$+\sum_{j=1}^{m}\sum_{i=1}^{n}G_iP_{ji}\int_0^{\tau}\left[\left|u_i(t)\right|-\left|u_i(t-s)\right|\right]ds. \tag{32}$$

Combining (28) and (32) yields

$$\begin{aligned}\frac{d^+V(t)}{dt}&=\sum_{i=1}^{n}\operatorname{sgn}(u_i(t))\left\{-a_iu_i(t)\right.\\&+\sum_{j=1}^{m}b_{ij}\left[f_j\left(y_j(t)\right)-f_j\left(y_j^*\right)\right]\\&\left.+\sum_{j=1}^{m}\int_0^{\tau}r_{ij}(s)\left[f_j\left(y_j(t-s)\right)-f_j\left(y_j^*\right)\right]ds\right\}\\&+\sum_{j=1}^{m}\operatorname{sgn}\left(v_j(t)\right)\left\{-c_jv_j(t)\right.\\&+\sum_{i=1}^{n}d_{ji}\left[g_i(x_i(t))-g_i(x_i^*)\right]\\&\left.+\sum_{i=1}^{n}\int_0^{\tau}p_{ji}(s)\left[g_ix_i(t-s)-g_i(x_i^*)\right]ds\right\}\\&+\sum_{i=1}^{n}\sum_{j=1}^{m}F_j\left|b_{ij}\right|\left[\left|v_j(t)\right|-\left|v_j(t-\tau)\right|\right]\\&+\sum_{j=1}^{m}\sum_{i=1}^{n}G_i\left|d_{ji}\right|\left[\left|u_i(t)\right|-\left|u_i(t-\tau)\right|\right]+\sum_{i=1}^{n}\sum_{j=1}^{m}F_jR_{ij}\\&\cdot\int_0^{\tau}\left[\left|v_j(t)\right|-\left|v_j(t-s)\right|\right]ds+\sum_{j=1}^{m}\sum_{i=1}^{n}G_iP_{ji}\\&\cdot\int_0^{\tau}\left[\left|u_i(t)\right|-\left|u_i(t-s)\right|\right]ds.\end{aligned} \tag{33}$$

By computations, we have

$$\begin{aligned}\frac{d^+V(t)}{dt}&\leqslant-\sum_{i=1}^{n}a_i\left|u_i(t)\right|-\sum_{j=m}^{n}c_j\left|v_j(t)\right|\\&+\sum_{i=1}^{n}\sum_{j=1}^{m}F_j\left|b_{ij}\right|\left|v_j(t-\tau)\right|\\&+\sum_{j=1}^{m}\sum_{i=1}^{n}G_i\left|d_{ji}\right|\left|u_i(t-\tau)\right|\\&+\sum_{i=1}^{n}\sum_{j=1}^{m}F_jR_{ij}\int_0^{\tau}\left|v_j(t-s)\right|ds\\&+\sum_{j=1}^{m}\sum_{i=1}^{n}G_iP_{ji}\int_0^{\tau}\left|u_i(t-s)\right|ds\\&+\sum_{i=1}^{n}\sum_{j=1}^{m}F_j\left|b_{ij}\right|\left[\left|v_j(t)\right|-\left|v_j(t-\tau)\right|\right]\\&+\sum_{j=1}^{m}\sum_{i=1}^{n}G_i\left|d_{ji}\right|\left[\left|u_i(t)\right|-\left|u_i(t-\tau)\right|\right]\\&+\sum_{i=1}^{n}\sum_{j=1}^{m}F_jR_{ij}\int_0^{\tau}\left[\left|v_j(t)\right|-\left|v_j(t-s)\right|\right]ds\\&+\sum_{j=1}^{m}\sum_{i=1}^{n}G_iP_{ji}\int_0^{\tau}\left[\left|u_i(t)\right|-\left|u_i(t-s)\right|\right]ds\\&\leqslant-\sum_{i=1}^{n}a_i\left|u_i(t)\right|-\sum_{j=m}^{n}c_j\left|v_j(t)\right|\\&+\sum_{i=1}^{n}\sum_{j=1}^{m}F_j\left|b_{ij}\right|\left|v_j(t)\right|\\&+\sum_{j=1}^{m}\sum_{i=1}^{n}G_i\left|d_{ji}\right|\left|u_i(t)\right|\\&+\sum_{i=1}^{n}\sum_{j=1}^{m}F_jR_{ij}\int_0^{\tau}\left|v_j(t)\right|ds\\&+\sum_{j=1i=1}^{m}\sum_{n}G_iP_{ji}\int_0^{\tau}\left|u_i(t)\right|ds\\&\leqslant\sum_{i=1}^{n}\left\{-a_i+G_i\sum_{j=1}^{m}\left(\left|d_{ji}\right|+\tau P_{ji}\right)\right\}\left|u_i(t)\right|\\&+\sum_{j=1}^{m}\left\{-c_j+F_j\sum_{i=1}^{n}\left(\left|b_{ij}\right|+\tau R_{ij}\right)\right\}\left|v_j(t)\right|\\&\leqslant-\frac{\varepsilon}{\Gamma(1-\alpha)}\sum_{i=1}^{n}\left|u_i(t)\right|\\&-\frac{\varepsilon}{\Gamma(1-\beta)}\sum_{j=1}^{m}\left|v_j(t)\right|,\quad t\neq t_k,\end{aligned} \tag{34}$$

which implies that $d^+V(t)/dt\leqslant 0$ as $t\neq t_k$. Hence, for any $t\in[t_{k-1},t_k)$, we get

$$V(t)+\int_{t_{k-1}}^{t_k}\left[\frac{\varepsilon}{\Gamma(1-\alpha)}\sum_{i=1}^{n}\left|u_i(s)\right|+\frac{\varepsilon}{\Gamma(1-\beta)}\sum_{j=1}^{m}\left|v_j(s)\right|\right]ds\leqslant V\left(t_{k-1}^+\right). \tag{35}$$

Case 2. For $t = t_k$, from (29), one has

$$\begin{aligned} V(t_k^+) = {}& {}_0D_{t_k^+}^{-(1-\alpha)}\left[\sum_{i=1}^{n}\left|u_i(t_k^+)\right|\right] \\ & + {}_0D_{t_k^+}^{-(1-\beta)}\left[\sum_{j=1}^{m}\left|v_j(t_k^+)\right|\right] \\ & + \sum_{i=1}^{n}\sum_{j=1}^{m}F_j\left|b_{ij}\right|\int_{t_k^+-\tau}^{t_k^+}\left|v_j(s)\right|ds \\ & + \sum_{j=1}^{m}\sum_{i=1}^{n}G_i\left|d_{ji}\right|\int_{t_k^+-\tau}^{t_k^+}\left|u_i(s)\right|ds \\ & + \sum_{i=1}^{n}\sum_{j=1}^{m}F_jR_{ij}\int_0^{\tau}\int_{t_k^+-s}^{t_k^+}\left|v_j(\eta)\right|d\eta\,ds \\ & + \sum_{j=1}^{m}\sum_{i=1}^{n}G_iP_{ji}\int_0^{\tau}\int_{t_k^+-s}^{t_k^+}\left|u_i(\eta)\right|d\eta\,ds. \end{aligned} \tag{36}$$

From (**H3**), we get

$$\begin{aligned} V(t_k^+) = {}& {}_0D_{t_k^+}^{-(1-\alpha)}\left[\sum_{i=1}^{n}\left|1-\lambda_{ik}^{(1)}\right|\left|u_i(t_k^-)\right|\right] \\ & + {}_0D_{t_k^+}^{-(1-\beta)}\left[\sum_{j=1}^{m}\left|1-\lambda_{jk}^{(2)}\right|\left|v_j(t_k^-)\right|\right] \\ & + \sum_{i=1}^{n}\sum_{j=1}^{m}F_j\left|b_{ij}\right|\int_{t_k^+-\tau}^{t_k^+}\left|v_j(s)\right|ds \\ & + \sum_{j=1}^{m}\sum_{i=1}^{n}G_i\left|d_{ji}\right|\int_{t_k^+-\tau}^{t_k^+}\left|u_{\mathrm{i}}(s)\right|ds \\ & + \sum_{i=1}^{n}\sum_{j=1}^{m}F_jR_{ij}\int_0^{\tau}\int_{t_k^+-s}^{t_k^+}\left|v_j(\eta)\right|d\eta\,ds \\ & + \sum_{j=1}^{m}\sum_{i=1}^{n}G_iP_{ji}\int_0^{\tau}\int_{t_k^+-s}^{t_k^+}\left|u_i(\eta)\right|d\eta\,ds. \end{aligned} \tag{37}$$

Note that the inequalities $|1-\lambda_{ik}^{(1)}| < 1$ and $|1-\lambda_{jk}^{(2)}| < 1$ hold; then

$$\begin{aligned} V(t_k^+) \leqslant {}& {}_0D_{t_k^-}^{-(1-\alpha)}\left[\sum_{i=1}^{n}\left|u_i(t_k^-)\right|\right] \\ & + {}_0D_{t_k^-}^{-(1-\beta)}\left[\sum_{j=1}^{m}\left|v_j(t_k^-)\right|\right] \\ & + \sum_{i=1}^{n}\sum_{j=1}^{m}F_j\left|b_{ij}\right|\int_{t_k^+-\tau}^{t_k^+}\left|v_j(s)\right|ds \\ & + \sum_{j=1}^{m}\sum_{i=1}^{n}G_i\left|d_{ji}\right|\int_{t_k^+-\tau}^{t_k^+}\left|u_i(s)\right|ds \\ & + \sum_{i=1}^{n}\sum_{j=1}^{m}F_jR_{ij}\int_0^{\tau}\int_{t_k^+-s}^{t_k^+}\left|v_j(\eta)\right|d\eta\,ds \\ & + \sum_{j=1}^{m}\sum_{i=1}^{n}G_iP_{ji}\int_0^{\tau}\int_{t_k^+-s}^{t_k^+}\left|u_i(\eta)\right|d\eta\,ds = V(t_k^-) \\ = {}& V(t_k). \end{aligned} \tag{38}$$

Let $U(t) = \sum_{i=1}^{n}|u_i(t)| + \sum_{j=1}^{m}|v_j(t)|$, for any $t \in [t_{k-1}, t_k)$; then we have the following estimations:

$$\begin{aligned} V(t) &\leqslant -\int_{t_{k-1}}^{t}U(s)\,ds + V(t_{k-1}^+) \\ &\leqslant -\int_{t_{k-1}}^{t}U(s)\,ds + V(t_{k-1}^-) \\ &\leqslant -\int_{t_{k-2}}^{t}U(s)\,ds + V(t_{k-2}^-) \leqslant \cdots \\ &\leqslant -\int_0^t U(s)\,ds + V(0); \end{aligned} \tag{39}$$

Thus, we can get the following inequality:

$$V(t) + \int_0^t U(s)\,ds \leqslant V(0), \tag{40}$$

which implies that $\lim_{t\to+\infty}U(t)$ is bounded. From (28), $|{}_0^{\mathrm{RL}}D_t^{\alpha}u_i(t)|$ and $|{}_0^{\mathrm{RL}}D_t^{\beta}v_j(t)|$ are also bounded. From Lemma 5, we have $\lim_{t\to+\infty}\sum_{i=1}^{n}|u_i(t)| = 0$ and $\lim_{t\to+\infty}\sum_{j=1}^{m}|v_j(t)| = 0$. Therefore, according to Lyapunov stability theory, a unique equilibrium solution $(x^{*T}, y^{*T})^T$ for system (6) is globally asymptotically stable. This completes the proof. □

The following corollary is the direct result of Theorem 11.

Corollary 12. *Suppose that (**H1**)–(**H3**) hold; then a unique equilibrium solution for system (6) is globally asymptotically stable, if the following inequalities simultaneously hold for a small enough constant* $\varepsilon > 0$

$$\begin{aligned} \omega_1 &= \max_{1\leqslant i\leqslant n}\left\{\frac{\varepsilon}{\Gamma(1-\alpha)}\cdot\frac{1}{a_i} + \frac{G_i}{a_i}\sum_{j=1}^{m}\left[\left|d_{ji}\right| + \tau P_{ji}\right]\right\} \\ &< 1, \\ \omega_2 &= \max_{1\leqslant j\leqslant m}\left\{\frac{\varepsilon}{\Gamma(1-\beta)}\cdot\frac{1}{c_j} + \frac{F_j}{c_j}\sum_{i=1}^{n}\left[\left|b_{ij}\right| + \tau R_{ij}\right]\right\} \\ &< 1. \end{aligned} \tag{41}$$

Remark 13. Different from fractional Lyapunov functional method in [30, 32, 37], an appropriate Lyapunov functional composed of fractional integral and definite integral terms in the proof of Theorem 11 is presented, and we only

need to calculate its first-order derivative to derive stability conditions. As discussed in [35], in general speaking, it is very difficult to calculate the fractional-order derivatives of a Lyapunov functional. The main advantage of our constructed method is that we can avoid computing the fractional-order derivatives of the Lyapunov functional.

Remark 14. The globally asymptotic stability criteria of a unique equilibrium solution for system (6) are described by the algebraic inequalities, which are dependent on the orders α and β of fractional derivatives and reflect the close relation between the coefficients, neuron activation functions, and time-delay of network parameters. Moreover, the globally asymptotic stability criteria are more easily checked and contribute to reducing the computational burden.

Remark 15. When $\alpha = \beta = 1$, system (6) is reduced to integer-order BAM neural networks with distributed delays and impulses [23]. Note that the Riemann-Liouville derivative is a continuous operator of the order (see [9–11]); then we can obtain globally asymptotic stability criteria for impulsive integer-order hybrid BAM neural networks from the proof of Theorem 11.

Remark 16. In [33, 34, 44], the authors have focused on studying the finite-time stability of fractional-order delayed neural networks. However, it should be pointed out that the finite-time stability and asymptotic stability in the sense of Lyapunov are different concepts, because finite-time stability does not contain Lyapunov asymptotic stability and vice versa [34, 47]. This is also the motivation of this paper.

5. An Illustrative Example

In this section, an example for impulsive fractional-order hybrid BAM neural networks with distributed delays is given to illustrate the effectiveness and feasibility of the theoretical results.

Example 17. Consider the four-state Riemann-Liouville fractional-order hybrid BAM neural network model with distributed delays and impulsive effects described by

$$
\begin{aligned}
{}^{\mathrm{RL}}_{0}D_{t}^{0.2}\, x_1(t) &= -0.7x_1(t) - 0.2f_1\left(y_1(t)\right) \\
&\quad + 0.1f_2\left(y_2(t)\right) \\
&\quad + 2\int_0^{0.2} sf_1\left(y_1(t-s)\right)ds \\
&\quad + \int_0^{0.2} sf_2\left(y_2(t-s)\right)ds, \\
{}^{\mathrm{RL}}_{0}D_{t}^{0.2}\, x_2(t) &= -0.6x_2(t) + 0.3f_1\left(y_1(t)\right) \\
&\quad + 0.2f_2\left(y_2(t)\right) \\
&\quad + \int_0^{0.2} sf_1\left(y_1(t-s)\right)ds \\
&\quad - \int_0^{0.2} s^3 f_2\left(y_2(t-s)\right)ds, \\
\Delta x_i\left(t_k\right) &= -0.3\left(x_i\left(t_k\right) - x_i^*\right), \\
&\qquad i = 1,2;\ k = 1,2,\ldots, \\
{}^{\mathrm{RL}}_{0}D_{t}^{0.6}\, y_1(t) &= -0.7y_1(t) + 0.4g_1\left(y_1(t)\right) \\
&\quad + 0.2g_2\left(y_2(t)\right) \\
&\quad - \int_0^{0.2} sg_1\left(y_1(t-s)\right)ds \\
&\quad + \int_0^{0.2} s^2 g_2\left(y_2(t-s)\right)ds, \\
{}^{\mathrm{RL}}_{0}D_{t}^{0.6}\, y_2(t) &= -0.6y_2(t) + 0.1g_1\left(y_1(t)\right) \\
&\quad - 0.3g_2\left(y_2(t)\right) \\
&\quad + \int_0^{0.2} s^2 g_1\left(y_1(t-s)\right)ds \\
&\quad + \int_0^{0.2} sg_2\left(y_2(t-s)\right)ds, \\
\Delta y_j\left(t_k\right) &= -0.4\left(y_j\left(t_k\right) - y_i^*\right), \\
&\qquad j = 1,2;\ k = 1,2,\ldots,
\end{aligned}
\tag{42}
$$

where $\alpha = 0.2$, $\beta = 0.6$, $\tau = 0.2$, $a_1 = c_1 = 0.7$, $a_2 = c_2 = 0.6$, $b_{11} = -0.2$, $b_{12} = 0.1$, $b_{21} = 0.3$, $b_{22} = 0.2$, $d_{11} = 0.4$, $d_{12} = 0.2$, $d_{21} = 0.1$, $d_{22} = -0.3$, $r_{11}(s) = 2s$, $r_{12}(s) = s$, $r_{21}(s) = s$, $r_{22}(s) = -s^3$, $p_{11}(s) = -s$, $p_{12}(s) = s^2$, $p_{21}(s) = s^2$, $p_{22}(s) = s$, and

$$
\begin{aligned}
f_j\left(y_j\right) &= \frac{1}{2}\left(\left|y_j + 1\right| - \left|y_j - 1\right|\right), \quad j = 1,2, \\
g_i\left(x_i\right) &= \frac{1}{2}\left(\left|x_i + 1\right| - \left|x_i - 1\right|\right), \quad i = 1,2.
\end{aligned}
\tag{43}
$$

From (43), we know that $F_1 = F_2 = G_1 = G_2 = 1$. Since $f_1(0) = f_2(0) = 0$, $g_1(0) = g_2(0) = 0$, then $(x_1^*, x_2^*, y_1^*, y_1^*)^T = (0,0,0,0)^T$ is an equilibrium solution for system (42). Next, we apply Theorem 11 or Corollary 12 to check the uniqueness and global asymptotic stability of the equilibrium point for system (42).

In fact, by computations, one can get that $R_{11} = 0.4$, $R_{12} = R_{21} = 0.2$, $R_{22} = 0.008$, $P_{11} = P_{22} = 0.2$, and $P_{12} = P_{21} = 0.04$. Choosing a positive constant $\varepsilon = 0.04 > 0$, then we can obtain

$$
\begin{aligned}
\eta_1 &= \min_{1\leqslant i\leqslant 2}\left\{a_i - G_i\sum_{j=1}^{2}\left[\left|d_{ji}\right| + \tau P_{ji}\right]\right\} = 0.052 \\
&> \frac{\varepsilon}{\Gamma(1-\alpha)} = 0.044, \\
\eta_2 &= \min_{1\leqslant j\leqslant 2}\left\{c_j - F_j\sum_{i=1}^{2}\left[\left|b_{ij}\right| + \tau R_{ij}\right]\right\} = 0.116 \\
&> \frac{\varepsilon}{\Gamma(1-\beta)} = 0.045,
\end{aligned}
$$

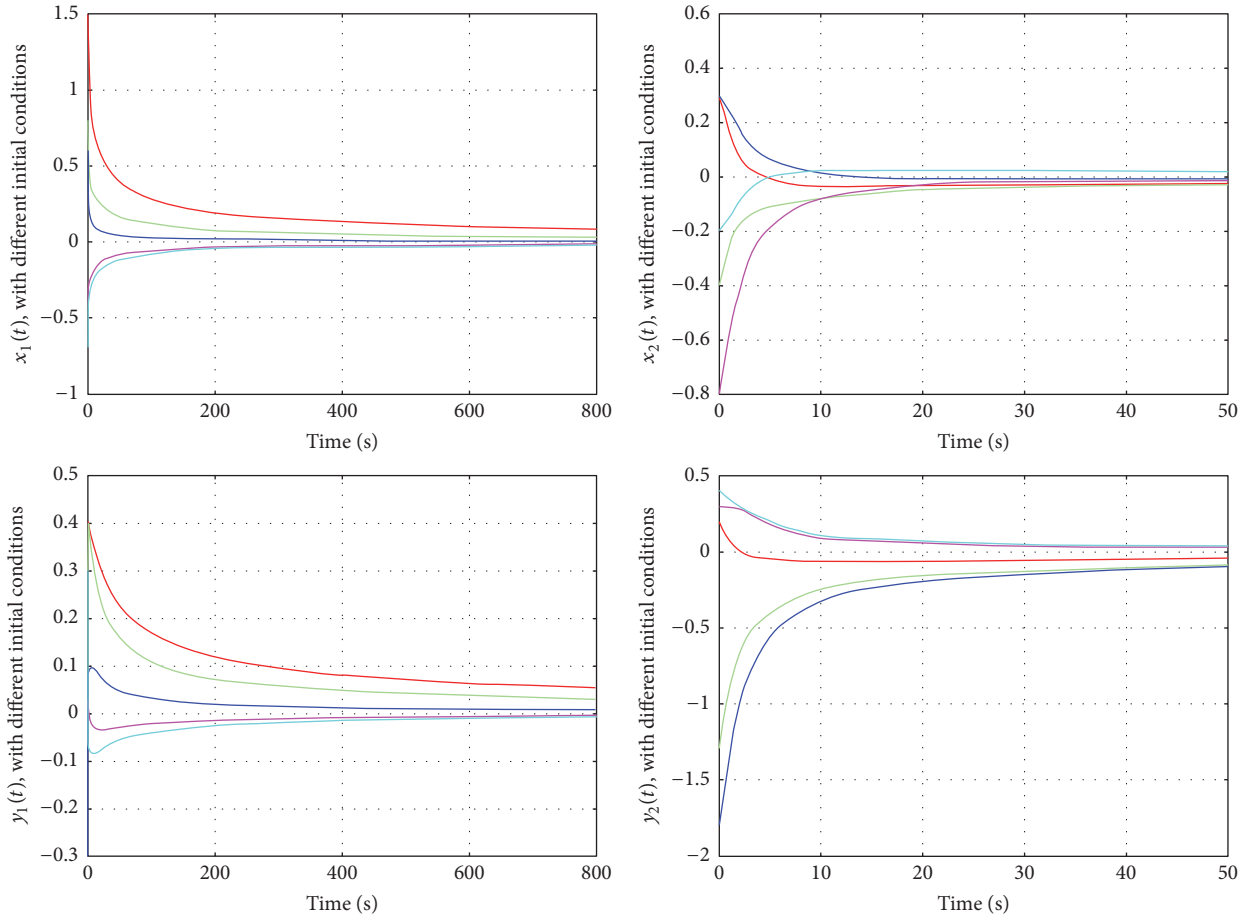

FIGURE 1: State trajectories of BAM neural network (42) with $\alpha = 0.2$; $\beta = 0.6$ under different initial conditions.

$$\omega_1 = \max_{1\leqslant i\leqslant 2}\left\{\frac{\varepsilon}{\Gamma(1-\alpha)}\cdot\frac{1}{a_i}+\frac{G_i}{a_i}\sum_{j=1}^{2}\left[\left|d_{ji}\right|+\tau P_{ji}\right]\right\}$$
$$= 0.856 < 1,$$
$$\omega_2 = \max_{1\leqslant j\leqslant 2}\left\{\frac{\varepsilon}{\Gamma(1-\beta)}\cdot\frac{1}{c_j}+\frac{F_j}{c_j}\sum_{i=1}^{2}\left[\left|b_{ij}\right|+\tau R_{ij}\right]\right\}$$
$$= 0.722 < 1. \tag{44}$$

Thus, the conditions of Theorem 11 or Corollary 12 are satisfied. For numerical simulations, Figure 1 depicts the state trajectories of system (42) under different initial conditions with $\alpha = 0.2$, $\beta = 0.6$. It can be directly observed that the unique equilibrium solution $(0, 0, 0, 0)^T$ for system (42) is globally asymptotically stable with $\alpha = 0.2$, $\beta = 0.6$. Therefore, the numerical simulations further confirm the theoretical results of this paper.

6. Conclusions

In this paper, the sufficient conditions for the existence and uniqueness of the equilibrium solution are presented based on the contraction mapping principle. By constructing a suitable Lyapunov functional composed of fractional integral and definite integral terms, we calculate its first-order derivative to derive global asymptotic stability of the equilibrium point. The constructed method avoids calculating the fractional-order derivative of the Lyapunov functional. Furthermore, the presented results are described as the algebraic inequalities, which are convenient and feasible to verify the existence and asymptotic stability of the equilibrium solution. For further research, it is interesting and challenging to discuss the chaos phenomena, Hopf bifurcation, and synchronization control problem for fractional-order memristor-based hybrid BAM neural networks with leakage, time-varying, and distributed delays.

Conflicts of Interest

The authors declare that there are no conflicts of interest with regard to the publication of this paper.

Acknowledgments

This work is jointly supported by the National Natural Science Fund of China (11301308, 61573096, and 61272530),

the 333 Engineering Fund of Jiangsu Province of China (BRA2015286), the Natural Science Fund of Anhui Province of China (1608085MA14), the Key Project of Natural Science Research of Anhui Higher Education Institutions of China (gxyqZD2016205 and KJ2015A152), and the Natural Science Youth Fund of Jiangsu Province of China (BK20160660).

References

[1] R. Metzler and J. Klafter, "The random walk's guide to anomalous diffusion: a fractional dynamics approach," *Physics Reports. A Review Section of Physics Letters*, vol. 339, no. 1, pp. 1–77, 2000.

[2] R. Hilfer, *Applications of Fractional Calculus in Physics*, World Scientific, Toh Tuck Link, Singapore, 2000.

[3] N. Laskin, "Fractional market dynamics," *Physica A. Statistical Mechanics and its Applications*, vol. 287, no. 3-4, pp. 482–492, 2000.

[4] J. Sabatier, O. P. Agrawal, and J. A. Tenreiro Machado, *Advances in Fractional Calculus: Theoretical Developments and Applications in Physics and Engineering*, Springer, Dordrecht, Netherlands, 2007.

[5] D. Baleanu, J. A. Tenreiro Machado, and A. C. J. Luo, *Fractional Dynamics and Control*, Springer, New York, NY, USA, 2012.

[6] R. L. Magin, "Fractional calculus models of complex dynamics in biological tissues," *Computers & Mathematics with Applications*, vol. 59, no. 5, pp. 1586–1593, 2010.

[7] W. C. Chen, "Nonlinear dynamics and chaos in a fractional-order financial system," *Chaos, Solitons and Fractals*, vol. 36, no. 5, pp. 1305–1314, 2008.

[8] E. Ahmed and A. S. Elgazzar, "On fractional order differential equations model for nonlocal epidemics," *Physica A: Statistical Mechanics and Its Applications*, vol. 379, no. 2, pp. 607–614, 2007.

[9] I. Podlubny, *Fractional Differential Equations*, vol. 198 of *Mathematics in Science and Engineering*, Academic Press, San Diego, Calif, USA, 1999.

[10] A. A. Kilbas, H. M. Srivastava, and J. J. Trujillo, *Theory and Applications of Fractional Differential Equations*, New York, NY, USA, Elsevier, 2006.

[11] K. Diethelm, *The Analysis of Fractional Differential Equations*, vol. 2004 of *Lecture Notes in Mathematics*, Springer, Berlin, Germany, 2010.

[12] B. Xin, T. Chen, and Y. Liu, "Projective synchronization of chaotic fractional-order energy resources demand-supply systems via linear control," *Communications in Nonlinear Science and Numerical Simulation*, vol. 16, no. 11, pp. 4479–4486, 2011.

[13] A. E. Matouk, "Chaos synchronization of a fractional-order modified van der Pol-Duffing system via new linear control, backstepping control and Takagi-Sugeno fuzzy approaches," *Complexity*, vol. 21, no. S1, pp. 116–124, 2016.

[14] A. Y. Leung, X.-F. Li, Y.-D. Chu, and X.-B. Rao, "Synchronization of fractional-order chaotic systems using unidirectional adaptive full-state linear error feedback coupling," *Nonlinear Dynamics*, vol. 82, no. 1-2, pp. 185–199, 2015.

[15] A. M. El-Sayed, H. M. Nour, A. Elsaid, A. E. Matouk, and A. Elsonbaty, "Dynamical behaviors, circuit realization, chaos control, and synchronization of a new fractional order hyperchaotic system," *Applied Mathematical Modelling. Simulation and Computation for Engineering and Environmental Systems*, vol. 40, no. 5-6, pp. 3516–3534, 2016.

[16] A. M. El-Sayed, A. Elsonbaty, A. A. Elsadany, and A. E. Matouk, "Dynamical analysis and circuit simulation of a new fractional-order hyperchaotic system and its discretization," *International Journal of Bifurcation and Chaos in Applied Sciences and Engineering*, vol. 26, no. 13, Article ID 1650222, pp. 1–35, 2016.

[17] J. Cao, "Global exponential stability of hopfield neural networks," *International Journal of Systems Science*, vol. 32, no. 2, pp. 233–236, 2001.

[18] S. Dharani, R. Rakkiyappan, and J. Cao, "New delay-dependent stability criteria for switched Hopfield neural networks of neutral type with additive time-varying delay components," *Neurocomputing*, vol. 151, no. 2, pp. 827–834, 2015.

[19] J. Cao, D.-S. Huang, and Y. Qu, "Global robust stability of delayed recurrent neural networks," *Chaos, Solitons & Fractals*, vol. 23, no. 1, pp. 221–229, 2005.

[20] Y. Liu, Z. Wang, and X. Liu, "Global exponential stability of generalized recurrent neural networks with discrete and distributed delays," *Neural Networks*, vol. 19, no. 5, pp. 667–675, 2006.

[21] Q. Zhang, X. Wei, and J. Xu, "Stability of delayed cellular neural networks," *Chaos, Solitons & Fractals*, vol. 31, no. 2, pp. 514–520, 2007.

[22] W. Xiong, Y. Shi, and J. Cao, "Stability analysis of two-dimensional neutral-type Cohen–Grossberg BAM neural networks," *Neural Computing and Applications*, vol. 28, no. 4, pp. 703–716, 2017.

[23] Z.-T. Huang, X.-S. Luo, and Q.-G. Yang, "Global asymptotic stability analysis of bidirectional associative memory neural networks with distributed delays and impulse," *Chaos, Solitons & Fractals*, vol. 34, no. 3, pp. 878–885, 2007.

[24] J. H. Park, C. H. Park, O. M. Kwon, and S. M. Lee, "A new stability criterion for bidirectional associative memory neural networks of neutral-type," *Applied Mathematics and Computation*, vol. 199, no. 2, pp. 716–722, 2008.

[25] Y. Li and S. Gao, "Global exponential stability for impulsive BAM neural networks with distributed delays on time scales," *Neural Processing Letters*, vol. 31, no. 1, pp. 65–91, 2010.

[26] C. Song and J. Cao, "Dynamics in fractional-order neural networks," *Neurocomputing*, vol. 142, pp. 494–498, 2014.

[27] H.-B. Bao and J.-D. Cao, "Projective synchronization of fractional-order memristor-based neural networks," *Neural Networks*, vol. 63, pp. 1–9, 2015.

[28] F. Ren, F. Cao, and J. Cao, "Mittag-Leffler stability and generalized Mittag-Leffler stability of fractional-order gene regulatory networks," *Neurocomputing*, vol. 160, pp. 185–190, 2015.

[29] X. Yang, C. Li, Q. Song, T. Huang, and X. Chen, "Mittag-Leffler stability analysis on variable-time impulsive fractional-order neural networks," *Neurocomputing*, vol. 207, pp. 276–286, 2015.

[30] Y. Li, Y. Chen, and I. Podlubny, "Stability of fractional-order nonlinear dynamic systems: Lyapunov direct method and generalized Mittag-Leffler stability," *Computers & Mathematics with Applications*, vol. 59, no. 5, pp. 1810–1821, 2010.

[31] H. Bao, J. H. Park, and J. Cao, "Adaptive synchronization of fractional-order memristor-based neural networks with time delay," *Nonlinear Dynamics. An International Journal of Nonlinear Dynamics and Chaos in Engineering Systems*, vol. 82, no. 3, pp. 1343–1354, 2015.

[32] I. Stamova, "Global Mittag-Leffler stability and synchronization of impulsive fractional-order neural networks with time-varying delays," *Nonlinear Dynamics. An International Journal of Nonlinear Dynamics and Chaos in Engineering Systems*, vol. 77, no. 4, pp. 1251–1260, 2014.

[33] Y. Ke and C. Miao, "Stability analysis of fractional-order Cohen-Grossberg neural networks with time delay," *International Journal of Computer Mathematics*, vol. 92, no. 6, pp. 1102–1113, 2015.

[34] X. Ding, J. Cao, X. Zhao, and F. E. Alsaadi, "Finite-time stability of fractional-order complex-valued neural networks with time delays," *Neural Processing Letters*, pp. 1–20, 2017.

[35] H. Zhang, R. Ye, J. Cao, and A. Alsaedi, "Delay-independent stability of Riemann–Liouville fractional neutral-type delayed neural networks," *Neural Processing Letters*, pp. 1–16, 2017.

[36] R. Rakkiyappan, J. Cao, and G. Velmurugan, "Existence and uniform stability analysis of fractional-order complex-valued neural networks with time delays," *IEEE Transactions on Neural Networks and Learning Systems*, vol. 26, no. 1, pp. 84–97, 2015.

[37] R. Rakkiyappan, R. Sivaranjani, G. Velmurugan, and J. Cao, "Analysis of global O(t-α) stability and global asymptotical periodicity for a class of fractional-order complex-valued neural networks with time varying delays," *Neural Networks*, vol. 77, pp. 51–69, 2016.

[38] D. Matignon, "Stability results for fractional differential equations with applications to control processing," *Computational Engineering in Systems Applications*, vol. 2, pp. 963–968, 1996.

[39] A. E. Matouk, "Stability conditions, hyperchaos and control in a novel fractional order hyperchaotic system," *Physics Letters A: General, Atomic and Solid State Physics*, vol. 373, no. 25, pp. 2166–2173, 2009.

[40] D. Bainov and P. Simeonov, *Impulsive Differential Equations: Periodic Solutions and Applications*, John Wiley and Sons, New York, NY, USA, 1993.

[41] M. Benchohra, J. Henderson, and S. Ntouyas, *Impulsive Differential Equations and Inclusions*, vol. 2 of *Contemporary Mathematics and Its Applications*, Hindawi Publishing Corporation, New York, NY, USA, 2006.

[42] F. Wang, Y. Yang, and M. Hu, "Asymptotic stability of delayed fractional-order neural networks with impulsive effects," *Neurocomputing*, vol. 154, pp. 239–244, 2015.

[43] B. Kosko, "Adaptive bidirectional associative memories," *Applied Optics*, vol. 26, no. 23, pp. 4947–4960, 1987.

[44] C. Rajivganthi, F. A. Rihan, S. Lakshmanan, and P. Muthukumar, "Finite-time stability analysis for fractional-order Cohen–Grossberg BAM neural networks with time delays," *Neural Computing and Applications*, pp. 1–12, 2016.

[45] J. Xiao, S. Zhong, Y. Li, and F. Xu, "Finite-time Mittag-Leffler synchronization of fractional-order memristive BAM neural networks with time delays," *Neurocomputing*, vol. 219, pp. 431–439, 2017.

[46] F. Wang, Y. Yang, X. Xu, and L. Li, "Global asymptotic stability of impulsive fractional-order BAM neural networks with time delay," *Neural Computing and Applications*, vol. 28, no. 2, pp. 345–352, 2017.

[47] L. V. Hien, "An explicit criterion for finite-time stability of linear nonautonomous systems with delays," *Applied Mathematics Letters. An International Journal of Rapid Publication*, vol. 30, pp. 12–18, 2014.

[48] A. Granas and J. Dugundji, *Fixed Point Theory*, Springer, New York, NY, USA, 2003.

Hindawi
Complexity
Volume 2017, Article ID 4948392, 12 pages
https://doi.org/10.1155/2017/4948392

Research Article

Dynamic Analysis of Complex Synchronization Schemes between Integer Order and Fractional Order Chaotic Systems with Different Dimensions

Adel Ouannas,[1] Xiong Wang,[2] Viet-Thanh Pham,[3] and Toufik Ziar[4,5]

[1]*Laboratory of Mathematics, Informatics and Systems (LAMIS), University of Larbi Tebessi, 12002 Tebessa, Algeria*
[2]*Institute for Advanced Study, Shenzhen University, Shenzhen, Guangdong 518060, China*
[3]*Hanoi University of Science and Technology, Hanoi, Vietnam*
[4]*Department of Matter Sciences, University of Larbi Tebessi, Tebessa, Algeria*
[5]*Active Devices and Materials Laboratory (LCAM), Larbi Ben M'hidi University, Oum El Bouaghi, Algeria*

Correspondence should be addressed to Viet-Thanh Pham; pvt3010@gmail.com

Received 15 February 2017; Revised 18 April 2017; Accepted 31 May 2017; Published 28 June 2017

Academic Editor: Delfim F. M. Torres

We present new approaches to synchronize different dimensional master and slave systems described by integer order and fractional order differential equations. Based on fractional order Lyapunov approach and integer order Lyapunov stability method, effective control schemes to rigorously study the coexistence of some synchronization types between integer order and fractional order chaotic systems with different dimensions are introduced. Numerical examples are used to validate the theoretical results and to verify the effectiveness of the proposed schemes.

1. Introduction

Nature is intrinsically nonlinear. So, it is not surprising that most of the systems we encounter in the real world are nonlinear. And what is interesting is that some of these nonlinear systems can be described by fractional order differential equations which can display a variety of behaviors including chaos and hyperchaos [1–5]. Recently, study on synchronization of fractional order chaotic systems has started to attract increasing attention of many researchers [6–12], since the synchronization of chaotic systems with integer order is understood well and widely explored [13–15]. Many scientists who are interested in the field of chaos synchronization have struggled to achieve the synchronization between integer order and fractional order chaotic systems.

At present, many schemes of control have been proposed to study the problem of synchronization between integer order and fractional order chaotic systems such as anticipating synchronization [16], function projective synchronization [17], complete synchronization [18], antisynchronization [19], Q-S synchronization [20], and generalized synchronization [21]. Also, different techniques have been introduced to synchronize integer order and fractional order chaotic systems. For example, a nonlinear feedback control method has been introduced in [22]. The idea of tracking control has been applied in [23, 24]. In [25], general control scheme has been described. A new fuzzy sliding mode method has been proposed in [26], and a sliding mode method has been designed in [27, 28]. Synchronization of a class of hyperchaotic systems has been studied in [29]. A practical method, based on circuit simulation, has been presented in [30], and in [31] a robust observer technique has been tackled.

Complete synchronization (CS), projective synchronization (PS), full state hybrid function projective synchronization (FSHFPS), and generalized synchronization (GS) are effective approaches to achieve synchronization and have been used widely in integer order chaotic systems [32–35] and fractional order chaotic systems [36–39]. Studying inverse problems of synchronization is an attractive and important idea. Recently, some interesting types of synchronization have

been introduced such as inverse projective synchronization (IPS) [40], inverse full state hybrid projective synchronization (IFSHPS) [41], inverse full state hybrid function projective synchronization (IFSHFPS) [42], and inverse generalized synchronization (IGS) [43]. Coexistence of several types of synchronization produces new complex type of chaos synchronization. Not long ago, many approaches for the problem of coexistence of synchronization types have been proposed in discrete time chaotic systems, integer order chaotic systems, and fractional order chaotic systems [44–47]. The coexistence of different type of synchronization is very useful in secure communication and chaotic encryption schemes.

This paper introduces new approaches to study the coexistence of some types of synchronization between integer order and fractional order chaotic systems with different dimensions. The new results, derived in this paper, are established in the form of simple conditions about the linear parts of the slave system and the master system, respectively, which are very convenient to verify. Using fractional Lyapunov approach, the coexistence of complete synchronization (CS), projective synchronization (PS), full state hybrid function projective synchronization (FSHFPS), and generalized synchronization (GS) between integer order master system and fractional order slave system is investigated. Based on integer order Lyapunov method, the coexistence of inverse projective synchronization (IPS), inverse full state hybrid function projective synchronization (IFSHFPS), and inverse generalized synchronization (IGS) between fractional order master system and integer order slave system is studied. The capability of the approaches is illustrated by numerical examples.

The rest of this paper is arranged as follows. Some theoretical bases of fractional calculus are introduced in Section 2. In Section 3, our main results of the paper are presented. In Section 4, our approaches are applied between some typical chaotic and hyperchaotic systems to show the effectiveness of the derived results. Section 5 is the conclusion of the paper.

2. Theoretical Basis

2.1. Fractional Integration and Derivative. There are several definitions of fractional derivatives [48, 49]. The two most commonly used are the Riemann-Liouville and Caputo definitions. Each definition uses Riemann-Liouville fractional integration and derivatives of whole order. The difference between the two definitions is in the order of evaluation. The Caputo derivative is a time domain computation method [50]. In real applications, the Caputo derivative is more popular since the unhomogenous initial conditions are permitted if such conditions are necessary [51, 52]. Furthermore, these initial values are prone to measure since they all have idiographic meanings. The Riemann-Liouville fractional integral operator of order $q \geq 0$ of the function $f(t)$ is defined as

$$J^q f(t) = \frac{1}{\Gamma(q)} \int_0^t (t-\tau)^{q-1} f(\tau)\, d\tau, \quad q > 0,\ t > 0. \tag{1}$$

Some properties of the operator J^q can be found, for example, in [53]. In this study, Caputo definition is used and the fractional derivative of $f(t)$ is defined as

$$\begin{aligned} D_t^p f(t) &= J^{m-p}\left(\frac{d^m}{dt^m} f(t)\right) \\ &= \frac{1}{\Gamma(m-p)} \int_0^t \frac{f^{(m)}(\tau)}{(t-\tau)^{p-m+1}} d\tau, \end{aligned} \tag{2}$$

for $m-1 < p \leq m$, $m \in \mathbb{N}$, $t > 0$. The fractional differential operator D_t^p is left-inverse (and not right-inverse) to the fractional integral operator J^p; that is, $D_t^p J^p = I$, where I is the identity operator.

2.2. Lyapunov Stability for Integer Order Systems. Consider the following integer order system:

$$\dot{X}(t) = F(X(t)), \tag{3}$$

where $X(t) = (x_1(t), x_2(t), \ldots, x_n(t))^T$ and $F : \mathbf{R}^n \to \mathbf{R}^n$.

Lemma 1 (see [54]). *If there exists a positive definite Lyapunov function $V(X(t))$ such that $\dot{V}(X(t)) < 0$, for all $t > 0$, then the trivial solution of system (3) is asymptotically stable.*

2.3. Fractional Order Lyapunov Stability. Consider the following fractional order system:

$$D_t^p X(t) = F(X(t)), \tag{4}$$

where $X(t) = (x_1(t), x_2(t), \ldots, x_n(t))^T$, p is a rational number between 0 and 1 and D_t^p is the Caputo fractional derivative of order p, and $F : \mathbf{R}^n \to \mathbf{R}^n$. For stability analysis of fractional order systems, a fractional extension of Lyapunov direct method has been proposed by the following theorem.

Theorem 2 (see [55]). *If there exists a positive definite Lyapunov function $V(X(t))$ such that $D_t^p V(X(t)) < 0$, for all $t > 0$, then the trivial solution of system (4) is asymptotically stable.*

Now, we present a new lemma which is helpful in the proving analysis of the proposed method.

Lemma 3 (see [56]). $\forall t > 0 : (1/2) D_t^p (X^T(t) X(t)) \leq X^T(t) D_t^p (X(t))$.

3. Main Results

3.1. Synchronization of Integer Oder Master System and Fractional Oder Slave System. The master system is defined by

$$\dot{x}_i(t) = f_i(X(t)), \quad i = 1, 2, 3, \tag{5}$$

where $X(t) = (x_1(t), x_2(t), x_3(t))^T$ is the state vector of the master system and $f_i : \mathbf{R}^3 \to \mathbf{R}$ $(i = 1, 2, 3)$. We consider the slave system as

$$D_t^q y_i(t) = \sum_{j=1}^{4} b_{ij} y_j(t) + g_i(Y(t)) + u_i, \quad i = 1, 2, 3, 4, \tag{6}$$

where $Y(t) = (y_1(t), y_2(t), y_3(t), y_4(t))^T$ is the state vector of the slave system, $(b_{ij}) \in \mathbf{R}^{4\times4}$, $g_i : \mathbf{R}^4 \to \mathbf{R}$ $(i = 1, 2, 3, 4)$ are nonlinear functions, $0 < q < 1$, and D_t^q is the Caputo fractional derivative of order q, and u_i $(i = 1, 2, 3, 4)$ are controllers.

Definition 4. We say that CS, PS, FSHFPS, and GS coexist in the synchronization of master system (5) and slave system (6), if there exist controllers u_i $(i = 1, 2, 3, 4)$ constant $\alpha \in \mathbf{R}^* - \{1\}$, differentiable functions $\beta_j(t) : \mathbf{R}^+ \to \mathbf{R}$ $(j = 1, 2, 3)$ and differentiable function $\varphi : \mathbf{R}^3 \to \mathbf{R}$, such that the synchronization errors

$$\begin{aligned} e_1(t) &= y_1(t) - x_1(t), \\ e_2(t) &= y_2(t) - \alpha x_2(t), \\ e_3(t) &= y_3(t) - \sum_{j=1}^{3} \beta_j(t)\, x_j(t), \\ e_4(t) &= y_4(t) - \varphi(X(t)) \end{aligned} \tag{7}$$

satisfy that $\lim_{t\to+\infty} e_i(t) = 0$, $i = 1, 2, 3, 4$.

Error system (7), between master system (5) and slave system (6), can be differentiated as follows:

$$\begin{aligned} D_t^q e_1(t) &= \sum_{j=1}^{4} b_{1j} y_j(t) + g_1(Y(t)) + u_1 - D_t^q x_1(t), \\ D_t^q e_2(t) &= \sum_{j=1}^{4} b_{2j} y_j(t) + g_2(Y(t)) + u_2 - \alpha D_t^q x_2(t), \\ D_t^q e_3(t) &= \sum_{j=1}^{4} b_{3j} y_j(t) + g_3(Y(t)) + u_3 \\ &\quad - D_t^q \left[\sum_{j=1}^{3} \beta_j(t)\, x_j(t) \right], \\ D_t^q e_3(t) &= \sum_{j=1}^{4} b_{4j} y_j(t) + g_4(Y(t)) + u_4 \\ &\quad - D_t^q \left[\varphi(X(t)) \right]. \end{aligned} \tag{8}$$

Error system (8) can be described as

$$D_t^q e_i(t) = \sum_{j=1}^{4} b_{ij} e_j(t) + R_i + u_i, \quad i = 1, 2, 3, 4, \tag{9}$$

where

$$\begin{aligned} R_1 &= \sum_{j=1}^{4} b_{1j} \left(y_j(t) - e_j(t) \right) + g_1(Y(t)) - D_t^q x_1(t), \\ R_2 &= \sum_{j=1}^{4} b_{2j} \left(y_j(t) - e_j(t) \right) + g_2(Y(t)) - \alpha D_t^q x_2(t), \\ R_3 &= \sum_{j=1}^{4} b_{3j} \left(y_j(t) - e_j(t) \right) + g_3(Y(t)) \\ &\quad - D_t^q \left[\sum_{j=1}^{3} \beta_j(t)\, x_j(t) \right], \\ R_4 &= \sum_{j=1}^{4} b_{4j} \left(y_j(t) - e_j(t) \right) + g_4(Y(t)) \\ &\quad - D_t^q \left[\varphi(X(t)) \right]. \end{aligned} \tag{10}$$

Rewrite error system (9) in the compact form

$$D_t^q e(t) = Be(t) + R + U, \tag{11}$$

where $D_t^q e(t) = [D_t^q e_1(t), D_t^q e_2(t), D_t^q e_3(t), D_t^q e_4(t)]^T$, $B = (b_{ij})_{4\times4}$, $R = (R_i)_{1\le i\le4}$, and $U = (u_i)_{1\le i\le4}$.

Theorem 5. *There exists a suitable feedback gain matrix $C \in \mathbf{R}^{4\times4}$ to realize the coexistence of CS, PS, FSHFPS, and GS between master system (5) and slave system (6) under the following control law:*

$$U = -R - Ce(t). \tag{12}$$

Proof. Substituting (12) into (11), one can have

$$D_t^q e(t) = (B - C)\, e(t). \tag{13}$$

If a Lyapunov function candidate is chosen as $V(e(t)) = (1/2)e^T(t)e(t)$, then, the time Caputo fractional derivative of V along the trajectory of system (13) is as follows:

$$D_t^q V(e(t)) = D_t^q \left(\frac{1}{2} e^T(t)\, e(t) \right), \tag{14}$$

and using Lemma 3 in (14) we get

$$D_t^q V(e(t)) \le e^T(t)\, D_t^q e(t) = e^T(t)\, (B - C)\, e(t). \tag{15}$$

If we select the feedback gain matrix C such that $B - C$ is a negative definite matrix, then we get $D_t^q V(e(t)) < 0$. From Theorem 2, the zero solution of system (13) is a globally asymptotically stable; that is, $\lim_{t\to+\infty} e_i(t) = 0$, $i = 1, 2, 3, 4$. We conclude that master system (5) and slave system (6) are globally synchronized. □

3.2. Synchronization of Fractional Oder Master System and Integer Oder Slave System. Now, the master system and the slave system can be described in the following forms:

$$D_t^{p_i} x_i(t) = \sum_{i=1}^{3} a_{ij} x_j(t) + f_i(X(t)), \quad i = 1, 2, 3, \tag{16}$$

$$\dot{y}_i(t) = g_i(Y(t)) + u_i, \quad i = 1, 2, 3, 4, \tag{17}$$

where $X(t) = (x_i(t))_{1\le i\le3}$, $Y(t) = (y_i(t))_{1\le i\le4}$ are the states of the master system and the slave system, respectively, $D_t^{p_i}$ is the Caputo fractional derivative of order p_i, $0 < p_i < 1$ $(i = 1, 2, 3)$, and $(a_{ij}) \in \mathbf{R}^{3\times3}$, $f_i : \mathbf{R}^3 \to \mathbf{R}$ $(i = 1, 2, 3)$, are nonlinear functions; for example, $g_i : \mathbf{R}^4 \to \mathbf{R}$ $(i = 1, 2, 3, 4)$ and u_i $(i = 1, 2, 3, 4)$ are controllers.

Definition 6. We say that IPS, IFSHFPS, and IGS coexist in the synchronization of master system (16) and slave system (17); if there exist controllers u_i $(i = 1, 2, 3, 4)$ differentiable function $h(t) : \mathbf{R}^+ \to \mathbf{R}^*$, differentiable functions $\Lambda_j(t) : \mathbf{R}^+ \to \mathbf{R}$ $(j = 1, 2, 3, 4)$ and differentiable function $\phi : \mathbf{R}^4 \to \mathbf{R}$, such that the synchronization errors

$$\begin{aligned} e_1(t) &= x_1(t) - h(t)\, y_1(t), \\ e_2(t) &= x_2(t) - \sum_{j=1}^{4} \Lambda_j(t)\, y_j(t), \\ e_3(t) &= x_3(t) - \phi(Y(t)) \end{aligned} \tag{18}$$

satisfy that $\lim_{t\to+\infty} e_i(t) = 0,\ i = 1, 2, 3$.

Error system (18), between master system (16) and slave system (17), can be derived as

$$\begin{aligned} \dot{e}_1(t) &= \dot{x}_1(t) - \dot{h}(t)\, y_1(t) - h(t)\, \dot{y}_1(t), \\ \dot{e}_2(t) &= \dot{x}_2(t) - \sum_{j=1}^{4} \dot{\Lambda}_j(t)\, y_j(t) - \sum_{j=1}^{4} \Lambda_j(t)\, \dot{y}_j(t), \\ \dot{e}_3(t) &= \dot{x}_3(t) - \sum_{j=1}^{4} \frac{\partial \phi}{\partial y_j} \dot{y}_j. \end{aligned} \tag{19}$$

Error system (19) can be written as

$$\begin{aligned} \dot{e}_1(t) &= \sum_{j=1}^{3} a_{1j} e_j(t) + T_1 - h(t)\, u_1, \\ \dot{e}_2(t) &= \sum_{j=1}^{3} a_{2j} e_j(t) + T_2 - \sum_{j=1}^{4} \Lambda_j(t)\, u_j, \\ \dot{e}_3(t) &= \sum_{j=1}^{3} a_{3j} e_j(t) + T_3 - \sum_{j=1}^{4} \frac{\partial \phi}{\partial y_j} u_j, \end{aligned} \tag{20}$$

where

$$\begin{aligned} T_1 &= \dot{x}_1(t) - \sum_{j=1}^{3} a_{1j} e_j(t) - \dot{h}(t)\, y_1(t) \\ &\quad - h(t)\, g_1(Y(t)), \\ T_2 &= \dot{x}_2(t) - \sum_{j=1}^{3} a_{2j} e_j(t) - \sum_{j=1}^{4} \dot{\Lambda}_j(t)\, y_j(t) \\ &\quad - \sum_{j=1}^{4} \Lambda_j(t)\, g_j(Y(t)), \\ T_3 &= \dot{x}_3(t) - \sum_{j=1}^{3} a_{3j} e_j(t) - \sum_{j=1}^{4} \frac{\partial \phi}{\partial y_j} g_j(Y(t)). \end{aligned} \tag{21}$$

Rewrite error system (20) in the compact form

$$\dot{e}(t) = Ae(t) + T - M \times \widehat{U} - u_4 W, \tag{22}$$

where $\dot{e}(t) = [\dot{e}_1(t), \dot{e}_2(t), \dot{e}_3(t)]^T$, $A = (a_{ij})_{3\times3}$, $T = (T_i)_{1\le i\le3}$, $\widehat{U} = (u_i)_{1\le i\le3}$, $W = (0, \Lambda_4(t), \partial\phi/\partial y_4)^T$, and

$$M = \begin{pmatrix} h(t) & 0 & 0 \\ \Lambda_1(t) & \Lambda_2(t) & \Lambda_3(t) \\ \dfrac{\partial \phi}{\partial y_1} & \dfrac{\partial \phi}{\partial y_2} & \dfrac{\partial \phi}{\partial y_3} \end{pmatrix}. \tag{23}$$

To achieve synchronization between systems (16) and (17), we assume that M is an invertible matrix and M^{-1} its inverse matrix. Hence, we have the following result.

Theorem 7. *IPS, IFSHFPS, and IGS coexist between master system (16) and slave system (17) under the following conditions:*

(i) M^{-1} *is bounded.*

(ii) $\widehat{U} = M^{-1}(Le(t) + T)$ *and* $u_4 = 0$.

(iii) *The feedback gain matrix* $L \in \mathbf{R}^{3\times3}$ *is selected such that* $(A - L)^T + (A - L)$ *is a negative definite matrix.*

Proof. By substituting the control law (ii) into (22), the error system can be written as

$$\dot{e}(t) = (A - L)\, e(t). \tag{24}$$

Construct the candidate Lyapunov function in the form $V(e(t)) = e^T(t)e(t)$, and we obtain

$$\begin{aligned} \dot{V}(e(t)) &= \dot{e}^T(t)\, e(t) + e^T(t)\, \dot{e}(t) \\ &= e^T(t)\, (A - L)^T\, e(t) + e^T(t)\, (A - L)\, e(t) \\ &= e^T(t) \left[(A - L)^T + (A - L) \right] e(t). \end{aligned} \tag{25}$$

Using (iii), then we get $\dot{V}(e(t)) < 0$. From Lemma 1, the zero solution of error system (24) is globally asymptotically stable and therefore, master system (16) the slave system (17) are globally synchronized. □

4. Numerical Examples

In this section, two numerical examples are considered to validate the proposed chaos synchronization schemes.

4.1. Example 1. Her, in this example, as the master system we consider the chaotic Chen system [57] and the controlled fractional hyperchaotic Liu system [58] as the slave system. The master system is defined as

$$\begin{aligned} \dot{x}_1 &= \alpha (x_2 - x_1), \\ \dot{x}_2 &= (\gamma - \alpha) x_1 + \gamma x_2 - x_1 x_3, \\ \dot{x}_3 &= \beta x_3 + x_1 x_2, \end{aligned} \tag{26}$$

where $x_i, i = 1, 2, 3$, are the states of the master system. System (26) has a chaotic behavior when $\alpha = 35$, $\beta = -3$, and $\gamma = 28$. Chaotic attractors of master system (26) are shown in Figure 1.

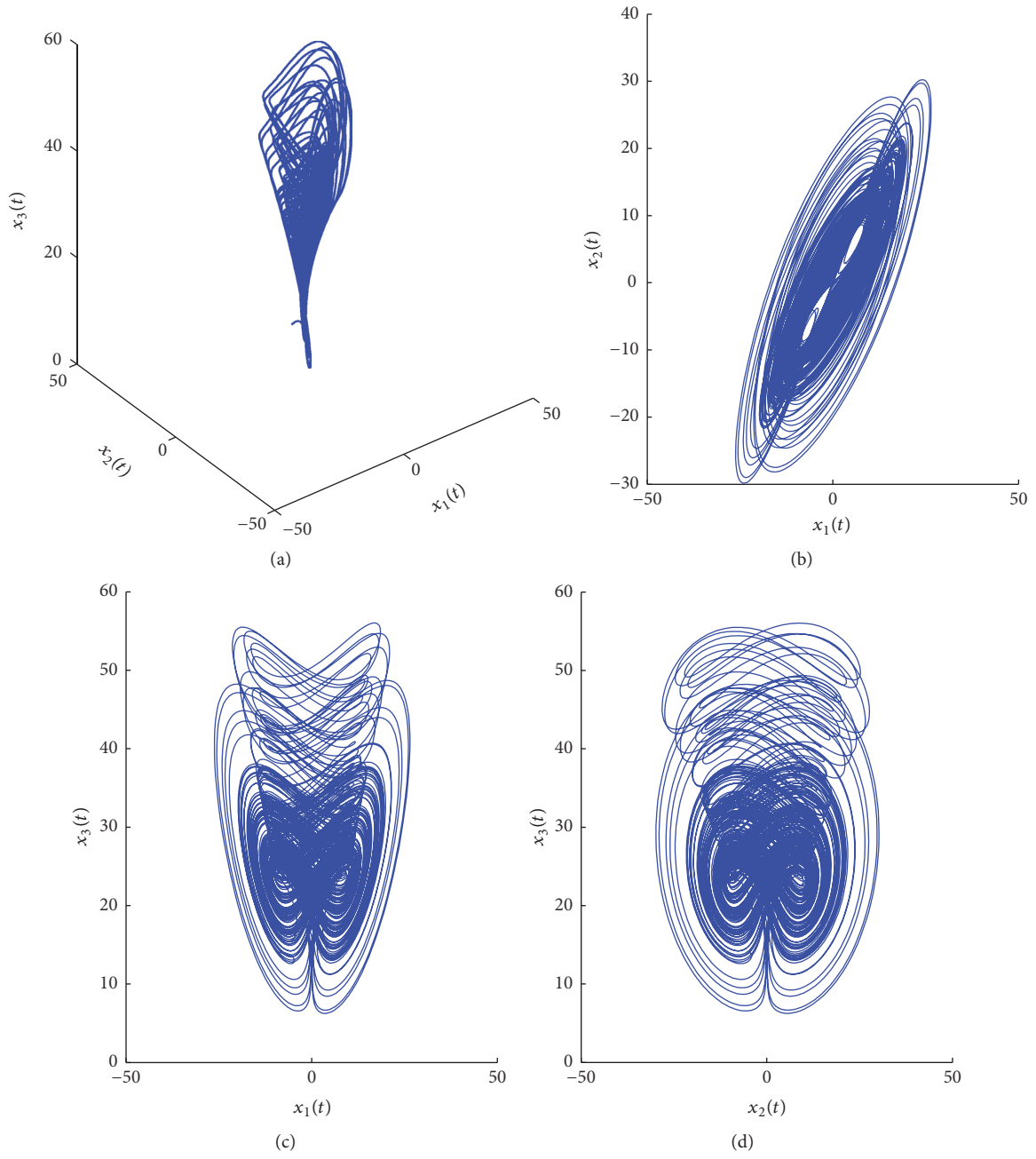

FIGURE 1: 3D and 2D chaotic attractors of Chen system (26).

The slave system is described by

$$\begin{aligned} D^q y_1 &= b_1 (y_2 - y_1) + y_4 + u_1, \\ D^q y_2 &= b_2 y_1 + 0.5 y_4 - y_1 y_3 + u_2, \\ D^q y_3 &= -b_3 y_3 - y_4 + 4 y_1^2 + u_3, \\ D^q y_4 &= -b_4 y_2 - y_4 + u_4, \end{aligned} \tag{27}$$

where y_i, $i = 1, 2, 3, 4$, are the states of the slave system and $U = (u_i)_{1 \le i \le 4}$ is the vector controller. This system, as shown in [58], exhibits hyperchaotic behavior when $(u_1, u_2, u_3, u_4) = (0, 0, 0, 0)$, $(b_1, b_2, b_3, b_4) = (10, 40, 2.5, 10/15)$, and $q = 0.9$. The projections of the hyperchaotic Lorenz attractor are shown in Figure 2.

Comparing system (27) with system (6), we get

$$B = \left(b_{ij}\right)_{4\times 4} = \begin{pmatrix} -10 & 10 & 0 & 1 \\ 40 & 0 & 0 & 0.5 \\ 0 & 0 & -2.5 & -1 \\ 0 & -\dfrac{10}{15} & 0 & -1 \end{pmatrix},$$

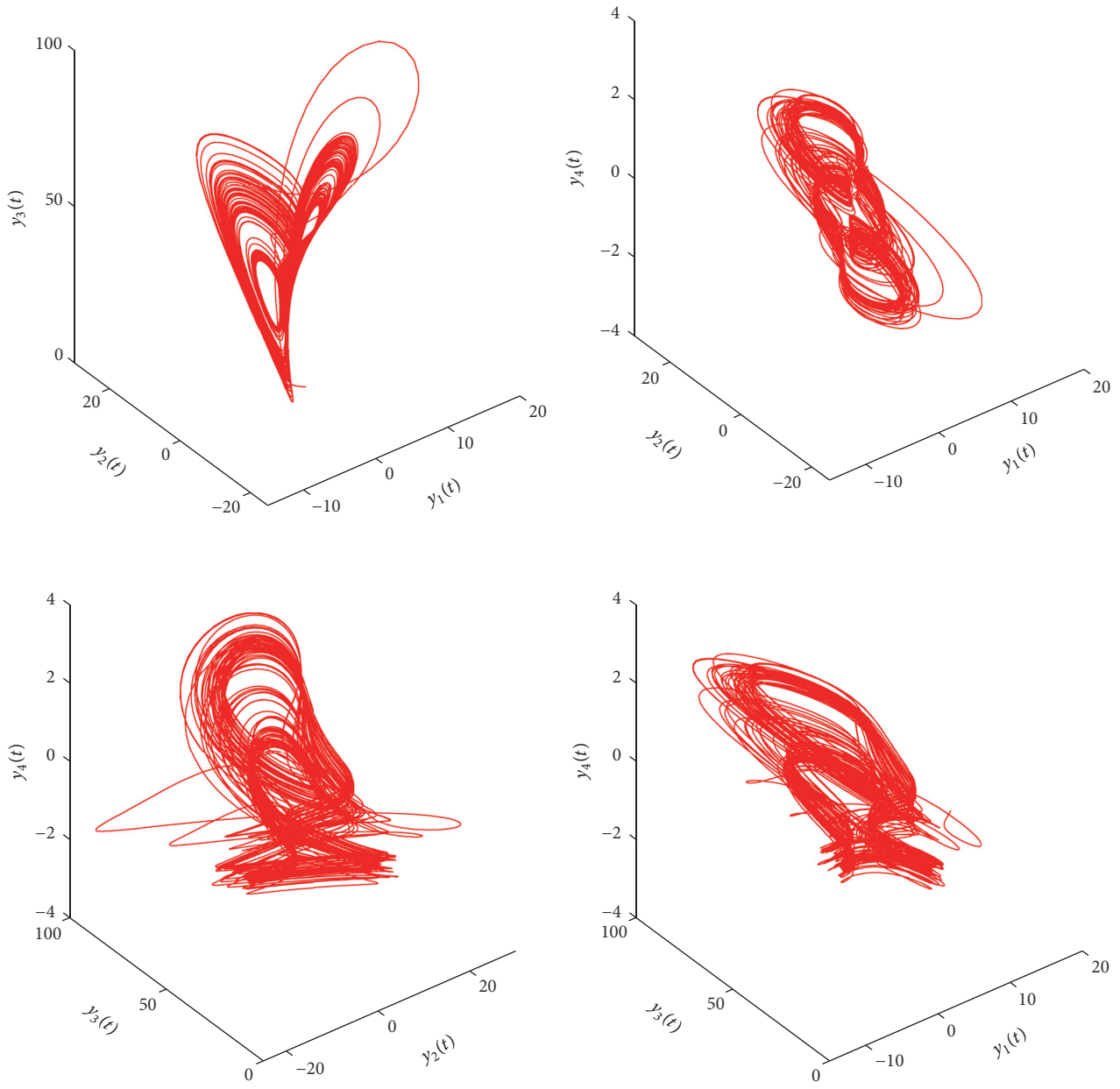

Figure 2: 3D phase portraits of the fractional hyperchaotic Liu system.

$$(g_i)_{1\le i\le 4} = \begin{pmatrix} 0 \\ -y_1 y_3 \\ 4y_1^2 \\ 0 \end{pmatrix}. \tag{28}$$

Using the notations described in Section 3.1, the errors between master system (26) and slave system (27) are defined as

$$\begin{aligned} e_1 &= y_1 - x_1, \\ e_2 &= y_2 - \alpha x_2, \\ e_3 &= y_3 - \sum_{j=1}^{3} \beta_j(t)\, x_j, \\ e_4 &= y_4 - \varphi(x_1, x_2, x_3), \end{aligned} \tag{29}$$

where $\alpha = 2$, $\beta_1(t) = t$, $\beta_2(t) = t^2$, $\beta_3(t) = t^3$, and $\varphi(x_1, x_2, x_3) = x_1 x_2 x_3$. According to Theorem 5, the control law $(u_1, u_2, u_3, u_4)^T$ can be designed as

$$(u_1, u_2, u_3, u_4)^T = -R - C \times (e_1, e_2, e_3, e_4)^T, \tag{30}$$

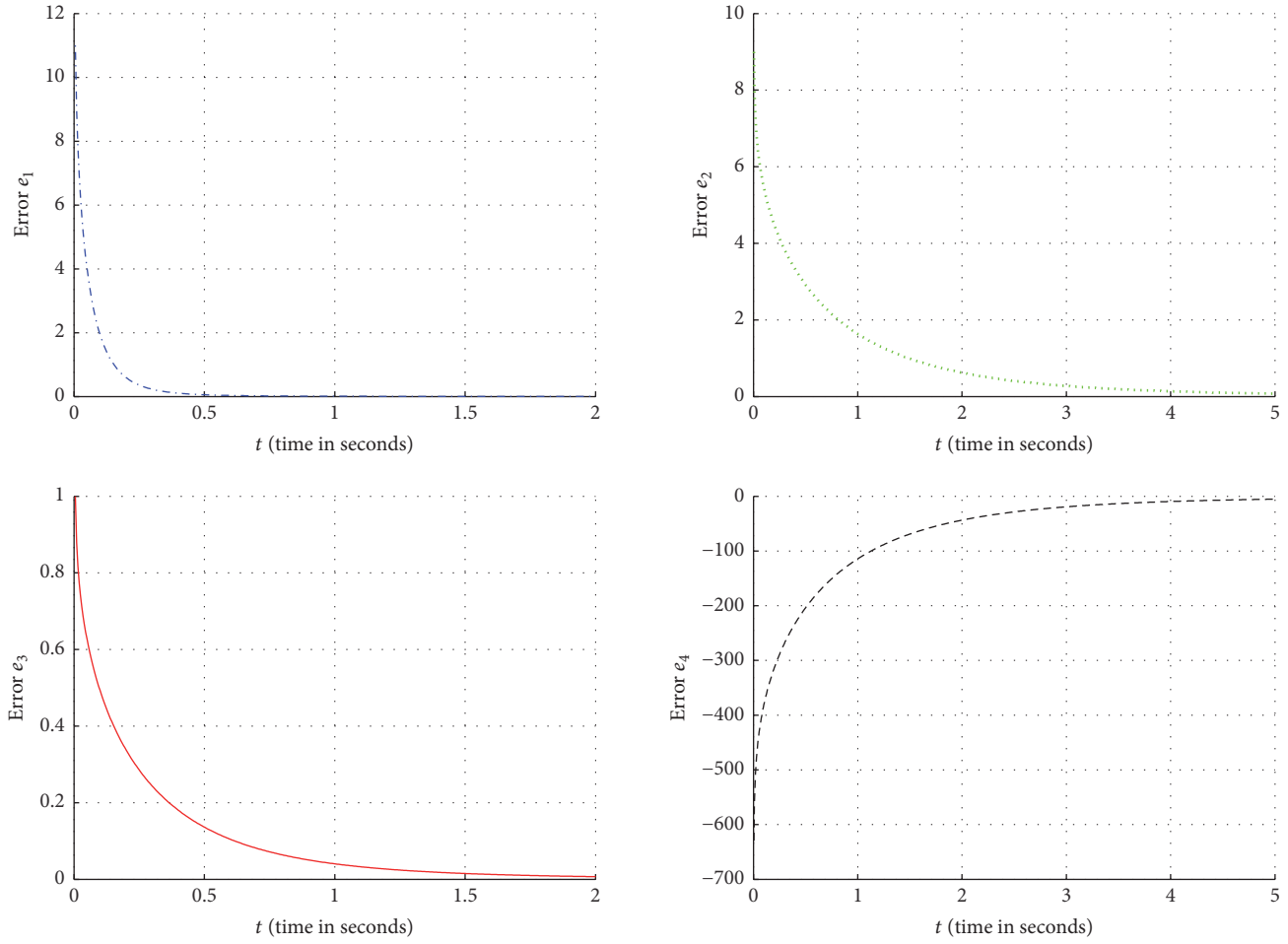

FIGURE 3: Time evolution of the synchronization errors e_1, e_2, e_3, and e_4 between master system (26) and slave system (27).

where

$$\begin{aligned} R_1 &= -10(y_1 - e_1) + 10(y_2 - e_2) + y_4 - e_4 - D^{0.9}x_1, \\ R_2 &= 40(y_1 - e_1) + 0.5(y_4 - e_4) - y_1 y_3 \\ &\quad - 2D^{0.9}x_2(t), \\ R_3 &= -2.5(y_3 - e_3) - (y_4 - e_4) + 4y_1^2 \\ &\quad - D^{0.9}\left(tx_1 + t^2 x_2 + t^3 x_3\right), \\ R_4 &= -\frac{10}{15}(y_2 - e_2) - (y_4 - e_4) - D^{0.9}(x_1 x_2 x_3), \end{aligned} \tag{31}$$

and C is a feedback gain matrix selected as

$$C = \begin{pmatrix} 0 & 10 & 0 & 1 \\ 40 & 1 & 0 & 0.5 \\ 0 & 0 & 0 & -1 \\ 0 & -\frac{10}{15} & 0 & 0 \end{pmatrix}. \tag{32}$$

It is easy to show that $B - C$ is a negative definite matrix. Hence, the synchronization between master system (26) and slave system (27) is achieved and the error system can be described as follows:

$$\begin{aligned} D^{0.9}e_1 &= -10e_1, \\ D^{0.9}e_2 &= -e_2, \\ D^{0.9}e_3 &= -2.5e_3, \\ D^{0.9}e_4 &= -e_4. \end{aligned} \tag{33}$$

For the purpose of numerical simulation, the fractional Euler integration method has been used to solve system (33). The initial values of the master and the slave systems are $[x_1(0), x_2(0), x_3(0)] = [-9, -5, 14]$ and $[y_1(0), y_2(0), y_3(0), y_4(0)] = [2, -1, 1, 1]$, respectively, and the initial states of error system (33) are $[e_1(0), e_2(0), e_3(0), e_4(0)] = [11, 9, 1, -629]$. Figure 3 displays the synchronization errors between systems (26) and (27).

4.2. Example 2. Now, in this example, as the master system we consider the fractional Lü system and the controlled

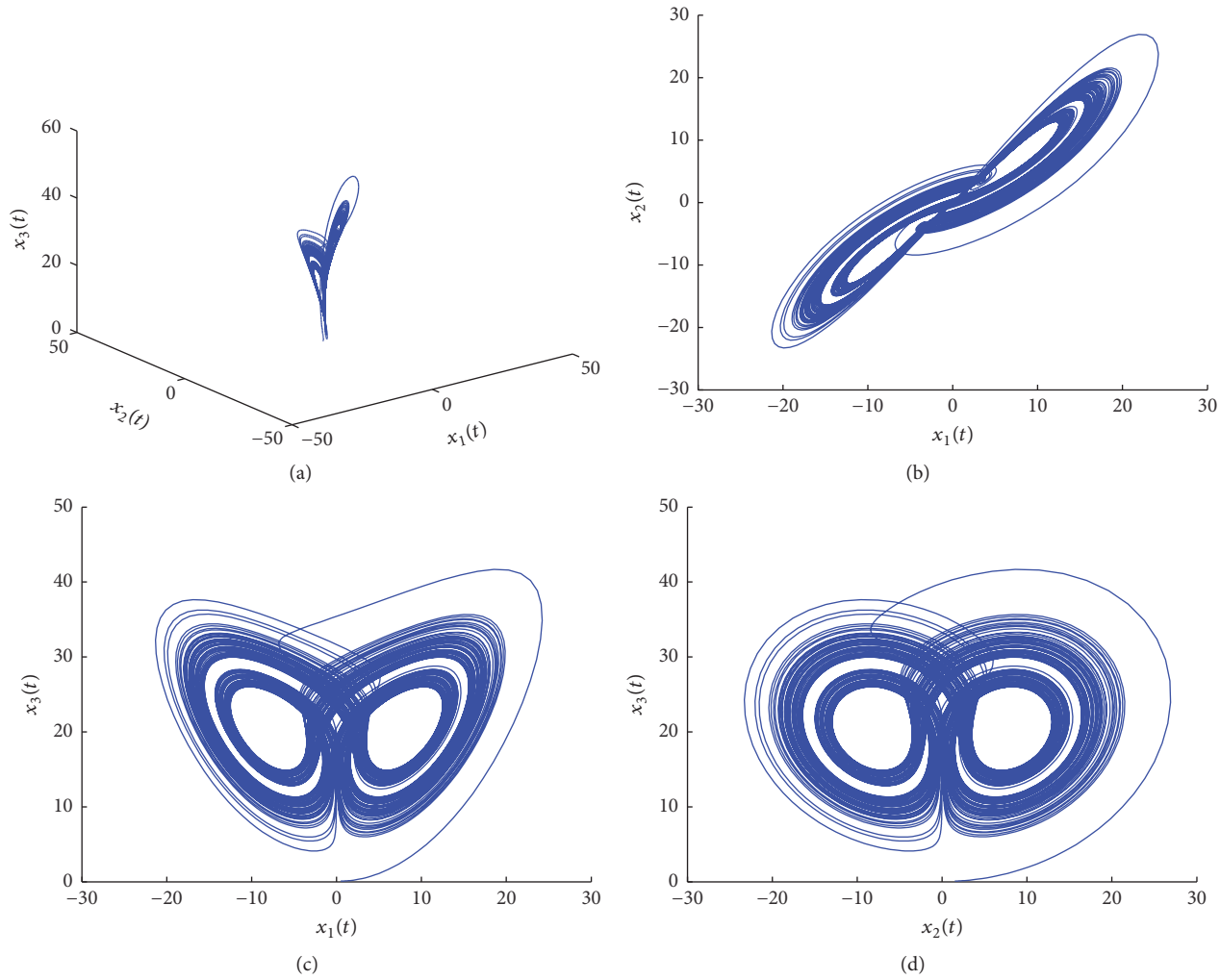

Figure 4: 3D and 2D chaotic attractors of fractional system (26).

hyperchaotic system, proposed by Zhang and Shen in [59], as the slave system. The master system is defined as

$$\begin{aligned} D^{p_1}x_1 &= \alpha(x_2 - x_1), \\ D^{p_2}x_2 &= \gamma x_2 - x_1 x_3, \\ D^{p_3}x_3 &= -\beta x_3 + x_1 x_2. \end{aligned} \tag{34}$$

It is found, in [60], that this system displays chaotic attractors when $(\alpha, \beta, \gamma) = (36, 3, 20)$ and $(p_1, p_2, p_3) = (0.985, 0.99, 0.98)$. Chaotic attractors of master system (34) are shown in Figure 4.

Comparing system (34) with system (16), one can have

$$A = (a_{ij}) = \begin{pmatrix} -36 & 36 & 0 \\ 0 & 20 & 0 \\ 0 & 0 & -3 \end{pmatrix},$$

$$(f_i)_{1\le i\le 3} = \begin{pmatrix} 0 \\ -x_1 x_3 \\ x_1 x_2 \end{pmatrix}. \tag{35}$$

The slave system is described by

$$\begin{aligned} \dot{y}_1 &= a y_1 - y_2 + u_1, \\ \dot{y}_2 &= y_1 - y_2 y_3^2 + u_2, \\ \dot{y}_3 &= b y_3 - y_2 - 6 y_4 + u_3, \\ \dot{y}_4 &= y_3 + c y_4 + u_4. \end{aligned} \tag{36}$$

The 4D Zhang-Shen system, that is, system (36) with $u_1 = u_2 = u_3 = u_4 = 0$, exhibits hyperchaotic behavior when $(a, b, c) = (0.56, -1, 0.8)$. Chaotic attractors in 3D of the uncontrolled system (36) are shown in Figure 5.

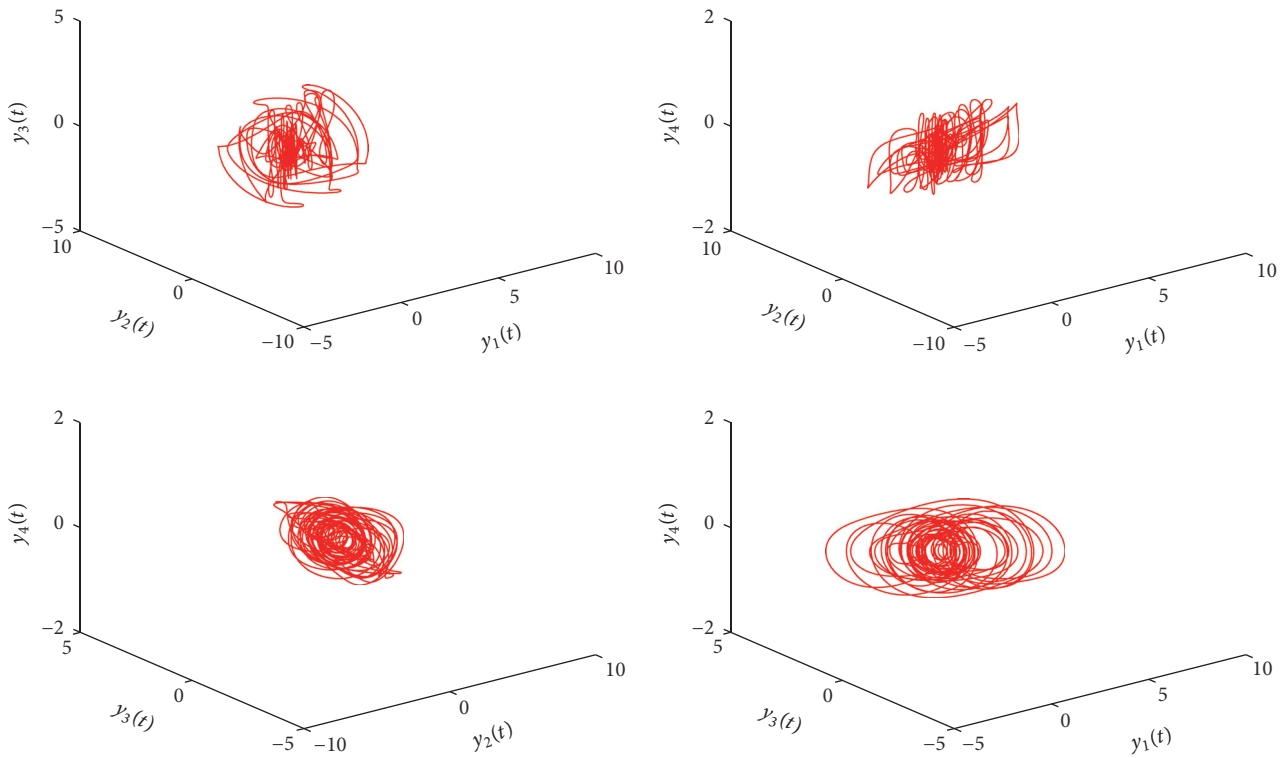

Figure 5: 3D phase portraits of the hyperchaotic Zhang-Shen system.

Based on the notations presented in Section 3.2, the errors between master system (34) and slave system (36) are given as

$$\begin{aligned} e_1 &= x_1 - h(t)\, y_1, \\ e_2 &= x_2 - \sum_{j=1}^{4} \Lambda_j(t)\, y_j, \\ e_3 &= x_3 - \phi(y_1, y_2, y_3, y_4), \end{aligned} \tag{37}$$

where $h(t) = t^2 + 1$, $\Lambda_1(t) = 0$, $\Lambda_2(t) = \exp(t)$, $\Lambda_3(t) = 0$, $\Lambda_4(t) = t^4$, and $\phi(y_1, y_2, y_3, y_4) = 3y_3 + y_4^2$. So, the matrix M defined by (23) is

$$M = \begin{pmatrix} t^2 + 1 & 0 & 0 \\ 0 & \exp(t) & 0 \\ 0 & 0 & 3 \end{pmatrix}. \tag{38}$$

According to Theorem 7, the control law $(u_1, u_2, u_3, u_4)^{\mathrm{T}}$ can be constructed as

$$\begin{aligned} (u_1, u_2, u_3)^T &= M^{-1}\left[T + L(e_1, e_2, e_3)^T\right], \\ u_4 &= 0, \end{aligned} \tag{39}$$

where

$$M^{-1} = \begin{pmatrix} \dfrac{1}{t^2+1} & 0 & 0 \\ 0 & \exp(-t) & 0 \\ 0 & 0 & \dfrac{1}{3} \end{pmatrix},$$

$$\begin{aligned} T_1 &= \dot{x}_1 + 36e_1 - 36e_2 - 2ty_1 \\ &\quad - \left(t^2 + 1\right)(0.56y_1 - y_2), \\ T_2 &= \dot{x}_2 - 20e_2 - \exp(t)\, y_2 - 4t^3 y_4 \\ &\quad - \exp(t)\left(y_1 - y_2 y_3^2\right) - t^4\left(y_3 + 0.8y_4\right), \\ T_3 &= \dot{x}_3 + 3e_3 + 3\left(y_3 + y_2 + 6y_4\right) \\ &\quad - 2y_4\left(y_3 + 0.8y_4\right), \end{aligned} \tag{40}$$

$$L = \begin{pmatrix} 0 & 36 & 0 \\ 0 & 30 & 0 \\ 0 & 0 & 0 \end{pmatrix}.$$

We can see that $(A - L)^T + (A - L)$ is a negative definite matrix. Hence, the synchronization between master system

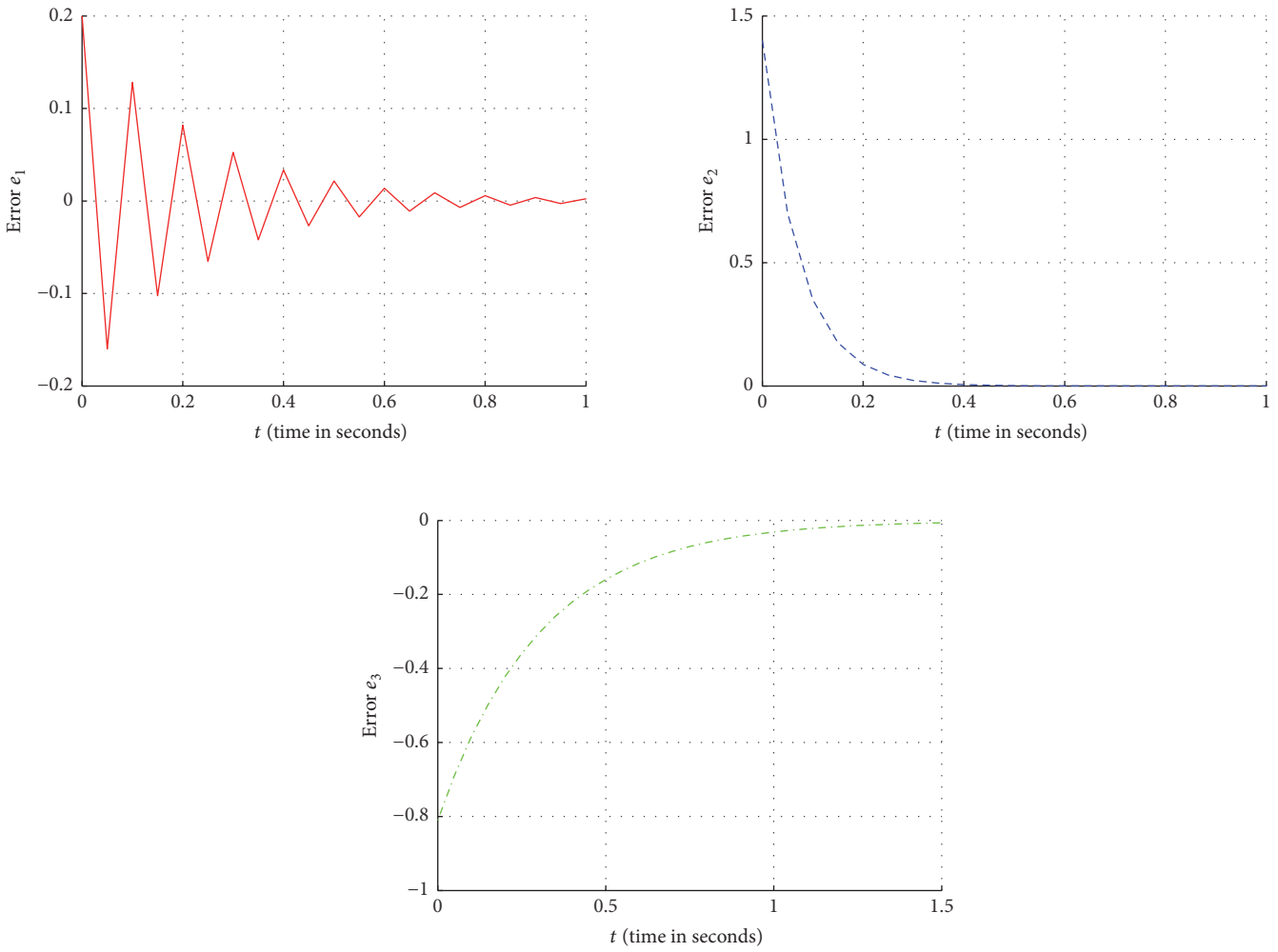

FIGURE 6: Time evolution of the synchronization errors e_1, e_2, and e_3 between master system (34) and slave system (36).

(34) and slave system (36) is achieved and the error system can be described as

$$\begin{aligned} \dot{e}_1 &= -36e_1, \\ \dot{e}_2 &= -10e_2, \\ \dot{e}_3 &= -3e_3. \end{aligned} \tag{41}$$

For the purpose of numerical simulation, the fourth order Runge–Kutta integration method has been used to solve system (41). The initial values of the master and the slave systems are $[x_1(0), x_2(0), x_3(0)] = [0.5, 1.5, 0.1]$ and $[y_1(0), y_2(0), y_3(0), y_4(0)] = [0.7, 0.1, 0.3, 0.1]$, respectively, and the initial states of the error system are $[e_1(0), e_2(0), e_3(0)] = [0.2, 1.4, -0.81]$. Figure 6 displays the synchronization errors between systems (34) and (36).

5. Conclusion

This paper has presented new schemes to study the coexistence of some types of chaos synchronization between nonidentical and different dimensional master and slave systems described by integer order and fractional order differential equations. The first scheme was constructed by combining CS, PS, FSHFPS, and GS in the synchronization of 3D integer order master system and 4D fractional order slave system. The second one was proposed when IPS, IFSHFPS, and IGS coexist between 3D fractional order master system and 4D integer order slave system. By exploiting fractional order Lyapunov approach and integer order Lyapunov method, the proposed synchronization approaches were rigorously proved to be achievable. The capability of the methods was illustrated by numerical examples and computer simulations.

Conflicts of Interest

The authors declare that there are no conflicts of interest regarding the publication of this paper.

Acknowledgments

The author Xiong Wang was supported by the National Natural Science Foundation of China (no. 61601306) and

Shenzhen Overseas High Level Talent Peacock Project Fund (no. 20150215145C).

References

[1] D. Cafagna and G. Grassi, "Fractional-order systems without equilibria: the first example of hyperchaos and its application to synchronization," *Chinese Physics B*, vol. 24, no. 8, Article ID 080502, 2015.

[2] Y. Gao, C. Liang, Q. Wu, and H. Yuan, "A new fractional-order hyperchaotic system and its modified projective synchronization," *Chaos, Solitons & Fractals*, vol. 76, pp. 190–204, 2015.

[3] A. M. El-Sayed, H. M. Nour, A. Elsaid, A. E. Matouk, and A. Elsonbaty, "Dynamical behaviors, circuit realization, chaos control, and synchronization of a new fractional order hyperchaotic system," *Applied Mathematical Modelling. Simulation and Computation for Engineering and Environmental Systems*, vol. 40, no. 5-6, pp. 3516–3534, 2016.

[4] J. Zhang, J. Nan, W. Du, Y. Chu, and H. Luo, "Dynamic analysis for a fractional-order autonomous chaotic system," *Discrete Dynamics in Nature and Society*, vol. 2016, Article ID 8712496, 13 pages, 2016.

[5] K. Rajagopal, L. Guessas, A. Karthikeyan, A. Srinivasan, and G. Adam, "Fractional order memristor no equilibrium chaotic system with its adaptive sliding mode synchronization and genetically optimized fractional order PID synchronization," *Complexity*, vol. 2017, Article ID 1892618, 19 pages, 2017.

[6] F. Zhang, G. Chen, C. Li, and J. Kurths, "Chaos synchronization in fractional differential systems," *Philosophical Transactions of the Royal Society of London. Series A. Mathematical, Physical and Engineering Sciences*, vol. 371, no. 1990, 26 pages, 2013.

[7] P. Muthukumar, P. Balasubramaniam, and K. Ratnavelu, "Sliding mode control design for synchronization of fractional order chaotic systems and its application to a new cryptosystem," *International Journal of Dynamics and Control*, vol. 5, no. 1, pp. 115–123, 2017.

[8] A. E. Matouk, "Chaos synchronization of a fractional-order modified van der Pol-Duffing system via new linear control, backstepping control and Takagi-Sugeno fuzzy approaches," *Complexity*, vol. 21, no. S1, pp. 116–124, 2016.

[9] R. Behinfaraz and M. Badamchizadeh, "Optimal synchronization of two different in-commensurate fractional-order chaotic systems with fractional cost function," *Complexity*, vol. 21, no. S1, pp. 401–416, 2016.

[10] A. Ouannas, M. M. Al-sawalha, and T. Ziar, "Fractional chaos synchronization schemes for different dimensional systems with non-identical fractional-orders via two scaling matrices," *Optik*, vol. 127, no. 20, pp. 8410–8418, 2016.

[11] W. S. Sayed, M. M. Henein, S. K. Abd-El-Hafiz, and A. G. Radwan, "Generalized dynamic switched synchronization between combinations of fractional-order chaotic systems," *Complexity*, vol. 2017, Article ID 9189120, 17 pages, 2017.

[12] A. Ouannas, G. Grassi, T. Ziar, and Z. Odibat, "On a function projective synchronization scheme for non-identical Fractional-order chaotic (hyperchaotic) systems with different dimensions and orders," *Optik - International Journal for Light and Electron Optics*, vol. 136, pp. 513–523, 2017.

[13] L. M. Pecora and T. L. Carroll, "Synchronization in chaotic systems," *Physical Review Letters*, vol. 64, no. 8, pp. 821–824, 1990.

[14] M. A. Aziz-Alaoui, "Synchronization of chaos," *Encyclopedia of Mathematical Physics*, vol. 5, pp. 213–226, 2006.

[15] A. C. Luo, "A theory for synchronization of dynamical systems," *Communications in Nonlinear Science and Numerical Simulation*, vol. 14, no. 5, pp. 1901–1951, 2009.

[16] P. Dong, G. Shang, and J. Liu, "Anticipating synchronization of integer order and fractional order hyper-chaotic Chen system," *International Journal of Modern Physics B*, vol. 26, no. 32, Article ID 1250211, 15 pages, 2012.

[17] Z. Ping and Y.-X. Cao, "Function projective synchronization between fractional-order chaotic systems and integer-order chaotic systems," *Chinese Physics B*, vol. 19, no. 10, Article ID 100507, 2010.

[18] A. Khan and P. Tripathi, "Synchronization between a fractional order chaotic system and an integer order chaotic system," *Nonlinear Dynamics and Systems Theory*, vol. 13, no. 4, pp. 425–436, 2013.

[19] Y. Wu and G. Wang, "Synchronization and anti-synchronization between a class of fractional-order and integer-order chaotic systems with only one controller term," *Journal of Theoretical & Applied Information Technology*, vol. 48, no. 1, pp. 145–151, 2013.

[20] A. Ouannas and R. Abu-Saris, "A robust control method for $Q-S$ synchronization between different dimensional integer-order and fractional-order chaotic systems," *Journal of Control Science and Engineering*, vol. 2015, Article ID 703753, 7 pages, 2015.

[21] A. Ouannas and A. Karouma, "Different generalized synchronization schemes between integer-order and fractional-order chaotic systems with different dimensions," *Differential Equations and Dynamical Systems*, pp. 1–13, 2016.

[22] L.-X. Jia, H. Dai, and M. Hui, "Nonlinear feedback synchronisation control between fractional-order and integer-order chaotic systems," *Chinese Physics B*, vol. 19, no. 11, Article ID 110509, 2010.

[23] Z. Ping, Y.-M. Cheng, and K. Fei, "Synchronization between fractional-order chaotic systems and integer orders chaotic systems (fractional-order chaotic systems)," *Chinese Physics B*, vol. 19, no. 9, Article ID 090503, 2010.

[24] L.-X. Yang, W.-S. He, and X.-J. Liu, "Synchronization between a fractional-order system and an integer order system," *Computers & Mathematics with Applications*, vol. 62, no. 12, pp. 4708–4716, 2011.

[25] G.-Q. Si, Z.-Y. Sun, and Y.-B. Zhang, "A general method for synchronizing an integer-order chaotic system and a fractional-order chaotic system," *Chinese Physics B*, vol. 20, no. 8, Article ID 080505, 2011.

[26] D. Chen, R. Zhang, J. Clinton Sprott, and X. Ma, "Synchronization between integer-order chaotic systems and a class of fractional-order chaotic system based on fuzzy sliding mode control," *Nonlinear Dynamics. An International Journal of Nonlinear Dynamics and Chaos in Engineering Systems*, vol. 70, no. 2, pp. 1549–1561, 2012.

[27] D.-Y. Chen, R.-F. Zhang, X.-Y. Ma, and J. Wang, "Synchronization between a novel class of fractional-order and integer-order chaotic systems via a sliding mode controller," *Chinese Physics B*, vol. 21, no. 12, Article ID 120507, 2012.

[28] Y.-P. Wu and G.-D. Wang, "Synchronization between fractional-order and integer-order hyperchaotic systems via sliding mode controller," *Journal of Applied Mathematics*, vol. 2013, Article ID 151025, 5 pages, 2013.

[29] Y. Wu and G. Wang, "Synchronization of a class of fractional-order and integer order hyperchaotic systems," *Journal of Vibration and Control*, vol. 20, no. 10, pp. 1584–1588, 2014.

[30] D. Chen, C. Wu, H. H. Iu, and X. Ma, "Circuit simulation for synchronization of a fractional-order and integer-order chaotic system," *Nonlinear Dynamics. An International Journal of Nonlinear Dynamics and Chaos in Engineering Systems*, vol. 73, no. 3, pp. 1671–1686, 2013.

[31] I. E. Gammoudi and M. Feki, "Synchronization of integer order and fractional order Chua's systems using robust observer," *Communications in Nonlinear Science and Numerical Simulation*, vol. 18, no. 3, pp. 625–638, 2013.

[32] S. Vaidyanathan, "Complete synchronization of hyperchaotic Xu and hyperchaotic Lü systems via active control," *International Journal of Computer Science & Engineering Survey*, vol. 3, no. 3, pp. 29–43, 2012.

[33] S. P. Ansari and S. Das, "Projective synchronization of time-delayed chaotic systems with unknown parameters using adaptive control method," *Mathematical Methods in the Applied Sciences*, vol. 38, no. 4, pp. 726–737, 2015.

[34] G. Cai, L. Yao, P. Hu, and X. Fang, "Adaptive full state hybrid function projective synchronization of financial hyperchaotic systems with uncertain parameters," *Discrete and Continuous Dynamical Systems. Series B. A Journal Bridging Mathematics and Sciences*, vol. 18, no. 8, pp. 2019–2028, 2013.

[35] S.-Y. Li, S.-A. Chen, C.-T. Lin, L.-W. Ko, C.-H. Yang, and H.-H. Chen, "Generalized synchronization of nonlinear chaotic systems through natural bioinspired controlling strategy," *Abstract and Applied Analysis*, Article ID 725674, 14 pages, 2015.

[36] A. Razminia and D. Baleanu, "Complete synchronization of commensurate fractional order chaotic systems using sliding mode control," *Mechatronics*, vol. 23, no. 7, pp. 873–879, 2013.

[37] S. K. Agrawal and S. Das, "Projective synchronization between different fractional-order hyperchaotic systems with uncertain parameters using proposed modified adaptive projective synchronization technique," *Mathematical Methods in the Applied Sciences*, vol. 37, no. 14, pp. 2164–2176, 2014.

[38] L. Zhang and T. Liu, "Full state hybrid projective synchronization of variable-order fractional chaotic/hyperchaotic systems with nonlinear external disturbances and unknown parameters," *Journal of Nonlinear Science and its Applications. JNSA*, vol. 9, no. 3, pp. 1064–1076, 2016.

[39] R. Martínez-Guerra and J. L. Mata-Machuca, "Fractional generalized synchronization in a class of nonlinear fractional order systems," *Nonlinear Dynamics. An International Journal of Nonlinear Dynamics and Chaos in Engineering Systems*, vol. 77, no. 4, pp. 1237–1244, 2014.

[40] G. Ahlem and A. Ouannas, "A general control method for inverse hybrid function projective synchronization of a class of chaotic systems," *International Journal of Mathematical Analysis*, vol. 9, no. 9-12, pp. 429–436, 2015.

[41] A. Ouannas and G. Grassi, "Inverse full state hybrid projective synchronization for chaotic maps with different dimensions," *Chinese Physics B*, vol. 25, no. 9, Article ID 090503, 2016.

[42] A. Ouannas, A. T. Azar, and T. Ziar, "On inverse full state hybrid function projective synchronization for continuous-time chaotic dynamical systems with arbitrary dimensions," *Differential Equations and Dynamical Systems*, pp. 1–14, 2017.

[43] A. Ouannas and Z. Odibat, "On inverse generalized synchronization of continuous chaotic dynamical systems," *International Journal of Applied and Computational Mathematics*, vol. 2, no. 1, pp. 1–11, 2016.

[44] A. Ouannas and G. Grassi, "A new approach to study the coexistence of some synchronization types between chaotic maps with different dimensions," *Nonlinear Dynamics*, vol. 86, no. 2, pp. 1319–1328, 2016.

[45] A. Ouannas, A. T. Azar, and S. Vaidyanathan, "New hybrid synchronisation schemes based on coexistence of various types of synchronisation between master-slave hyperchaotic systems," *International Journal of Computer Applications in Technology*, vol. 55, no. 2, p. 112, 2017.

[46] A. Ouannas, A. T. Azar, and S. Vaidyanathan, "A robust method for new fractional hybrid chaos synchronization," *Mathematical Methods in the Applied Sciences*, vol. 40, no. 5, pp. 1804–1812, 2017.

[47] A. Ouannas, S. Abdelmalek, and S. Bendoukha, "Co-existence of some chaos synchronization types in fractiona-order differential equations," *Electronic Journal of Differential Equations*, vol. 2017, no. 5, pp. 1804–1812, 2017.

[48] K. B. Oldham and J. Spanier, *The Fractional Calculus*, Academic Press, New York, NY, USA, 1974.

[49] R. Gorenflo and F. Mainardi, "Fractional calculus: integral and differential equations of fractional order," in *Fractals and Fractional Calculus in Continuum Mechanics*, A. Carpinteri and F. Mainardi, Eds., pp. 223–276, Springer, New York, NY, USA, 1997.

[50] M. Caputo, "Linear Models of Dissipation whose Q is almost Frequency Independent-II," *Geophysical Journal of the Royal Astronomical Society*, vol. 13, no. 5, pp. 529–539, 1967.

[51] S. G. Samko, A. A. Kilbas, and O. I. Marichev, *Fractional Integrals and Derivatives, Theory and Applications*, Gordon and Breach, Amsterdam, 1993.

[52] A. A. Kilbas, H. M. Srivastava, and J. J. Trujillo, *Theory and Applications of Fractional Differential Equations*, Elsevier, 2006.

[53] I. Podlubny and S. G. Samko, *Fractional Differential Equations*, vol. 198 of *Mathematics in Science and Engineering*, Academic Press, San Diego, Calif, USA, 1999.

[54] S. Wiggins, *Introduction to Applied Nonlinear Dynamical Systems and Chaos*, Springer, New York, NY, USA, 2003.

[55] D. Chen, R. Zhang, X. Liu, and X. Ma, "Fractional order Lyapunov stability theorem and its applications in synchronization of complex dynamical networks," *Communications in Nonlinear Science and Numerical Simulation*, vol. 19, no. 12, pp. 4105–4121, 2014.

[56] N. Aguila-Camacho, M. A. Duarte-Mermoud, and J. A. Gallegos, "Lyapunov functions for fractional order systems," *Communications in Nonlinear Science and Numerical Simulation*, vol. 19, no. 9, pp. 2951–2957, 2014.

[57] G. Chen and T. Ueta, "Yet another chaotic attractor," *International Journal of Bifurcation and Chaos in Applied Sciences and Engineering*, vol. 9, no. 7, pp. 1465-1466, 1999.

[58] Q. Han, C.-X. Liu, L. Sun, and D.-R. Zhu, "A fractional order hyperchaotic system derived from a Liu system and its circuit realization," *Chinese Physics B*, vol. 22, no. 2, Article ID 020502, 2013.

[59] X. Zhang and K. Shen, "The control action of the periodic perturbation on a hyperchaotic system," *Acta Physica Sinica*, vol. 8, no. 9, pp. 651–656, 1999.

[60] W. H. Deng and C. P. Li, "Chaos synchronization of the fractional Lü system," *Physica A: Statistical Mechanics and Its Applications*, vol. 353, no. 1–4, pp. 61–72, 2005.

Hindawi
Complexity
Volume 2017, Article ID 8979408, 16 pages
https://doi.org/10.1155/2017/8979408

Research Article

Hyperchaotic Chameleon: Fractional Order FPGA Implementation

Karthikeyan Rajagopal, Anitha Karthikeyan, and Prakash Duraisamy

Centre for Non-Linear Dynamics, Defense University, Bishoftu, Ethiopia

Correspondence should be addressed to Karthikeyan Rajagopal; rkarthiekeyan@gmail.com

Received 9 January 2017; Revised 2 March 2017; Accepted 2 March 2017

Academic Editor: Abdelalim Elsadany

There are many recent investigations on chaotic hidden attractors although hyperchaotic hidden attractor systems and their relationships have been less investigated. In this paper, we introduce a hyperchaotic system which can change between hidden attractor and self-excited attractor depending on the values of parameters. Dynamic properties of these systems are investigated. Fractional order models of these systems are derived and their bifurcation with fractional orders is discussed. Field programmable gate array (FPGA) implementations of the systems with their power and resource utilization are presented.

1. Introduction

Many recent works on dynamical systems are categorized into self-excited and hidden attractors [1–3]. A self-excited attractor has a basin of attraction that is associated with an unstable equilibrium, while a hidden attractor has a basin of attraction that does not intersect with small neighborhoods of any equilibrium points. Hidden attractors are important in most of the engineering problems as they allow chaotic responses [4, 5]. Control of such hidden oscillations is a big challenge because of the multistability nature of the systems [6, 7]. Chaotic attractors are with no equilibrium points [8–15], with only stable equilibria [16–19], and with curves of equilibria [20]. Fractional order with no equilibrium systems with its FPGA implementation has also been reported recently [21, 22].

Recently many researchers have discussed fractional order calculus and its applications [23–25]. Fractional order nonlinear systems with different control approaches are investigated [26–28]. Fractional order memristor based with no equilibrium chaotic system is proposed by Rajagopal et al. [21, 22]. A novel fractional order with no equilibrium chaotic system is investigated by Li and Chen [29]. Cafagna and Grassi investigated a fractional order hyperchaotic system without equilibrium points [30]. Memristor based fractional order system with a capacitor and an inductor is discussed [31]. Numerical analysis and methods for simulating fractional order nonlinear system are proposed by Petras [32] and MATLAB solutions for fractional order chaotic systems are discussed by Trzaska Zdzislaw [33]. A FPGA implementation of fractional order chaotic system using approximation method is investigated recently for the first time [21, 22].

Recently Jafari et al. announced a 3D chaotic system [34] which can belong to three famous categories of hidden attractors plus systems with self-excited attractors. Motivated by this, in this paper we announce a hyperchaotic chameleon which can be self-excited or a hidden attractor depending on the values of the parameters. This system helps us to better understand the hidden chaotic flows of higher dimension.

2. Novel Chaotic System (NCS)

In this section we introduce a class of novel chaotic and hyperchaotic systems with flux controlled memristor [35, 36], derived from the hyperchaotic system [37] by including parameter a which governs the equilibrium of the system and parameter b controls the number of Lyapunov exponents in the system, that is, chaotic and hyperchaotic case. The

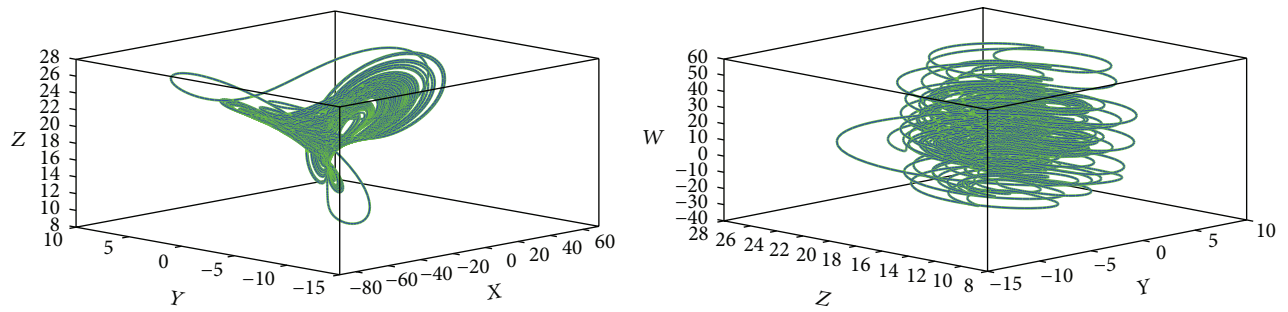

Figure 1: 3D phase portraits of NCS_1 system.

Table 1: Different cases for the parameters a and b.

Name of the system	Parameters a and b	Type of system
NCS_1	$a = 0, b \neq 0$	Hyperchaotic system with single equilibrium at origin
NCS_2	$a \neq 0, b \neq 0$	Hyperchaotic system with no equilibrium
NCS_3	$a = 0, b = 0$	Hyperchaotic system with single equilibrium at origin
NCS_4	$a \neq 0, b = 0$	Chaotic system with no equilibrium

novel hyperchaotic system's dimensionless state equations are

$$\begin{aligned} \dot{x} &= 15\left(y - x\right) + 13yz, \\ \dot{y} &= 18x - xz - bxW\left(\phi\right) - a, \\ \dot{z} &= xy - cz, \\ \dot{w} &= -dx, \end{aligned} \tag{1}$$

where $W(\phi) = \alpha + 3\beta\phi^2$ is the memductance of the flux controller memristor where the flux element ϕ is defined by the fourth state w with $\alpha = 4$ and $\beta = 0.01$. The parameters c and d are fixed at 2 and 1.4, respectively. We investigate four different choices for the parameters a and b as in Table 1.

Figures 1–4 show the 3D phase portraits of the systems NCS_1, NCS_2, NCS_3, and NCS_4, respectively.

3. Dynamic Properties of the NCS

3.1. Equilibrium Points. The equilibrium points for the NCS can be calculated by equating the state equations to 0. It can be seen that $18x - xz - bxW(\phi) - a = 0$ shows two cases of equilibrium points; that is, when $a = 0$ the system has origin as the only defined equilibrium point and when $a \neq 0$ the system has no defined equilibrium and hence exhibits hidden attractors. Table 2 shows the equilibrium points for different choices of a and b. The characteristic equation of NCS_1 and NCS_3 is $2\lambda^4 + 19\lambda^3 - 270\lambda^2 - 600\lambda$ and the Eigenvalues are $\lambda_1 = 0; \lambda_2 = -16.55; \lambda_3 = 9.06; \lambda_4 = -2$ and λ_3 is an unstable

Table 2: Equilibrium points of the NCS systems.

Name of the system	Parameters a and b	Equilibrium points
NCS_1	$a = 0, b = 0.5$	[0, 0, 0, 0]
NCS_2	$a \neq 0, b = 0.5$	No equilibrium
NCS_3	$a = 0, b = 0$	[0, 0, 0, 0]
NCS_4	$a \neq 0, b = 0$	No equilibrium

focus and thus the two systems are self-excited attractors. As investigated by many researchers [8–15], chaotic attractors with no equilibrium are hidden thus making NCS_2 and NCS_4 hidden attractors.

3.2. Lyapunov Exponents and Kaplan-Yorke Dimension. Lyapunov exponents of a nonlinear system define the convergence and divergence of the states. The existence of a positive Lyapunov exponent confirms the chaotic behavior of the system [38, 39]. Lyapunov exponents (LEs) are necessary and more convenient for detecting hyperchaos in fractional order hyperchaotic system. A definition of LEs for fractional differential systems was given in [40] based on frequency-domain approximations, but the limitations of frequency-domain approximations are highlighted by Tavazoei and Haeri [41]. Time series based LEs calculation methods like Wolf algorithm [11], Jacobian method [12], and neural network algorithm [13] are popularly known ways of calculating Lyapunov exponents for integer and fractional order systems. Hence we use the Jacobian method to calculate the LEs. Table 3 shows the Lyapunov exponents of the NCS.

3.3. Bifurcation. In this section we derive the bifurcation contours for the NCS. The chaotic behavior of the system largely depends on the parameters a, b, c, and d. As discussed in [42], the transient behaviors occurring in memristor based nonlinear systems may result in longer simulation times to reach steady states. Hence we used the ode45 solver for numerical simulations. Four different cases of bifurcations are investigated for the NCS. In case 1 the parameter a is varied and the bifurcation of the attractor is investigated. Figure 5 shows the bifurcation plot for a. In the second case parameter b is varied and the bifurcation of the NCS is studied which is shown in Figure 6. In case 3 the parameter c is varied and bifurcation analysis of the system is investigated. Finally

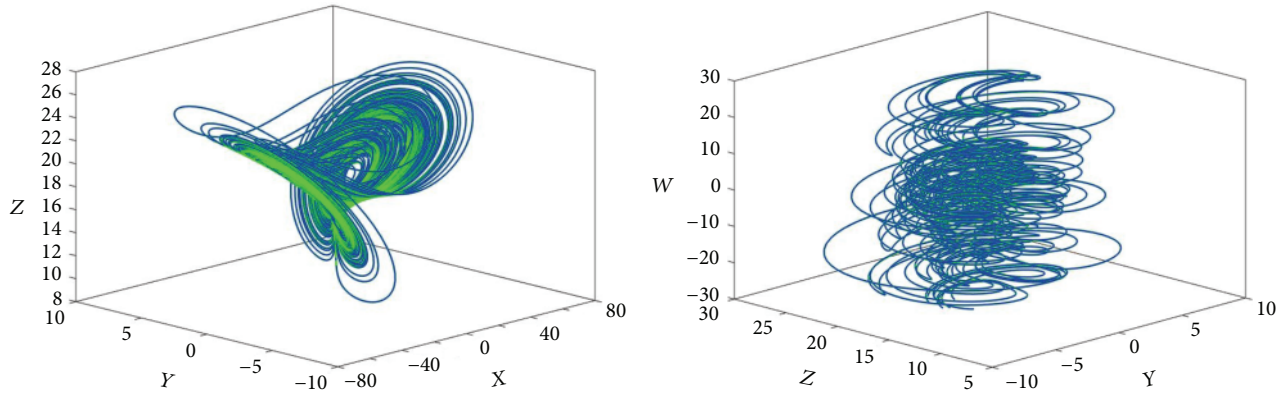

Figure 2: 3D phase portraits of NCS_2 system.

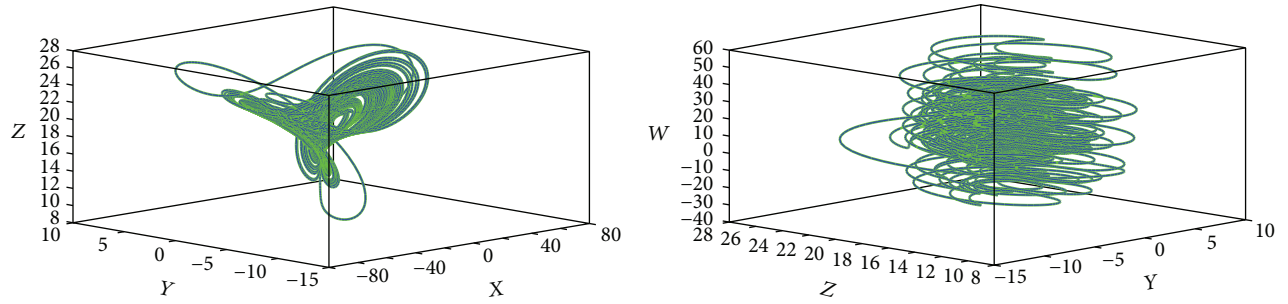

Figure 3: 3D phase portraits of the NCS_3 system.

Table 3: Lyapunov exponents and KY dimension of NCS systems.

System	Lyapunov exponents	Kaplan-Yorke (KY) dimension
NCS_1	$L_1 = 19.3050$, $L_2 = 1.0627$, $L_3 = -0.1084$, $L_4 = -37.2591$	3.5465
NCS_2	$L_1 = 19.7244$; $L_2 = 1.2240$; $L_3 = 0$; $L_4 = -38.0565$	3.5506
NCS_3	$L_1 = 3.5123$; $L_2 = 0.0026$; $L_3 = 0$; $L_4 = -20.5149$	3.1714
NCS_4	$L_1 = 3.1029$; $L_2 = 0$; $L_3 = 0$; $L_4 = -20.1029$	3.1543

bifurcation plot for parameter d is derived in case 4. Figures 7 and 8 show the bifurcation contours of c and d, respectively. As can be seen from the figures the NCS shows strange attractor, hyperchaos, chaos, and quasiperiodic systems. For $0 \leq a \leq 0.25$, $0.51 \leq b \leq 0.72$, $0.8 \leq c \leq 1.2$, and $1.34 \leq d \leq 1.45$ the NCS shows strange attractor and the transient behavior of the memristor prevents the bifurcation plots to show the period doubling property even after reducing the transients to 70%. The system exhibits hyperchaotic attractor with hidden oscillations for $0.26 \leq a \leq 0.8$, $0.2 \leq b \leq 0.5$, $1.8 \leq c \leq 2.3$, and $1.04 \leq d \leq 1.25$. For a small band of $0 \leq b \leq 0.1$ with $0.8 \leq a \leq 1.4$, $2.4 \leq c \leq 2.8$, and $1.31 \leq d \leq 1.45$ the system shows chaotic oscillations with hidden attractors. A quasichaotic system is seen for $1.5 \leq a \leq 1.8$, $0.8 \leq b \leq 2$, $0.42 \leq c \leq 0.7$, and $1.47 \leq d \leq 1.5$.

3.4. Bicoherence. The motivation to study the bicoherence is twofold. First, the bicoherence can be used to extract information due to deviations from Gaussianity and suppress additive (colored) Gaussian noise. Second, the bicoherence can be used to detect and characterize asymmetric nonlinearity in signals via quadratic phase coupling or identify systems with quadratic nonlinearity. The bicoherence is the third-order spectrum. Whereas the power spectrum is a second-order statistic, formed from $X'(f) * X(f)$, where $X(f)$ is the Fourier transform of $x(t)$, the bispectrum is a third-order statistic formed from $X(f_j) * X(f_k) * X'(f_j + f_k)$. The bispectrum is therefore a function of a pair of frequencies (f_j, f_k). It is also a complex-valued function. The (normalized) square amplitude is called the bicoherence (by analogy with the coherence from the cross-spectrum). The bispectrum is calculated by dividing the time series into M segments of length N_seg, calculating their Fourier transforms and biperiodogram and then averaging over the ensemble. Although the bicoherence is a function of two frequencies the default output of this function is a one-dimensional output, the bicoherence refined as a function of

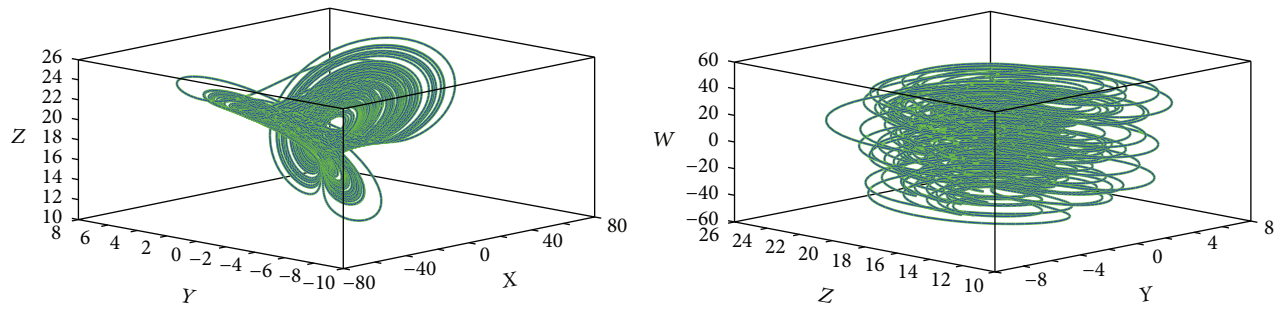

Figure 4: 3D phase portraits of the NCS_4 system.

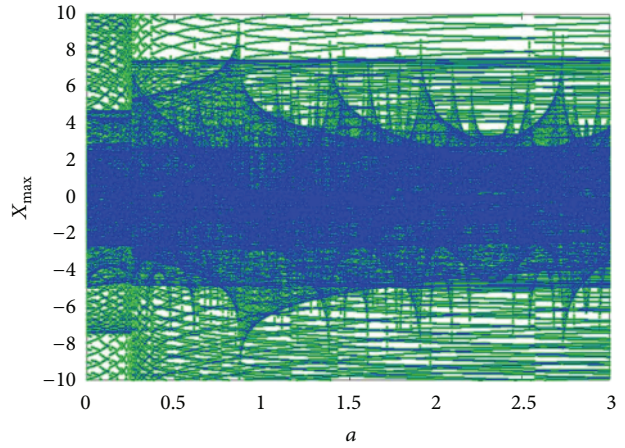

Figure 5: Bifurcation plots for parameter a.

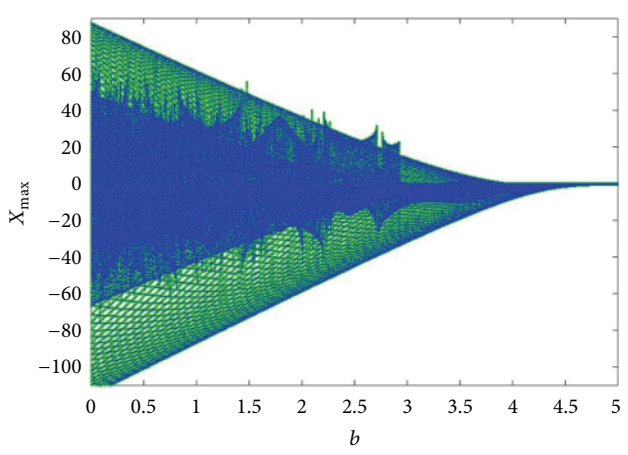

Figure 6: Bifurcation plots for parameter b.

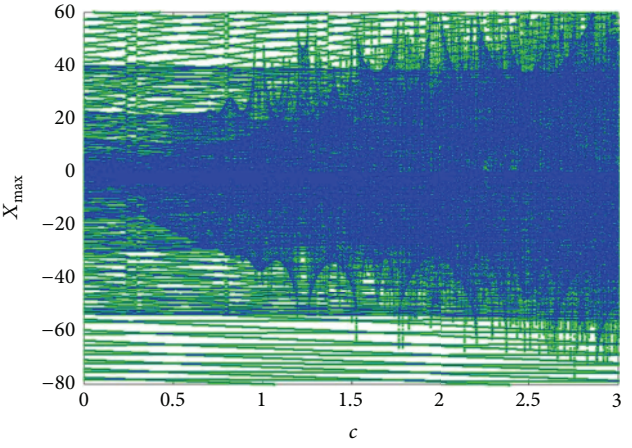

Figure 7: Bifurcation plots for parameter c.

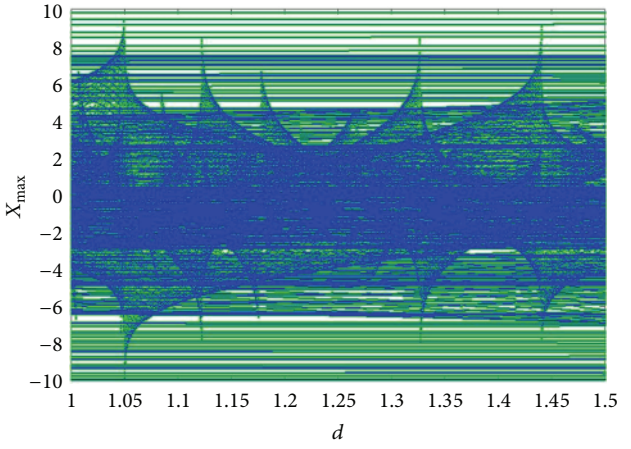

Figure 8: Bifurcation plots for parameter d.

only the sum of the two frequencies. The autobispectrum of a chaotic system is given by Pezeshki et al. [43]. They derived the autobispectrum with the Fourier coefficients.

$$B(\omega_1, \omega_2) = E\left[A(\omega_1) A(\omega_2) A^*(\omega_1 + \omega_2)\right], \quad (2)$$

where ω_n is the radian frequency and A is the Fourier coefficients of the time series. The normalized magnitude spectrum of the bispectrum known as the squared bicoherence is given by

$$b(\omega_1, \omega_2) = \frac{\left|B(\omega_1, \omega_2)\right|^2}{P(\omega_1) P(\omega_2) P(\omega_1 + \omega_2)}, \quad (3)$$

where $P(\omega_1)$ and $P(\omega_2)$ are the power spectrums at f_1 and f_2.

Figures 9 and 10 show the bicoherence contours of the NCS for $a \neq 0$ and $b \neq 0$ and $a = 0$ and $b = 0$,

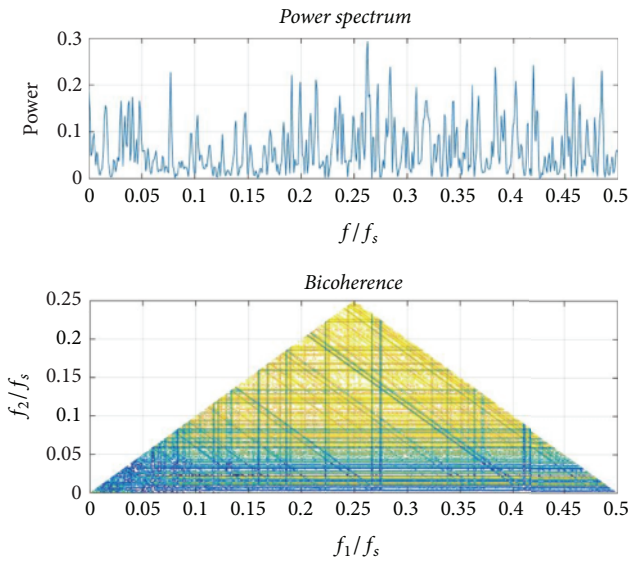

Figure 9: Bicoherence plots of NCS ($a \neq 0$, $b \neq 0$).

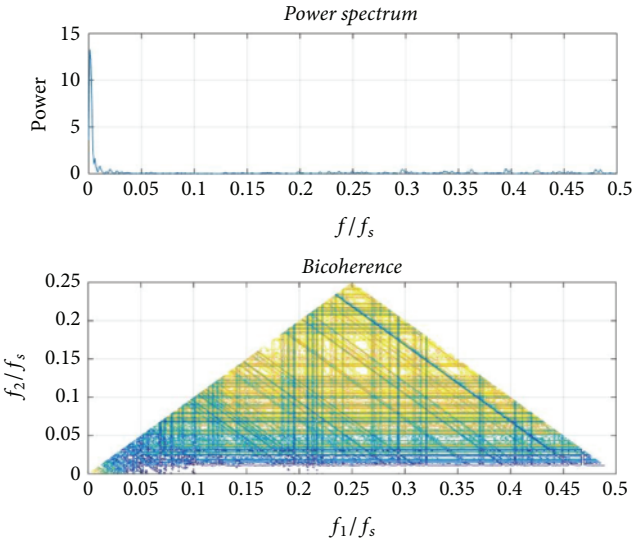

Figure 10: Bicoherence plot of NCS ($a = 0$, $b = 0$).

respectively. As can be seen from the figures, the NCS shows wider band of power spectrum when $a \neq 0$ and $b \neq 0$ because of the hyperchaotic hidden attractor as when $b \neq 0$ the memristor element introduces a quadratic nonlinearity resulting in the cross-bicoherence. Shades in yellow represent the multifrequency components contributing to the power spectrum. From Figures 9 and 10 the cross-bicoherence is significantly nonzero and nonconstant, indicating a nonlinear relationship between the states. The yellow shades and nonsharpness of the peaks, as well as the presence of structure around the origin in figures (cross-bicoherence), indicate that the nonlinearity between the states x, y, z, and w is not of the quadratic nonlinearity and hence may be because of nonlinearity of higher dimensions. The most two dominant frequencies (f_1, f_2) are taken for deriving the contour of bicoherence. The sampling frequency (f_s) is taken as the reference frequency. Direct FFT is used to derive the power spectrum for individual frequencies and Hankel operator is used as the frequency mask. Hanning window is used as the FIR filter to separate the frequencies.

4. Fractional Order NCS (FONCS)

In this section we derive the fractional order model novel chaotic system (FONCS). There are three commonly used definitions of the fractional order differential operator, *namely,* those of Grunwald–Letnikov, Riemann–Liouville, and Caputo [23–25].

In this section, we will study the dynamical behavior of fractional order system derived from the NCS with the Grunwald-Letnikov (GL) definition, which is defined as

$$\begin{aligned} {}_aD_t^q f(t) &= \lim_{h\to 0}\left\{\frac{1}{h^q}\sum_{j=0}^{[(t-q)/h]}(-1)^j\binom{q}{j}f(t-jh)\right\} \\ &= \lim_{h\to 0}\left\{\frac{1}{h^q}\Delta_h^q f(t)\right\}, \end{aligned} \tag{4}$$

where a and t are limits of the fractional order equation, $\Delta_h^q f(t)$ is generalized difference, h is the step size, and q is the fractional order of the differential equation.

For numerical calculations the above equation is modified as

$${}_{(t-L)}D_t^q f(t) = \lim_{h\to 0}\left\{h^{-q}\sum_{j=0}^{N(t)} b_j\left(f(t-jh)\right)\right\}. \tag{5}$$

Theoretically fractional order differential equations use infinite memory. Hence when we want to numerically calculate or simulate the fractional order equations we have to use finite memory principal, where L is the memory length and h is the time sampling.

$$N(t) = \min\left\{\left[\frac{t}{h}\right], \left[\frac{L}{h}\right]\right\}. \tag{6}$$

The binomial coefficients required for the numerical simulation are calculated as

$$b_j = \left(1 - \frac{a+q}{j}\right)b_{j-1}. \tag{7}$$

Using (4)–(6) the fractional order NCS is defined as

$$\begin{aligned} D^{q_x}x &= 15(y-x) + 13yz, \\ D^{q_y}y &= 18x - xz - bxW(\phi) - a, \\ D^{q_z}z &= xy - cz, \\ D^{q_w}w &= -dx. \end{aligned} \tag{8}$$

As discussed in Section 1, the FONCS also shows chaotic and hyperchaotic systems with no equilibrium and single equilibrium points for a choice of parameter values a and b as shown in Table 4.

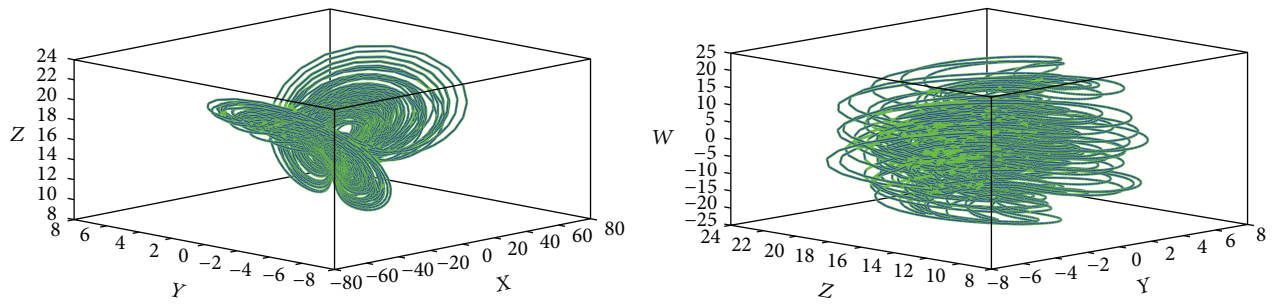

Figure 11: 3D phase portraits of NCS ($a \neq 0$, $b \neq 0$).

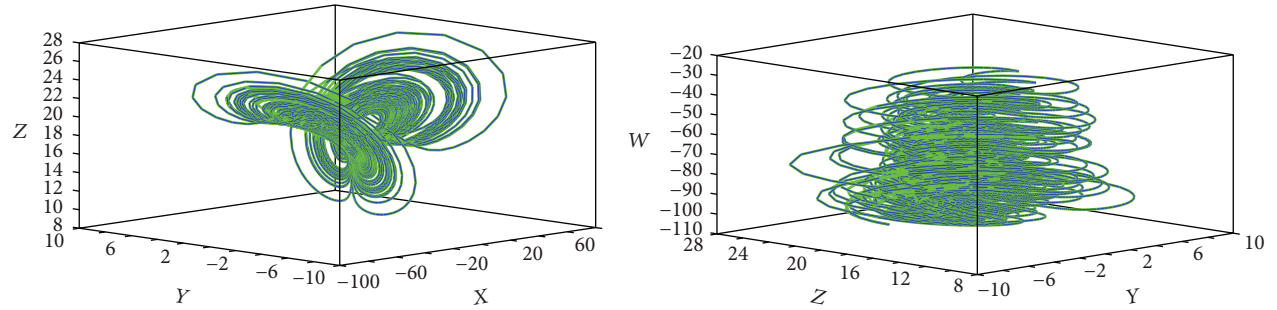

Figure 12: 3D phase portraits of NCS ($a \neq 0$, $b = 0$).

Table 4: Choice of parameters and type of the system.

Name of the system	Parameters a and b	Type of system
$FONCS_1$	$a = 0, b = 0.5$	Hyperchaotic system with single equilibrium at origin
$FONCS_2$	$a \neq 0, b = 0.5$	Hyperchaotic system with no equilibrium
$FONCS_3$	$a = 0, b = 0$	Hyperchaotic system with single equilibrium at origin
$FONCS_4$	$a \neq 0, b = 0$	Chaotic system with no equilibrium

The 3D phase portraits of the FONCS are shown in Figures 11–14. The commensurate fractional orders of the system for $a = 0, b \neq 0$, $a \neq 0, b \neq 0$, $a = 0, b = 0$, $a \neq 0$, and $b = 0$ are taken as $q = 0.991$, $q = 0.995$, $q = 0.989$, and $q = 0.990$, respectively.

4.1. Dynamic Analysis of the FONCS. Most of the dynamic properties of the NCS like the Lyapunov exponents and bifurcation with parameters are preserved in the FONCS [44] if $q_i > 0.98$, where $i = x, y, z,$ and w. The most important analysis of interest when investigating a fractional order system is the bifurcation with fractional order. The largest positive Lyapunov exponents ($L_1 = 19.8942$, $L_2 = 1.1436$) of the NCS for $a = 0$ and $b \neq 0$ appear when $q = 0.991$ against their largest integer order Lyapunov exponents ($L_1 = 19.3050$, $L_2 = 1.0627$), largest positive Lyapunov exponents ($L_1 = 20.1613$, $L_2 = 1.4108$) of the NCS for $a \neq 0$ and $b \neq 0$ appear when $q = 0.995$ against their largest integer order Lyapunov exponents ($L_1 = 19.7244$, $L_2 = 1.2208$), largest positive Lyapunov exponents ($L_1 = 3.8407$, $L_2 = 0.0134$) of the NCS for $a = 0$ and $b = 0$ appear when $q = 0.989$ against their largest integer order Lyapunov exponents ($L_1 = 3.51$, $L_2 = 0.0026$) and largest positive Lyapunov exponent ($L_1 = 3.1187$) of the NCS for $a \neq 0$ and $b = 0$ appear when $q = 0.990$ against its largest integer order Lyapunov exponent ($L_1 = 3.1029$). It can also be seen that as the fractional order q decreases, the FONCS starts losing its largest positive Lyapunov exponent. When $q \leq 0.90$ the positive Lyapunov exponents of the system become negative and thus the chaotic oscillation in the system disappears. Figures 15 and 16 show the bifurcation of the FONCS for variation in fractional orders $q_x = q_y = q_z = q_w = q$ for the two distinctive cases $a \neq 0$ and $b \neq 0$ and $a = 0$ and $b = 0$.

4.2. Stability Analysis of FONCS

4.2.1. Commensurate Order. For commensurate FONCS of order q, the system is stable and exhibits chaotic oscillations if $|\arg(\mathrm{eig}(J_E))| = |\arg(\lambda_i)| > q\pi/2$, where J_E is the Jacobian matrix at the equilibrium E and λ_i are the Eigenvalues of the FONCS, where $i = 1, 2, 3,$ and 4. As seen from the FONCS, the Eigenvalues should remain in the unstable region and the necessary condition for the FONCS to be stable is $q > (2/\pi)\tan^{-1}(|\mathrm{Im}\,\lambda|/\mathrm{Re}\,\lambda)$. The Eigenvalues of $FONCS_1$ and $FONCS_3$ are $\lambda_1 = 0$; $\lambda_2 = -16.55$; $\lambda_3 = 9.06$; $\lambda_4 = -2$ and λ_3 is an unstable focus contributing to the existence of chaotic oscillations.

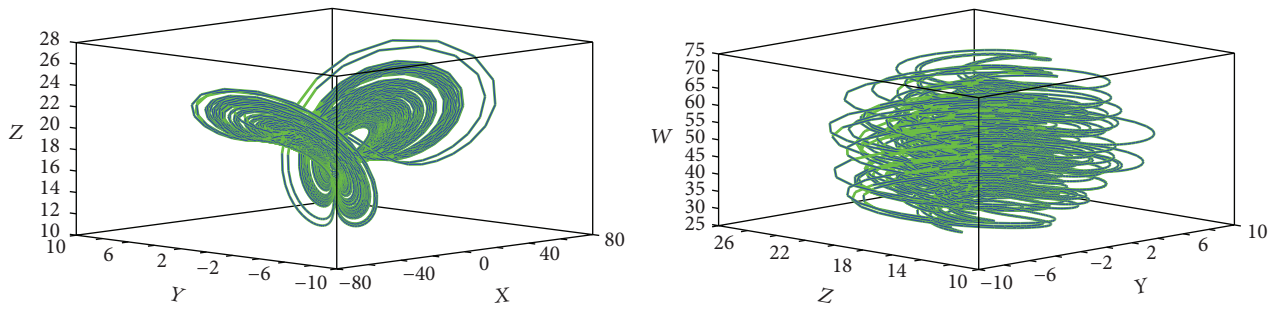

Figure 13: 3D phase portraits of NCS ($a = 0$, $b = 0$).

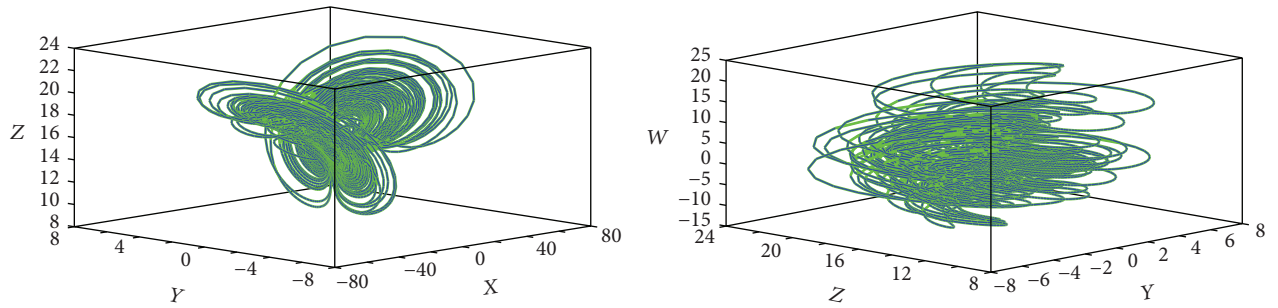

Figure 14: 3D phase portraits of NCS ($a = 0$, $b \neq 0$).

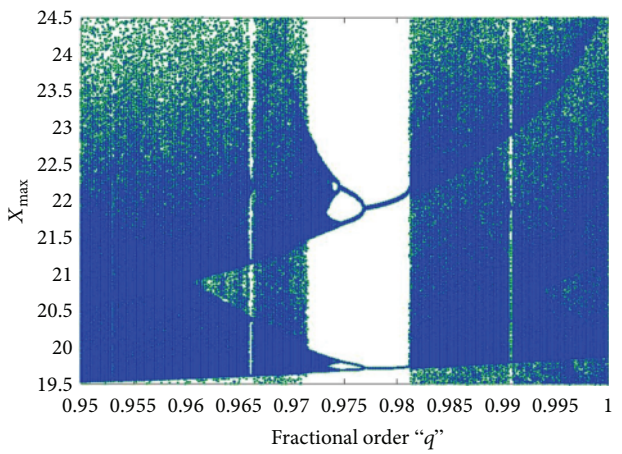

Figure 15: Bifurcation of NCS versus fractional order q ($a \neq 0$, $b \neq 0$).

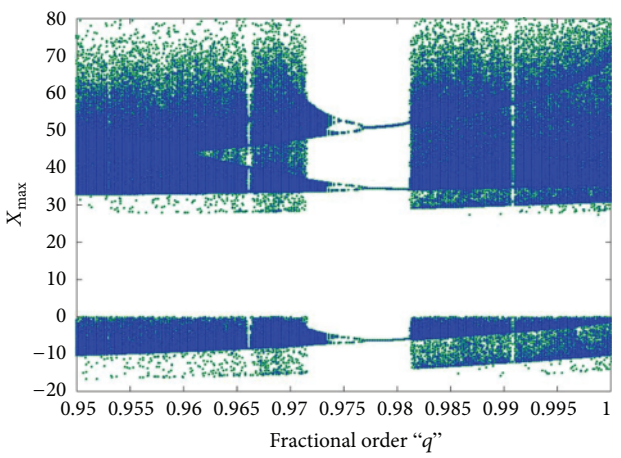

Figure 16: Bifurcation of NCS versus fractional order q ($a = 0$, $b = 0$).

4.2.2. Incommensurate Order. The necessary condition for the FONCS to exhibit chaotic oscillations in the incommensurate case is $\pi/2M - \min_i(|\arg(\lambda i)|) > 0$, where M is the LCM of the fractional orders. If $q_x = 0.9$, $q_y = 0.9$, $q_z = 0.8$, and $q_w = 0.8$, then $M = 10$. The characteristic equation of the system evaluated at the equilibrium is $\det(\mathrm{diag}[\lambda^{Mq_x}, \lambda^{Mq_y}, \lambda^{Mq_z}, \lambda^{Mq_w}] - J_E) = 0$ and by substituting the values of M and the fractional orders, $\det(\mathrm{diag}[\lambda^9, \lambda^9, \lambda^8, \lambda^8] - J_E) = 0$, the characteristic equation is $\lambda^{34} + 2\lambda^{27} + 4\lambda^{26} + 15\lambda^{25} + \lambda^{20} + 6\lambda^{19} + 35\lambda^{18} + 45\lambda^{17} - 300\lambda^{16} + 2\lambda^{12} + 21\lambda^{11} + 62\lambda^{10} - 570\lambda^9 - 600\lambda^8 + \lambda^4 + 17\lambda^3 - 270\lambda^2 - 600\lambda$ and is the same for both FONCS_1 and FONCS_3. The approximated solution of the characteristic equation is $\lambda_{34} = 0.912$ whose argument is zero and which is the minimum argument and hence the stability necessary condition becomes $\pi/20 - 0 > 0$ which solves for $0.0785 > 0$ and hence the FONCS is stable and chaos exists in the incommensurate system.

5. FPGA Implementation of the Fractional Order Novel Cubic Nonlinear Systems

In this section we discuss the implementation of the proposed FONCS in FPGA [21, 22, 38, 45–48] using the Xilinx (Vivado)

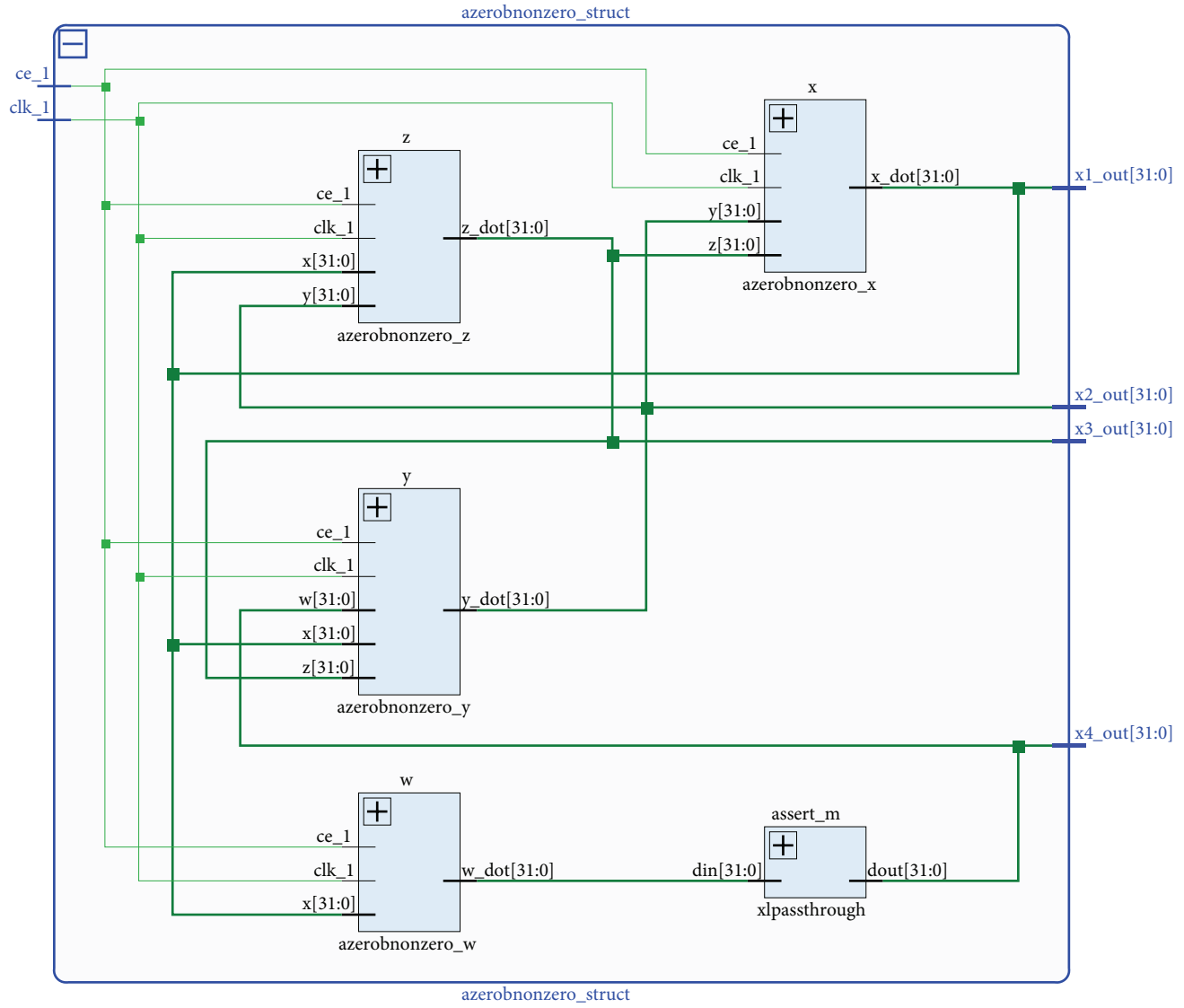

Figure 17: RTL schematics of FONCS-1 system.

Table 5: Resource utilization of FONCS-1 system.

Resource	Utilization	Available	Utilization %	Clock frequency	
				f_{max}	Used
LUT	1165	101400	1.15	300 Mhz	167 Mhz
FF	256	202800	0.13	500 Mhz	226 Mhz
DSP	20	600	3.33	250 Mhz	140 Mhz
IO	129	285	45.26	300 Mhz	108 Mhz
BUFG	1	32	3.13	300 Mhz	47 Mhz

System Generator toolbox in Simulink. The challenge while implementing the systems in FPGAs is to design the fractional order integrator which is not a readily available block in the System Generator [21, 22]. Hence we implement the fractional integrators using the mathematical relation [32, 33] discussed in (4), (5), and (6) and the value of h is taken as 0.001 with the initial conditions as described in Table 1 and the commensurate fractional order taken as $q = 0.991$ for FONCS-1, $q = 0.995$ for FONCS-2, $q = 0.989$ for FONCS-3, and $q = 0.99$ for FONCS-4. Figures 17, 18(a), and 18(b) show the Xilinx RTL schematics of the FONCS-1 system implemented in Kintex-7 (device = 7k160t, package = fbg484 S), power utilized by the system, and power utilized for various fractional orders, respectively. Table 5 shows the

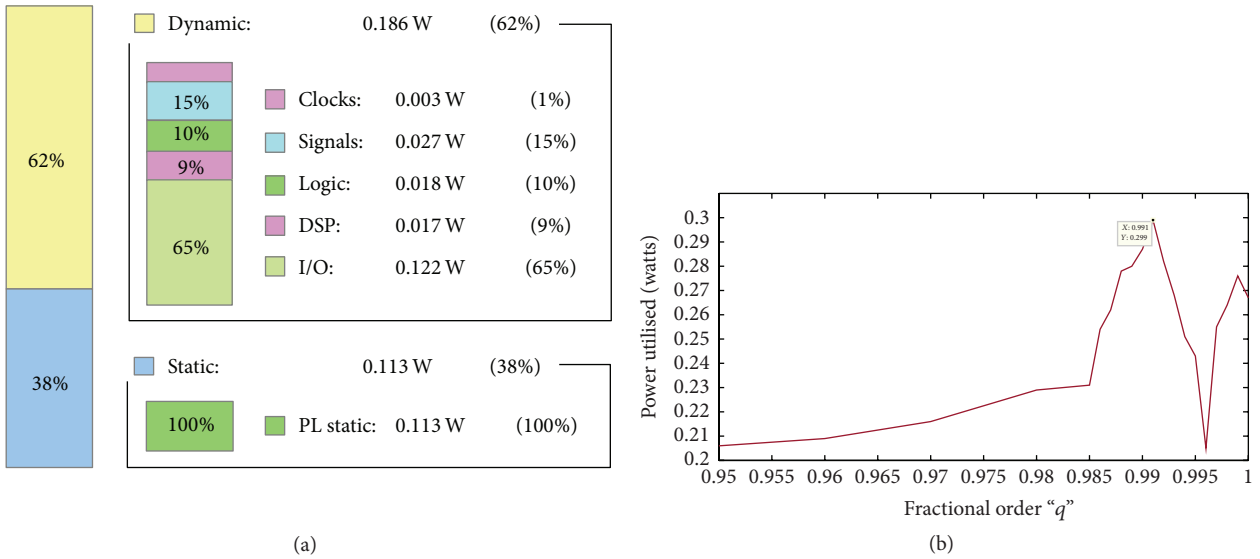

FIGURE 18: (a) Power utilized and (b) power utilization versus fractional order of FONCS-1 system.

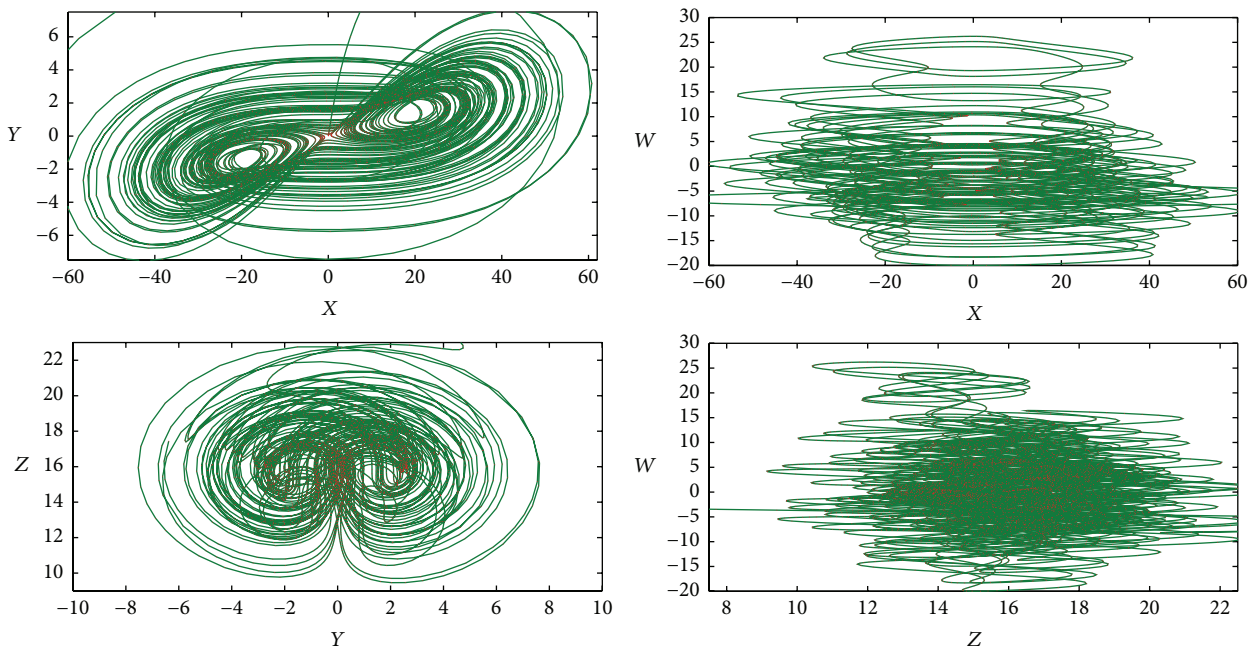

FIGURE 19: 2D phase portraits of the FPGA implemented FONCS-1 system (XY, XW, YZ, and ZW).

resources utilized by the FONCS-1 system including the clock frequency. Figure 19 shows the 2D state portraits of the FPGA implemented FONCS-1 system. Figures 20, 21(a), and 21(b) show the Xilinx schematics of the FONCS-2 system implemented in Kintex-7 (Device = 7k160t Package = fbg484 S), power utilized by the system and power utilization for various fractional orders, respectively. Table 6 shows the resources utilized by the FONCS-2 system including the clock frequency. Figure 22 shows the 2D state portraits of the FPGA implemented FONCS-2 system. Figures 23, 24(a), and 24(b) show the Xilinx schematics of the FONCS-3 system implemented in Kintex-7 (device = 7k160t, package = fbg484 S), power utilized by the system, and power utilization for various fractional orders, respectively. Table 7 shows the resources utilized by the FONCS-3 system including the clock frequency. Figure 25 shows the 2D state portraits of the FPGA implemented FONCS-3 system. Figures 26, 27(a), and 27(b) show the Xilinx schematics of the FONCS-4 system implemented in Kintex-7 (device = 7k160t, package = fbg484 S), power utilized by the system, and power utilization for various fractional orders, respectively. Table 8 shows the resources utilized by the FONCS-3 system including the clock frequency. Figure 28 shows the 2D state portraits of the FPGA implemented FONCS-3 system. The sampling rates of the FPGA blocks play a crucial role in the existence of Lyapunov exponents and also increasing the sampling time

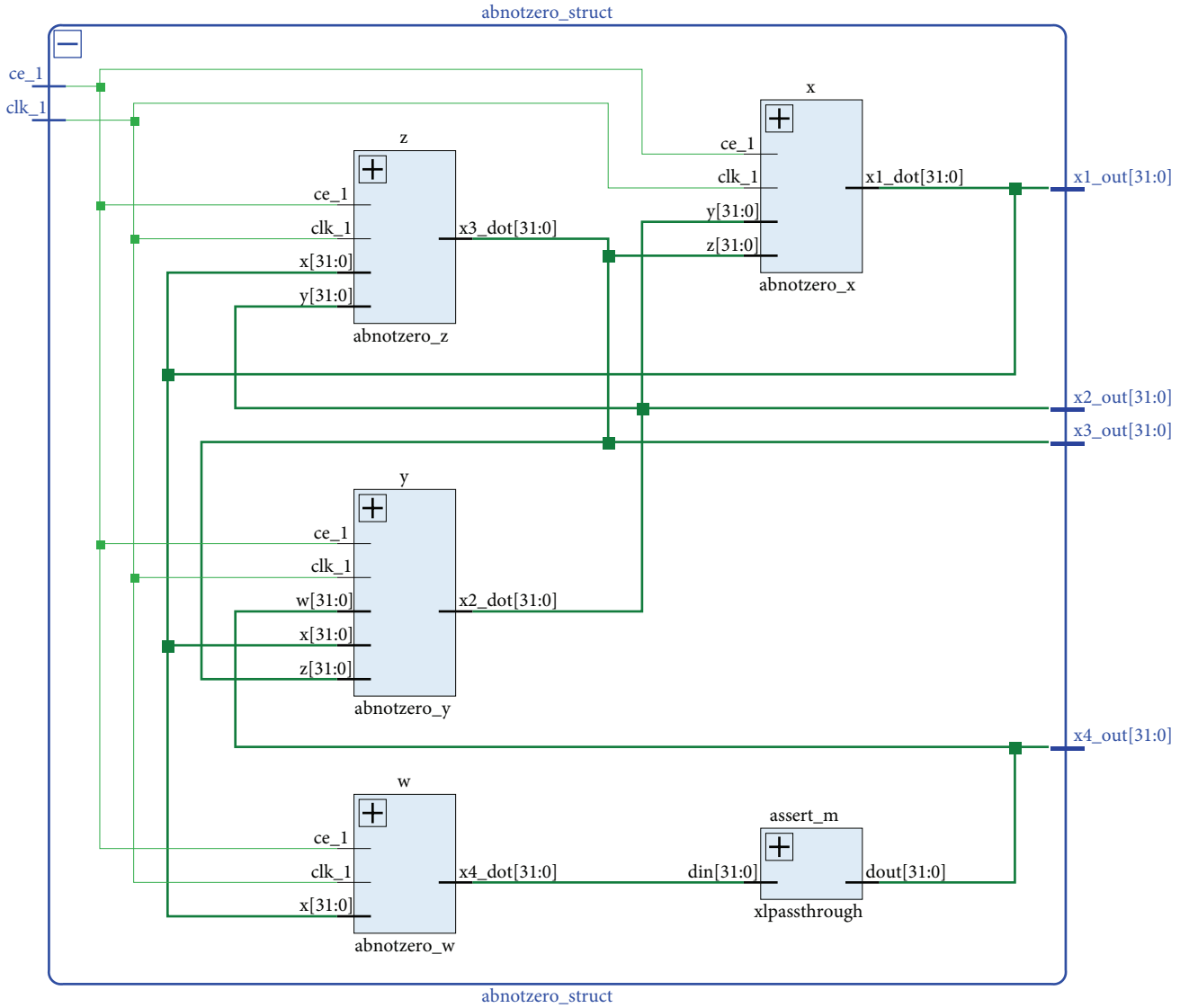

Figure 20: RTL schematics of FONCS-2 system.

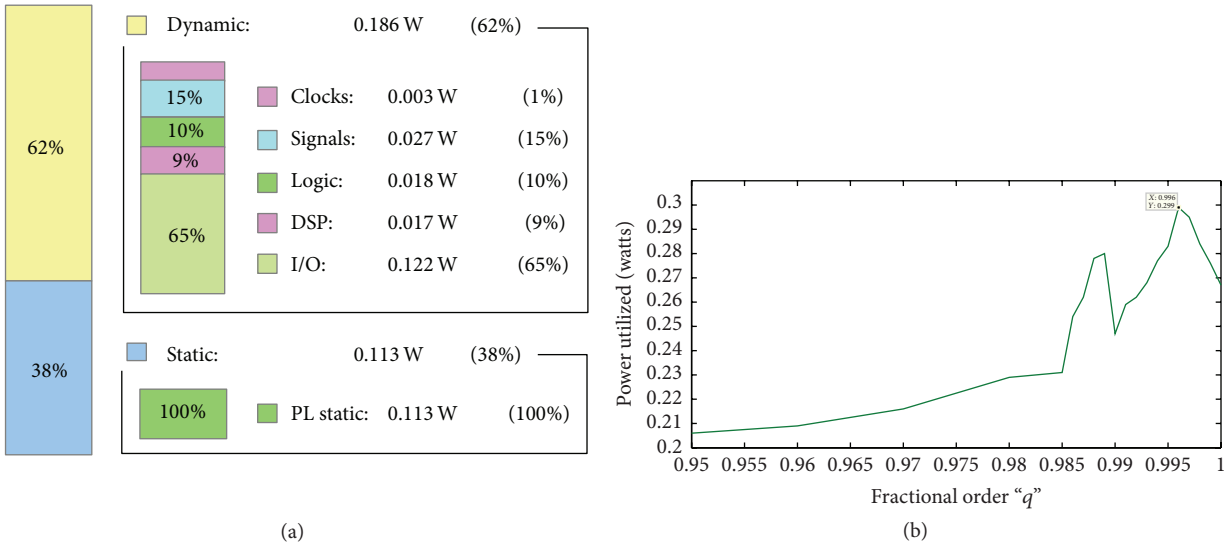

(a) (b)

Figure 21: (a) Power utilized and (b) power utilization versus fractional order of FONCS-2 system.

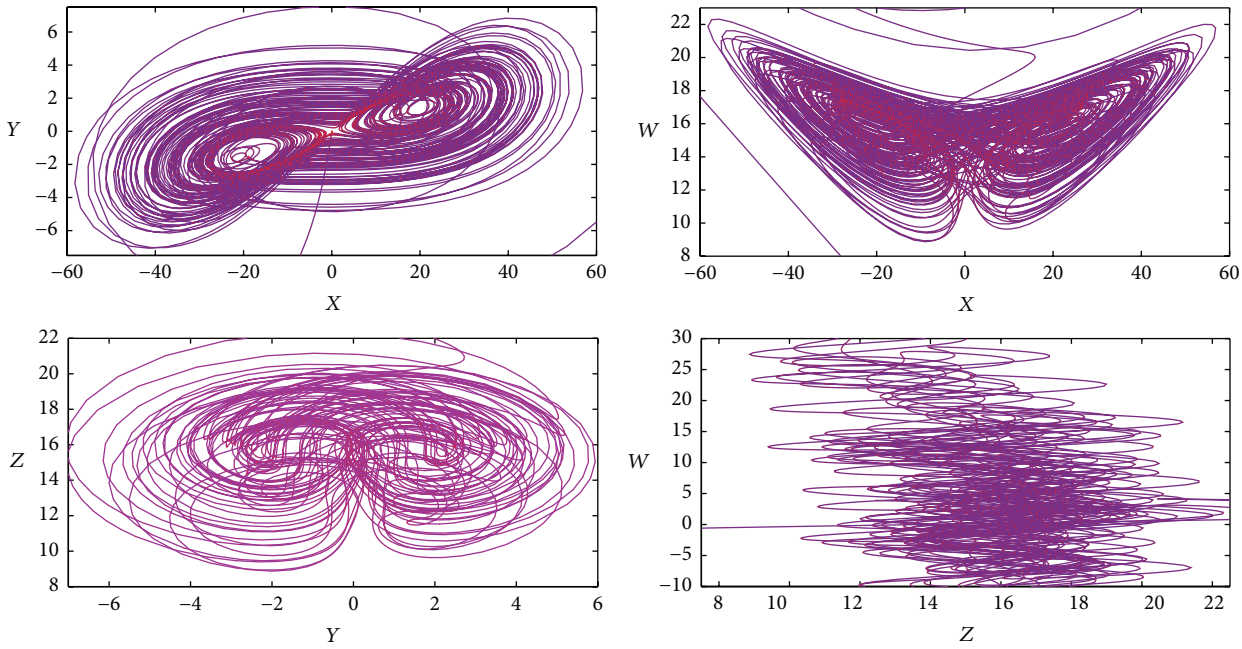

Figure 22: 2D phase portraits of the FPGA implemented FONCS-2 system (XY, XW, YZ, and ZW).

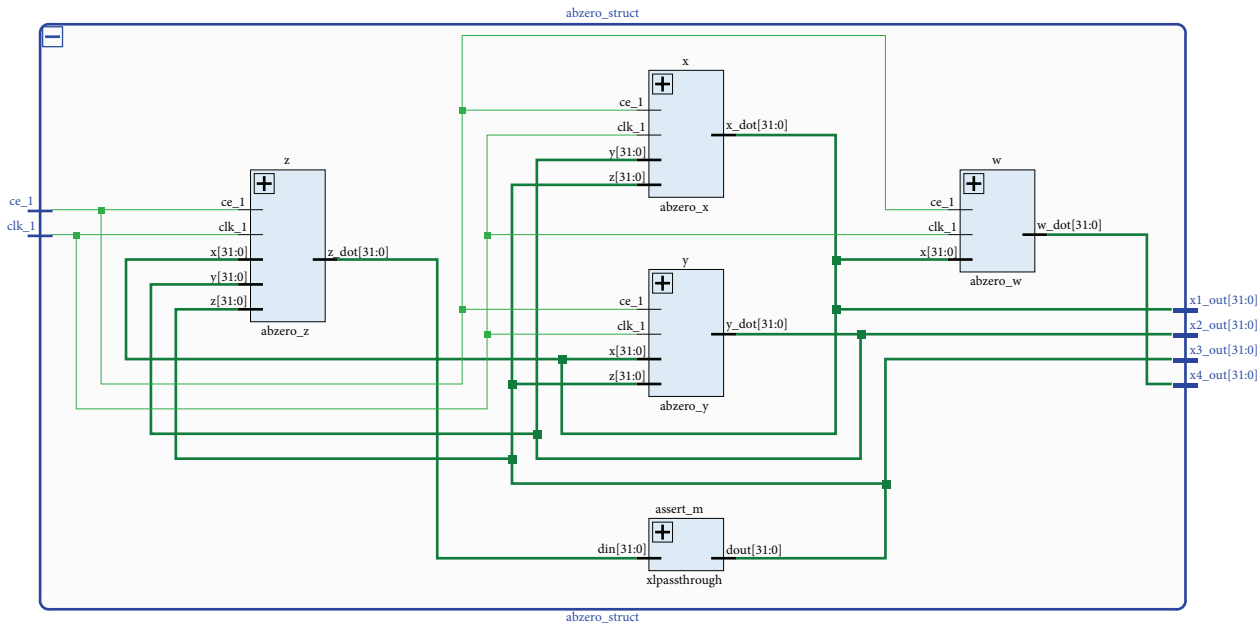

Figure 23: RTL schematics of FONCS-3 system.

period in some implementations may lead to a clock frequency mismatch. Maximum power will be consumed by the system when the FONCS shows largest Lyapunov exponents (FONCS-1 $q = 0.991$, FONCS-2 $q = 0.995$, and FONCS-3 $q = 0.996$). To utilize the power of FPGA, the computation needs to be divided into several independent blocks of threads that can be executed simultaneously [39, 49]. The FONCS power efficiency also depends on the parameter b as can be observed from the power efficiency Figures 18, 21, 24, and 27. When $b \neq 0$ the FONCS uses a maximum power of 299 w against 280 w when $b = 0$. This is because of the reason that the system shows their largest positive Lyapunov exponents when $b \neq 0$. The effect of parameter a on the power efficiency is quiet minimal and negligible. The performance on FPGA is directly related to the number of threads and its performances and hence the FONCS are designed as four parallel threads. The fractional order operators are implemented as building blocks and the so-called "frame delay" is not noticeable in the FPGA hardware implementation due to its parallel data structure, unlike a microprocessor-based implementation.

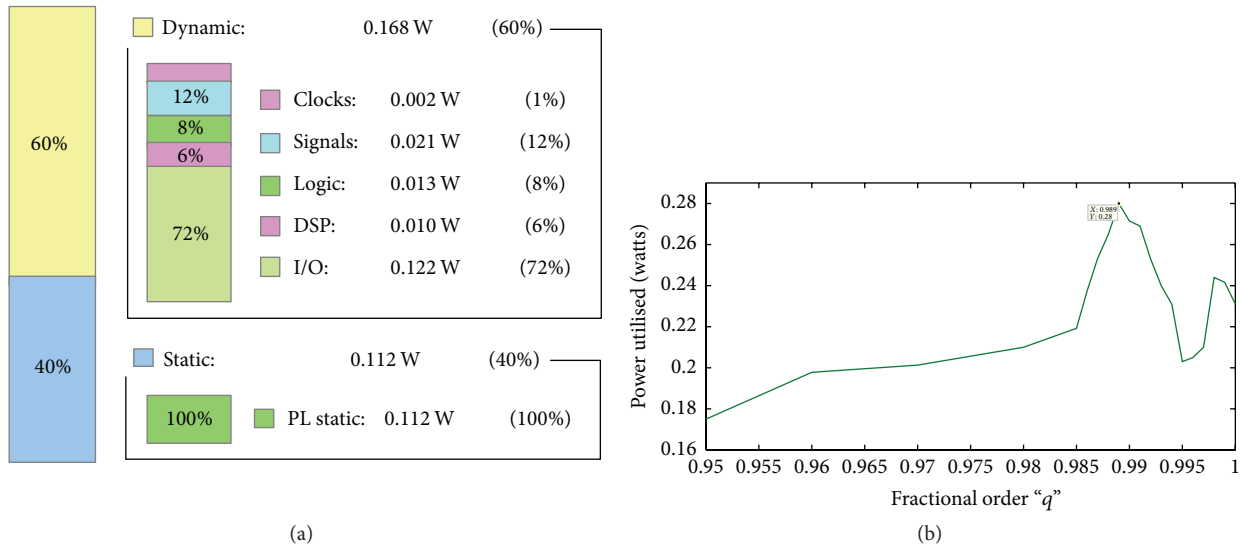

(a) (b)

Figure 24: (a) Power utilized and (b) power utilization versus fractional order of FONCS-1 system.

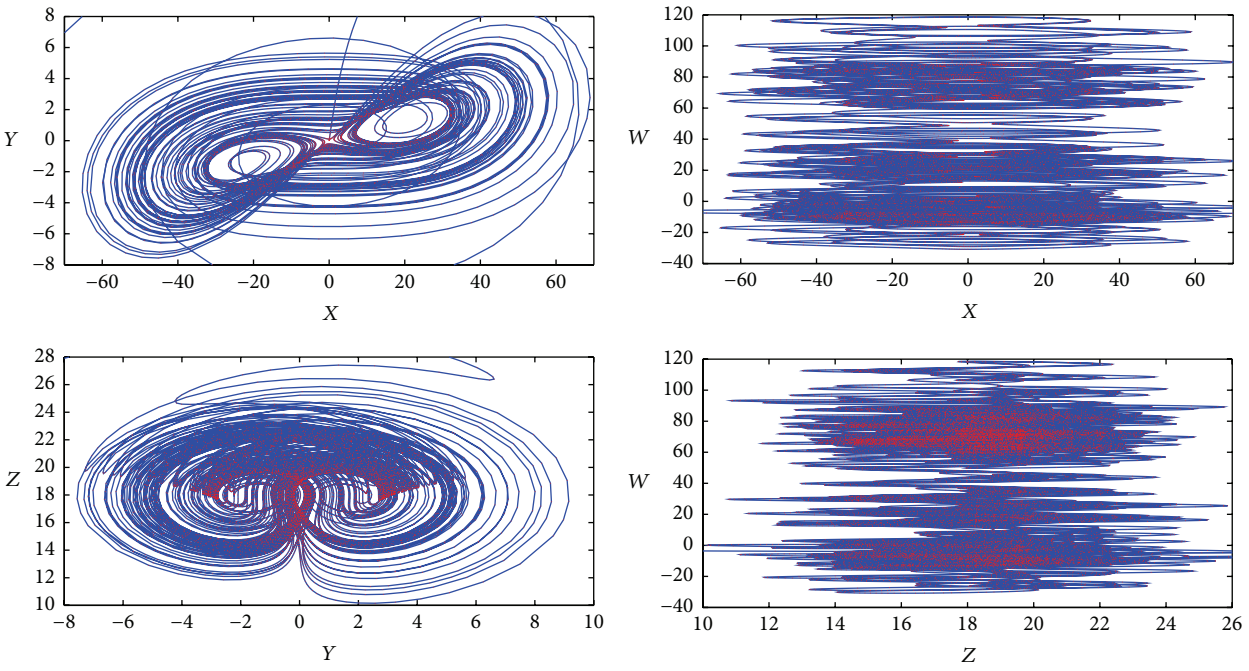

Figure 25: 2D phase portraits of the FPGA implemented FONCS-3 system.

Table 6: Resource utilization of FONCS-2 system.

Resource	Utilization	Available	Utilization %	Clock frequency	
				f_{max}	Used
LUT	1196	101400	1.18	300 Mhz	172 Mhz
FF	256	202800	0.13	500 Mhz	226 Mhz
DSP	20	600	3.33	250 Mhz	123 Mhz
IO	129	285	45.26	300 Mhz	108 Mhz
BUFG	1	32	3.13	300 Mhz	47 Mhz

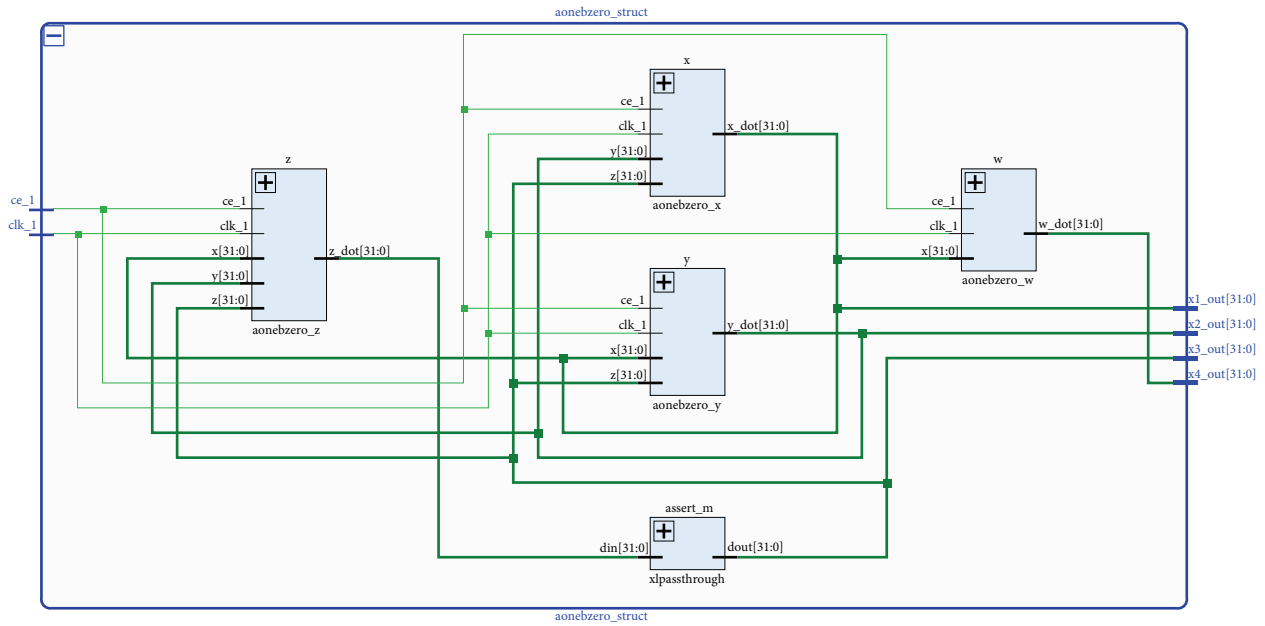

Figure 26: RTL schematics of FONCS-4 system.

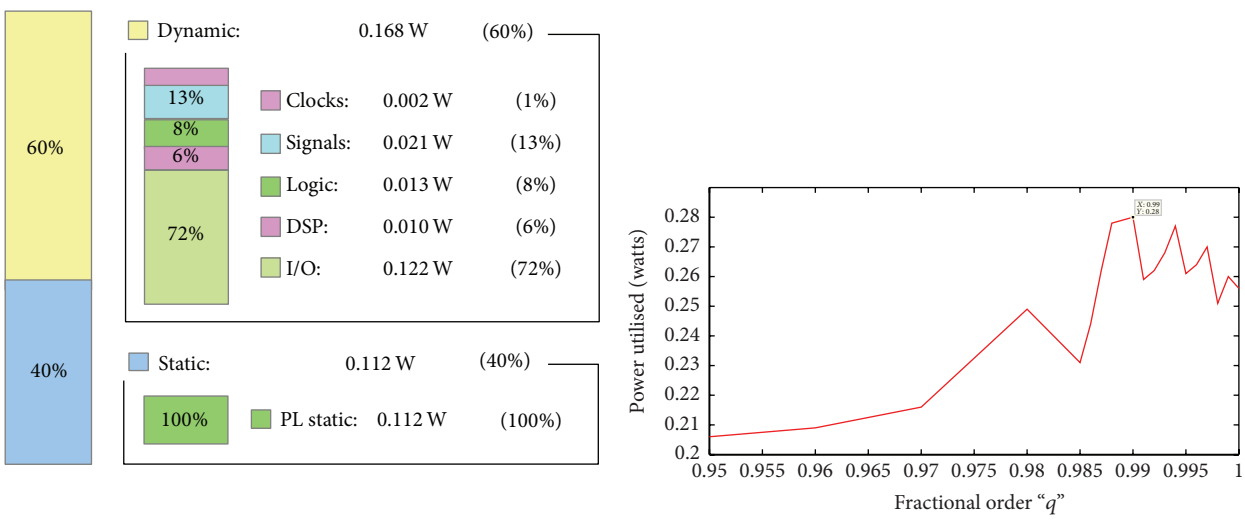

(a) (b)

Figure 27: (a) Power utilized and (b) power utilization versus fractional order of FONCS-4 system.

Table 7: Resource utilization of FONCS-3 system.

Resource	Utilization	Available	Utilization %	Clock frequency	
				f_{max}	Used
LUT	880	101400	0.87	300 Mhz	142 Mhz
FF	256	202800	0.13	500 Mhz	226 Mhz
DSP	12	600	2.00	250 Mhz	123 Mhz
IO	129	285	45.26	300 Mhz	108 Mhz
BUFG	1	32	3.13	300 Mhz	47 Mhz

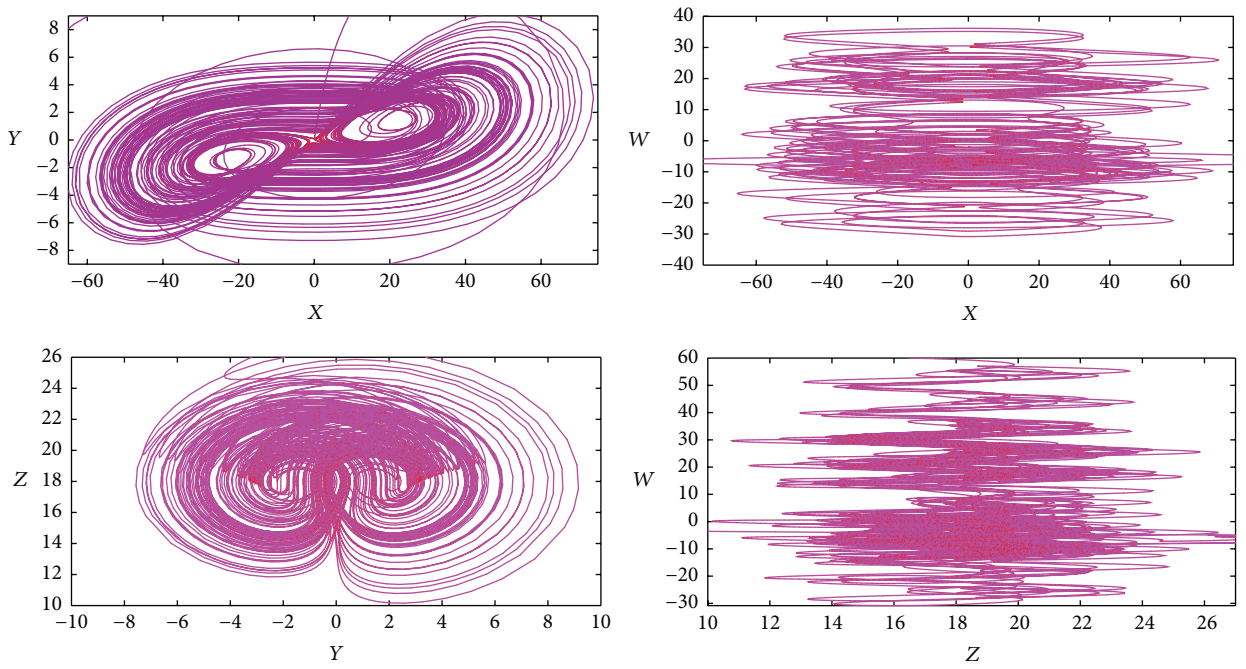

Figure 28: 2D phase portraits of the FPGA implemented FONCS-4 system.

Table 8: Resource utilization of FONCS-4 system.

Resource	Utilization	Available	Utilization %	Clock frequency	
				f_{max}	Used
LUT	911	101400	0.90	300 Mhz	151 Mhz
FF	256	202800	0.13	500 Mhz	226 Mhz
DSP	12	600	2.00	250 Mhz	123 Mhz
IO	129	285	45.26	300 Mhz	108 Mhz
BUFG	1	32	3.13	300 Mhz	47 Mhz

6. Conclusion

This paper introduces a new hyperchaotic system which when changing the values of parameters exhibits self-excited and hidden attractors. Dynamic analyses of the proposed hyperchaotic system are investigated. Fractional order model of the hyperchaotic system is derived and implemented in FPGA. Power efficiency analyses for various fractional orders are derived and it is shown that the system uses maximum power when exhibiting its largest Lyapunov exponent.

Conflicts of Interest

The authors declare that there are no conflicts of interest regarding the publication of this paper.

Acknowledgments

The authors wish to extend their sincere thanks and gratitude to *Dr. Sajad Jafari*, Department of Biomedical Engineering, Amirkabir University of Technology, for guiding in achieving crucial results.

References

[1] G. A. Leonov, N. V. Kuznetsov, and V. I. Vagaitsev, "Localization of hidden Chua's attractors," *Physics Letters A*, vol. 375, no. 23, pp. 2230–2233, 2011.

[2] G. A. Leonov, N. V. Kuznetsov, and V. I. Vagaitsev, "Hidden attractor in smooth Chua systems," *Physica D. Nonlinear Phenomena*, vol. 241, no. 18, pp. 1482–1486, 2012.

[3] G. A. Leonov and N. V. Kuznetsov, "Hidden attractors in dynamical systems. From hidden oscillations in Hilbert-Kolmogorov, Aizerman, and Kalman problems to hidden chaotic attractor in Chua circuits," *International Journal of Bifurcation and Chaos*, vol. 23, no. 01, Article ID 1330002, 2013.

[4] G. A. Leonov, N. V. Kuznetsov, and T. N. Mokaev, "Hidden attractor and homoclinic orbit in Lorenz-like system describing convective fluid motion in rotating cavity," *Communications in Nonlinear Science and Numerical Simulation*, vol. 28, no. 1–3, pp. 166–174, 2015.

[5] G. A. Leonov, N. V. Kuznetsov, and T. N. Mokaev, "Homoclinic orbits, and self-excited and hidden attractors in a Lorenz-like system describing convective fluid motion," *The European Physical Journal Special Topics*, vol. 224, no. 8, pp. 1421–1458, 2015.

[6] P. R. Sharma, M. D. Shrimali, A. Prasad, N. V. Kuznetsov, and G. A. Leonov, "Control of multistability in hidden attractors," *The European Physical Journal: Special Topics*, vol. 224, no. 8, pp. 1485–1491, 2015.

[7] P. R. Sharma, M. D. Shrimali, A. Prasad, N. V. Kuznetsov, and G. A. Leonov, "Controlling dynamics of hidden attractors," *International Journal of Bifurcation and Chaos*, vol. 25, no. 4, Article ID 1550061, 2015.

[8] S. Jafari, J. C. Sprott, V.-T. Pham, S. M. Hashemi Golpayegani, and A. Homayoun Jafari, "A new cost function for parameter estimation of chaotic systems using return maps as fingerprints," *International Journal of Bifurcation and Chaos*, vol. 24, no. 10, Article ID 1450134, 2014.

[9] V.-T. Pham, C. Volos, S. Jafari, Z. Wei, and X. Wang, "Constructing a novel no-equilibrium chaotic system," *International Journal of Bifurcation and Chaos in Applied Sciences and Engineering*, vol. 24, no. 5, Article ID 1450073, 6 pages, 2014.

[10] F. R. Tahir, S. Jafari, V.-T. Pham, C. Volos, and X. Wang, "A novel no-equilibrium chaotic system with multiwing butterfly attractors," *International Journal of Bifurcation and Chaos in Applied Sciences and Engineering*, vol. 25, no. 4, 2015.

[11] S. Jafari, V.-T. Pham, and T. Kapitaniak, "Multiscroll chaotic sea obtained from a simple 3D system without equilibrium," *International Journal of Bifurcation and Chaos*, vol. 26, no. 2, Article ID 1650031, 2016.

[12] S.-K. Lao, Y. Shekofteh, S. Jafari, and J. C. Sprott, "Cost function based on Gaussian mixture model for parameter estimation of a chaotic circuit with a hidden attractor," *International Journal of Bifurcation and Chaos in Applied Sciences and Engineering*, vol. 24, no. 1, 2014.

[13] S. Jafari, V.-T. Pham, and T. Kapitaniak, "Multiscroll chaotic sea obtained from a simple 3D system without equilibrium," *International Journal of Bifurcation and Chaos*, vol. 26, no. 2, Article ID 1650031, 2016.

[14] V.-T. Pham, S. Vaidyanathan, C. Volos, S. Jafari, and S. T. Kingni, "A no-equilibrium hyperchaotic system with a cubic nonlinear term," *Optik*, vol. 127, no. 6, pp. 3259–3265, 2016.

[15] V.-T. Pham, S. Vaidyanathan, C. K. Volos, S. Jafari, N. V. Kuznetsov, and T. M. Hoang, "A novel memristive time–delay chaotic system without equilibrium points," *European Physical Journal: Special Topics*, vol. 225, no. 1, pp. 127–136, 2016.

[16] M. Molaie, S. Jafari, J. C. Sprott, and S. M. R. H. Golpayegani, "Simple chaotic flows with one stable equilibrium," *International Journal of Bifurcation and Chaos*, vol. 23, no. 11, Article ID 1350188, 2013.

[17] S. T. Kingni, S. Jafari, H. Simo, and P. Woafo, "Three-dimensional chaotic autonomous system with only one stable equilibrium: analysis, circuit design, parameter estimation, control, synchronization and its fractional-order form," *The European Physical Journal Plus*, vol. 129, no. 5, pp. 1–16, 2014.

[18] M. Molaie, S. Jafari, J. C. Sprott, and S. M. Hashemi Golpayegani, "Simple chaotic flows with one stable equilibrium," *International Journal of Bifurcation and Chaos in Applied Sciences and Engineering*, vol. 23, no. 11, Article ID 1350188, 7 pages, 2013.

[19] S. T. Kingni, S. Jafari, H. Simo, and P. Woafo, "Three-dimensional chaotic autonomous system with only one stable equilibrium: analysis, circuit design, parameter estimation, control, synchronization and its fractional-order form," *The European Physical Journal Plus*, vol. 129, no. 5, article 76, pp. 1–16, 2014.

[20] V. Pham, S. Jafari, C. Volos, A. Giakoumis, S. Vaidyanathan, and T. Kapitaniak, "A chaotic system with equilibria located on the rounded square loop and its circuit implementation," *IEEE Transactions on Circuits and Systems II: Express Briefs*, vol. 63, no. 9, pp. 878–882, 2016.

[21] R. Karthikeyan, A. Prasina, R. Babu, and S. Raghavendran, "FPGA implementation of novel synchronization methodology for a new chaotic system," *Indian Journal of Science and Technology*, vol. 8, no. 11, 2015.

[22] K. Rajagopal, A. Karthikeyan, and A. K. Srinivasan, "FPGA implementation of novel fractional-order chaotic systems with two equilibriums and no equilibrium and its adaptive sliding mode synchronization," *Nonlinear Dynamics. An International Journal of Nonlinear Dynamics and Chaos in Engineering Systems*, vol. 87, no. 4, pp. 2281–2304, 2017.

[23] D. Baleanu, K. Diethelm, E. Scalas, and J. J. Trujillo, *Fractional Calculus: Models and Numerical Methods*, World Scientific, Singapore, 2014.

[24] Y. Zhou, *Basic Theory of Fractional Differential Equations*, World Scientific, Singapore, 2014.

[25] K. Diethelm, *The Analysis of Fractional Differential Equations*, Springer, Berlin, Germany, 2010.

[26] M. Pourmahmood Aghababa, "Robust finite-time stabilization of fractional-order chaotic systems based on fractional lyapunov stability theory," *Journal of Computational and Nonlinear Dynamics*, vol. 7, no. 2, Article ID 021010, 2012.

[27] E. A. Boroujeni and H. R. Momeni, "Non-fragile nonlinear fractional order observer design for a class of nonlinear fractional order systems," *Signal Processing*, vol. 92, no. 10, pp. 2365–2370, 2012.

[28] R. Zhang and J. Gong, "Synchronization of the fractional-order chaotic system via adaptive observer," *Systems Science & Control Engineering*, vol. 2, no. 1, pp. 751–754, 2014.

[29] R. H. Li and W. S. Chen, "Complex dynamical behavior and chaos control in fractional-order Lorenz-like systems," *Chinese Physics B*, vol. 22, no. 4, Article ID 040503, 2013.

[30] D. Cafagna and G. Grassi, "Fractional-order systems without equilibria: the first example of hyperchaos and its application to synchronization," *Chinese Physics B*, vol. 24, no. 8, Article ID 080502, 2015.

[31] M.-F. Danca, W. K. Tang, and G. Chen, "Suppressing chaos in a simplest autonomous memristor-based circuit of fractional order by periodic impulses," *Chaos, Solitons & Fractals*, vol. 84, pp. 31–40, 2016.

[32] I. Petras, "Methos for simulation of the fractional order chaotic systems," *Acta Montanastica Slovaca*, vol. 11, no. 4, pp. 273–277, 2006.

[33] W. Trzaska Zdzislaw, *Matlab Solutions of Chaotic Fractional Order Circuits*, InTech, Rijeka, Croatia, 2013, http://www.intechopen.com/download/pdf/21404.

[34] M. A. Jafari, E. Mliki, A. Akgul et al., "Chameleon: the most hidden chaotic flow," *Nonlinear Dynamics*, pp. 1–15, 2017.

[35] Q. Li, H. Zeng, and J. Li, "Hyperchaos in a 4D memristive circuit with infinitely many stable equilibria," *Nonlinear Dynamics*, vol. 79, no. 4, pp. 2295–2308, 2015.

[36] Q.-H. Hong, Y.-C. Zeng, and Z.-J. Li, "Design and simulation of chaotic circuit for flux-controlled memristor and charge-controlled memristor," *Acta Physica Sinica*, vol. 62, no. 23, Article ID 230502, 2013.

[37] S. Sampath, S. Vaidyanathan, and V.-T. Pham, "A novel 4-D hyperchaotic system with three quadratic nonlinearities, its adaptive control and circuit simulation," *International Journal of Control Theory and Applications*, vol. 9, no. 1, pp. 339–356, 2016.

[38] V. Rashtchi and M. Nourazar, "FPGA implementation of a real-time weak signal detector using a duffing oscillator," *Circuits, Systems, and Signal Processing*, vol. 34, no. 10, pp. 3101–3119, 2015.

[39] E. Tlelo-Cuautle, J. J. Rangel-Magdaleno, A. D. Pano-Azucena, P. J. Obeso-Rodelo, and J. C. Nunez-Perez, "FPGA realization of multi-scroll chaotic oscillators," *Communications in Nonlinear Science and Numerical Simulation*, vol. 27, no. 1–3, pp. 66–80, 2015.

[40] C. Li, Z. Gong, D. Qian, and Y. Chen, "On the bound of the Lyapunov exponents for the fractional differential systems," *Chaos*, vol. 20, no. 1, Article ID 013127, 2010.

[41] M. S. Tavazoei and M. Haeri, "Unreliability of frequency-domain approximation in recognising chaos in fractional-order systems," *IET Signal Processing*, vol. 1, no. 4, pp. 171–181, 2007.

[42] B. Bao, P. Jiang, H. Wu, and F. Hu, "Complex transient dynamics in periodically forced memristive Chua's circuit," *Nonlinear Dynamics*, vol. 79, no. 4, pp. 2333–2343, 2015.

[43] C. Pezeshki, S. Elgar, and R. C. Krishna, "Bispectral analysis of systems possessing chaotic motion," *Journal of Sound and Vibration*, vol. 137, no. 3, pp. 357–368, 1990.

[44] D. Dudkowski, S. Jafari, T. Kapitaniak, N. V. Kuznetsov, G. A. Leonov, and A. Prasad, "Hidden attractors in dynamical systems," *Physics Reports. A Review Section of Physics Letters*, vol. 637, pp. 1–50, 2016.

[45] E. Tlelo-Cuautle, A. D. Pano-Azucena, J. J. Rangel-Magdaleno, V. H. Carbajal-Gomez, and G. Rodriguez-Gomez, "Generating a 50-scroll chaotic attractor at 66 MHz by using FPGAs," *Nonlinear Dynamics*, vol. 85, no. 4, pp. 2143–2157, 2016.

[46] Q. Wang, S. Yu, C. Li et al., "Theoretical design and FPGA-based implementation of higher-dimensional digital chaotic systems," *IEEE Transactions on Circuits and Systems I-Regular Papers*, vol. 63, no. 3, pp. 401–412, 2016.

[47] E. Dong, Z. Liang, S. Du, and Z. Chen, "Topological horseshoe analysis on a four-wing chaotic attractor and its FPGA implement," *Nonlinear Dynamics*, vol. 83, no. 1-2, pp. 623–630, 2016.

[48] E. Tlelo-Cuautle, V. H. Carbajal-Gomez, P. J. Obeso-Rodelo, J. J. Rangel-Magdaleno, and J. C. Núñez-Pérez, "FPGA realization of a chaotic communication system applied to image processing," *Nonlinear Dynamics*, vol. 82, no. 4, pp. 1879–1892, 2015.

[49] Y.-M. Xu, L.-D. Wang, and S.-K. Duan, "A memristor-based chaotic system and its field programmable gate array implementation," *Wuli Xuebao/Acta Physica Sinica*, vol. 65, no. 12, Article ID 120503, 2016.